WL-TR-
90-45

(2)

LASER-BASED DIAGNOSTICS FOR $N_2(X,v)$

L. G. Piper, et al

Physical Sciences Inc.
20 New England Business Center
Andover, Massachusetts 01810

October 1990

Final Report

Approved for public release; distribution unlimited.

Weapons Laboratory
Air Force Systems Command
Kirtland Air Force Base, NM 87117-6008

This final report was prepared by Physical Sciences Inc, Andover, Massachusetts, under contract F29601-87-C-0056 Job Order 3005AR14 with the Weapons Laboratory, Kirtland Air Force Base, New Mexico. The Laboratory Project Officer-in-Charge was Captain Robert P. Crannage, Jr. (ARDJ).

When Government drawings, specifications, or other data are used for any purpose other than in connection with a definitely Government-related procurement, the United States Government incurs no responsibility or any obligation whatsoever. The fact that the Government may have formulated or in any way supplied the said drawings, specifications, or other data, is not to be regarded by implication, or otherwise in any manner construed, as licensing the holder, or any other person or corporation; or as conveying any rights or permission to manufacture, use, or sell any patented invention that may in any way be related thereto.

This report has been authored by a contractor of the United States Government. Accordingly, the United States Government retains a nonexclusive, royalty-free license to publish or reproduce the material contained herein, or allow others to do so, for the United States Government purposes.

This report has been reviewed by the Public Affairs Office and is releasable to the National Technical Information Service (NTIS). At NTIS, it will be available to the general public, including foreign nationals.

If your address has changed, if you wish to be removed from our mailing list, or if your organization no longer employs the addressee, please notify WL/ARDJ, Kirtland AFB, NM 87117-6008 to help us maintain a current mailing list.

This report has been reviewed and is approved for publication.

Robert P Crannage, Jr

ROBERT P. CRANNAGE, JR.
Captain, USAF
Project Officer

FOR THE COMMANDER

Robert A Hildreth

ROBERT A. HILDRETH
Major, USAF
Chief, Advanced Concepts Branch

David K Neumann

DAVID K. NEUMANN
Lieutenant Colonel, USAF
Chief, Devices Division
Technology Directorate

DO NOT RETURN COPIES OF THIS REPORT UNLESS CONTRACTUAL OBLIGATIONS OR NOTICE ON A SPECIFIC DOCUMENT REQUIRES THAT IT BE RETURNED.

REPORT DOCUMENTATION PAGE

Form Approved
OMB No. 0704-0188

1. AGENCY USE ONLY (Leave blank)	2. REPORT DATE	3. REPORT TYPE AND DATES COVERED
	October 1990	Final Report; Sep 87 - Oct 89

4. TITLE AND SUBTITLE

LASER-BASED DIAGNOSTICS FOR $N_2(X,v)$

5. FUNDING NUMBERS

PE: 65502F
C: F29601-87-C-0056
PR: 3005
TA: AR
WU: 14

6. AUTHOR(S)

Piper, L. G.; Donohue, K.; Kessler, W. J.; Tucker, T. R.; Cummings, W. P.; Marinelli, W. J.; and Davis, S. J.

7. PERFORMING ORGANIZATION NAME(S) AND ADDRESS(ES)

Physical Sciences Inc.
20 New England Business Center
Andover, Massachusetts 01810

8. PERFORMING ORGANIZATION REPORT NUMBER

PSI-1045/TR-960

9. SPONSORING MONITORING AGENCY NAME(S) AND ADDRESS(ES)

Weapons Laboratory
Kirtland AFB, New Mexico 87117-6008

10. SPONSORING/MONITORING AGENCY REPORT NUMBER

WL-TR-90-45

11. SUPPLEMENTARY NOTES

12a. DISTRIBUTION AVAILABILITY STATEMENT

Approved for public release; distribution unlimited.

12b. DISTRIBUTION CODE

13. ABSTRACT (Maximum 200 words)

This program has developed successful laser-based diagnostics including 2 + 2 and 1 + 1 multiphoton ionization (MPI) and two- and one-photon laser-induced fluorescence (LIF). All techniques relied upon excitation of the $N_2(X,v'')$ to the intermediate $a^1\Pi$ level of molecular nitrogen. Two energy-transfer diagnostics were developed. One was Penning ionization in which metastable helium atoms excited the $N_2(x,v'')$ to $N_2^+(B^2\Sigma^+)$ with subsequent observation of the resulting nitrogen first-negative emission, $N_2^+(B^2\Sigma^+)$. Another energy-transfer technique involved excitation of the $N_2(X,v'')$ by $N_2(A^3\Sigma u)$ to $N_2(B^3\Pi g)$, with subsequent observation of the nitrogen first-positive system. Penning-ionization characterization showed that microwave and radio-frequency discharges were efficient sources of $N_2(X,v'')$. The recombination of N_3 radicals produced $N_2(X,v'')$ with a Treanor vibrational distribution having a characteristic temperature of 3300 K, while the reaction between N and NO produced $N_2(X,v'')$ having an inverted vibrational population distribution. Studies on the excitation of IF(B) in active nitrogen. Active nitrogen excites IF(B) with an efficiency that is greater than that which would be obtained were $N_2(A)$ the only metastable involved in the energy-transfer reaction.

14. SUBJECT TERMS	15. NUMBER OF PAGES
Nitrogen, Vibrational, Diagnostic, Penning Ionization, Multiphoton Ionization, Laser Induced Fluorescence, $N_2(X,v)$, Detection, $N_2(A^3\Sigma u^+)$, $N_2(B^3\Pi g)$	152
	16. PRICE CODE

17. SECURITY CLASSIFICATION OF REPORT	18. SECURITY CLASSIFICATION OF THIS PAGE	19. SECURITY CLASSIFICATION OF ABSTRACT	20. LIMITATION OF ABSTRACT
UNCLASSIFIED	UNCLASSIFIED	UNCLASSIFIED	

SUMMARY

This program was designed to study diagnostics for $N_2(X,v'')$ and the kinetics of $N_2(X,v'')$ energy transfer reactions, particularly those which might be important in chemical laser systems. The program had four primary components: 1) the development of $N_2(X,v'')$ diagnostics; 2) the quantitative correlation of these various diagnostics; 3) the characterization of various sources of $N_2(X,v'')$; and 4) the study of $N_2(X,v'')$ energy transfer reactions. The key accomplishments are as follows:

I. Diagnostic Development

A. Laser-Based Diagnostics

1) 2+2 MPI
Range of vibrational levels: 0 to 4
Sensitivity: 10^{14} molecules cm^{-3}
Absolutely quantifiable with difficulty

2) 1+1 MPI
Range of vibrational levels: 9 to 27
Sensitivity: 10^{8} molecules cm^{-3}
Cannot be quantified

3) 2+2 LIF
Range of vibrational levels: 0 to 4
Sensitivity: 10^{14} molecules cm^{-3}
Absolutely quantifiable with difficulty

4) 1+1 LIF
Range of vibrational levels: 9 to 15
Sensitivity: 10^{8} molecules cm^{-3}
Quantifiable in relative sense

B. Energy-Transfer Diagnostics

1) He^{*} Penning Ionization
Range of vibrational levels: 0 to 6
Sensitivity: 10^{11} molecules cm^{-3}
Absolutely quantifiable

2) $N_2(A)$ Excitation to $N_2(B)$
Range of vibrational levels: 5 to 15
Sensitivity: 10^{11} molecules cm^{-3}
Quantifiable to factor of two

II. Quantitative Correlations

He^* Penning ionization and 2+2 MPI agree to within experimental error

III. Source Characterization

A. Discharge

1) Microwave (2.54 GHz)
> 70 percent of N_2 vibrationally excited

2) Radio-Frequency (13.56 MHz)
> 50 percent of N_2 vibrationally excited

3) Hollow-Cathode Direct Current
< 2 percent of N_2 vibrationally excited

4) Dielectric Barrier
< 2 percent of N_2 vibrationally excited

B. Chemical

1) $N_3 + N_3 \rightarrow 3\ N_2(X,v'')$
Treanor Distribution
Vibrational Temperature = 3300 K

2) $N + NO \rightarrow N_2(X;v'') + O$
Inverted vibrational distribution

3) $H + NF_2$ Reaction Sequence
Penning ionization inappropriate
MPI not sufficiently sensitive

IV. Energy Transfer Reactions

A. $IF(B^3\Pi_O{}^+)$ Excitation Studies

1) Active Nitrogen - slow-flow conditions
IF(B) excited strongly
Exciting species generated from $N + N \rightarrow N_2{}^*$
$N_2(A)$ probably not implicated
$[IF(B)] > 3 \times 10^8$ produced

2) Active Nitrogen - fast-flow conditions
IF(B) not excited by $N_2(X,v'' \leq 15)$

N_2^* excitation > excitation by $N_2(A)$
IF(B) excitation source remains unidentified

3) $N_3 + N_3 \rightarrow N_2^* + 2\ N_2$
IF(B) excitation like that from $N_2(A)$
yield of $N_2(A)$ from $N_3 + N_3 < 10^{-5}$

B. $N_2(X,v'')$ Quenching Studies

1) 1+1 LIF

$$k_{CF_4} = 3.6 \times 10^{-13}\ cm^3\ molecule^{-1}\ s^{-1}$$

2) $N_2(A) + N_2(X,v'') \rightarrow N_2(B) + N_2(X)$
$N_2(x,v''=5\text{-}15)$ and $N_2(B)$ quenching surveyed

$10^{-16} < k_Q < 5 \times 10^{-14}\ cm^3\ molecule^{-1}\ s^{-1}$ for $N_2(X,v'')$ quenching by CO_2, N_2, CF_4, and H_2

$10^{-11} < k_Q < 10^{-9}\ cm^3\ molecule^{-1}\ s^{-1}$ for $N_2(B)$ quenching by CH_4, H_2, CO_2, N_2 CF_4, SF_6, and N_2O

CONTENTS

SUMMARY iii

1.0 INTRODUCTION 1
1.1 PROGRAM MOTIVATION 1
1.2 PHASE I RESEARCH ACCOMPLISHMENTS 3

2.0 DIAGNOSTIC DEVELOPMENT 7
2.1 EXTENSION OF PENNING IONIZATION DIAGNOSTIC 8
2.2 THE EXCITATION OF $N_2(B^3\Pi_g, v'=1\text{-}12)$ IN THE REACTION BETWEEN $N_2(A^3\Sigma_u^+)$ AND $N_2(X, v \geq 5)$ 18
2.3 LASER-BASED DIAGNOSTICS FOR $N_2(X,v)$ 42

3.0 QUANTITATIVE CORRELATIONS 63

4.0 SOURCE CHARACTERIZATION 68
4.1 CHARACTERIZATION OF DISCHARGE SOURCES OF $N_2(X,v)$ 68
4.2 CHARACTERIZATION OF CHEMICAL SOURCES OF $N_2(X,v)$ 74

5.0 ENERGY TRANSFER MEASUREMENTS 100
5.1 INTRODUCTION 101
5.2 ACTIVE NITROGEN PRODUCED UNDER "SLOW FLOW" CONDITIONS (REGIME I) 101
5.3 ACTIVE NITROGEN PRODUCED UNDER "FAST FLOW" CONDITIONS (REGIME II) 113
5.4 IF(B) EXCITATION BY THE PRODUCTS OF N_3 RECOMBINATION 118
5.5 QUENCHING OF $N_2(X,v'')$ AND $N_2(B)$ 120

6.0 PROGRAM SUMMARY 125

REFERENCES 127

LIST OF FIGURES

Figure		Page
1	Calculated time evolution of discharge-created $N_2(X,v)$ illustrating the effects of collisional up-pumping	3
2	Strategies for $N_2(X,v)$ detection	4
3	Flow reactor for Penning-ionization studies of $N_2(X,v)$	9
4	Penning-ionization spectrum of vibrationally cold N_2	16
5	Penning-ionization spectrum of vibrationally excited $N_2(X)$	16
6	Observed and fit vibrational distribution of $N_2^+(B,v)$ produced in the Penning-ionization of $N_2(X,v)$ by $He(2^3S)$	17
7	Penning-ionization spectrum of N in N_2/He mixtures	19
8	Distribution of $N_2^+(B)$ vibrational levels of $N_2(v)$ produced in Penning ionization of the effluents of a 6-W microwave discharge	20
9	Observed (■) and calculated (-) intensities of $N_2^+(B\text{-}X)$ emission produced by Penning-ionization of $N_2(v)$ from a 6-W microwave discharge	21
10	Vibrational distribution of ground state $N_2(v)$ from a 6-W microwave discharge as determined by the iterative technique	22
11	$N_2^+(B)$ distribution produced from Penning-ionization of the effluents of a 90-W microwave discharge	23
12	Relative intensities from $N_2^+(B\text{-}X)$ emission produced from Penning-ionization of a 90-W microwave discharge	24
13	Relative populations of $N_2(X,v'')$ determined from iterative fitting of Penning ionization intensities of the effluents of a 90-W microwave discharge	25
14	Schematic of discharge flow apparatus for studying $N_2(A)$ and $N_2(X,v)$	26
15	Spectrum of N first-positive bands, $N_2(B^3\Pi_g - A\Sigma_u^+)$, excited in the reaction between $N_2(A)$ and $N_2(X,v)$	27

LIST OF FIGURES (Continued)

Figure		Page
16	Variation in the intensity of the 2,0 band of the first-positive system as a function of the intensity of the 0,6 band of the N Vegard-Kaplan system $N_2(A^3\Sigma_g^+ - X^1\Sigma_g^-)$	28
17	Variation in the number density of different vibrational levels of $N_2(B)$ as a function of power of the microwave discharge under conditions of constant $N_2(A)$ number density	29
18	Relative vibrational distributions for $N_2(B,v)$ for two different levels of $N_2(X,v)$ vibrational excitation	32
19	Variation in the ratio of the number density of $N_2(B)$, after correcting for quenching, to that for $N_2(A)$ with the number density of $N_2(X,v=5\text{-}10)$	33
20	Variation in intensity of the 0,6 Vegard-Kaplan band as a function of time in the absence and presence of $N_2(X,v)$	34
21	Nitrogen ultraviolet spectrum	37
22	Ratio of the number densities of $N_2(A,v=1)$ to $N_2(A,v=0)$ as a function of time	39
23	Laser detection strategies	43
24	Schematic diagram of 1-in flow reactor	44
25	Block diagram of 5 cm ID flow reactor	45
26	MPI electrodes and electronics	46
27	The 2+2 MPI signal dependence on $[N_2]$	47
28	The 2+2 MPI signal dependence on electrode bias	48
29	The 2+2 MPI signal dependence on laser energy	49
30	The 1+1 MPI spectrum of $N_2(a^1\Pi_g,v'=5 \leftarrow X^1\Sigma_g^+,v''=13)$ band	51
31	The 1+1 MPI spectrum of $N_2(a^1\Pi_g,v' \leftarrow X^1\Sigma_g^+,v'')$ band	52

LIST OF FIGURES (Continued)

Figure		Page
32	Variation in $N_2(a^1\Pi_g, v'=0)$ fluorescence efficiency as a function of N_2 mole fraction in Ar at 1.0 torr total pressure	54
33	One-photon LIF excitation spectrum of $N_2(a^1\Pi_g, v'=2 \leftarrow X^1\Sigma_g^+, v''=9)$ band	56
34	One-photon LIF signal dependence on laser energy	57
35	$[N_2(X,v'')]$ determination via LIF signal intensity versus time	58
36	LIF temporal decay of $N_2(a^1\Pi_g, v'=4 \rightarrow X^1\Sigma_g^+, v''=13)$ band	58
37	$N_2(X^1\Sigma_g^+, v''=14)$ quenching by CF_4	60
38	The 2+2 MPI spectrum of the $N_2(a^1\Pi_g, v'=0 \rightarrow X^1\Sigma_g^+, v''=0)$ band, overlay with 70 W microwave discharge and without microwave discharge	64
39	The 2+2 MPI spectrum of $N_2(a^1\Pi_g, v'=1 \rightarrow X^1\Sigma_g^+, v''=1)$ band, 70 W microwave discharge production of $N_2(X^1\Sigma_g^+, v''=1)$	64
40	Variation in effective N vibrational temperature as a function of discharge power	69
41	Fraction of total N that is vibrationally excited as a function of discharge power	70
42	Variation in effective vibrational temperature with N mole fraction	71
43	Variation in vibrational level number densities with N mole fraction through the discharge	72
44	Variation in effective N vibrational temperature with flow time from the discharge	73
45	Variation in effective vibrational temperature of $N_2(X,v)$ as a function of discharge power for microwave and rf discharge	73
46	Variation in effective vibrational temperature of $N_2(X,v)$ as a function of N mole fraction for a 50-W microwave discharge and a 70-W rf discharge	74
47	Flow reactor configurations	77
48	N + NO titration plot	79

LIST OF FIGURES (Continued)

Figure		Page
49	Penning-ionization in absence of added NO	79
50	Penning-ionization spectrum of $N_2(v)$ generated from N + NO	80
51	First negative distributions without NO	80
52	First negative distributions with NO	81
53	The $N_2(X,v)$ distribution produced from N + NO reaction	82
54	The $N_2(X,v)$ distributions from N + NO at various pressures	84
55	Loss of $N_2(X,v=0)$ with increasing N_2-N_2 collisions	85
56	The NF(b) chemiluminescence versus $[HN_3]$ at 528.8 nm : 21 cm	87
57	The NF(b) chemiluminescence versus $[HN_3]$ at 528.8 nm : 1 cm	88
58	$N_2^+(B^2\Sigma_u^+ - X^2\Sigma_g^+)$ emission from Penning ionization of the product of N_3 recombination	89
59	Reciprocal of the signal intensity versus reaction length	89
60	Excited state distributions of $N_2(v)$ from N_3 recombination	90
61	Expected ground state distributions of $N_2(v)$ from N_3 recombination	90
62	Excited state distribution as a function of flow tube pressure	92
63	N_3 kinetics plot	94
64	Flow reactor configuration for $N_2(A) + N_2(v)$ studies	95
65	Flow reactor configuration for N + N_3 reaction	96
66	N_2(B-A) emission from N + N_3 reaction	97
67	Flow reactor configuration for scaling experiments	102

LIST OF FIGURES (Concluded)

Figure		Page
68	IF($B^3\Pi_0^+$ - $X^1\Sigma_g^+$) emission from active N_2 excitation of IF(X) produced in the F + CF_3I reaction	103
69	The IF(B) vibrational distributions in active N_2	104
70	The IF(B) intensity versus [CF_3I]	104
71	The IF(B) intensity versus N_2 mole fraction in discharge	105
72	The IF(B) intensity versus microwave power	105
73	The N_2 mole fraction in discharge dependence of N-atoms produced in an N_2/He microwave discharge	107
74	Discharge power dependence of N-atoms produced in an N_2/He microwave discharge	108
75	IF(B-X) (0,2) intensity versus [N]	108
76	Flow reactor configuration for Penning-ionization studies	110
77	Penning ionization of $N_2(v)$ generated in active N_2 with a glass wool plug	110
78	Penning-ionization spectra of $N_2(v)$ generated from active N_2 with Ni screen	111
79	Flow reactor configuration for IF(B) excitation studies comparing iodine donor	112
80	The IF(B) intensity versus iodine donor concentration	113
81	Flow reactor for studying the excitation of IF(B) by $N_2(X,v'')$	114
82	Excitation of the IF(B) 0,4 band by $N_2(A)$ and $N_2(X,v'')$	116
83	Flow reactor configuration for $N_2(v)$ + IF studies	118
84	IF(B) excited by N_3 + N_3 recombination products	119
85	The IF(B) vibrational distributions from N_2^* excitation	119
86	Stern-Volmer plot for $N_2(B)$ quenching by CH_4	123

LIST OF TABLES

Table

1 Vibrational transitions from $N_2(X,v'')$ observed using laser-based techniques 7

2 Multiphoton ionization detection of $N_2(a,v') \leftarrow N_2(X,v'')$ 53

3 Selected a←X bands suitable for LIF probing 55

4 The $N_2(X^1\Sigma_g^+)$ vibrational populations 66

5 Comparison of $N_2(X,v)$ detection by MPI versus Penning ionization 67

6 The N_3 recombination results: absolute number densities for $N_2(X,v)$ 91

7 Previously reported values for the N_3 recombination rate coefficient 93

8 Rate coefficients for global quenching of $N_2(B)$ and $N_2(X,v'')$ 123

1.0 INTRODUCTION

This report details the activities and accomplishments on a Phase II Small Business Innovative Research (SBIR) program designed to develop diagnostics for vibrationally excited nitrogen, and to use these diagnostics to investigate energy transfer reactions of $N_2(X,v)$ that might be important in visible chemical laser systems. This program had four goals:

1. To extend the diagnostics for vibrationally excited nitrogen developed during the Phase I program (Ref. 1) to make them more comprehensive diagnostics of the total N_2 ground-state vibrational distribution as well as to extend their range of utility to environments more hostile to their implementation.

2. To correlate the multiphoton ionization (MPI) and laser-induced fluorescence (LIF) techniques with the Penning-ionization technique developed previously under Strategic Defense Initiative Organization (SDIO) sponsorship (Ref. 2).

3. To compare the vibrational distributions produced by a number of $N_2(X,v)$ sources, both discharge and chemical.

4. To investigate the kinetics of $N_2(X,v)$ to gain an experimental insight into v-v pumping within the N_2 vibrational manifold as well as to characterize the quenching and relaxation of $N_2(X,v)$ by a number of partners including several potential laser candidates that possibly are excited electronically from quenching specific, high vibrational levels of $N_2(X,v)$.

The remainder of this section of the report gives the program motivation and summarizes the Phase I activities that served as the foundation for this program. Sections 2.0 through 5.0 detail the accomplishments in the various areas of activity of this program. Finally, Section 6.0 gives conclusions derived from the work.

1.1 PROGRAM MOTIVATION

The recent interest in the development of visible chemical lasers has focused on the use of energetic nitrogen (N) species to excite potential laser candidates. At Physical Sciences Inc. (PSI), experiments funded by the Weapons Laboratory (WL) showed that $N_2(A^3\Sigma_u^+)$ was 40 percent efficient in exciting $IF(B^3\Pi_{O+})$ and that active N produced by discharging N_2/Ar mixtures also strongly excited IF(B) (Refs. 3 and 4). The exciting agent in active N_2 could not be positively identified, but an analysis of the concentrations of possible exciting species showed that only $N_2(X,v>>0)$ appeared to be present in sufficient quantities to excite IF(B) with the measured excitation rates. This assignment is consistent with the observed lifetime of the exciting species and the observation that emission from $N_2(B)$, which has an internal electronic term energy T_e, of 7.4 eV and is further vibrationally excited up to energies of 9.8 eV, varies linearly with IF(B) emission. Subsequent work in this area, supported by both WL and SDIO/IST, provided further evidence that IF(B) excitation by active N_2 was indeed closely correlated with $N_2(B^3\Pi_g)$ concentrations (Refs. 5 and 6). A technique

employing Penning-ionization to obtain $N_2(X,v>>0)$ concentrations (Ref. 2) showed that $N_2(B)$ and $N_2(X,v>>0)$ were also closely linked. Hence, research conducted subsequent to the award of the Phase I effort continued to provide evidence of a link between IF(B) excitation and $N_2(X,v>>0)$ concentrations. These Penning-ionization studies were sensitive only to $N_2(X,v\leq 6)$. These levels do not have sufficient energy to excite IF(B) but their behavior does provide information about the concentration of highly excited levels within the context of a model for $N_2(X,v>>0)$. The goal of the current effort was to develop diagnostics for $N_2(X,v>>0)$ which would further enable understanding its role in exciting a visible chemical laser.

Current short wavelength visible chemical laser research efforts are directed at developing chemical methods for the generation of $N_2(A)$ and other forms of metastable N. Among the methods under investigation are the disproportionation of N_3 radicals produced from thermal decomposition of ionic azides (Ref. 7) and the reaction of $N(^2D)$ with $NF(a^1\Delta)$ (Ref. 8). The research is expected to produce fundamental rate constants and product yields for these reactions with the primary emphasis on the production of $N_2(A)$. A significant problem in generating and maintaining large amounts of $N_2(A)$ is its subsequent rapid depletion in energy pooling reactions (Refs. 9 and 10):

$$N_2(A) + N_2(A) \rightarrow N_2(C,B,A') + N_2^+(X,v) \qquad (1)$$

It is possible that if large amounts of $N_2(A)$ could be produced, it would rapidly relax to a mixture quite similar to active N_2 and would contain significant amounts of $N_2(X,v>>0)$. Even if $N_2(A)$ could not be used as a transfer agent because of rapid energy pooling, the $N_2(X,v>>0)$ produced may still prove effective in exciting a lasant molecule. It has been shown recently that this reaction is quite rapid and results in the excitation of several excited electronic states of N_2 (Refs. 6, 9 and 10). Methods which fail to produce $N_2(A)$ efficiently might still produce large amounts of vibrationally excited N_2. These points make clear the need to study the reactions of vibrationally excited N_2 and the need for an effective diagnostic tool for monitoring the concentrations of high vibrational states of N_2.

The $N_2(X,v>>0)$ may be stable against collisional deactivation on wall materials. Once produced, it should undergo collisional up-pumping in which two vibrationally excited N_2 molecules pool their energy to produce one molecule with a greater degree of excitation. This is illustrated in Figure 1 where the calculated time evolution of discharge-created $N_2(v)$ is shown following termination of the discharge (Ref. 11). It is in conjunction with models such as these that the previously mentioned Penning-ionization technique can be employed to predict the behavior of $N_2(X,v>>0)$.

Among the techniques presently available for detecting $N_2(X,v)$ are coherent anti-Stokes Raman spectroscopy (CARS) (Ref. 12), pulsed multichannel Raman spectroscopy (PMRS) (Ref. 13), laser-induced fluorescence (LIF) (Refs. 1 and 14), CO infrared emission tracers (Ref. 15), Franck-Condon excitation by He metastables to $N_2^+(B)$ followed by detection of

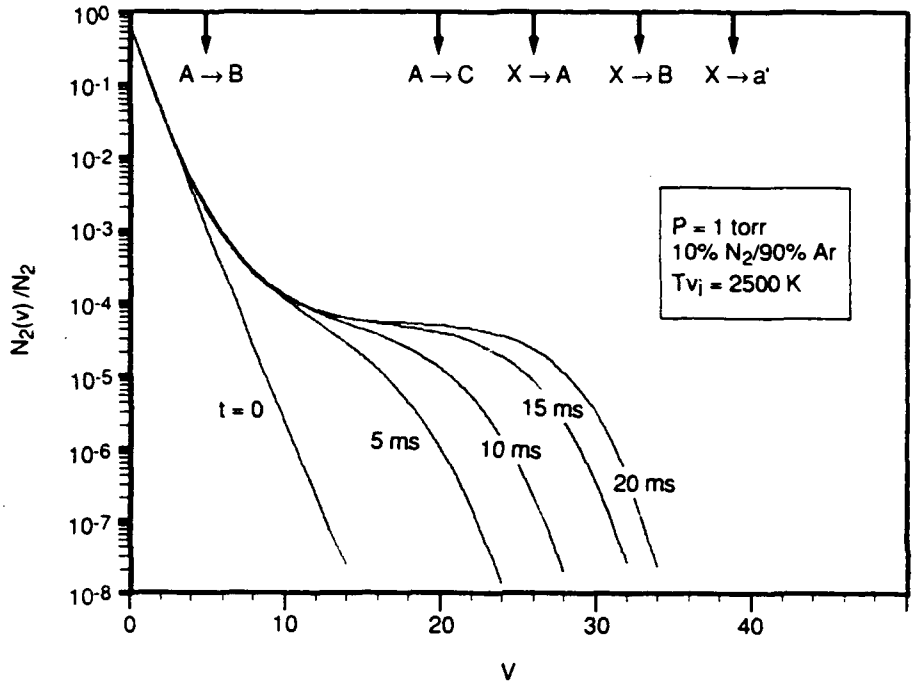

Figure 1. Calculated time evolution of discharge-created $N_2(X,v)$ illustrating the effects of collisional up-pumping. Time is referenced with respect to termination of the discharge.

emission (Refs. 2 and 16), and VUV absorption spectroscopy (Ref. 17). The Raman methods have been used to observe $N_2(X,v)$ to levels as high as 7 in both active N_2 and in N discharges, but suffer from problems of low sensitivity and calibration difficulties. Two-photon LIF on the $a^1\Pi_g$ - $X^1\Sigma_g$ transition has been employed to observe $v = 0$, but rapid quenching of the $a^1\Pi_g$ state by N_2 may result in poor sensitivity for this method (Ref. 18). The CO infrared tracer method is only sensitive for $N_2(v=1)$. Absorption spectroscopy using the $a^1\Pi_g$ - $X^1\Sigma_g$ transition requires long optical path lengths and is a line-of-sight method requiring often-complicated Abel-type inversion techniques to obtain point densities. Franck-Condon excitation by the metastable He atoms to the $N_2^+(B)$ state can be used to detect vibrational levels as high as $v'' = 7$, but requires the introduction of an ion-free stream of metastables into the gas. These metastables sometimes are efficiently quenched by other species in the flow and might modify the chemical system which is under observation. None of these methods have been used to detect local concentrations of the high vibrational levels ($v \geq 9$) capable of exciting IF(B) or other visible chemical laser candidates.

1.2 PHASE I RESEARCH ACCOMPLISHMENTS

In the Phase I program several potential laser-based diagnostics for measuring $N_2(X,v>>0)$ were pursued. These diagnostics were evaluated qualitatively with respect to detection sensitivity and range of levels which could be detected, potential interferences from other

species in the gas flow, and magnitude of background signals characteristic of the excited species in the flow. The purpose of this evaluation was to select the best technique(s) for development into a quantitative diagnostic in this, the Phase II effort.

Three techniques were evaluated in the Phase I research program. Two of these techniques involved the use of multiphoton excitation spectroscopy employing the $N_2(a^1\Pi_g)$ state. A third technique employed an optical-optical double resonance excitation scheme using the $A^3\Sigma_u^+$ and $B^3\Pi_g$ states. Each of these schemes is shown schematically in Figure 2 and is described in more detail below.

Detection of $N_2(X,v>>0)$ via multiphoton excitation of the $a^1\Pi_g$ state is achieved in two ways. The $a^1\Pi_g$ state can be excited in either one- or two-photon transitions from the ground state and weakly allowed fluorescence from the $a^1\Pi_g$ state (Lyman-Birge-Hopfield bands) can be observed in the vacuum ultraviolet region. The radiative lifetime of the excited state is fairly long, 56 μs (Ref. 19), and hence $N_2(a)$ quite susceptible to quenching even at moderate pressures. The quenching of this state by N_2 was briefly explored by van Veen and coworkers (Ref. 14) as well as Marinelli et al. (Ref. 18) and reinvestigated under the Phase I program. Because of predissociation of the a-state above $v' = 6$, fluorescence from higher levels is not observed, nonetheless the potential curves of the $a^1\Pi_g$ and $X^1\Sigma_g$ states are sufficiently shifted so that X-state levels as high as $v'' = 15$ have sufficient oscillator strength to nonpredissociated levels of $N_2(a)$ to make this technique attractive. Key

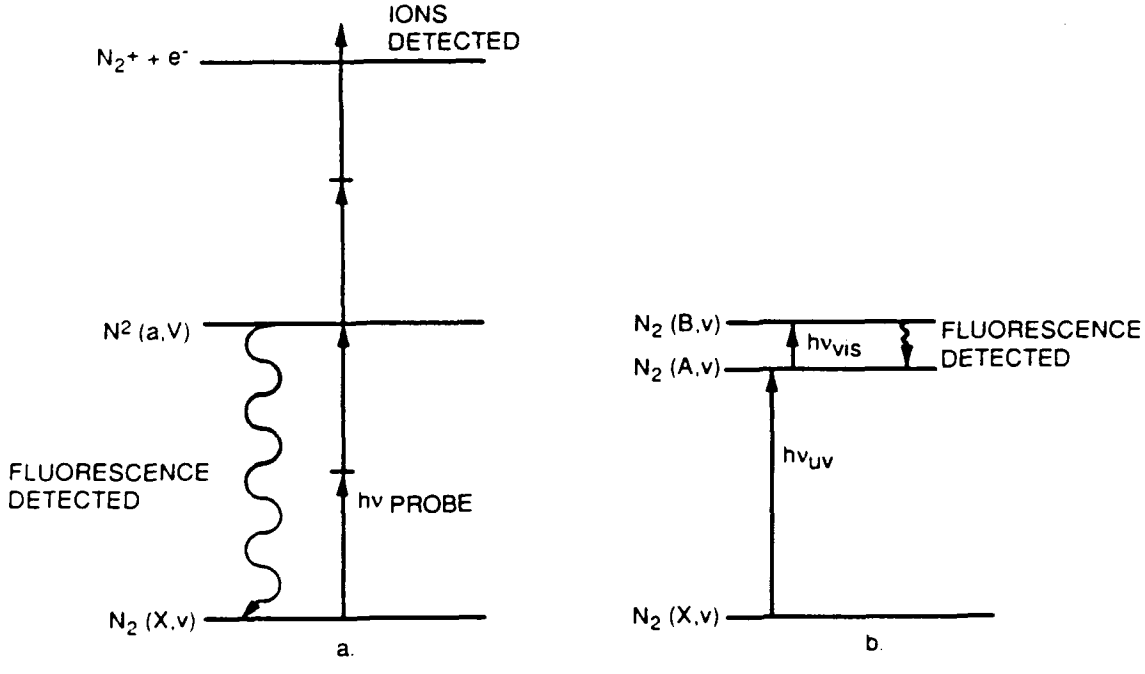

a) Schematic of energy levels used in MPI and LIF detection of $N_2(X,v)$

b) Energy levels used in two-step LIF detection of $N_2(X,v)$

Figure 2. Strategies for $N_2(X,v)$ detection.

issues in evaluating this method further are the extent to which quenching of the excited state reduces fluorescence efficiency, the magnitude of the one- and two-photon cross sections for excitation of $N_2(X,v>>0)$, and the amount of VUV emission present in the discharged gas mixture and its effect on detector performance.

Multiphoton excitation of the $a^1\Pi_g$ state from $N_2(X,v>>0)$ can also be followed by absorption of additional laser photons until the ionization limit of the molecule is reached. Ions and electrons produced by the absorption of the laser radiation are then detected as a measure of the ground-state vibrational population. This technique, known as MPI spectroscopy, has become an important tool for the detection of molecules in situations where the use of purely optical spectroscopy is not possible. This is most often due to a lack of allowed excitation transitions, long-lived, predissociated, or easily quenched excited states, or the presence of large luminous background emissions. The MPI technique has recently been reviewed (Ref. 20) and will be only briefly discussed here.

In MPI spectroscopy a high power, pulsed tunable laser is used to provide high photon fluxes so that a molecule absorbs a sufficient number of photons to ionize. The ions are detected by measuring the current flow in the gas using a set of biased electrodes or other suitable ion detection device. The MPI process usually is described as occurring in two steps: 1) the absorption of m photons to a real intermediate electronic state of the molecule, and 2) the absorption of n more photons, perhaps proceeding through several intermediate electronic states of the molecule, until ionization is achieved. In practice, the m photon step is almost always rate limiting. In scanning the frequency of the probe laser, one generally observes a spectrum characteristic of this transition. The entire process is commonly referred to as an m+n process.

The principal advantages in employing the MPI technique rather than the LIF technique with the $a^1\Pi_g$ state lie in three areas. First, large ion fluxes to electrodes in the gas may be effectively discriminated using ac coupling. Large photon fluxes to a PMT photocathode cannot be similarly ignored because of saturation or possible destruction of the photocathode material. Secondly, the technique is much less sensitive to the effective lifetime (fluorescence efficiency) of the excited state, as influenced by quenching or predissociation. The absorption of laser photons happens rapidly compared to both quenching times and the slow predissociation rate. The consequence of this rapid absorption of laser photons is that MPI is not restricted to the use of excitation transitions which terminate on levels which fluoresce. As a result, a wider range of transitions can be employed which sample higher vibrational levels in the $N_2(X)$ manifold. Finally, MPI electrode configurations are available which collect ions and electrons with essentially unit efficiency, as opposed to optical collection systems which generally collect only 1 percent of the fluorescence excited by the laser. Typical disadvantages for MPI lie in the low excitation cross sections and the potential to produce ions from other species in the gas stream having a lower ionization potential than the species of interest.

The third approach considered was to use a two-laser method in which a high power, tunable pulsed laser is used initially to excite $N_2(X,v)$ molecules to the $A^3\Sigma_u^+$ state. A lower-

power tunable pulsed visible laser was then used to excite these molecules from the A-state to the $B^3\Pi_g$ state and fluorescence was observed on the B-A (first positive) transition. While the A-X transition (Vegard-Kaplan) is forbidden, A-X emission is readily observed in the flow systems and the calculations indicate that a sizable number of $N_2(X,v)$ molecules can be excited to the A-state with commercially available laser systems. The $N_2(A)$ state is not easily quenched but its emission rate is very slow; therefore, subsequent excitation to the B-state could result in greater sensitivity. The $N_2(B)$ state is only weakly quenched by N_2 (Refs. 10 and 21), and its radiative lifetime varies from about 4 to 12 μs (Ref. 22). Therefore $N_2(B)$ emission should be easily detectable. This technique is most sensitive for moderately high vibrational levels of $N_2(X,v>>0)$ ($v'=5$-12) because of the shift in the potential curve of the $A^3\Sigma_u^+$ state to longer internuclear distances. The assignment of the features observed will be those of $N_2(X,v)$. The principal disadvantages in employing this technique are threefold. First, the method is equipment intensive in that it requires two tunable dye lasers. Secondly, the quenching of the $N_2(B^3\Pi_g)$ state is still poorly understood. Though the state appears to be quenched only moderately by N_2, the B-state lies at approximately the same energy as the $W^3\Delta_u$ state and collisional energy transfer between the states will strongly influence the B-state fluorescence efficiency (Refs. 23-26). Finally, emission from the N_2(B-A) first positive bands is quite strong in active N_2 and results in a significant background signal above which laser-induced signals must be observed. Selective filtering of these bands to isolate the region of interest may be required.

Because there was no UV laser appropriate for exciting $N_2(A^3\Sigma_u^+)$, only the second half of this technique was proved during the Phase I program. Generation of $N_2(A)$ was from a conventional discharge source and detection was via laser-induced fluorescence.

In summary, 2+2 MPI was successful for a number of low vibrational levels ($v = 0 - 3$), but was unsuccessful for the detection of highly vibrationally excited ground state N_2. The inability to detect the upper vibrational levels was caused by low absorption cross sections in the four-photon MPI process. These levels were detected using a 1+1 MPI process with observed MPI spectra originating from the $v = 15$ and 19 levels of $N_2(X)$. Two-photon LIF spectroscopy was plagued by low fluorescence efficiencies from the $N_2(a^1\Pi_g)$ state in N_2/Ar and by a large amount of background emission in the spectral region of interest. This background emission originated from $N_2(a^1\Pi_g)$ produced in the microwave discharge. The two-photon LIF via the $a^1\Pi_g$ state did not appear to be a sensitive technique for the detection of $N_2(v)$ originating from a microwave discharge of N_2/Ar mixtures.

The final technique which was evaluated was an optical-optical double resonance experiment. This technique requires two dye lasers to excite two distinct rovibronic states of N_2. The first dye laser excites the $N_2(A^3\Sigma_u^+,v,J)$ state with UV radiation, while the second dye laser further excites the N_2 molecule with visible radiation from the A-state to the $N_2(B^3\Pi_g,v,J)$ state. The subsequent B-A fluorescence would be detected by a filtered, red-sensitive photomultiplier tube. The N_2(B-A) fluorescence following single-photon excitation of $N_2(A)$ produced in a hollow cathode discharge was detected but attempts at the optical-optical double resonance experiment were prevented by an equipment failure. Thus the feasibility of this technique could not be evaluated fully.

2.0 DIAGNOSTIC DEVELOPMENT

Diagnostic development activities during this program took several parallel directions. Techniques were established using the Penning-ionization diagnostic developed previously that allowed determination of absolute number densities of $N_2(X,v)$ as well as estimation of $N_2(X,v)$ number density distributions from sources which could not be modeled analytically.

During the course of the Penning-ionization work this diagnostic was found to be essentially sensitive only to vibrational levels zero through six. Therefore, a second type of energy-transfer diagnostic which is a semiquantitative diagnostic of higher vibrational levels, primarily 5 through 15, was developed. This diagnostic is based upon the excitation of $N_2(X,v)$ to $N_2(B^3\Pi_g)$ in an energy transfer reaction with $N_2(A^3\Sigma_u^+)$.

Finally, considerable effort was expended in extending the laser-based diagnostics established previously. One- and two-photon LIF as well as 1+1 and 2+2 MPI were used. For either detection technique, the two-photon excitation works only for lower levels of $N_2(X,v)$, generally zero through four, while the one-photon laser excitation techniques were sensitive to much higher vibrational levels, generally those above nine. Table 1 summarizes the various vibrational levels detected with the laser-based techniques. They cover a wide range. The major problem with the laser-based diagnostics is that they are quite difficult to use quantitatively.

Table 1. Vibrational transitions from $N_2(X,v'')$ observed using laser-based techniques

Technique	Transition (v′, v″)	
2+2 MPI	0,0 1,0 6,0 7,0	1,1 2,1 0,3 0,4
1+1 MPI	2,9 5,13 6,14 7,15 12,23 12,24	13,24 13,25 14,25 15,26 16,27
Two-Photon LIF	0,0 1,0 2,0	
One-Photon LIF	2,9 4,13 5,14	

2.1 EXTENSION OF PENNING-IONIZATION DIAGNOSTIC

2.1.1 Introduction

Recently a diagnostic was developed for observing vibrationally-excited N molecules based upon Penning ionization of the $N_2(X,v)$ by metastable He atoms (Ref. 2). Extention of this work allows determination of absolute number densities of $N_2(X,v)$ and quantification of $N_2(X,v)$ in the effluents of discharges as well as $N_2(X,v)$ produced in several chemical reactions (Ref. 27). This report details the analysis of Penning-ionization data to extract absolute $N_2(X,v)$ number densities and describes the observations of discharge-based sources of $N_2(X,v)$.

The Penning-ionization diagnostic for vibrationally excited N in discharge afterglows follows along the lines of the pioneering work of Schmeltekopf et al. (Ref. 16) and Young and Horn (Refs. 15 and 28). Mixing metastable He atoms with a flow of molecular N results in strong emission of the N first-negative system, $N_2^+(B^2\Sigma_u^+ - X^2\Sigma_g^+)$. Since the Penning-ionization process follows a Franck-Condon excitation pathway, the vibrational distribution in the neutral, ground state will determine the distribution observed in the upper, ionic state. One problem with this approach is that care must be taken not to have any He^+ or He_2^+ in the flow of metastable He. Both of those species also excite $N_2^+(B)$ quite strongly in charge-transfer reactions, but with an $N_2^+(B)$ vibrational distribution that is decidely non-Franck-Condon (Ref. 29).

This diagnostic is most sensitive to vibrational excitation of the first few vibrational levels in the ground electronic state ($v''=0$-6). Recently a semiquantitative diagnostic for vibrational levels 5 to 15 based upon the excitation of $N_2(B^3\Pi_g)$ in the reaction between $N_2(A^3\Sigma_u^+)$ and $N_2(X,v)$ was reported (Ref. 30).

2.1.2 Experimental

Figure 3 is a schematic of the 4.6-cm inside-diameter (ID), quartz, discharge-flow reactor used in these studies. Various discharges at the upstream end of the flow reactor, through a flow of He and N, create vibrationally excited N. Small amounts of SF_6 flow through a loop injector placed at the entrance of the flow tube to attach electrons created in the Penning-ionization reactions. The metastable He atoms enter through one of four side arms off the reactor. Each is 10 cm distant from the preceding one. A 0.5 m monochromator, mounted on rails, views the region of the flow reactor 2 to 3 cm downstream from the He^* injector to observe the fluorescence created in the Penning-ionization reaction.

The characterization of discharge effluents involves determining $N_2(X,v)$ production as a function of discharge power, N mole fraction in the discharge, and flow time from the discharge to the observation region. Some of the measurements were repeated with a nickel (Ni) screen across the flow tube downstream from the discharge, but upstream from the observation region.

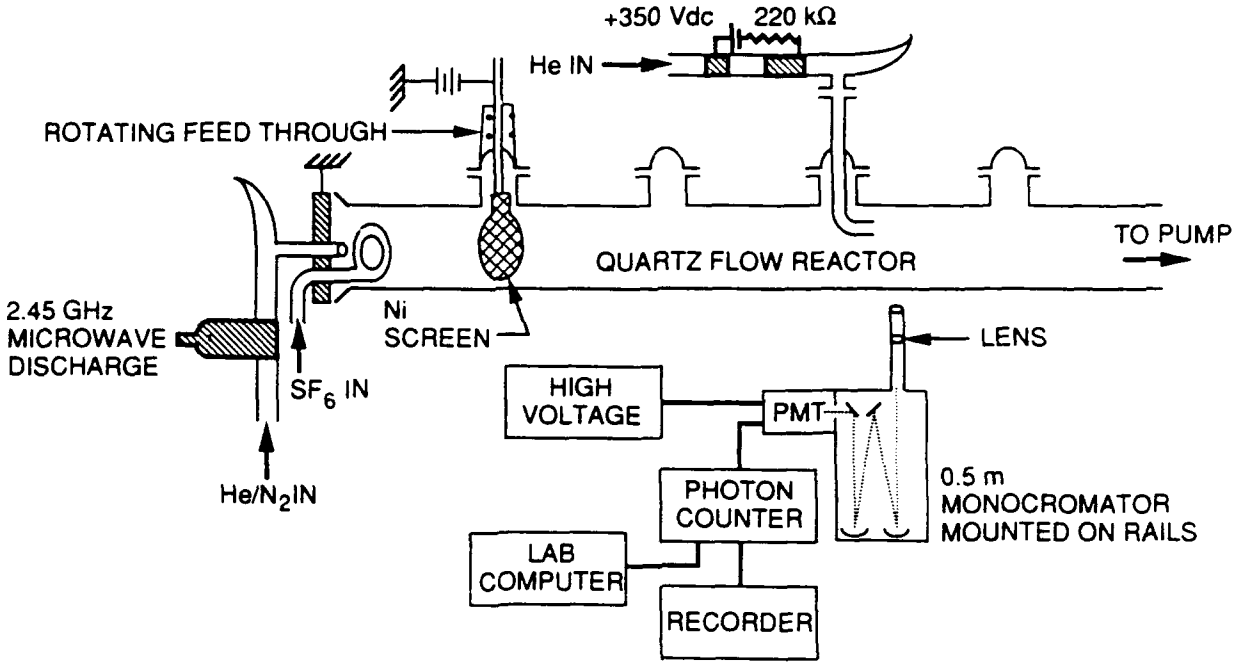

Figure 3. Flow reactor for Penning-ionization studies of $N_2(X,v")$

The Ni screen serves several purposes. First, it recombines most of the atoms created in the discharge, so that it is possible to test whether or not the presence of N atoms affects the metastable-He number density, and thereby the sensitivity of the diagnostic. Second, by grounding the Ni screen, and putting a slight positive bias on the aluminum end plate at the entrance to the flow reactor, it is possible to sweep any ions created in the discharge sources from the flow. This allows tests for the presence of ions in the flow - mostly molecular N ions - and their effect on observations. Third, it is possible to determine whether or not the Ni screen seriously reduces the $N_2(X,v)$ number density. If not, the presence of the Ni screen downstream from the discharge gives a clean source of $N_2(X,v)$, free from N atoms or molecular metastables. The latter two species recombine or are deactivated on the screen quite efficiently.

Four types of common laboratory discharges have been studied: microwave (2.54 GHz), radio frequency (13.56 MHz), dielectric barrier, and hollow-cathode dc. The microwave discharge operates at powers between 10 and 90 W and is coupled into the flowing gas via a McCarroll cavity (Ref. 31). The radio-frequency (rf) discharge is coupled to the flow via several turns of copper wire wrapped around the discharge tube. An LC tank circuit with an adjustable capacitance is adjusted to maximize coupling into the gas. Discharge powers between 20 and 150 W were investigated.

The dielectric-barrier discharge consists of a high voltage (0 to 12 kV), ac discharge between annular glass electrodes which are 30 cm long and have a 3 mm gap between them (Ref. 32).

The dc discharge consists of cylindrical tantalum electrodes separated by about 3 cm inside a 10 mm od glass tube. The discharge operates at about 350 Vdc and has its current limited to a few milliamps by a 2.2 kΩ resistor.

A hollow-cathode, dc discharge through a flow of purified He creates the metastable He atoms. Flowing the He through a molecular-sieve trap at liquid N temperature, upstream from the discharge, removes most of the impurities in the He, including N and O, with the exception of some residual Ne. The small amounts of Ne ($\leq$ 10 ppm) have no effect on observations. A number of years ago, it was shown that operating the hollow-cathode discharge at high voltage and high current tended to produce significant number densities of atomic and molecular He ions (Ref. 29). These ions are an anathema to the Penning-ionization measurements because they produce highly non-Franck-Condon distributions in the $N_2^+(B)$. Thus one could be led to false conclusions regarding the extent of ground-state vibrational excitation. The discharge was operated at 350 Vdc with a current, limited by a 200 kΩ resistor, below a milliamp. The absence of significant number densities of He ions was confirmed by failing to observe $N_2^+(B,v'>2)$ when the active-N discharge was off.

Typical conditions comprised flow rates of He through the $N_2(X,v)$-producing discharge and the metastable-producing dc discharge of 4200 and 1200 μmol s^{-1} respectively, N flow rates between 10 and 700 μmol s^{-1}, SF_6 flow rate of 5 μmol s^{-1}, total pressure of 1 to 3 torr, and transit time between the microwave discharge and observation region of 2 to 30 ms.

A spectral fitting procedure (Refs. 4, 22 and 23) analyzes the Penning-ionization spectra. Basis functions consisting of a synthetic electronic spectrum for a unit population in each vibrational level of each electronic state appearing in the spectral region of interest are generated. A linear least-squares routine then finds the populations of each vibronic band which, when multiplied by the appropriate basis function and summed with overlapping bands, gives a composite spectrum most nearly matching the experimental spectrum.

2.1.3 Theory Behind the Penning-Ionization Measurements

2.1.3.1 Relative Vibrational Distributions. The rate of Penning ionization between metastable He atoms and molecular N is proportional to the Franck-Condon factors which connect the $N_2^+(B)$ and $N_2(X)$ states. One can calculate the vibrational distribution in the final state, therefore, knowing only the vibrational distribution in the lower state and the Franck-Condon factors that couple the two states together. Thus,

$$N_{v'} \propto \sum_{v''} N_{v''} q_{v'v''} \qquad (2)$$

where v′ and v″ represent the vibrational levels of the upper and lower states, respectively, and $q_{v'v''}$ is the Franck-Condon factor coupling them. A set of Franck-Condon factors spanning the range of ground- electronic-state vibrational levels of 0 to 18, and $N_2^+(B)$-state vibrational levels of 0 to 9 has been reported previously (Ref. 2).

In theory, if the relative vibrational distribution in the upper state was measured, that in the ground state could be determined simply by inverting the Franck-Condon matrix, and multiplying this inverse matrix on both sides of Equation (2). This procedure did not work for PSI because the measurements of the upper-state populations have some uncertainty associated with them, and the uncertainties become greatly magnified by the matrix multiplication. The data were analyzed by adjusting $N_2(X,v)$ distributions in Equation (2) to predict $N_2^+(B)$ vibrational distributions which most nearly reproduced those observed experimentally. The $N_2(X,v)$ vibrational distributions used for the experimental comparison were chosen to follow a modified Treanor (Refs. 34-36) model or else were determined using an iterative empirical procedure (vide infra).

The modified Treanor distribution has been outlined by Caledonia and Center (Ref. 35) and Dilonardo and Capitelli (Ref. 36). For low vibrational levels the distribution is that given by Treanor et al. (Ref. 34):

$$\frac{N_{v''}}{N_{v''=0}} = \exp\left\{ - v'' \left[\frac{1.4388(\omega_e - 2\omega_e x_e)}{\Theta_1} - (v''-1)\frac{1.4388\omega_e x_e}{T} \right] \right\} \tag{3}$$

where Θ_1 is the Boltzmann vibrational temperature referenced to $v'' = 1$, T is the ambient gas temperature, and ω_e and $\omega_e x_e$ are spectroscopic constants in units of cm^{-1}. The Boltzmann vibrational temperature is given by

$$\Theta_1 = \frac{\omega_e - 2\omega_e x_e}{k \ln\left[\frac{N_{v''=1}}{N_{v''=0}}\right]} \tag{4}$$

This distribution goes through a minimum, called the Treanor minimum at v^*, which is given by

$$v^* = \frac{T(\omega_e - 2\omega_e x_e)}{2\,\omega_e x_e \Theta_1} + 0.5 \tag{5}$$

For vibrational levels above the Treanor minimum, the product vN_v is essentially constant (Ref. 35). Equating $(v^*-1)N_{v^*-1}$ with N_{v^*-1} calculated from Equation (3) gives

$$\frac{N_{v''}}{N_{v''=0}} = \frac{(v^*-1)\exp\left(-1.4388(v^{*2}-1)\omega_e x_e/T\right)}{v} \tag{6}$$

For this distribution, then, the Penning-ionization spectrum that is observed is compared to one calculated from Equation (2) using a ground-state distribution based upon Equations (3).

(4), and (6). Rather than use an explicit Θ_1 value, the distribution is based on an effective Θ_1 which best fits all the data points.

The iterative procedure determines ground-state vibrational distributions directly. The intensity of emission from an upper state vibrational level is

$$I_{v'} = k_{PI}[He^*]\sum_{v''} q_{v'v''}[N_2(X,v'')] \qquad (7)$$

where k_{PI} is the Penning-ionization rate coefficient and $q_{v'v''}$ are the Franck-Condon factors connecting the two states. Summing the Franck-Condon factors over v″ shows that even if all ground-state vibrational levels were populated equally, ≥ 75 percent of the intensity from level v′ is determined by the populations of vibrational levels v″ = v′ and below. Furthermore, ≥ 90 percent of the intensity is determined by vibrational levels v″ = v′ + 1 and below. Actually in most instances, more than 70 percent of the intensity is determined by only two ground state levels, v″ = v′ and v′ = 1.

This iterative procedure is based upon the assumption that in all cases $[N_2(v)] > [N_2(v+1)]$. This then allows finding the population of a given level, v″, to within better than 20 percent by knowing only the populations of the levels lower in energy than v″ and the intensity of emission from vibrational level v′ = v″. Beginning at the zeroth vibrational level, > 90 percent of the emission from v′ = 0 is determined by the population in v″ = 0. Thus the population in v″ = 0 can be found to within 10 percent by matching calculated and observed intensities. The population in v″ = 1 can then be determined reasonably well by adjusting it to give a match to the observed intensity from v′ = 1. The higher vibrational levels are treated in a similar manner. Several iterations of this process generally are required to find the best match between observed and calculated intensities. The major problem with this process is the tendency to overpredict the intensity from v′ = 1 given reasonable choices of v″ = 0, 1, and 2. Even so in most instances, the population determined for v″ = 1 seemed a bit low compared to the trend displayed by the other levels.

One additional piece of information helps to fix the population in v″ = 1. As discussed below, the procedure for determining absolute number densities for v″ = 0 involves noting changes in the intensities from v′ = 0 and v′ = 1 when the discharge is on and off. This procedure requires as input the ratio of the number densities of the various ground-state vibrational levels to that in v″ = 0. The ratio of the intensities from v′ = 1 with the discharge on to that with it off is particularly sensitive to the ratio of the number densities of v″ = 1 to v″ = 0. Thus the change in the intensities as well as the relative variation in intensities from the different vibrational levels was used to fix the population in v″ = 1.

2.1.3.2 Absolute $N_2(X,v)$ Number Densities. Fitting the Penning-ionization spectra to a ground-state vibrational model as just described gives only the relative distribution among ground-state vibrational levels. This relative distribution can be placed on an absolute basis, however, by first determining the absolute number density of $N_2(X,v''=0)$. This is done by

noting the changes in the intensity of $N_2^+(B,v'=0,1)$ when the discharge is struck relative to the intensities with the discharge off. Since both of these levels are excited by $N_2(X,v''=0)$, changes in their intensities reflect changes in the number density of $N_2(X,v''=0)$. The analysis rests upon three major assumptions:

1. The total $N_2(X)$ number density remains the same whether the discharge is on or not.

2. The rate coefficient for $N_2(X,v'')$ Penning-ionization is the same as that for the Penning-ionization of $N_2(X,v''=0)$.

3. The metastable He number density within the field of view of the monochromator remains unchanged when the discharge is struck.

The latter assumption actually follows from the other two. If no new quenching species are created by the discharge except for $N_2(X,v'')$, and if this newly created $N_2(X,v'')$ quenches the metastable He at the same rate as $N_2(X,v''=0)$, it follows that the metastable He number density will remain unchanged.

In practice, the discharge will dissociate some of the N so that some of the initial $N_2(X,v''=0)$ will be converted to atoms. In general, this dissociation fraction is not very large for N dissociation in a He buffer. Generally the dissociation amounts to <5 percent. In addition to producing ground-state atoms, the discharge also produces electronically excited metastable atoms, electronically excited metastable molecules, and some ions, principally molecular ions. In all cases, the number densities of these species will be on the order of 10^{-5} or less compared to ground-electronic-state, molecular N. The possible effect of these other species was tested by placing a Ni screen in the flow reactor to recombine the atoms, deactivate the metastables, and neutralize the ions produced by the discharge. The results with the screen were similar to those without.

Because the electronically excited N nitrogen ions formed in the Penning ionization have a radiative lifetime of about 60 ns (Ref. 37), they are in steady state within the field of view of the detector. Their formation and destruction rates can be equated:

$$k_{PI}\left[He^*\right]\sum_{v''} N_{v''} q_{v'v''} = k_{rad}\left[N_2^+(B,v')\right] = I_{v'} \tag{8}$$

where k_{rad} is the radiative decay rate of the observed level, k_{PI} is the Penning-ionization rate coefficient and $q_{v'v''}$ is the Franck-Condon factor coupling vibrational levels of the ground electronic state with those of the B-state of the ion.

The intensity from $v' = 0$ that is observed with the discharge off is

$$I_{v'=0} = 0.884\ k_{PI}\left[He^*\right]\left[N_2\right] \tag{9}$$

while that with the discharge on is

$$I_{v'=0} = 0.884 k_{PI}[He^*][N_2(X,v'=0)]$$

$$\times \left\{ 1 + 0.116 \frac{[N_2(X,v''=1)]}{[N_2(X,v''=0)]} + 0.014 \frac{[N_2(X,v'=2)]}{[N_2(X,v''=0)]} \right.$$

$$\left. + 0.0014 \frac{[N_2(X,v''=3)]}{[N_2(X,v''=0)]} \right\} \qquad (10)$$

Similar expressions hold for the intensity from $v' = 1$:

$$i_{v'=1} = 0.114\ k_{PI}[He^*][N_2] \qquad (11)$$

with the discharge off, and

$$I_{v'=0} = 0.116 k_{PI}[He^*][N_2(X,v'=0)]$$

$$\times \left\{ 1 + 6.06 \frac{[N_2(X,v''=1)]}{[N_2(X,v''=0)]} + 1.412 \frac{[N_2(X,v'=2)]}{[N_2(X,v''=0)]} \right.$$

$$\left. + 0.25 \frac{[N_2(X,v''=3)]}{[N_2(X,v''=0)]} + 0.035 \frac{[N_2(X,v''=4)]}{[N_2(X,v''=0)]} \right\} \qquad (12)$$

with it on.

Equations (9), (10), (11), and (12) can be combined and rearranged to give the number density of $N_2(X,v''=0)$ with the discharge on in terms of the total $N_2(X,v'')$ number density, the ratio of the intensities of the observed level with the discharge on and off, and the ratio of the number densities of the various ground-state vibrational levels to the number density in $v'' = 0$. This latter quantity is determined from the fits to the Penning-ionization data.

The resulting equations are

$$[N_2(v''=0)]^{on} = \frac{I^{on}_{v'=0}}{I^{off}_{v'=0}} \qquad (13)$$

$$\frac{[N_2(v''=0)]^{off}}{\left\{1 + 0.116\,\frac{[N_2(v''=1)]^{on}}{[N_2(v''=0)]^{on}} + 0.014\,\frac{[N_2(v''=2)]^{on}}{[N_2(v''=0)]^{on}} + 0.0014\,\frac{[N_2(v''=3)]^{on}}{[N_2(v''=0)]^{on}}\right\}}$$

and

$$[N_2(v''=0)]^{on} = \frac{I^{on}_{v'=0}}{I^{off}_{v'=0}} \qquad (14)$$

$$\frac{[N_2(v''=0)]}{\left\{1 + 6.06\,\frac{[N_2(v''=1)]^{on}}{[N_2(v''=0)]^{on}} + 1.41\,\frac{[N_2(v''=2)]^{on}}{[N_2(v''=0)]^{on}} + 0.25\,\frac{[N_2(v''=3)]^{on}}{[N_2(v''=0)]^{on}} + 0.035\,\frac{[N_2(v''=4)]^{on}}{[N_2(v''=0)]^{on}}\right\}}$$

where the superscripts "on" and "off" refer to whether the discharge is on or off.

2.1.3.3 Examples of Fitting Procedure. The two spectra shown in Figures 4 and 5 which show the $\Delta v = -2$ sequence of the $N_2^+(B^2\Sigma^+ - X^2\Sigma^+)$ system created in Penning ionization of vibrationally cold and vibrationally excited N, respectively illustrate the analysis procedure. Note that the ordinate in Figure 4, the vibrationally cold case, is roughly a factor of 2 greater than that in Figure 5. Upon striking the discharge, the intensity of the 0,2 band decreases by slightly more than a factor of 2. This is because the $v'' = 0$ level of the ground electronic state, which is the principle source of excitation of $N_2^+(B,v'=0)$, has dropped dramatically in its number density. Since the total $N_2(X)$ number density is conserved, the number densities of levels $v'' > 0$ must be increased accordingly. Comparison of Figures 4 and 5 shows that this must be so. The 1,3 band has almost doubled in intensity. Since this band is excited principally from $v'' = 1$, the number density of that state must have increased greatly upon striking the discharge.

Applying Equation (13) to the changes in intensity of the 0,2 band with the discharge on and off indicates that the number density of $N_2(X,v''=0)$ has dropped to 1.11×10^{15} molecules per cubic centimeter with the discharge on from 2.60×10^{15} molecules per cubic centimeter with the discharge off. Similar application of Equation (14) to changes in the 1,3 band gives

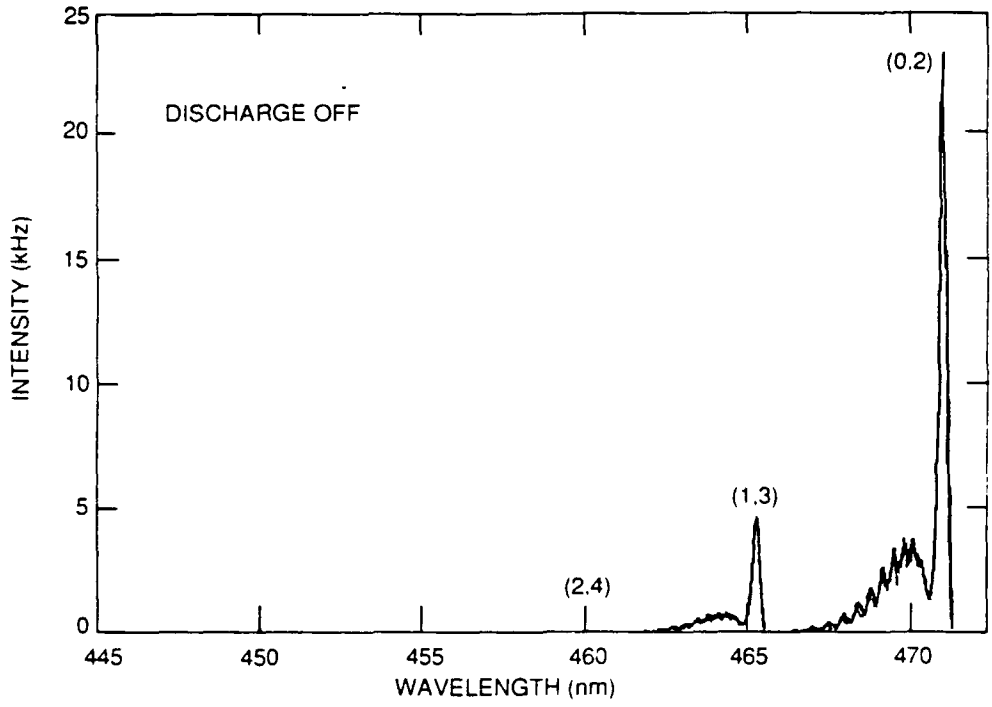

Figure 4. Penning-ionization spectrum of vibrationally cold N_2. The light line represents the data, the heavy line the least-squares fit to the data.

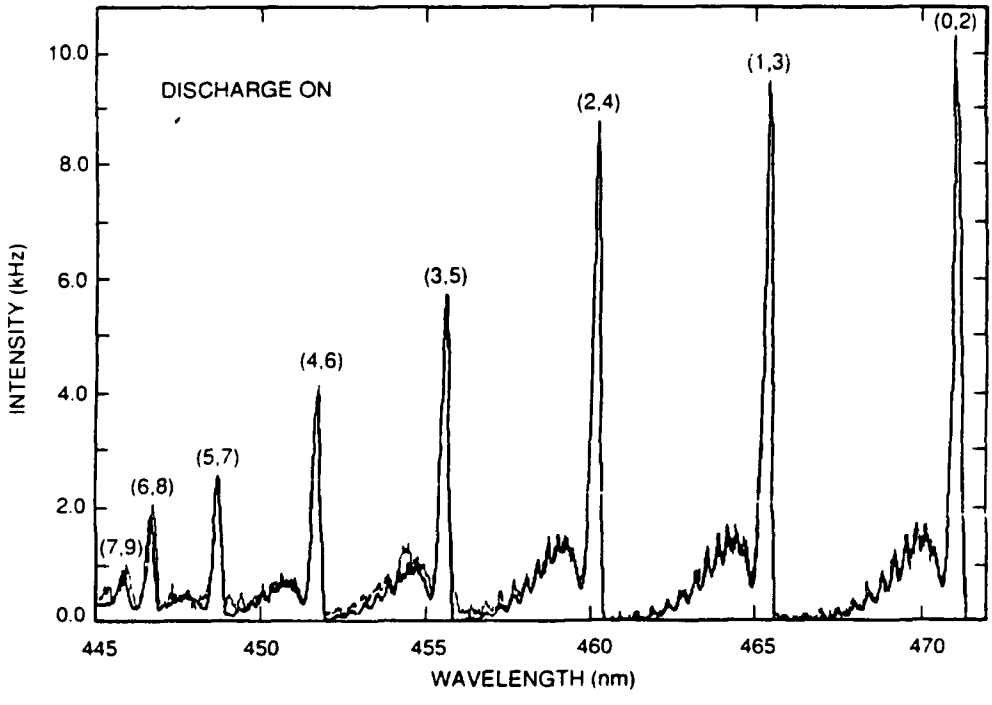

Figure 5. Penning-ionization spectrum of vibrationally excited $N_2(X)$. The light line shows the data, the heavy line the synthetic fit to the data.

$[N_2(X,v''=0)] = 1.19 \times 10^{15}$ molecules per cubic centimeter with the discharge on, in good agreement with the previous result. In this instance, therefore, striking the discharge places well over half of the ground-state N molecules in vibrationally excited states.

The $N_2^+(B)$ vibrational distribution in the spectrum shown in Figure 5 was determined using the spectral fitting procedure documented previously. The heavy line over the spectrum of Figure 5 shows the best fit synthetic spectrum. Figure 6 shows the $N_2^+(B,v)$ distribution. The curve through the experimental data shows the $N_2^+(B,v)$ distribution expected if the ground-state vibrational levels were characterized by a modified Treanor distribution. Also shown is a line denoting the $N_2^+(B)$ distribution which would obtain were the ground-state levels to follow a Boltzmann distribution with the same effective temperature as the modified Treanor. Clearly, the modified Treanor distribution more nearly represents the data.

The relative ground-state vibrational distribution determined from the modified Treanor fit shown in Figure 6 is placed upon an absolute basis by setting $[N_2(X,v''=0)] = 1.15 \times 10^{15}$ molecules per cubic centimeter as determined above. The result of this procedure is that upon summing up the absolute populations, the total population in $N_2(X,v'')$ is reached at $v'' = 7$. The total population, therefore, must fall off somewhat faster than would be predicted by a fully developed, nonequilibrium distribution as described by Equations (3) and (5). This is not particularly surprising since the Penning-ionization spectrum in Figure 5 was taken only 6 to 8 ms downstream from the discharge, and with a nitrogen partial pressure below 100 mtorr. At this low pressure, the v-v pumping process generally takes tens of

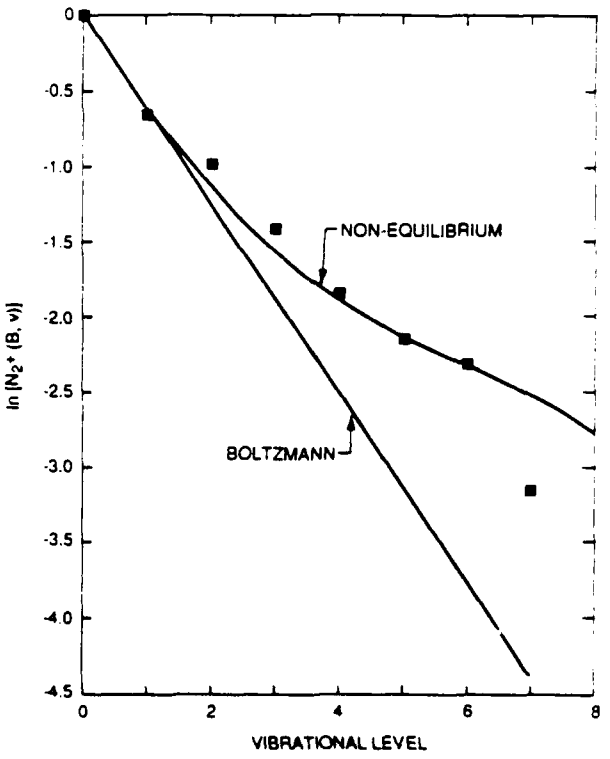

Figure 6. Observed and fit vibrational distribution of $N_2^+(B,v)$ produced in the Penning-ionization of $N_2(X,v)$ by $He(2^3S)$.

milliseconds to establish an equilibrium distribution. The fit to the data shown in Figure 6 is sensitive only to the vibrational distribution up through $v'' = 6$. There is no information, therefore, on the distribution in higher vibrational levels. Evidently, it falls off fairly steeply after about $v'' = 5$ or 6. This might be one reason that the $v' = 7$ level of $N_2^+(B)$ generally appears to be substantially underpopulated compared to the trend suggested by the rest of the data.

Typical data requiring the use of this iterative procedure are shown in Figures 7 through 10. Figure 7 is a portion of the Penning-ionization spectrum with the discharge off and with the discharge on at a power of only 6 W. Figure 8 shows the failure to fit the observed intensities with either a Boltzmann or a modified Treanor distribution. Figures 9 and 10 illustrate the match between the observed and calculated intensities and the relative number densities of the ground-state vibrational levels, respectively, determined from the iterative procedure. Interestingly, while the ratio of ground-state vibrational levels 0 to 1 would imply a vibrational temperature on the order of 1100 K, the higher vibrational levels are populated much more strongly than such a temperature would indicate. For the higher vibrational levels, a temperature on the order of 2500 K would seem more appropriate.

Under conditions where the modified Treanor distribution does give good fits to the observed intensities, the iterative technique gives concurring results. Figures 11 through 13 illustrate this. Figures 11 and 12 compare the fits to the observed intensities from the modified Treanor and iterative fits, respectively, while Figure 13 compares the ground-state populations derived from the iterative procedure to those predicted by a modified Treanor distribution.

2.2 THE EXCITATION OF $N_2(B^3\Pi_g, v'=1\text{-}12)$ IN THE REACTION BETWEEN $N_2(A^3\Sigma_u^+)$ AND $N_2(X, v \geq 5)$

The excitation of $N_2(B^3\Pi_g, v=1\text{-}12)$ in the interaction between $N_2(A^3\Sigma_u^+)$ and $N_2(X^1\Sigma_g^+, v \geq 5)$ has been studied. The $N_2(A)$ and $N_2(B)$ are observed spectroscopically between 220 to 400 nm and 560 to 900 nm, respectively, while the $N_2(X,v)$ number densities are determined by metastable-He Penning-ionization. The experiments are performed in a discharge-flow reactor with separate discharge sources of $N_2(A)$, $N_2(X,v)$ and $He^*(2^3S)$. The excitation rate coefficient is $(3 \pm 1.5) \times 10^{-11}$ cm^3 molecule^{-1} s^{-1}. Observations of $N_2(A)$ decay indicate that the $N_2(A)$ is removed by $N_2(X,v)$ with an apparent rate coefficient of about 3.5×10^{-12} cm^3 molecule^{-1} s^{-1}. The discrepancy between the excitation and removal rate coefficients probably results from $N_2(A)$ regeneration via cascade from the excited $N_2(B)$. The appearance of vibrationally excited $N_2(A)$ when $N_2(X,v)$ is added to a flow of $N_2(A, v=0)$ demonstrates this regeneration process. The reaction appears to be a transfer of electronic energy from the $N_2(A)$ to the $N_2(X,v)$ rather than an excitation of the $N_2(A)$ to $N_2(B)$ resulting from the input of energy from the $N_2(X,v)$.

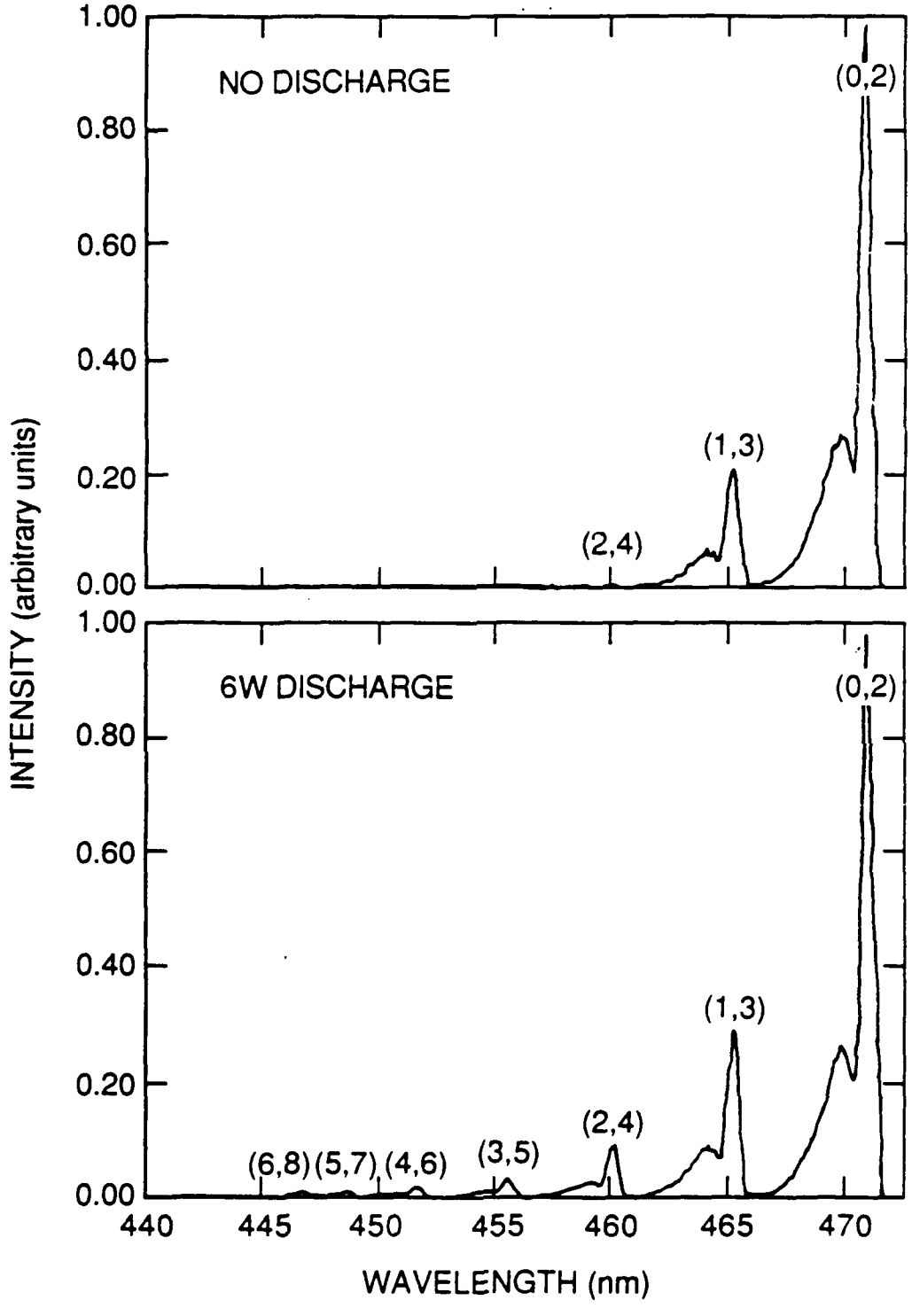

Figure 7. Penning-ionization spectrum of N in N_2/He mixtures. Upper spectrum - undischarged N_2; low spectrum = 6-W discharge. The light line represents the experimental data, the heavy line the synthetic best fit to the experimental spectrum.

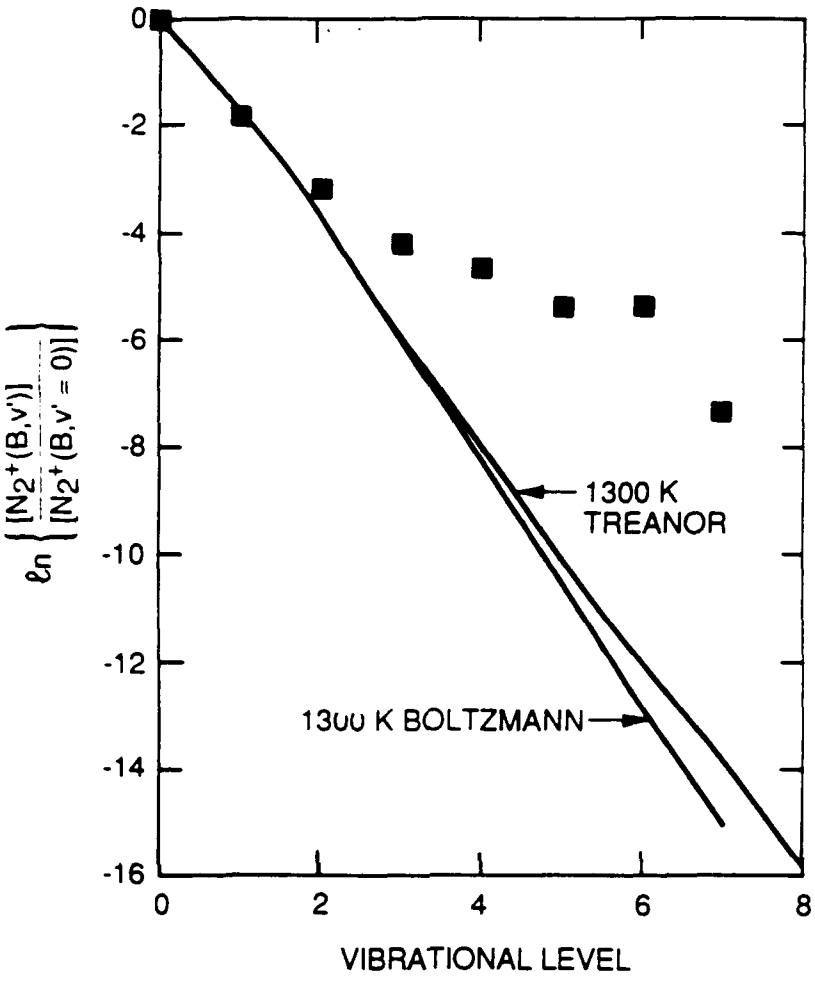

Figure 8. Distribution of $N_2^+(B)$ vibrational levels of $N_2(v)$ produced in Penning ionization of the effluents of a 6-W microwave discharge.

2.2.1 Introduction

A number of researchers have speculated on a possible energy-pooling reaction between $N_2(A^3\Sigma_u^+)$ and $N_2(X^1\Sigma_g^+,v)$ to generate $N_2(B^3\Pi_g)$ (Refs. 36-40). This speculation has been fueled to some extent by observations of long-lived $N_2(B)$ radiation in discharge afterglows. For the most part, however, the observations also could be explained by alternative mechanisms. There is no known direct experimental evidence for this reaction. A direct observation of the reaction is reported here, with estimates of its efficiency.

These observations cover the range of $N_2(B)$ vibrational levels 1 to 12. The energetics of the reaction are such that $N_2(X)$ vibrational levels between 5 and 14 are required to excite the observed B-state levels from $N_2(A,v=0)$. Observations of enhanced B-state emission upon adding $N_2(A)$ to an active N afterglow, therefore, provide a diagnostic of these moderately energetic ground-state vibrational levels. Metastable-He Penning-ionization as a diagnostic of $N_2(X,v)$ (Refs. 2 and 43), can provide quantitative estimates of number

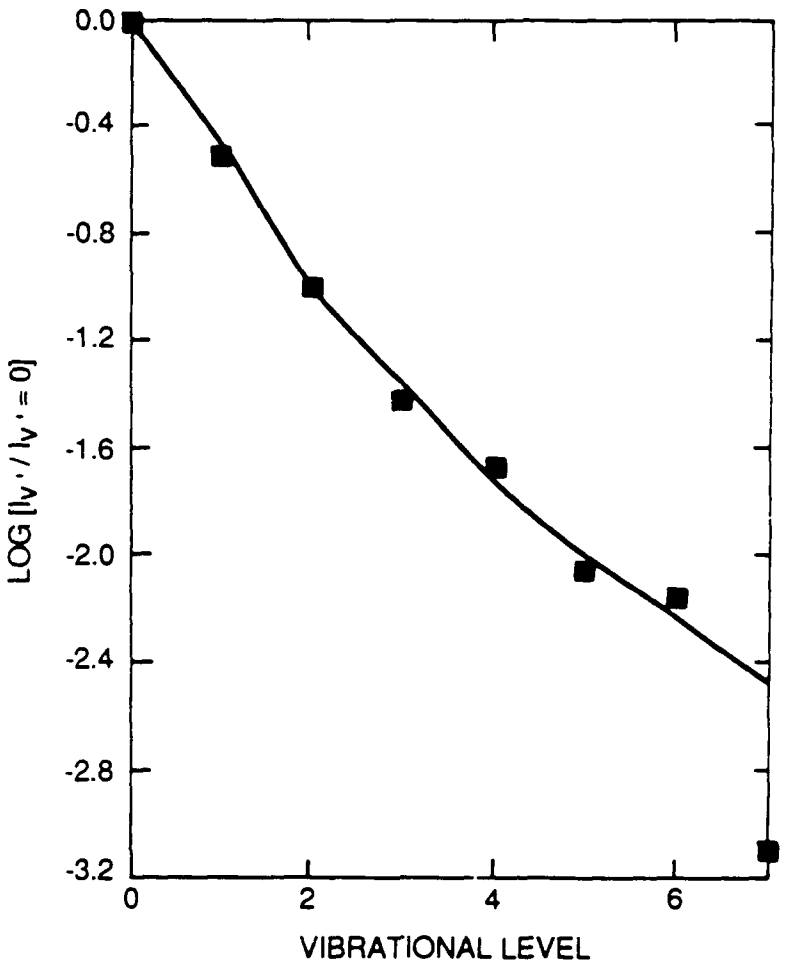

Figure 9. Observed (■) and calculated (-) of N_2^+(B-X) emission produced by Penning-ionization of N_2(v) from a 6-W microwave discharge. The calculated intensities result from the iterative procedure for determining the N_2(v) population distribution.

densities in vibrational levels 0 to 6 (Ref. 43). The current research is directed towards developing a diagnostic of higher vibrational levels.

2.2.2 Experimental

These studies employed the 4.6-cm diameter quartz discharge-flow reactor shown schematically in Figure 14. The N_2(A), generated by energy transfer between metastable-Ar atoms and molecular N (Refs. 44 and 45) enters the reactor at its upstream end and mixes further downstream with a flow of vibrationally excited, ground-electronic-state, N molecules. The N_2(X,v) is prepared in a side arm and introduced into the reactor through a hook-shaped injector. A 0.5 m monochromator equipped with photoelectric detection capability detects the luminescence generated in the reaction further downstream from the N_2(X,v) injector. The monochromator is mounted on rails so that observations can be made

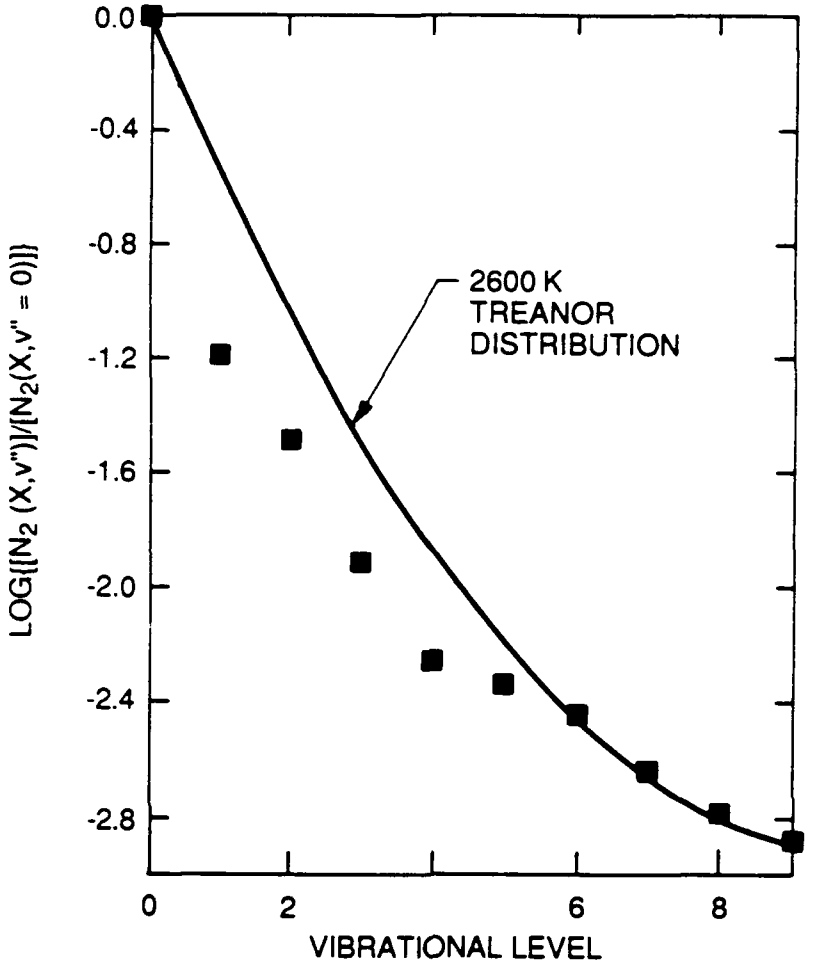

Figure 10. Vibrational distribution of ground state $N_2(v)$ from a 6-W microwave discharge as determined by the iterative technique.

at various distances from the injector, and thereby various interaction times. A second injector further downstream disgorges a flow of metastable He atoms which reveal the presence of $N_2(X,v)$ via a Penning-ionization reaction (Refs. 2, 15, 16, and 43).

A hollow-cathode, dc discharge through a flow of 3 to 10 percent Ar in He generates metastable Ar atoms. The Ar metastables mix immediately downstream from the discharge with a flow of N. The Ar metastables excite $N_2(C^3\Pi_u)$ which immediately radiates to the $N_2(B)$ state:

$$Ar^*(^3P_{2,0}) + N_2(X,^1\Sigma_g^+) \rightarrow N_2(C^3\pi_u) + Ar(^1S_0) \qquad (15)$$

Radiation and quenching of the B-state then results in $N_2(A)$-state production. The number densities of $N_2(A)$ generated in the predominantly He buffer are similar to those

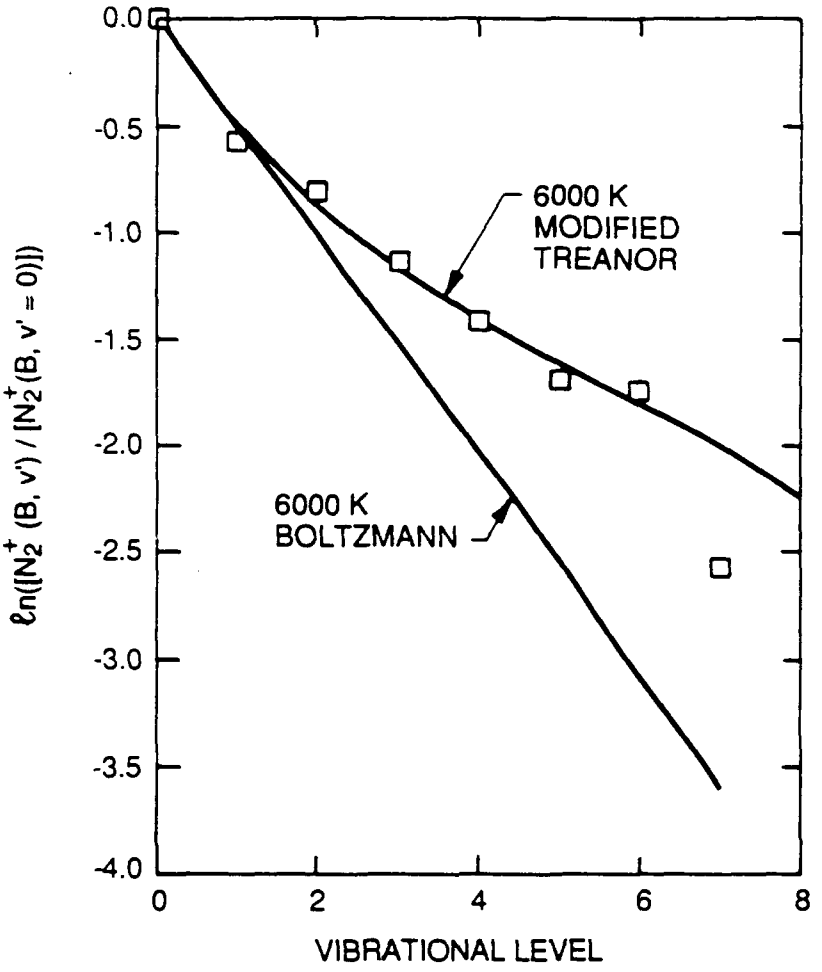

Figure 11. N_2^+(B) distribution produced from Penning-ionization of the effluents of a 90-W microwave discharge.

obtained in a pure Ar buffer. The N_2(A) vibrational distribution, however, tends to be slightly more relaxed because He is much more efficient than Ar at relaxing the vibrational energy in the A-state (Ref. 46).

A microwave discharge through a flow of N_2 in He, or just pure N_2 generates the N_2(X,v). Downstream from the discharge, the active N_2 flows through a Ni screen. The screen recombines most of the atoms and, in addition, deactivates electronically excited metastables produced in the discharge. It has little effect on the N_2(X,v), however (Refs. 43 and 47). Failure to observe Lewis-Rayleigh afterglow downstream from the Ni screen demonstrates the absence of N-atoms. The N_2(X,v) is introduced into the main flow after atom recombination and metastable deactivation have occurred.

A hollow-cathode, dc discharge in the upstream portion of the second injector generates metastable-He atoms. The Penning ionization of N_2 produces $N_2^+(B^2\Sigma_u^+)$ which is observed readily in emission on the N first-negative system, $N_2^+(B^2\Sigma_u^+ - X^2\Sigma_g^+)$. The

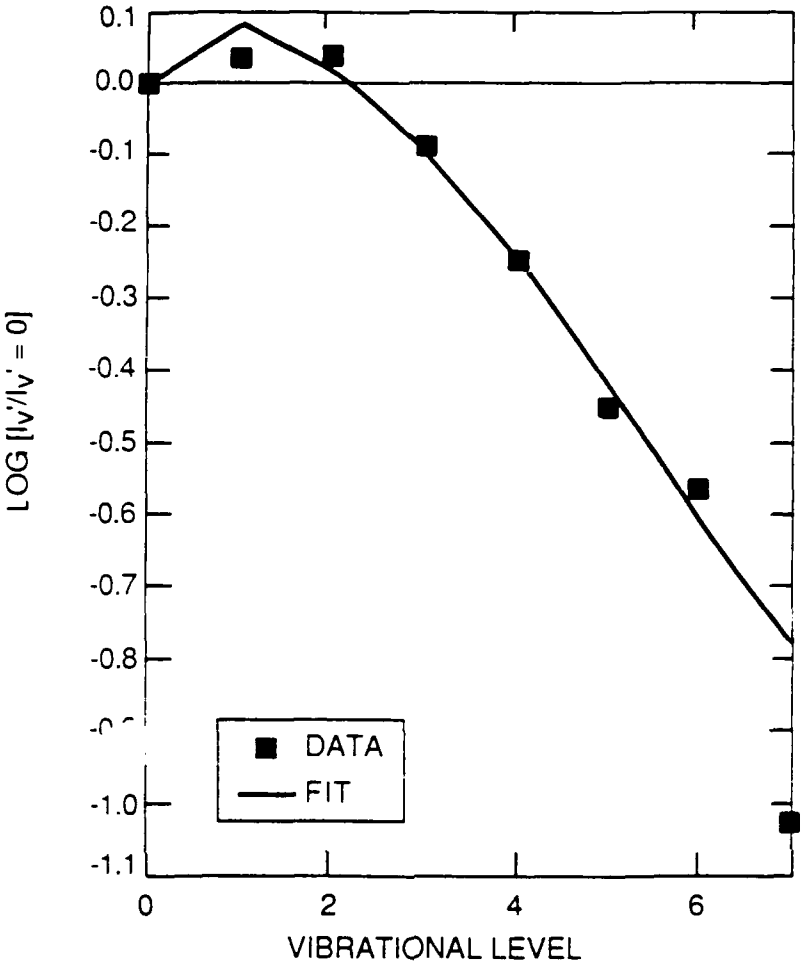

Figure 12. Relative intensities from N_2^+(B-X) emission produced from Penning-ionization of a 90-W microwave discharge. The solid line represents intensities calculated from N_2(v) populations determined by the iterative fitting procedure.

vibrational distribution of N_2^+(B) mirrors that of the N_2(X,v) from which it was generated. The procedures and analysis relating to monitoring N_2(X,v) using a Penning-ionization diagnostic have been described in some detail previously (Refs. 2 and 43). The previous work indicated that N_2(X,v) was deactivated only very slowly in collisions with the reactor walls.

The N_2(X,v) distributions as determined by Penning ionization downstream from the second hook injector, therefore, ought to be a reasonable reflection of the actual distributions within the observation zone just downstream from the first hook injector. This conjecture was tested experimentally in this series of experiments by comparing the N_2(B) distribution and intensity immediately downstream from the N_2(X,v) injector with that observed downstream from the metastable-He injector. The results at the two locations, after correcting for differences in N_2(A) number densities, were the same.

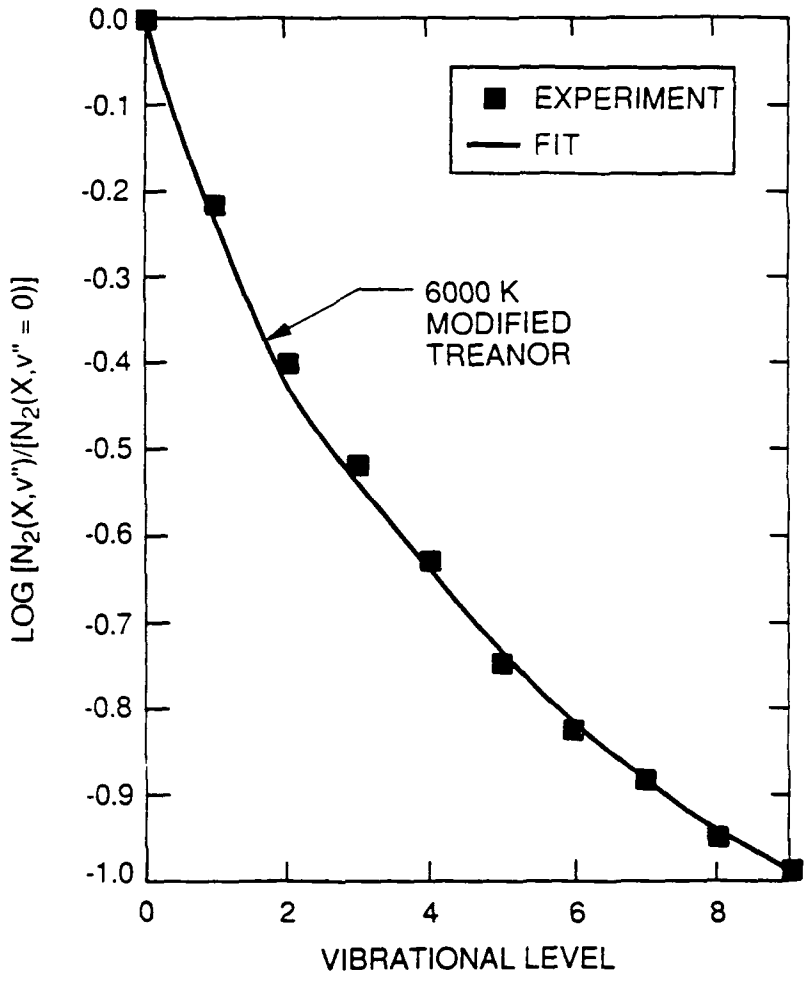

Figure 13. Relative populations of $N_2(X,v'')$ determined from iterative fitting of Penning ionization intensities of the effluents of a 90-W microwave discharge.

The relative spectral response of the detection system was calibrated by comparing observed intensity distributions as a function of wavelength with those emitted by standard quartz-halogen and deuterium lamps. Light from the lamps was reflected into the monochromator from a $BaSO_4$ screen (Ref. 48) so as to ensure that the optics were filled. The response was calibrated absolutely at 538 nm by comparison with air-afterglow intensities (Refs. 49-55). Detailed procedures for making air-afterglow calibrations were reported previously (Refs. 56 and 57).

With the detection system calibrated absolutely, absolute number densities of all emitting species could be determined by dividing absolute band intensities by the appropriate Einstein coefficients. The spectral fitting procedure described previously determined the band intensities. Shemansky's (Ref. 58) Einstein coefficients were used to reduce $N_2(A)$ observations while those of Piper et al. (Ref. 22) were used for $N_2(B)$.

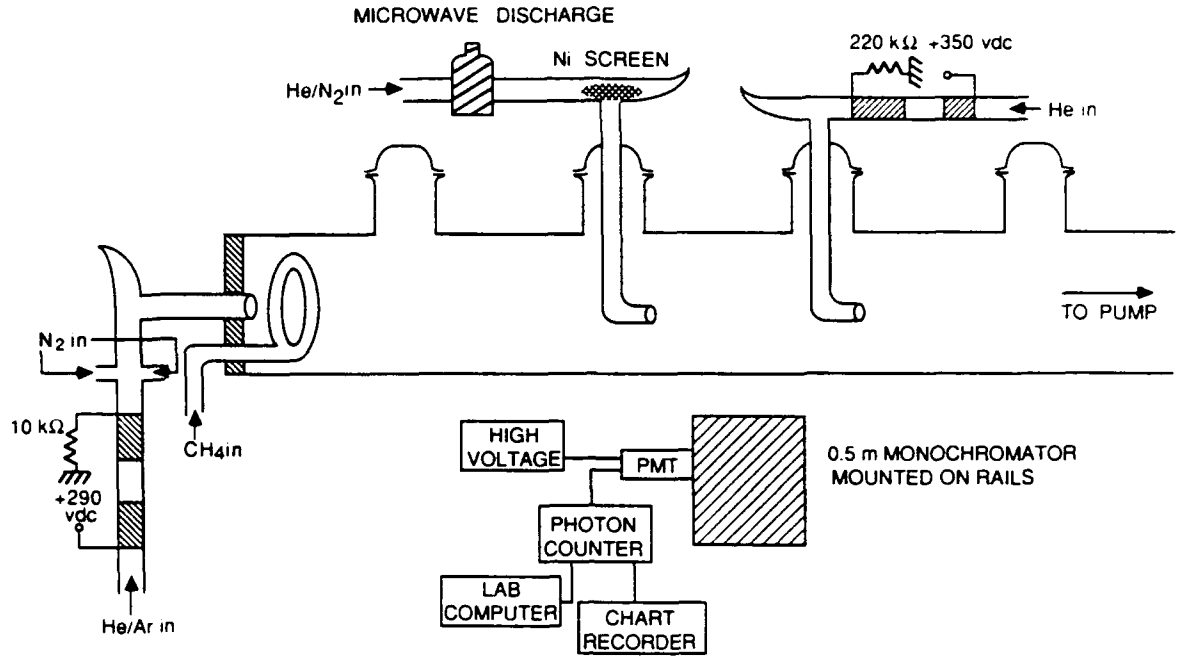

Figure 14. Schematic of discharge flow apparatus for studying $N_2(A)$ and $N_2(X,v)$.

Mass-flow meters or rotameters monitored the flow rates of all gases. The calibrations of all mass-flow meters and most rotameters were checked by monitoring the pressure rise with time in a calibrated volume. Some of the rotameters were calibrated by comparison with a calibrated mass-flow meter. This was done by establishing the dependence of flow-tube pressure on gas-flow rate using the calibrated mass-flow meter for flow-rate measurements. This correlation could then be used to derive flow rates of the uncalibrated flow meter from measurements of flow tube pressure for various flow-meter settings. A capacitance manometer monitored the flow-tube pressure.

Typical conditions included main flow of 2500 to 5000 μmol s^{-1}, flow of He and N_2 through the $N_2(X,v)$ injector of 275 and 140 μmol s^{-1} respectively, and flow of He through the He* injector of 1600 μmol s^{-1}. In some instances flows of methane were added to the flow of $N_2(A)$, at flow rates up to 90 μmol s^{-1}, in order to relax the vibrational energy in the $N_2(A)$ (Refs. 4 and 59). Flow tube pressures ranged between 0.9 and 3.3 torr.

2.2.3 Results

2.2.3.1 $N_2(B)$ Excitation. When the discharges producing $N_2(A)$ and $N_2(X,v)$ are both on, one sees an orange afterglow streaming from the $N_2(X,v)$ injector. When either discharge is extinguished the afterglow vanishes. Figure 15 shows the spectrum, with $N_2(X,v)$ in the reactor, between 560 and 900 nm in the presence and absence of $N_2(A)$. Quite strong N first-positive emission, $N_2(B^3\Pi_g$ -- $A^3\Sigma_u^+)$, results from the addition of $N_2(A)$ while

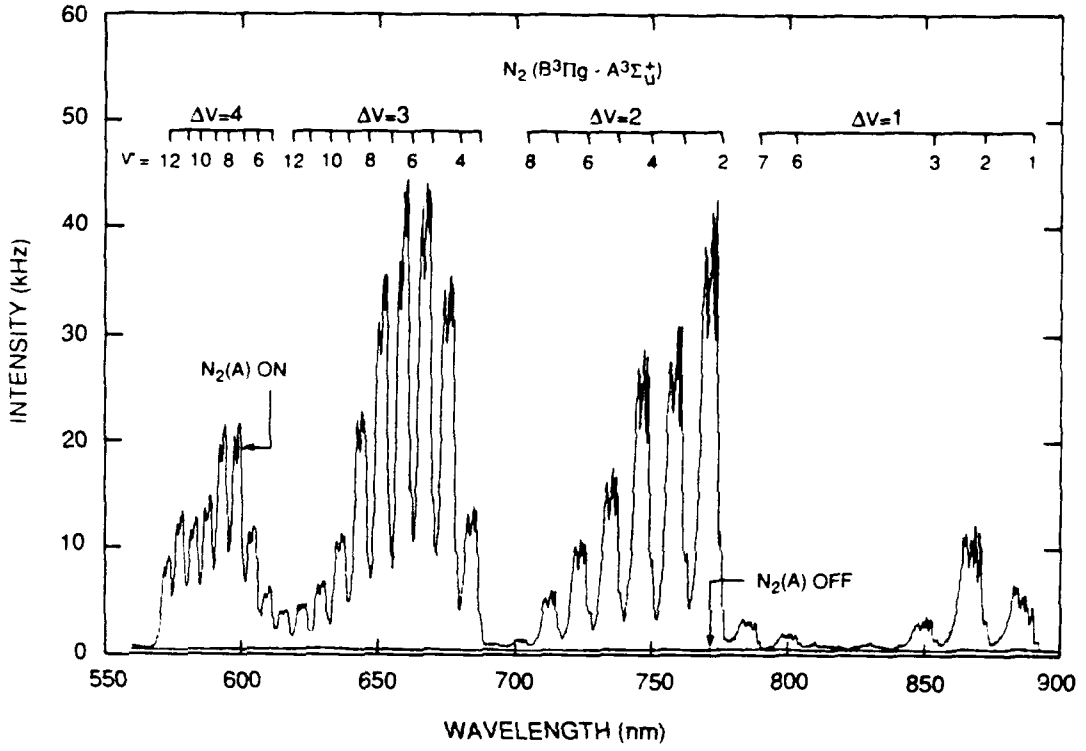

Figure 15. Spectrum of nitrogen first-positive bands, $N_2(B^3\Pi_g - A\Sigma_u^+)$, excited in the reaction between $N_2(A)$ and $N_2(X,v)$. The baseline shows the spectrum in the absence of $N_2(A)$. The spectrum has not been corrected for relative spectral response.

radiation is undetectable in the absence of $N_2(A)$. The $N_2(A)$ number densities were small and the spectrometer slit widths narrow so that $N_2(B)$ formed by $N_2(A)$ energy pooling (Ref. 10) could not be observed.

Figure 16 shows that the intensity of the 2,0 band of the first-positive system varies linearly with the intensity of the Vegard-Kaplan system, $N_2(A^3\Sigma_u^+ -- X^1\Sigma_g^+)$. Since the Vegard-Kaplan intensity is directly proportional to $N_2(A)$ number density, these results show that the $N_2(B)$ excitation is first-order in $N_2(A)$ number density.

The $N_2(X,v)$ number densities have been shown previously to vary (Ref. 43), although not linearly, with discharge power. The number densities increase fairly rapidly as the power is increased to ~50 W, but appear to level off around 70 W. Figure 17 shows how the observed $N_2(B)$ number densities vary with discharge power. In this set of experiments, the discharge power was varied under otherwise constant conditions of flow rates and $N_2(A)$ number density. The similarity between the variations in $N_2(B)$ with discharge power and the previous observations on $N_2(X,v)$ production with discharge power is strong evidence for $N_2(B)$ generation in the reaction between $N_2(A)$ and $N_2(X,v)$.

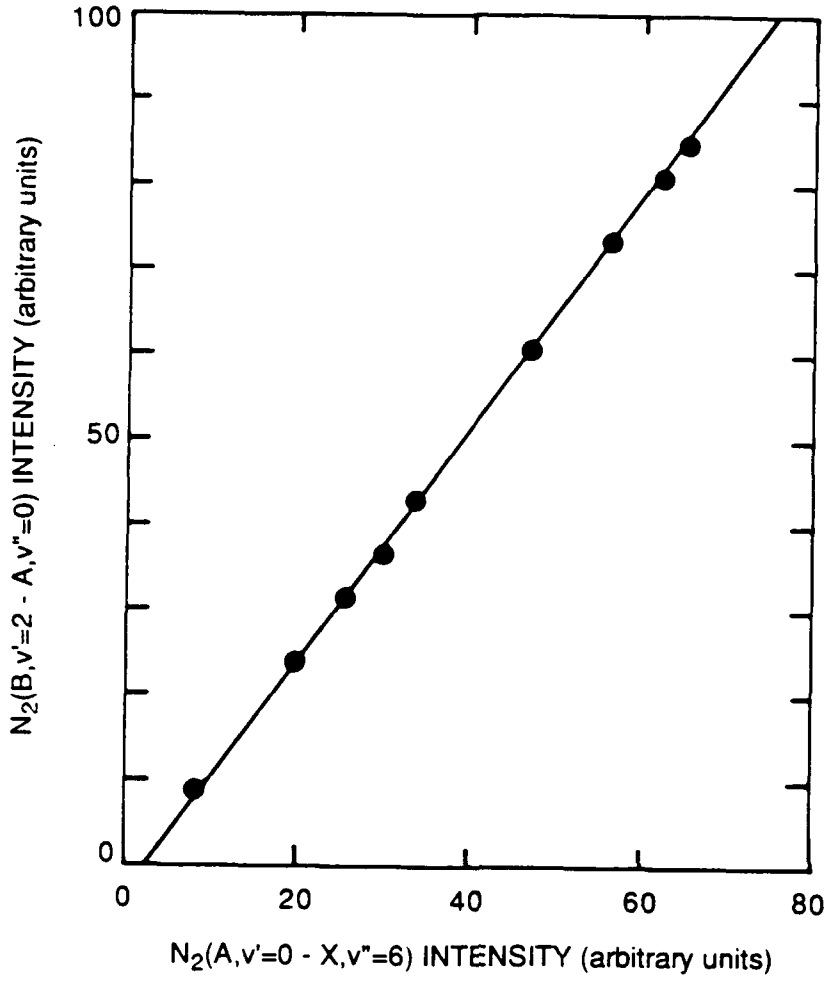

Figure 16. Variation in the intensity of the 2,0 band of the first-positive system as a function of the intensity of the 0,6 band of the nitrogen Vegard-Kaplan system $N_2(A^3\Sigma_g^+ - X^1\Sigma_g^-)$.

These observations can be rationalized by the following reactions which govern the formation and destruction of $N_2(B)$:

$$N_2\left(A^3\Sigma_u^+\right) + N_2\left(X^1\Sigma_g^+, v\right) \rightarrow N_2\left(B^3\Pi_g, v'\right) + N_2\left(X^1\Sigma_g^+, v''\right) \qquad (16)$$

$$N_2\left(B^3\Pi_g\right) \rightarrow N_2\left(A^3\Sigma_u^+\right) + h\nu \qquad (17)$$

$$N_2\left(B^3\Pi_g\right) + N_2 \rightarrow 2N_2 \qquad (18)$$

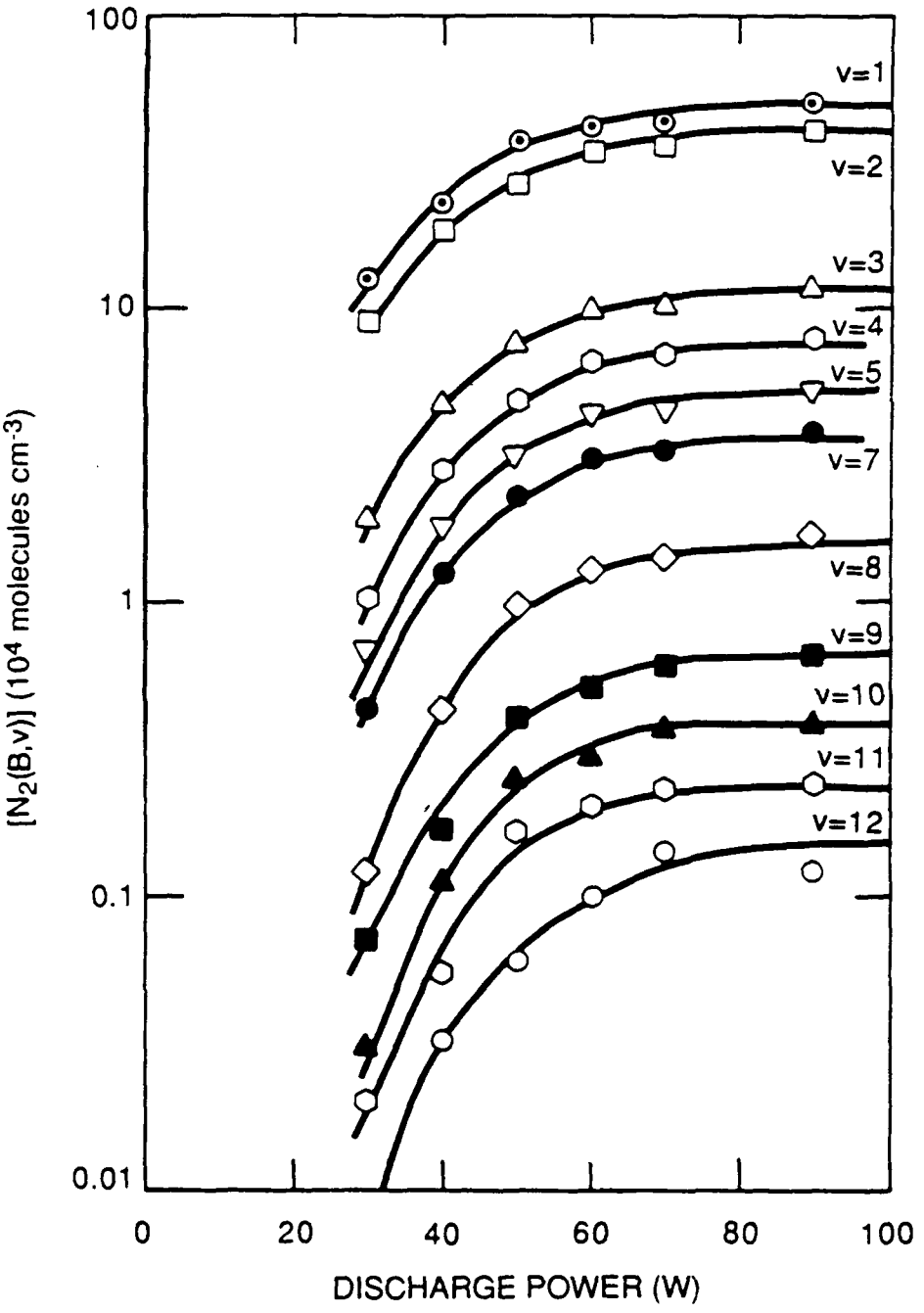

Figure 17. Variation in the number density of different vibrational levels of $N_2(B)$ as a function of power of the microwave discharge under conditions of constant $N_2(A)$ number density. $N_2(X,v)$ number densities scale with discharge power in a manner similar to the $N_2(B,x)$ in tihs figure.

$$N_2\left(B^3\Pi_g\right)+Q \rightarrow N_2(X)+Q \qquad (19)$$

Both the radiative decay rate (Refs. 22 and 60) of $N_2(B)$ and the rate coefficient for quenching $N_2(B)$ by N are vibrational-level dependent (Refs. 10, 26, 61 and 62). To analyze the data average values are used for these quantities: $k_{17} \sim 2 \times 10^5$ s^{-1} and $k_{18} \sim 2.5 \times 10^{-11}$ cm^3 $molecule^{-1}$ s^{-1}.

The quenching of $N_2(B)$ by molecular N is a complex process with the likely production of a number of states including $N_2(W^3\Delta_u)$, $N_2(B'^3\Sigma_u^-)$, $N_2(A^3\Sigma_u^+)$, and $N_2(X^1\Sigma_g^+,v)$. Reaction (19), therefore, encompasses all possibilities. It accounts for removal of molecules from the B-state. Ultimately most of the B-state quenching by N_2 probably results in cascade down through the triplet manifold to the A-state.

Reaction (19) accounts for possible quenching of the $N_2(B)$ fluorescence by methane, Ar, and He. The Ar partial pressure generally was well below 75 mtorr, whereas the half-quenching pressure for Ar is greater than 1 torr (Refs. 63 and 64). Thus quenching by Ar should be less than a 10 percent effect. Observations on the excitation of $N_2(B)$ in the reaction between $N(^2D)$ and $NF(a^1\Delta)$[8] indicated a half-quenching pressure for helium of about 5 torr. Thus quenching by He at pressures near 1 torr is a minor, but not insignificant, loss process for $N_2(B)$. The partial pressure of methane remained below 25 mtorr. So long as the rate coefficient for quenching $N_2(B)$ by methane is no greater than 3×10^{-11} cm^3 $molecule^{-1}$ s^{-1}, i.e., is less than one-tenth gas kinetic, methane quenching will be unimportant for these studies. Bayes and Kistiakowsky (Ref. 65) indicate that methane does quench $N_2(B)$ emission, but they failed to provide any estimate of its quenching efficiency. PSI is unaware of any other observations of $N_2(B)$ quenching by methane. Any strong dependence of the $N_2(B)$ fluorescence yield did not appear to depend upon methane number density, so the conclusion was that methane quenching is indeed of little importance in these studies.

The differential equation describing the rates of formation and destruction of $N_2(B)$ as governed by the processes in Equations (16) through (19) is

$$\frac{d[N_2(B)]}{dt} = k_1[N_2(A)][N_2(X,v)] - \{k_2 = k_3[N_2] + k_4[Q]\}[N_2(b)] \qquad (20)$$

Because the radiative lifetime of $N_2(B)$ (~ 5 μs) (Ref. 60) is much shorter than the transit time through the detector's field of view, the $N_2(B)$ is in local steady state at every point in the reactor. The variation in $[N_2(B)]$ with time vanishes, therefore, and Equation (20) can be rearranged to give

$$[N_2(B)] = \frac{k_1[N_2(A)][N_2(X,v)]}{k_2 + k_3[N_2] + k_4[Q]} \qquad (21)$$

This equation demonstrates the first-order dependence between $N_2(B)$ excitation and the number densities of $N_2(A)$ and $N_2(X,v)$.

In order to observe how the $N_2(B)$ excitation varied with $N_2(A)$ vibrational level, varying amounts of methane were mixed with the total $N_2(A)$ at the head of the flow reactor. The added methane appeared to affect the total $N_2(A)$ number density only minimally, but reduced the $N_2(B)$ intensity by more than a factor of 2.5 as the methane number density was increased to 7.5×10^{14} molecules per cubic centimeter. Penning-ionization measurements showed a concomitant drop in the number density of $N_2(X,v)$. The reduced $N_2(B)$-state population appears, therefore, to result from $N_2(X,v)$ quenching rather than from quenching of $N_2(B)$ fluorescence by methane.

The relative $N_2(B)$ vibrational distribution, however, showed little variation with methane number density. This observation indicates that vibrational energy in the $N_2(A)$ does not have a major impact on the $N_2(B)$ vibrational distribution. A hotter vibrational distribution in the $N_2(X,v)$, on the other hand, does produce a hotter $N_2(B)$ vibrational distribution. Figure 18 illustrates this difference. The data points denoted by circles were taken under conditions where the $N_2(X,v)$ vibrational distribution could be characterized roughly by a vibrational temperature of 1800 K, and where only about 12 percent of the nitrogen was vibrationally excited. The points denoted as squares, however, were taken under conditions of a roughly 3700 K vibrational temperature of the $N_2(X,v)$ and with about 50 percent of the nitrogen vibrationally excited. Clearly the hotter ground-state distribution results in a hotter $N_2(B)$ distribution. The lines through the data points show for comparison Boltzmann distributions of the B-state resulting from vibrational temperatures of 3700 and 5000 K.

A slight rearrangement of Equation (21) gives the result

$$\frac{[N_2(B)]}{[N_2(A)]} \left\{ 1 + \frac{k_{18}}{k_{17}}[N_2] + \frac{k_{19}}{k_{17}}[Q] \right\} = \frac{k_{16}}{k_{17}} [N_2(X,v)] \qquad (22)$$

Figure 19 shows the ratio of the $N_2(B)$ to $N_2(A)$ number densities, after correcting for quenching, plotted against the number density estimated to be in vibrational levels 5 to 10 of the ground-electronic state. These vibrational levels are responsible for the bulk of the observed excitation. The number-density estimates were obtained from the Penning-ionization data with some extrapolation outside the region of greatest validity of the Penning-ionization diagnostic. While the data are somewhat scattered, they do indicate a clear trend with increasing $N_2(X,v)$ number density. The slope of the line through the data gives the result $k_{16}/k_{17} = (1.4 \pm 0.2) \times 10^{-16}$ cm^3 molecule^{-1}. Given $k_{17} \sim 2 \times 10^5$ s^{-1} the rate coefficient for exciting $N_2(B)$ found in the interaction between $N_2(A)$ and $N_2(X,v)$ is

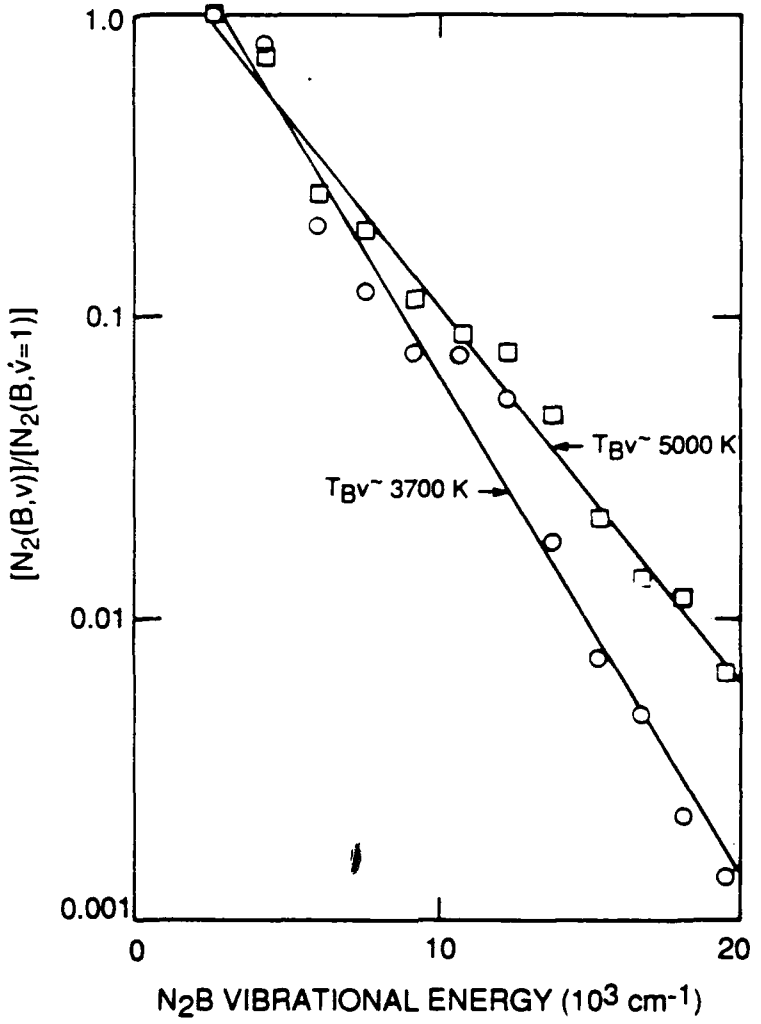

Figure 18. Relative vibrational distributions for $N_2(B,v)$ for two different levels of $N_2(X,v)$ vibrational excitation. [○]: T_x ~ 1800 K, $[N_2(X,v)]/[N_2(X)]$ ~ 0.12; [□]: T_x ~ 3700 K, $[N_2(X,v)]/[N_2(x)]$ ~ 0.50

2.8×10^{-11} cm^3 $molecule^{-1}$ s^{-1}. Given the uncertainties in the experimental data used to derive this value, a realistic value for k_{16} is $(3.0 \pm 1.5) \times 10^{-11}$ cm^3 $molecule^{-1}$ s^{-1}.*

If it is assumed that all $N_2(X)$ vibrational levels excite each energetically accessible $N_2(B)$ vibrational level with the same rate coefficient, a distribution can be estimated for the $N_2(X,v)$ by difference. That is, $N_2(B,v'=1)$ can be excited by $N_2(X,v \geq 5)$, but excitation of $N_2(B,v'=2)$ is possible only from $N_2(X,v \geq 6)$, and so on up to $N_2(B,v'=12)$ which requires $N_2(X,v \geq 13)$. The $N_2(X,v)$ distribution obtained under these assumptions lies midway between modified Treanor and Boltzmann distributions with a common characteristic

* After this work was completed, CH_4 quenching was found to be nonnegligible. The corrected value for k_{16} is $(3.5 \pm 1.5) \times 10^{-11}$ cm^3 $molecule^{-1}$ s^{-1}. See L.G. Piper, "Energy Transfer Studies on $N_2(X^1\Sigma_g^+, v)$ and $N_2B^3\pi_g$)," PSI-1045/SR-467, Physical Sciences Inc. Andover, MA, 1990.

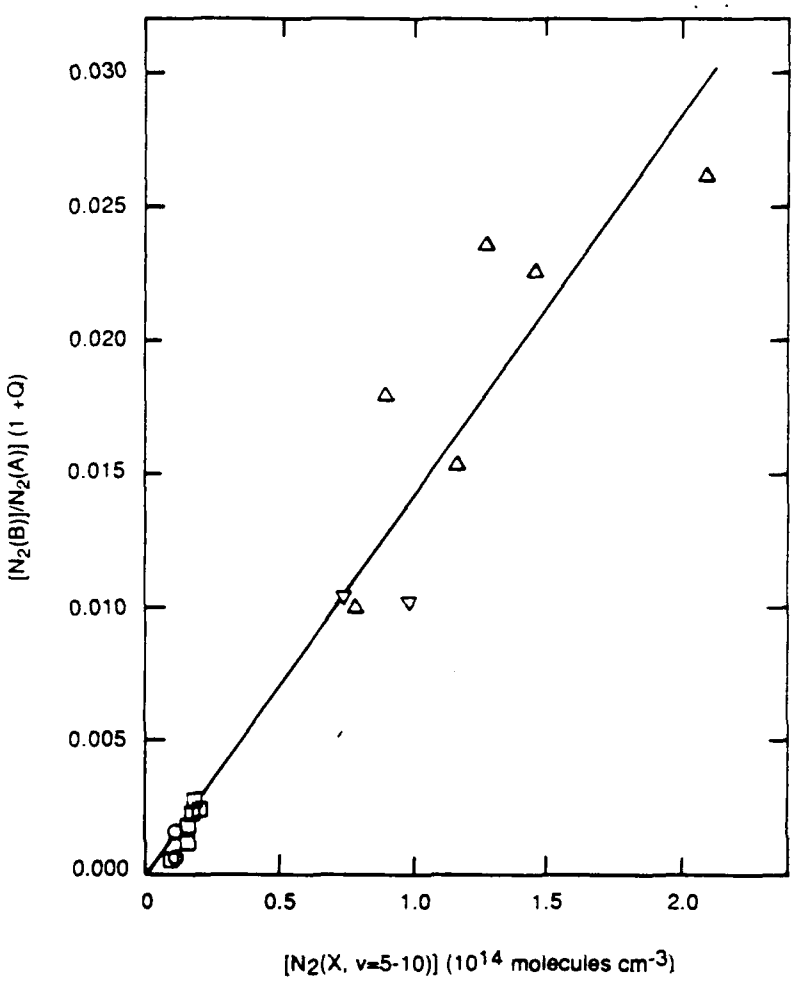

Figure 19. Variation in the ratio of the number density of $N_2(B)$, after correcting for quenching, so that for $N_2(A)$ with the number density of $N_2(X,v = 5 - 10)$.

temperature. The modified Treanor distribution changes from a Treanor distribution for vibrational levels less than the Treanor minimum to one which varies as 1/v above the Treanor minimum. The estimates of $N_2(X,v)$ number densities assume a modified Treanor distribution which the Penning-ionization measurements indicate is appropriate for vibrational levels 0 to 6. At some point the distribution should decrease more rapidly than 1/v. Perhaps this increased drop off is reflected in $N_2(X,v)$ distribution estimated above to lie below a modified Treanor distribution. Equally likely, however, would be values of k_{16} which varied with vibrational level. Without a more accurately determined $N_2(X,v)$ distribution, such variations cannot be determined.

2.2.3.2 Quenching of $N_2(A)$. Figure 20 shows how $N_2(A,v=0)$ varies as a function of time in the flow reactor in the absence and presence of $N_2(X,v)$. Clearly the $N_2(X,v)$ enhances the destruction of $N_2(A)$ dramatically. In the absence of $N_2(X,v)$, $N_2(A)$ decays principally by deactivation at the walls. When $N_2(X,v)$ enters the reactor, the $N_2(A)$ decay increases

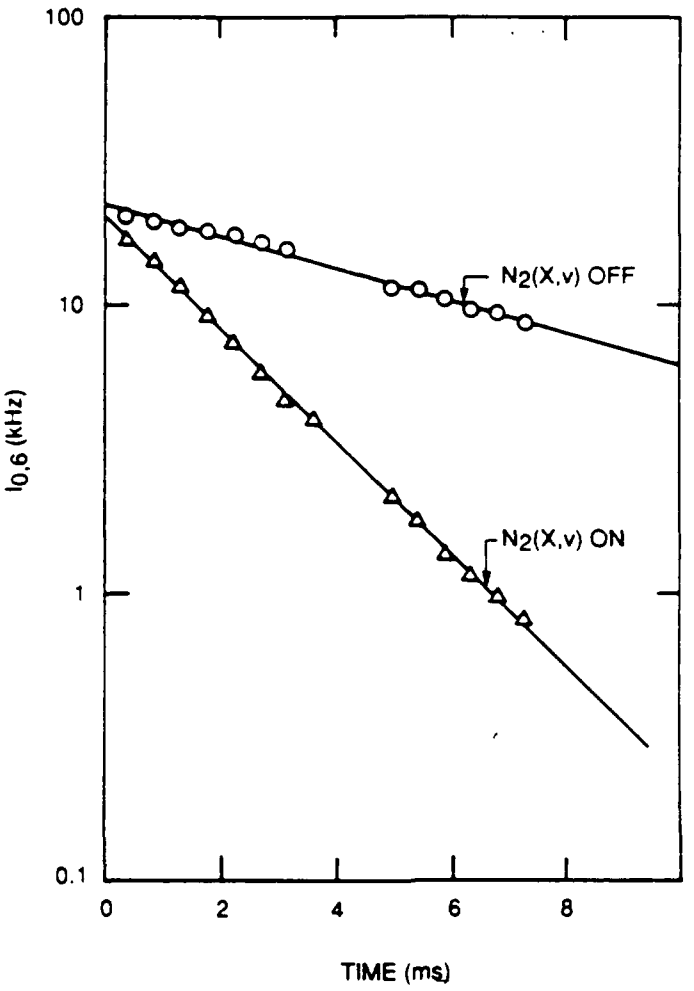

Figure 20. Variation in intensity of the 0,6 Vegar-Kaplan band as a function of time in the absence and presence of $N_2(X,v)$.

due to quenching by the $N_2(X,v)$ and perhaps a small amount of quenching from residual N-atoms which did not recombine on the nickel screen. The relevant reactions are

$$N_2(A) + \text{wall} \rightarrow N_2(X) + \text{wall} \tag{23}$$

$$N_2(A) + N_2(X,v) \rightarrow 2N_2(X) \tag{24}$$

$$N_2(A) + N \rightarrow N_2(X) + N(^2P) \tag{25}$$

An alternative to reaction (24) would be excitation to the B-state followed by quenching out of the B-state into the X-state. Reaction (24), therefore, represents removal of molecules from the triplet manifold.

The rate equation describing these reactions is

$$\frac{d[N_2(A)]}{dt} = -\{k_{23} + k_{24}[N_2(X,v)] + k_{25}[N]\}\ [N_2(A)] \tag{26}$$

Under conditions where the number densities of $N_2(X,v)$ and N remain essentially invariant with time, Equation (26) has the solution

$$\ln\left\{\frac{[N_2(A)](t)}{[N_2(A)](t=0)}\right\} = -K_\ell t \tag{27}$$

where the loss rate, K_ℓ, is given by

$$K_\ell = 0.62\ \{k_{23} + k_{24}[N_2(X,v)] + k_{25}[N]\} \tag{28}$$

The factor of 0.62 corrects for the coupling of the radial number density gradient of $N_2(A)$ with the parabolic velocity profile in the reactor (Refs. 66-75). The semi-log plot in Figure 20 displays the expected linear behavior between the natural log of the $N_2(A)$ number density and the reaction time.

In the absence of $N_2(X,v)$, the decay of the metastables is determined principally by wall deactivation. This process is controlled by the rate of diffusion of the metastables to the walls. The wall-loss rate, k_{23}, is given by (Ref. 66)

$$k_{23} = \frac{D_o\lambda_o^2}{r^2 p} \tag{29}$$

where D_0 is the diffusion coefficient in centimeters squared per second at 1 torr, λ_0 is the root of the zero-order Bessel function, 2.405, r is the flow tube radius, and p is the flow tube pressure. For the data in Figure 20, the decay rate in the absence of $N_2(X,v)$ is 210 s^{-1}. This value agrees moderately well with the value of 180 s^{-1} which can be calculated from Equation (29). For the diffusion coefficient of $N_2(A)$ in He an experimental value of 540 $cm^2\ s^{-1}$ at 1 torr, which was calculated for $N_2(X)$ in He using procedures described by Hirschfelder, Curtiss and Bird (Ref. 76) was used. The slight discrepancy could result from an incompletely developed flow profile in the reactor because of perturbations to the flow induced by the injectors or perhaps just increased surface area for deactivation because of the presence of the injectors.

The addition of $N_2(X,v)$ increases the decay rate of $N_2(A)$ to 731 s^{-1}. Since the N-atom number density is less than 10^{12} atoms per cubic centimeter, and the rate coefficient for quenching $N_2(A)$ by N is 4.0×10^{-11} cm^3 $molecule^{-1}$ s^{-1} (Ref. 77), < 10 percent of this increase in $N_2(A)$ decay can be attributed to quenching by atomic N. The balance, therefore, must result from quenching by $N_2(X,v)$. The rate of quenching $N_2(A)$ by $N_2(X,v)$ under the conditions of Figure 20 is about 520 s^{-1}. From the Penning-ionization measurements an $N_2(X,v)$ number density of $\approx 1.4 \times 10^{14}$ molecules per cubic centimeter is estimated. This value estimates a quenching rate coefficient of $N_2(A)$ by $N_2(X,v)$ of about 3.7×10^{-12} cm^3 $molecule^{-1}$ s^{-1}. This is just over 10 percent of the previously estimated rate coefficient for reaction (16). The discrepancy between the two rate coefficients probably arises from the fact that little $N_2(A)$ is actually lost in pumping it from the A-state to the B-state. Most molecules pumped to the B-state eventually return to the A-state via radiative or collisional cascade. Evidently some are lost by quenching out of the triplet manifold.

2.2.3.3 Regeneration of $N_2(A)$. Figure 21 shows direct evidence of this repopulation of the A-state from pumping to the B-state followed by cascade back to the A-state. It shows the ultraviolet spectrum in the absence and presence of $N_2(X,v)$. The spectra were taken in the presence of methane, so that the $N_2(A)$ initially in the field of view was entirely in vibrational level 0. When the $N_2(X,v)$ mixes with the $N_2(A,v=0)$. however, vibrational levels 1 and 2 of the $N_2(A)$ are regenerated as is evident in Figure 21(b).

The question arises as to whether the pumping of the $N_2(A,v)$ could be a direct excitation from $N_2(A,v=0)$ or if it is the result of cascade from the B-state which has itself been pumped directly. The time evolution of the ratio of the number densities of $N_2(A,v=1,2)$ to $N_2(A,v=0)$ was followed to investigate this issue.

In the following discussion a short-hand notation is used in which a N molecule in a specific vibronic state is identified by the letter of the electronic state with a superscript corresponding to the vibrational level in that state. For example, A^1 represents $N_2(A^3\Sigma_u^+,v'=1)$.

In addition to reactions (16), (17), (23), (24) the relevant reactions for $N_2(A,v=1)$ excitation and quenching include the following:

$$N_2(A,v=0) + N_2(X,v) \rightarrow N_2(A,v=1,2) + N_2(X,v) \qquad (30)$$

$$N_2(A,v) + CH_4 \rightarrow N_2(A,v=1) + CH_4 \qquad (31)$$

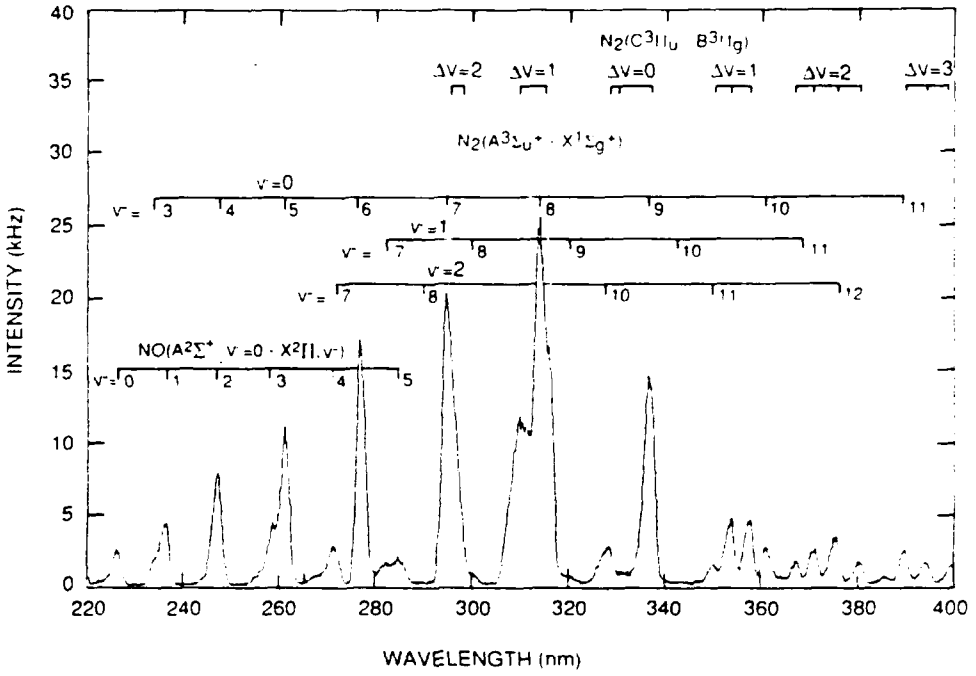

(a) Spectrum of the N Vegard-Kaplan and second-positive $N_2(C^3\Pi_u - B^3\Pi_g)$, bands in the presence of 6.1×10^{14} molecules per cubic centimeter of Methane, but the absence of $N_2(X,v)$. Note the absence of vibrationally excited $N_2(A)$ in the spectrum.

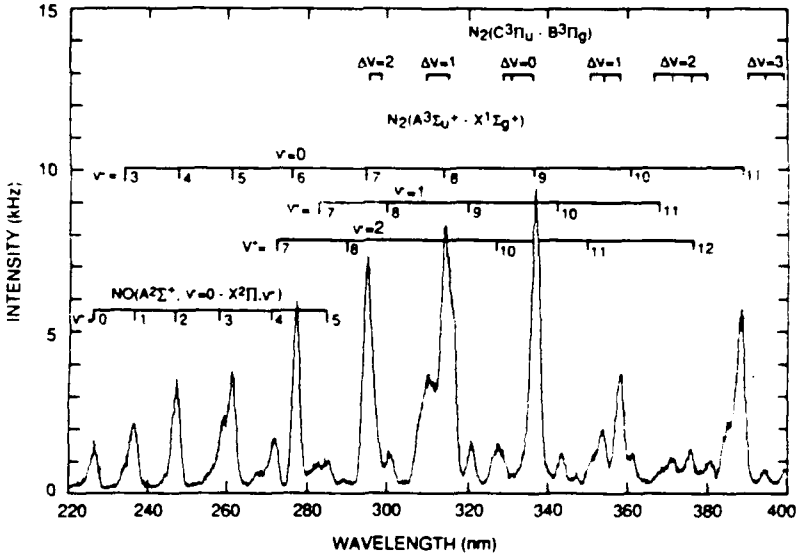

(b) Spectrum of the N Vegard-Kaplan and second-positive bands in the presence of 6.1×10^{14} molecules per cubic centimeter of methane and also in the presence of $N_2(X,v)$. Note the appearance of bands from vibrational levels 1 and 2 of the Vegard-Kaplan system.

Figure 21. Nitrogen ultraviolet spectrum.

The rate of change in the number density of $N_2(A,v=1)$ with time is

$$\frac{d[A^1]}{dt} = \zeta_1 k_{17}[B] + k_{30}[A^0][X^v] + k_{31}^{v=2}[A^2][CH_4] - \left\{k_{23} + k_{24}[X^v] + k_{31}^{v=1}[CH_4]\right\}[A^1] \tag{32}$$

where ζ_1 is the fraction of $N_2(B)$ excitations which cascade down to $N_2(A)$ vibrational level 1. Inserting Equation (21) into Equation (32) and rearranging gives the result

$$\frac{d[A^1]}{dt} = \left[\frac{\zeta_1 k_{16}}{1 + \frac{k_{18}}{k_{17}}[N_2] + \frac{k_{19}}{k_{17}}[Q]} + k_{30}\right][A^0][X^v] - \left\{k_{23} + k_{24}[X^v] + \left[k_{31}^{v=1} - k_{31}^{v=2}\frac{[A^2]}{[A^1]}\right] - \left[1 + \frac{[A^2]}{[A^1]}\right]\frac{\zeta_1 k_{16}[X^v]}{1 + \frac{k_{18}}{k_{17}}[N_2] + \frac{k_{19}}{k_{17}}[Q]}\right\}[A^1] \tag{33}$$

If the number-density ratio $[A^2]/[A^1]$ is constant, and if $[X^v]$ is constant, Equation (33) can be solved analytically upon inserting the exponential form of Equation (27) into it. The result is

$$\frac{[A^1]}{[A^0]} = \frac{K_f e^{-K_\ell^{v=0} t}}{K_\ell^{v=1} - K_\ell^{v=0}}\left\{1 - e^{\left(K_\ell^{v=1} - K_\ell^{v=0}\right) t}\right\} \tag{34}$$

where the substitutions for the formation and loss rates, K_f and K_ℓ, have been made respectively,

$$K_f = 0.62\left[\frac{\zeta_1 k_{16}}{1 + \frac{k_{18}}{k_{17}}[N_2] + \frac{k_{19}}{k_{17}}[Q]} + k_{30}\right][X^v] \tag{35}$$

and

$$K_\ell^{v=1} = 0.62\left\{k_{23} + k_{24}X^v + \left[k_{31}^{v=1} - k_{31}^{v=2}\frac{[A^2]}{[A^1]}\right][CH_4] - \left[1 + \frac{[A^2]}{[A^1]}\right]\frac{\zeta_1 k_{16}[X^v]}{1 + \frac{k_{18}}{k_{17}}[N_2] + \frac{k_{19}}{k_{17}}[Q]}\right\} \quad (36)$$

Figure 22 shows the data plotted according to Equation (34). The curve through the data is a least-squares fit. The result from the fit is $K_f = 174\ s^{-1}$ and $K_\ell^{v=1} = -184\ s^{-1}$.

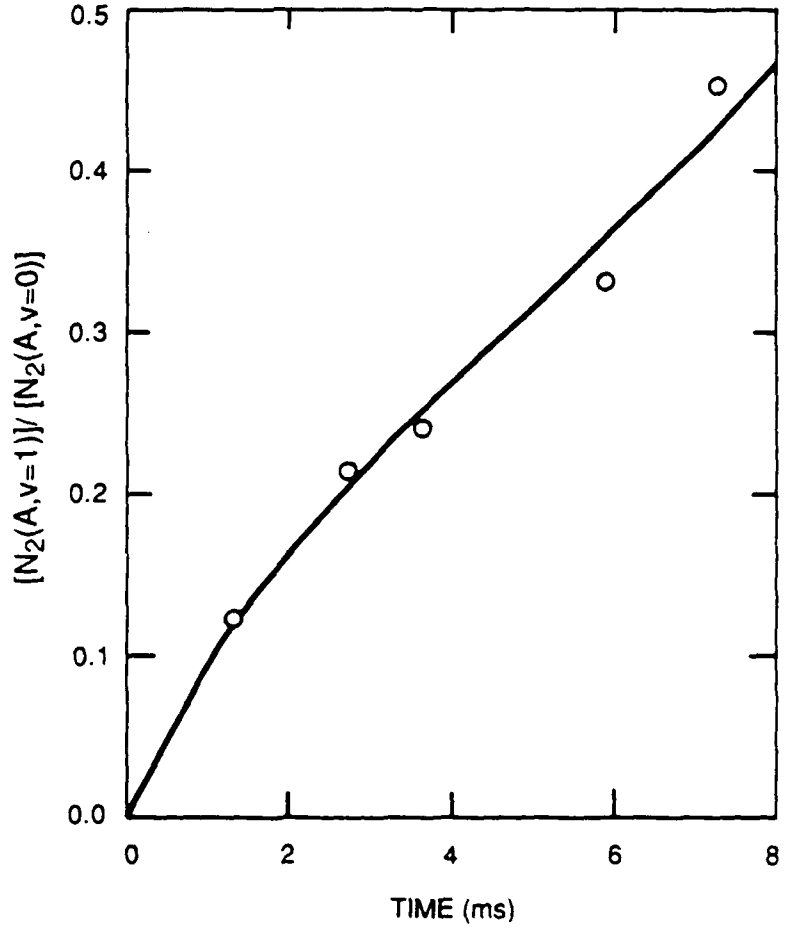

Figure 22. Ratio of the number densities of $N_2(A,v=1)$ to $N_2(A,v=0)$ as a function of time. The line through the data is the least-square fit to Equation 34.

Using the $N_2(B)$ vibrational distribution from reaction 1, $\zeta_1 = 0.2$ and the ratio $[A^2]/[A^1]=0.7$ are calculated. These values agree quite well with our observations from this series of experiments. The rate coefficient for reaction (31) is 1.5×10^{-12} cm^3 $molecule^{-1}$ s^{-1} for v = 1 and 3.1×10^{-12} cm^3 $molecule^{-1}$ s^{-1} for v = 2 (Ref. 26). Combining these values with the value of k_1, the quenching rate coefficients given above, and the number density for $N_2(X,v=5\text{-}10)$ estimated from Penning-ionization measurements to be 1.4×10^{14} molecules cm^{-3}, a value for K_f of 280 s^{-1} is calculated if the direct excitation channel to produce $N_2(A,v=1)$ from $N_2(A,v=0)$ is neglected. Assuming that k_{23} and k_{24} are the same for v = 1 as they were for v = 0, a value for $K_\ell^{v=1}$ of -154 s^{-1} is calculated. Given the experimental uncertainties in this study, the much better than factor of 2 agreement between observed and calculated formation and loss rates must be considered quite good. This agreement doesn't preclude a direct excitation channel. Rather a direct excitation is not required to explain the observations.

2.2.4 Discussion

2.2.4.1 Mechanism. The reaction between $N_2(A)$ and $N_2(X,v)$ results in efficient excitation of $N_2(B)$. The question arises as to whether the molecule originally in the A-state is excited to the B-state by the influx of the vibrational energy from the X-state molecule, or whether the X-state molecule is excited to the B-state in an electronic-energy transfer from the A-state. Apparently the latter is more likely.

One model that has become quite popular for rationalizing energy-transfer observations involves comparing rate coefficients with the product of the Franck-Condon factors of the two transitions involved in the energy transfer and multiplying that result by the absolute value of the energy defect of the reaction (Refs. 78-82). These studies (Refs. 10, 57, and 83) and others (Refs. 84 and 85) have shown on several occasions that this model is inadequate to describe the details of state-to-state observations, it may have some validity as a qualitative predictor.

For the case of direct excitation of the A-state by the X-state, the Franck-Condon factors coupling vibrational level 0 of the A-state with various B-state vibrational levels become vanishingly small ($q_{v'v''} < 10^{-4}$) for transitions to B-state levels greater than v = 5. The implication is that population rates of the higher B-state vibrational levels should be negligible. The higher vibrational B-state levels would be more readily excited from vibrationally excited $N_2(A)$. Thus where the A-state excited directly to the B-state one would see a strong dependence of the B-state vibrational distribution on that of the A-state. This dependence is not observed.

The situation is markedly different for the case of electronic energy exchange. When $N_2(A,v=0)$ transfers all of its energy to a given X-state level, the Franck-Condon factor coupling that level to the most nearly resonant B-state level is in all cases greater than 2×10^{-3}, and in most instances greater than 10^{-2}. The Franck-Condon factor coupling vibrational levels zero of the X- and A-states is small, 1×10^{-3}, but nonnegligible.

On the basis of just the Franck-Condon factors, the transfer appears even more facile if the A-state doesn't give up all its energy in the transfer. For example, the collision between $N_2(A,v=0)$ and $N_2(X,v=16)$ to produce $N_2(X,v=5)$ and $N_2(B,v=8)$ has a Franck-Condon product three orders of magnitude greater than does the generation of $N_2(B,v=8)$ and $N_2(X,v=0)$ from the reaction between $N_2(X,v=11)$ and $N_2(A,v=0)$. This advantage will be offset somewhat by the lower number density in vibrational level 16 of the X-state compared to that in vibrational level 11. The main point is that the Franck-Condon model appears to favor quite strongly the electronic-energy exchange channel.

The somewhat related observations of Pravilov et al. (Ref. 82) demonstrate rather unequivocally that electronic-energy exchange does occur in collisions between ground-state and electronically excited N molecules. They studied the formation of the $N_2(B)$ state produced from N-atom recombination. Upon adding isotopically labeled N to their afterglow, they noted a strong shift in the positions of the first-positive bands. The observed fluorescence was from the isotopically labeled molecules which had been excited in an energy-transfer reaction with B-state molecules initially excited in the N-atom recombination.

2.2.4.2 Related Studies. Hayes and Oskam (Ref. 38) monitored the decays of $N_2(A)$ and $N_2(B)$ in the afterglow following a discharge pulse in a static cell. They attributed the excitation of $N_2(B)$ primarily to energy pooling of two $N_2(A)$ molecules. They noted, however, that the variation in the ratios of the A-state intensity to that of the B-state was less than quadratic throughout the afterglow. Quadratic behavior would be expected in the event of excitation by $N_2(A)$ energy pooling. Furthermore, this deviation from quadratic behavior was greater for longer discharge pulses. They suggested reaction (16) as a second mechanism which might be responsible for some of the $N_2(B)$ excitation.

The results reported here show that reaction (16) is indeed efficient. Evidently, the longer discharge pulses in Hayes and Oskam's apparatus result in increased production of $N_2(X,v)$. The $N_2(B)$ excited from reaction (16) as opposed to the energy-pooling reaction, therefore, would become more and more significant as discharge-pulse lengths grew. Hayes and Oskam tried to eliminate the effects of reaction (16) by extrapolating their results to vanishingly small discharge-pulse lengths. The much larger value they reported for the energy-pooling reaction than that reported recently (Ref. 10) indicates that they were not completely successful in this endeavor. The energy-pooling results should not have been contaminated by reaction (16). Penning-ionization measurements of this $N_2(A)$ discharge source indicate an absence of $N_2(X,v)$ (Ref. 2).

Over a number of years, Kenty (Refs. 41, 86-89) studied the orange afterglow resulting from passing current pulses through high pressure mixtures of rare gases containing a trace of N. He showed that these afterglows did not result from $N_2(B)$ excitation caused by N-atom recombination, and suggested that the B-state was excited by collisional transfer from a long-lived metastable in the afterglow. He proposed that this metastable was $N_2(W^3\Delta_u)$. The results reported here indicate that a more likely explanation for Kenty's observations is the energy-transfer reaction between $N_2(A)$ and $N_2(X,v)$. He did suggest this possibility himself in one of his later publications (Ref. 41), but even his last publication (Ref. 89)

championed $N_2(W)$ as being primarily responsible for his observations. Clearly the close coupling between the B- and W-states (Refs. 25, 26, and 90) means that the characteristics of the latter state might affect the observed B-state fluorescence. The primary excitation channel, however, is most likely reaction (16).

2.3 LASER-BASED DIAGNOSTICS FOR $N_2(X,v)$

2.3.1 Introduction

A number of laser-based $N_2(X,v'')$ detection techniques were investigated. There was enough information to rate the usefulness of each of the techniques, their sensitivities and their applicability to various experimental settings. The $N_2(X,v''=14)$ quenching rate was measured by an interhalogen precursor. This measurement is important as proof of principle in using laser-based detection of $N_2(X,v'')$ in kinetic studies. It is also important in that it identifies potential problems associated with measuring $N_2(X,v'')$ energy transfer rates for interhalogens such as iodine monofluoride, IF.

The four laser-based $N_2(X,v'')$ detection techniques which have been investigated in this program are 2+2 MPI, 1+1 MPI, two-photon LIF and one-photon LIF. Each technique has been successful in detecting $N_2(X,v'')$ produced from a microwave discharge source. The theory behind MPI and LIF has been reviewed in a number of journal articles (Refs. 20, 91-94), thus they will be discussed here only briefly. The four techniques each involve excitation of the vibrationally excited, ground-state N molecule, $N_2(X^1\Sigma_g^+,v'')$ to the $N_2(a^1\Pi_g,v')$ state. Each technique is shown schematically in Figure 23 and is described in more detail below.

Detection of $N_2(X,v''>0)$ via multiphoton excitation to the $a^1\Pi_g$ state may be accomplished using four methods which can be classified into two groups, MPI and LIF. In LIF one or two photons are absorbed by the ground-state molecule, exciting it to the $a^1\Pi_g$ state (through a virtual intermediate state in the two-photon process). The weakly allowed fluorescence from the $a^1\Pi_g$ state (Lyman-Birge-Hopfield bands) is observed in the vacuum ultraviolet region. By scanning the frequency of the probe laser and detecting the undispersed VUV fluorescence, one observes an excitation spectrum characteristic of the $N_2(a,v' \leftarrow X,v'')$ system. The radiative lifetime of the excited state has been measured to be 56 μs (Ref. 19) and hence is quite susceptible to quenching at even moderate pressures (Refs. 14, 18 and 95). Because of predissociation of the a-state above $v' = 6$, fluorescence from higher levels is not observed.

Multiphoton excitation of the $a^1\Pi_g$ state from $N_2(X,v''>0)$ may also be followed by absorption of additional laser photons until the ionization limit of the molecules is reached. Ions and electrons produced by the absorption of the laser radiation may then be detected as a measure of the ground-state vibrational population. In MPI spectroscopy high photon fluxes are utilized so that the molecule absorbs a sufficient number of photons to ionize. The ions are detected by measuring the current flow in the gas using a set of biased electrodes or other suitable ion detection device. The MPI process can usually be described as occurring

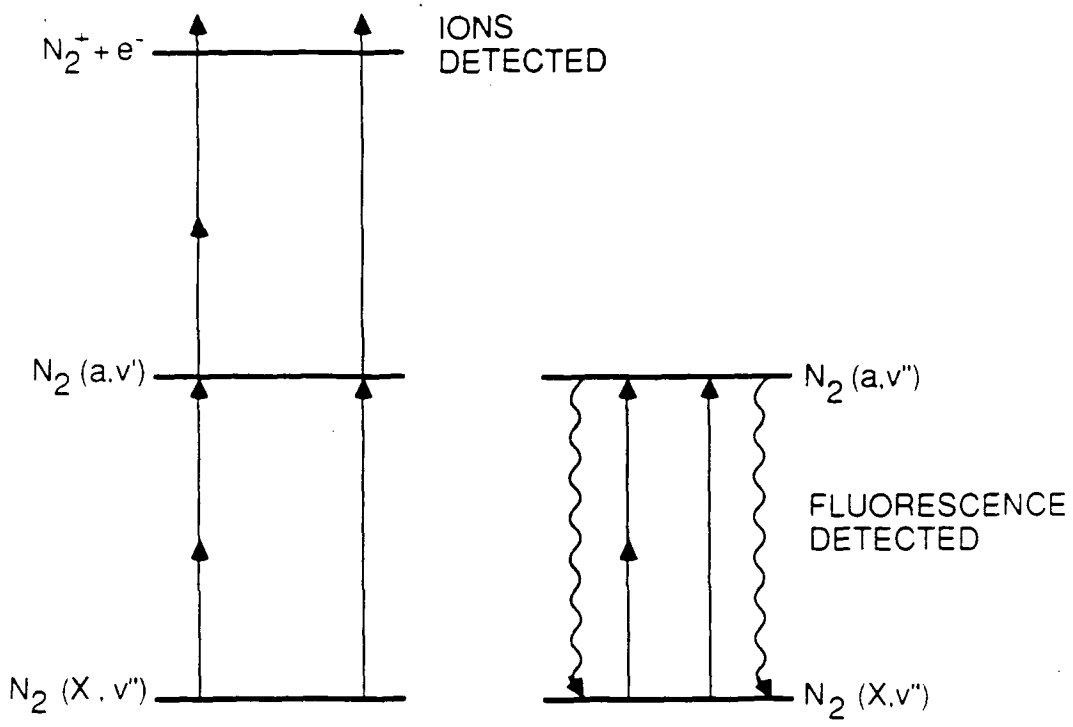

(a) Schematic of 2+2 and 2+1 MPI for $N_2(X,v'')$ detection

(b) $N_2(X,v'')$ Detection via one- and two-photon LIF

Figure 23. Laser detection strategies.

in two steps: 1) the absorption of m photons to a real intermediate electronic state of the molecule, and 2) the absorption of n more photons, perhaps through several intermediate electronic states of the molecule, until ionization is achieved. In particular, the m photon step is almost always rate limiting. So, as in LIF spectroscopy, by scanning the frequency of the probe laser and detecting the current flow within the gas one achieves a spectrum characteristic of the $N_2(a,v' \leftarrow X,v'')$ system.

2.3.2 Experimental

2.3.2.1 Flow System. The 1-in flow reactor shown in Figure 24 was used for most of the laser-based experiments. It is a conventional discharge flow reactor run at ambient temperature (295 K). The flow tube is constructed from 2.54 cm ID Pyrex® connected to a 2.54 cm ID aluminum detection block. The Pyrex flow tube is coated with halocarbon wax and the detection block is coated with Teflon (Dupont Poly TFE #852-201) to slow atom recombination and quenching of vibrational energy. The apparatus is attached using 25 mm Viton O-ring joints making the setup adaptable to many experimental configurations. The excitation axis (laser ports) of the detection block is fitted with skimmer-type optical baffles (Ref. 96) and S1-UV grade quartz windows mounted at Brewster's angle. This configuration helped to reduce scattered light during LIF studies. The flow tube is evacuated by a (Sargent

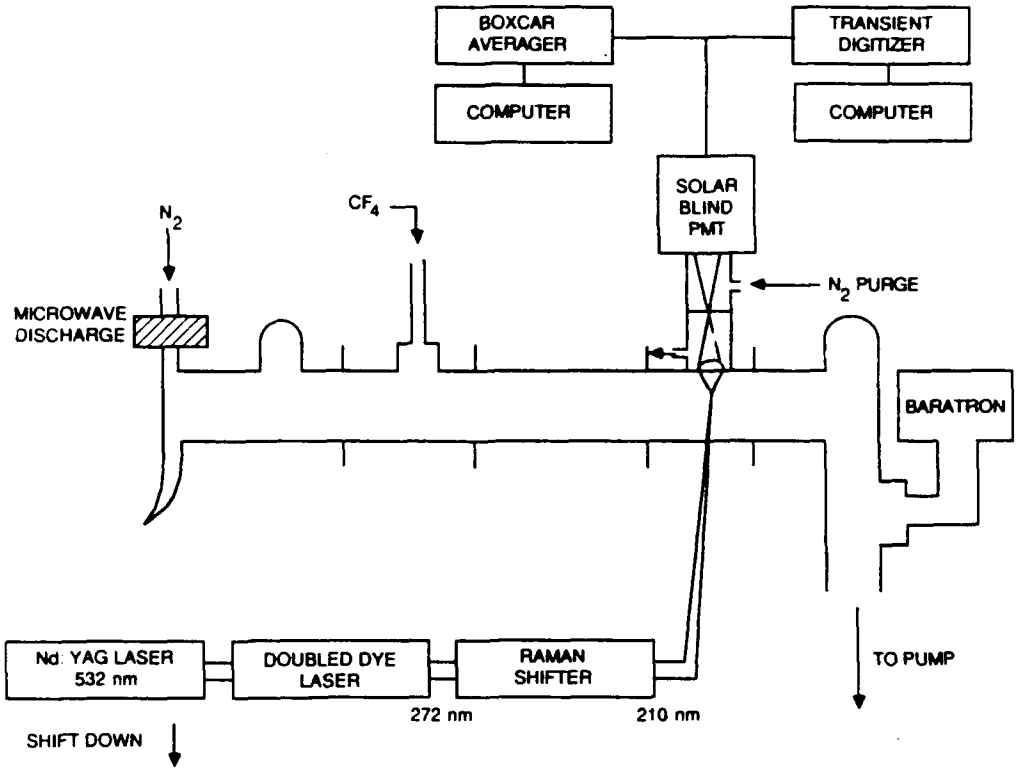

Figure 24. Schematic diagram of 1-in flow reactor.

Welch Model 1397) rotary pump and is capable of flow velocities up to 1000 cm s^{-1}. Flow rates of all species are determined by calibrated electronic linear mass flow meters (Teledyne Hastings-Raydist, Models ST-10, ST-100, ST-500) and the pressure is determined by a 0 to 100 torr capacitance manometer (MKS Model 226-66100AB). Various ports are available for the introduction of reactants into the flow tube and a standard electrodeless microwave discharge of N_2 or N_2/He mixtures supplies the $N_2(X,v'' > 0)$. The discharge tube is equipped with a Wood's horn to help eliminate scattered light and the discharge cavity typically runs between 70 and 100 W forward power.

The flow tube can be equipped with either electrodes or a photomultiplier tube (PMT) for MPI or LIF spectroscopy, respectively. Figure 24 shows the flow tube setup for LIF detection. Note that a 25-mm diameter, f/1, CaF_2 lens collects the VUV fluorescence and focuses it onto an iris diaphragm. This optical configuration helps to reduce scattered laser light and VUV background chemiluminescence produced directly in the microwave discharge. The entire optical train is purged with N_2 to prevent atmospheric O absorption of the VUV fluorescence.

Some of the early experiments were conducted on the CONAN flow tube which has been described previously (Refs. 6 and 8). Briefly, it is a 5 cm ID flow tube coated with halocarbon wax and pumped by a Roots blower. Flow rates of all species are determined by calibrated electronic mass-flow meters and the pressure is determined by a 0 to 10 torr capacitance manometer. Flow velocities range from 500 to 5300 cm s^{-1}. A schematic diagram of this flow reactor is shown in Figure 25.

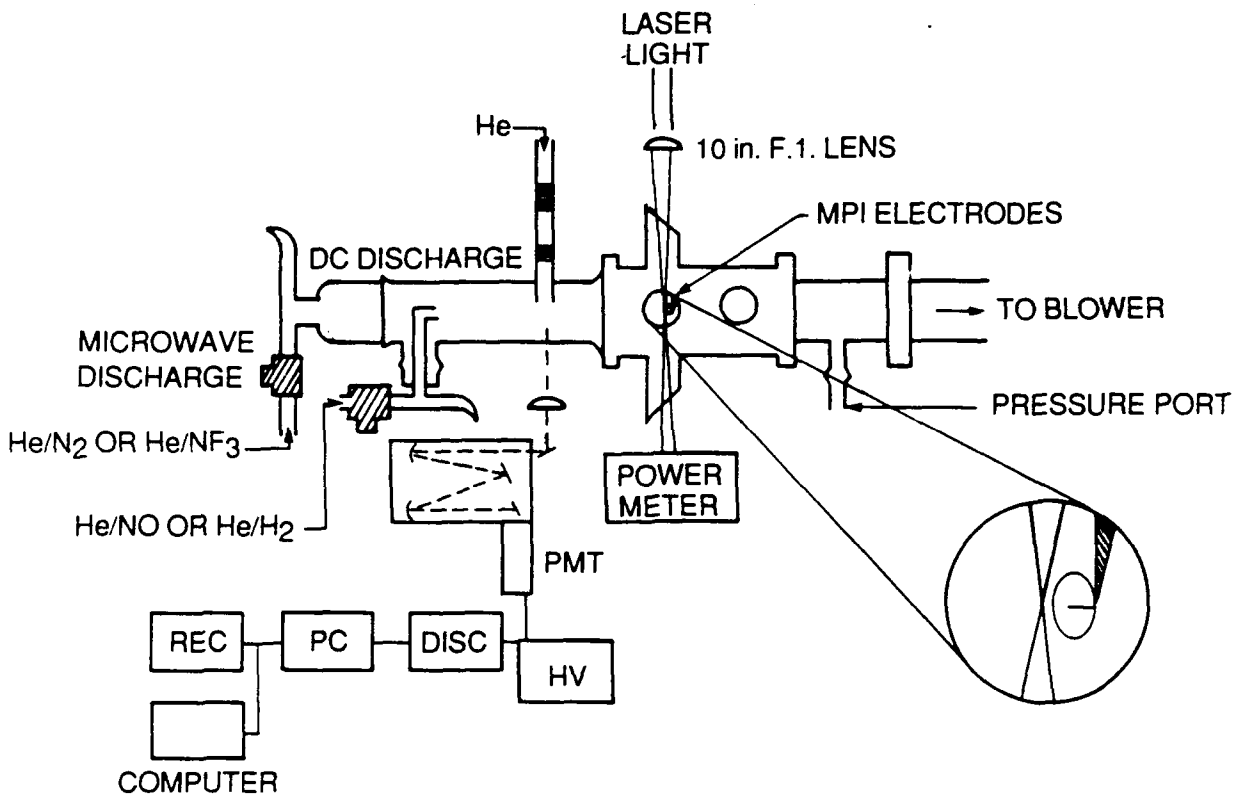

Figure 25. Block diagram of 5 cm ID flow reactor.

The MPI detection system for $N_2(X,v'')$ is shown schematically in Figure 26. The system consists of two copper electrodes inserted into the gas stream in which the negative electrode (positive ion collector) was formed into a circular loop concentric with the flow tube axis. The positively biased electrode (electron collector) was a blunt tipped section of copper wire which ran through the center of the negatively biased loop, colinear with the gas flow. The electrodes were biased with a stabilized high voltage power supply (EMI Model 3000R) or a 90V radio battery and placed in series with a high speed current amplifier (Ithaco Model 1211). The ionization laser beam was focused to a spot $\approx$2 mm upstream from the positive electrode by a 15-cm focal length quartz lens. The placement of the laser focus upstream of the collection electrodes was essential in order to detect the metastables before they came in contact with the potentially deactivating electrode surfaces. The electrode geometry was optimized for detection of both ions and electrons by providing a strong field gradient across the diameter of the reactor. The faster moving electrons were formed near the positive electrode while the slower moving positive ions were provided with a larger surface area electrode in the downstream direction to enhance ion capture.

2.3.2.2 Detection Electronics. The signals from the MPI electrodes were sent to a high speed current amplifier and were then captured by a gated integrator (Stanford Research Systems Model SR250, SR280) triggered by the excitation laser. The VUV fluorescence was detected by a solar-blind PMT (EMR Photoelectric Model 541G-08-18) and these signals were also captured by the gated integrator. A computerized data acquisition system, consisting of an IVY® personal computer equipped with a DT 2801A A/D board, was used in

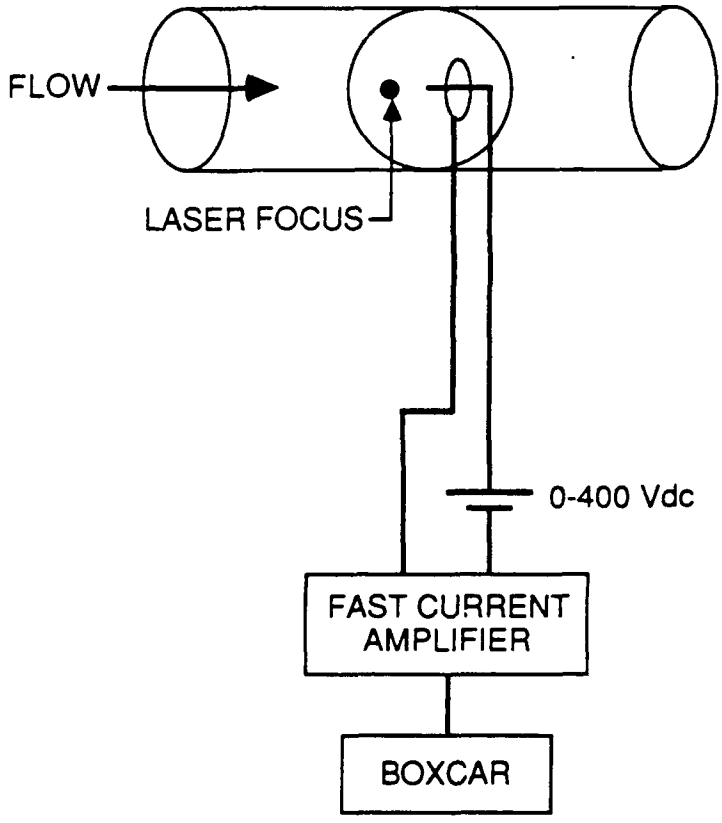

Figure 26. MPI electrodes and electronics.

conjunction with a strip chart recorder to record the spectral scans. The data acquisition software used on the computer was REAL TIME Lab Notebook® written by Laboratory Technologies Corporation, Wilmington, Massachusetts. The LIF experiments, which were used to determine electronic state lifetimes and quenching rates, were recorded by a LeCroy® 200 MHz transient digitizer (Model TR 8828C), 150 MHz programmable preamp (Model 6103), IEEE 488 bus controller (Model 8103A), run by CATALYST® waveform digitizing software on the personal computer.

2.3.2.3 Laser System. The excitation laser employed in the detection system was a pulsed Nd:YAG-pumped tunable dye laser (Quantel International®). The YAG pump was a YG580 series Nd:YAG capable of output up to 500 mJ at 532 nm and 10 Hz. The dye laser, which the Nd:YAG laser pumped, was a model TDL50 equipped with a narrow bandwidth package (prism beam expanders) capable of 0.08 cm^{-1} bandwidth. The dye laser was pulsed at 10 Hz with a pulse duration of 10 ns. A variety of laser dyes and dye mixtures (Exciton: FL548, R590, R610, R640, DCM, and LD700) were employed to produce light in the region from 545 nm to 700 nm at pulse energies as large as 150 mJ. These studies required light in the region of 190 nm to 400 nm, hence nonlinear frequency generation and Raman shifting techniques were employed. Tunable laser light in the 350 to 400 nm range was produced by mixing the fundamental dye laser radiation with the 1.064 μm fundamental of the Nd:YAG in an angle-tuned KDP crystal. The crystal tuning was controlled by a servoloop, so that optimum generation of UV light was achieved while the dye laser wavelength was scanned

using a microprocessor-controlled grazing incidence grating. Pulse energies as large as 30 mJ were attained in this wavelength region. Tunable laser output in the 272 to 350 nm range was produced by second harmonic generation in KDP crystal. Pulse energies as large as 40 mJ were attained in this region. Generation of light in the 220 to 260 nm region was accomplished by subsequent mixing of the tunable second harmonic of the dye laser with the 1.064 μm radiation from the Nd:YAG laser in a second set of servo-controlled KDP crystals. The maximum pulse energy in this wavelength region was 6 mJ. Finally, radiation in the 190 to 220 nm region was generated via Raman shifting of the second harmonic tunable dye laser radiation in a (Quantel International, Model RS-2-IR) Raman cell filled with 100 to 250 psi of hydrogen. Pulse energies ranged from 1000 to 20 μJ respectively for the first and fourth anti-Stokes lines. Transmission of wavelengths below 200 nm was accomplished via N-purged light pipes to prevent atmospheric O absorption of the laser radiation. The multiple outputs from the nonlinear harmonic generation system and Raman shifting were dispersed using a Pellin-Brocha prism and the proper wavelengths were directed through the detection cell via 45 deg S1-UV turning prisms.

2.3.3 Summary of Results

2.3.3.1 2+2 MPI. To use 2+2 MPI as a quantitative tool, the signal must have a linear dependence on $[N_2]$ (Refs. 20, 91-94). To check this linearity the (0-0) band S-branch bandhead was excited with no microwave discharge. This allowed $[N_2(X,v''=0)]$ to be known exactly. Signal intensity as a function of $[N_2]$ was recorded and is shown in Figure 27. This plot shows a limited linear region followed by a rolling off of the MPI

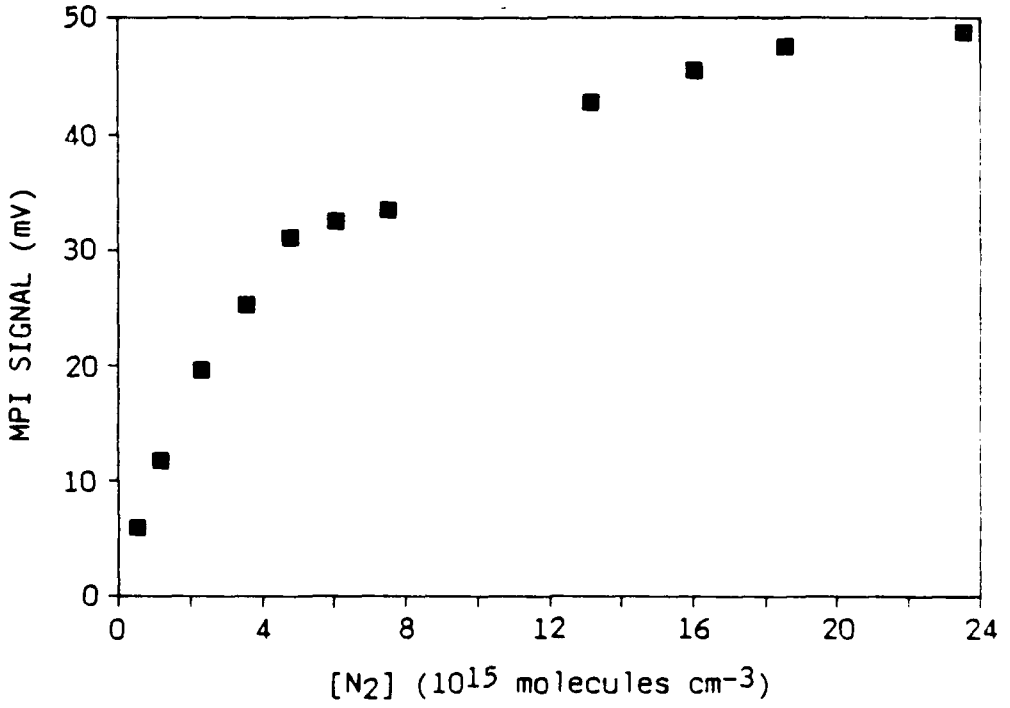

Figure 27. The 2+2 MPI signal dependence on $[N_2]$.

signal as [N_2] increases. This is an unexpected result, but it is believed to be due to an experimental artifact. The [N_2] was changed by throttling the pump valve, thus changing the reactor flow velocity. The change in flow velocity might affect ion-collection efficiency and thus signal levels. This illustrates a potential problem with MPI detection of $N_2(X,v'')$. In a practical application flow velocities may well vary, and the MPI signal level, therefore, would have to be calibrated for each flow setting. This calibration would be time consuming and is a major drawback to MPI detection of $N_2(X,v'')$.

In order to obtain measurable MPI signals a bias voltage must be applied to the electrode pair. The higher the bias applied, the larger the MPI signal detected. In a recent study on 2+1 MPI detection of NO in Ar, Cool (Ref. 97) has shown that there is a range of bias voltages for which the ion collection efficiency of the electrodes is unity. Below a certain voltage ($\sim$ 100 V) only a few of the ions are captured, while at higher voltages breakdown can occur in the gas and additional ion-electron pairs are created. This latter regime should be avoided since other external factors can influence any gain occurring in the gas and influence calibrations. The former regime fails to maximize the sensitivity of the technique. Experiments conducted at 2.5 torr N_2 with the laser wavelength set to the (0-0) band S-branch bandhead, showed the ion signal varied only weakly over a limited range of bias voltages from 0 to 420 V.

Figure 28 shows that from 0 to 180 V a relatively flat response to bias is observed, indicating little or no gain (avalanching) due to breakdown. Above 420 V the avalanche breakdown was so severe that a glow discharge was struck around the electrodes. Therefore

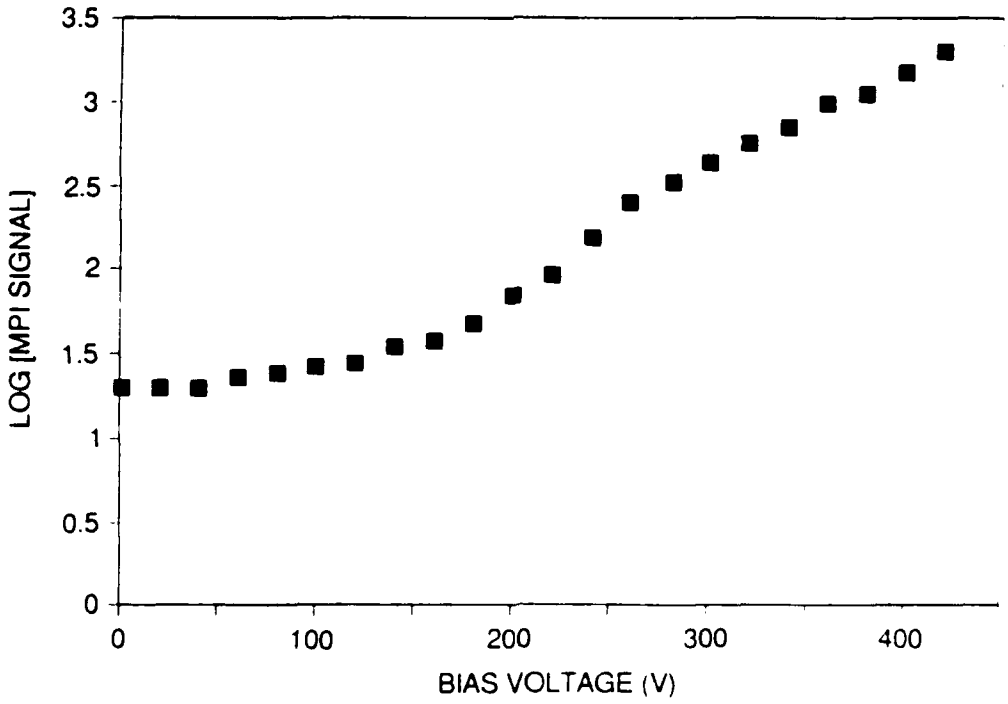

Figure 28. The 2+2 MPI signal dependence on electrode bias.

all subsequent MPI experiments were performed with bias voltages between 0 and 180 V. In this range there was some confidence that the results were not severely affected by gain in the gas mixture. Though it was not always possible to obtain adequate signals at these low bias voltages.

Finally the dependence of the MPI signal on laser energy was measured. In a 2+2 MPI system, where the two-photon initial excitation is the rate limiting step and is not saturated, the MPI signal should vary as the square of the laser intensity. The energy dependence of the (0-0) MPI signal at a pressure of 2.5 torr and a +90 V electrode bias was measured. The probe laser energy was varied by placing 7-54 Corning glass filters in the laser beam in front of or before the reactor laser port. The highest laser pulse energy used was 10 mJ. The data, presented in Figure 29, show that the MPI signal varies as the laser energy squared to within the experimental error, indicating that the transition is not saturated. Note the error bars on the largest and smallest data points. Data points taken at low laser energies have much larger potential errors than those taken at high laser energies. This may account for the slight curvature seen in the plot.

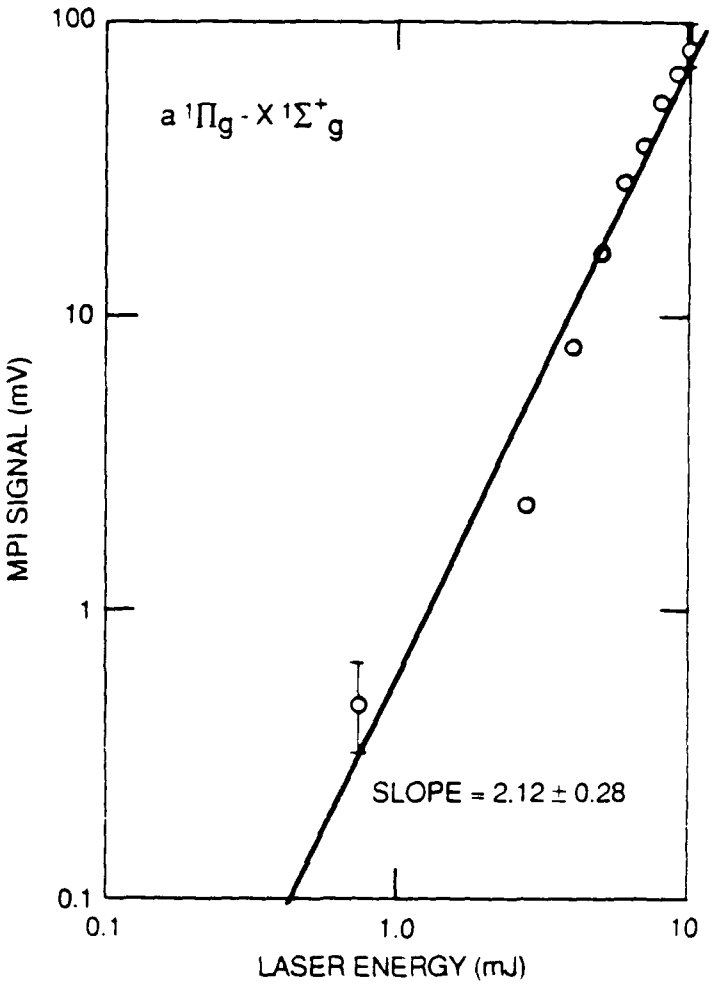

Figure 29. The 2+2 MPI signal dependence on laser energy.

One additional observation thought to be important was the effect of beam position on collection efficiency. A comprehensive study was not attempted, but observations did reveal a potential drawback to the MPI detection technique. The position of the probe laser focus had a large effect on the shape of the pulse of current observed following each laser pulse. As the focus was moved further away from the electrodes the pulse peak broadened, and as the focus moved still further away there was near total loss of the signal. Thus focus position reproducibility becomes important when trying to quantify $N_2(X,v'')$ number densities.

Related to this problem is the problem of "laser-beam walk" as the dye laser wavelength is scanned. The doubled laser beam is separated from the fundamental with a prism. As the wavelength changes during a scan, the angle at which the laser beam exits the prism shifts slightly, thus causing laser-beam walk. Over short distances and small changes in wavelength, beam walk is not significant, but this experimental setup required sending the laser beam $\approx$30 ft. Over this long distance there is substantial beam walk and great care must be taken to assure laser beam position reproducibility from one laser scan to the next. This is a considerable problem in applying MPI to practical systems. This problem could be alleviated by using a second, compensating, separation prism, or by using filters to separate the UV beam from the fundamental.

When the laser beam was set up to probe $N_2(X,v'')$ in the 5-cm diameter flow reactor attempts were made to detect $N_2(X,v''=0)$ produced from two chemical sources: $N_3 + N_3$, which the Penning-ionization work identified as a good source of $N_2(X,v'')$, and $H + NF_2$, from which the Penning-ionization work failed to detect $N_2(X,v'')$. No MPI signal was seen from either source. This was not a surprise for the $H + NF_2$ source, but it was, at least initially, for the $N_3 + N_3 \rightarrow N_2(X,v'')$ source. The 2+2 MPI with the electrode configuration used in the experiment at a +90 V bias allowed a 16:1 signal to noise ratio. The lowest possible $N_2(X,v'')$ density that could be detected was $\sim 2.5 \times 10^{14}$ molecules per cubic centimeter. The Penning-ionization work had determined that under similar operating conditions $[N_2(X,v''=0)]$ was 2.04×10^{12} molecules per cubic centimeter. Scaling the gas flows and increasing the electrode bias in attempts to detect $N_2(X,v''=0)$, were unsuccessful. It was determined that 2+2 MPI was not a sensitive enough technique to detect $N_2(X,v'')$ produced in these chemical sources.

2.3.3.2 1+1 MPI. Although the work showed the 2+2 MPI detection technique to be insensitive, the Phase I study determined that 1+1 MPI detection was somewhat more sensitive. The 2+2 MPI insensitivity results from poor absorption cross sections for the rate limiting multiphoton process. The 1+1 MPI process on the other hand needs the absorption of only a single photon in the initial rate limiting step and the absorption cross section is much higher for this process.

As the vibrational energy in $N_2(X,v'')$ increases, the amount of additional photon energy required to ionize the molecule decreases. The energy of transitions from $N_2(X,v'' \geq 9)$ to $N_2(a,v' \geq 2)$ become accessible to excitation in a single photon process. As a result the dye laser system excites $N_2(X,v'' \geq 9)$ to $N_2(a,v' \geq 2)$ in the much more efficien-

single photon transition and requiresthe absorption of only one additional photon for ionization. Though the vibrational levels of $N_2(a,v'>6)$ are known to predissociate and hence no fluorescence can be observed from these levels (Ref. 37), at high laser intensities MPI competes successfully with the apparently weak predissociation.

Figure 30 shows a 1+1 MPI spectrum of the 5-13 band. This spectrum was recorded in the 25 mm diameter flow reactor with 2.2 torr N_2, 300 V electrode bias, and 60 μJ of laser energy. The band appears precisely where the 5-13 band is expected, to within the calibration of the dye laser. The R and Q-branch bandheads appear characteristic of the one-photon excitation process.

Note that a 300 V electrode bias had to be used to record this spectrum -- a regime where signal gain in the gas is present. This is probably due to two factors; the low $N_2(X,v''=13)$ number densities and the low laser power at this excitation wavelength. In order to generate 204 nm light the doubled output of the 548 nm fundamental dye laser beam had to be shifted (anti-Stokes Raman). This process has a relatively poor conversion efficiency. Figure 31 shows a number of 1+1 MPI transitions and one 2+2 MPI transition (7-0). This spectrum shows the sensitivity of the 1+1 MPI technique with detection of the $N_2(X,v''=23$ through 26) levels. Note that the intensity units for this spectrum are much larger than those for Figure 30. This is because of the laser energy available at these wavelengths, ~5 mJ.

An attempt was made to tie the 1+1 and 2+2 MPI techniques by obtaining spectra of common levels with both techniques. The $N_2(X)$ v'' = 9 and v'' = 10 levels were chosen.

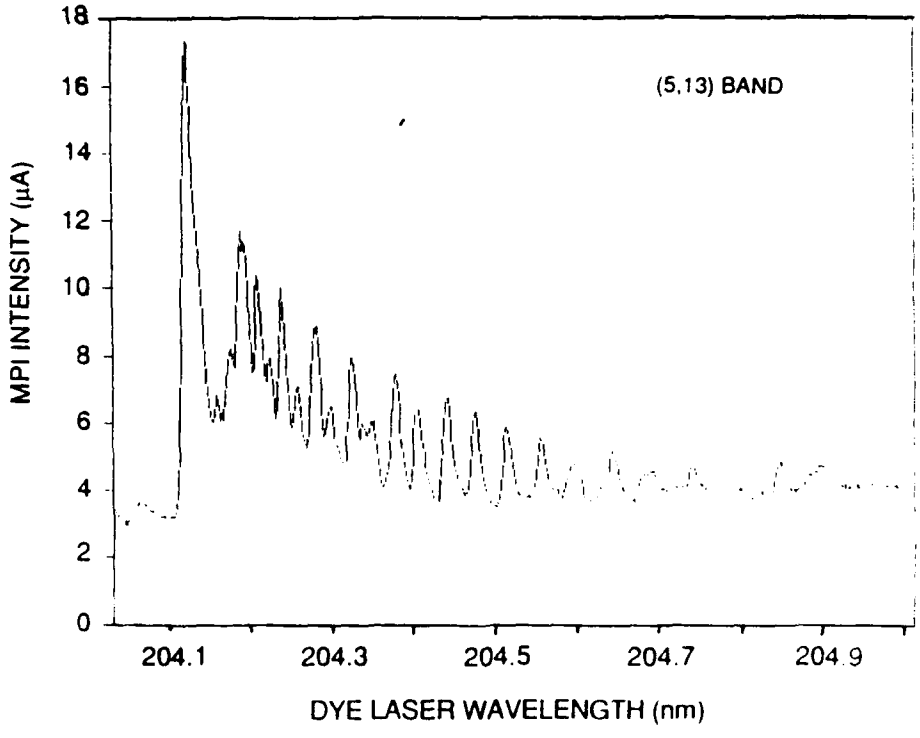

Figure 30. The 1+1 MPI spectrum of $N_2(a^1\Pi_g,v' = 5 \leftarrow X^1\Sigma_g{}^+,v'' = 13)$ band.

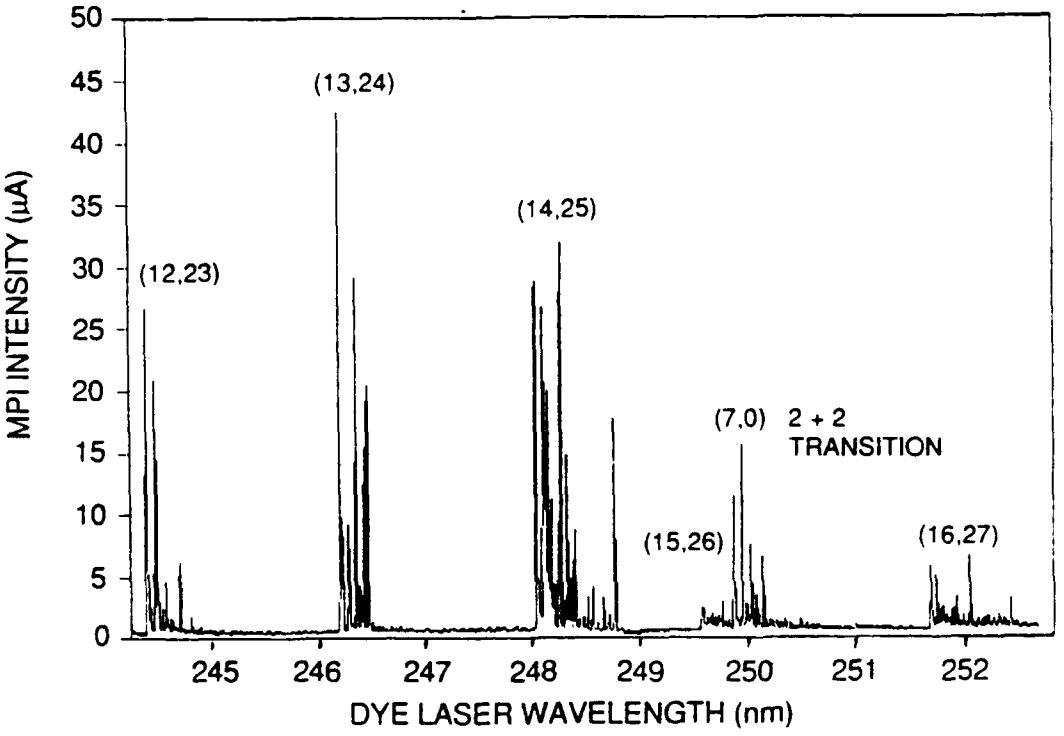

Figure 31. The 1+1 MPI spectrum of $N_2(a^1\Pi_g, v' \leftarrow X^1\Sigma_g^+, v'')$.

The $N_2(a,v'=2) \leftarrow N_2(X,v''=9)$ band was detected using 1+1 MPI, but attempts to detect the (3-9) and (3-10) transitions with 2+2 MPI were unsuccessful. The failure may have been due to low laser energy and low $N_2(X,v'')$ concentrations. Nor was there as much laser energy at the wavelength of interest as expected. The laser output was 30 percent lower than the output used in the early 2+2 MPI studies. Since the signal scales as the square of the laser intensity this 30 percent drop translates to a 50 percent drop in signal levels. If a 1700 K Treanor distribution describes the $N_2(X,v'')$ distribution from a microwave discharge, the populations of the $v'' = 9$ and $v'' = 10$ levels would be 1.6×10^{11} and 7.8×10^{10} molecules per cubic centimeter respectively. These values are far below the detection limits of the 2+2 MPI detection apparatus. In a separate calculation assuming unit ion/electron collection efficiency and based upon the lowest signal level the current amplifier/gated integrator can detect, the 1+1 MPI $N_2(x,v'')$ detection limit is 10^8 molecules per cubic centimeter.

These experiments concluded the study of 1+1 and 2+2 MPI detection of $N_2(X,v'')$. Table 2 lists the transition detected using MPI. This table is not meant to imply that v'' levels not listed here cannot be detected. The table shows that $N_2(X,v'' \leq 4)$ with 2+2 MPI was detected and $N_2(X,v'' \geq 9)$ with 1+1 MPI, but a common $N_2(X,v'')$ level was not detected with both techniques. This hindered turning MPI into a quantitative technique for those levels, $N_2(X,v'' \geq 9)$, which are required to excite most halogens or interhalogens.

Table 2. Multiphoton Ionization Detection of $N_2(a,v') \leftarrow N_2(X,v'')$

2 + 2 MPI (v'-v'')	1 + 1 MPI (v'-v'')
0-0	2-9
1-0	5-13
6-0	6-14
7-0	7-15
1-1	12-23
2-1	12-24
0-3	13-24
0-4	13-25
	14-25
	15-26
	16-27

Multiphoton ionization apparently cannot measure the absolute number densities of the many vibrational levels needed to determine if $N_2(X,v'')$ excites IF or other interhalogens. Some of the reasons for this are that MPI detection shows a nonlinear signal dependence on electrode bias (gain), the gain of the ion collection system changes with gas composition, the microwave-discharge source of $N_2(X,v'')$ produces a large ion background signal, and the MPI detection efficiency is highly dependent upon laser beam position. Multiphoton ionization spectroscopy is, however, a useful tool for surveying the extent of vibrational excitation in $N_2(X,v)$.

2.3.3.3 Two-Photon LIF. Two-photon laser-induced fluorescence (LIF) detection of $N_2(X,v'')$ was studied in Phase I of this program. At that time the fluorescence efficiency of the N_2(a-X) system as a function of pressure was studied. The fluorescence efficiency, ϕ_f, is defined in Equation (37):

$$\phi_f = \frac{k_{rad}}{k_{rad} + \sum_Q k_Q[Q]} \qquad (37)$$

where k_{rad} is the radiative decay rate for the N_2(a-X) transition, which is the reciprocal of the radiative lifetime, and k_Q is the rate coefficient for quenching $N_2(a)$ by species Q. The results from that study are summarized in Figure 32. At that time the fluorescence efficiency was determined to be 1.8 to 3.1 percent. Based on that finding and the problem of PMT saturation caused by VUV emission produced directly in the microwave discharge, two-photon LIF was dismissed as a sensitive $N_2(X,v'')$ detection technique. During the Phase I study the $N_2(X,v'')$ two-photon LIF detection limit was determined to be $\sim 1 \times 10^{13}$ molecules per cubic centimeter.

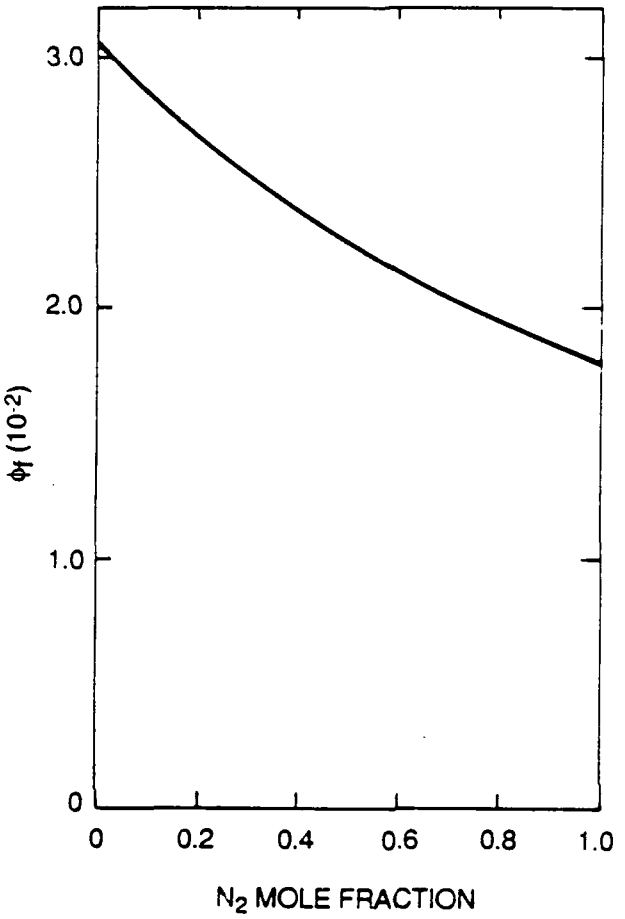

Figure 32. Variation in $N_2(a^1\Pi_g, v'=0)$ fluorescence efficiency as a function of N_2 mole fraction in Ar at 1.0 torr total pressure.

The detection optical train was improved to increase our detection sensitivity. These improvements reduced the VUV background generated by the microwave discharge. This allowed a larger bias on the PMT which increased detection sensitivity. Studies of the $N_2(a)$ lifetime subsequent to the Phase I work showed it to be 56 μs (Ref. 19), shorter than the previously assumed value of 80 μs (Ref. 17). This has resulted in a revised fluorescence efficiency of 2.6 to 4.4 percent. These factors suggested that two-photon LIF might have merit as a detection technique for $N_2(X,v'')$.

2.3.3.4 One-Photon LIF. The technique of one-photon LIF of the $a^1\Pi_g \leftarrow X^1\Sigma_g^+$ system is suitable only for probing $v'' \geq 9$ since laser wavelengths less than $\approx$191 nm otherwise would be required: $a^1\Pi_g(v' \leq 6)$ is excited from the various v'' levels and monitor total, spectrally unresolved fluorescence from the $a^1\Pi_g$ state. The $a^1\Pi_g$ state predissociates at levels above $v' = 6$. For reference, Table 3 contains a few transition wavelengths for the $a^1\Pi_g$ - $X^1\Sigma_g^+$ transition and the appropriate Franck-Condon factors ($q_{v',v''}$). These bands are suitable for one-photon LIF experiments.

Table 3. Selected a←X bands suitable for LIF probing

Band (v′,v″)	λ (nm)	$q_{v',v''}$
2,9	191.1	0.091
2,10	199.0	0.035
2,11	207.4	0.010
3,10	192.8	0.141
3,11	200.7	0.071
3,12	209.2	0.024
4,12	202.5	0.114
4,13	210.9	0.049
5,13	204.2	0.148
5,14	212.7	0.081
6,13	206.0	0.160
6,14	214.5	0.117
6,15	223.6	0.051

Even if calibrating the one-photon technique with the two-photon technique were unsuccessful, one-photon LIF could still be used to obtain information about energy transfer. Measuring population ratios would allow fitting Boltzmann or Treanor distributions to the data, allowing other $N_2(X,v'')$ number densities to be estimated by extrapolation. Table 3 shows that several absorption bands in the wavelength region between 191 nm and 225 nm, have reasonable $q_{v',v''}$ values terminating on $v' \leq 6$. Pumping the same v′ level for each v″ probed would reduce systematic errors in determining population ratios between any two v″ probed because the LIF signal would always originate from the same v′ level. Unfortunately this is difficult to do for the a-X system because of the short wavelength cutoff ($\lambda \sim 191$ nm of the dye laser). However, detection of the a → X LIF signal is accomplished with a solar-blind PMT. This allows all stable levels ($v' \leq 6$) to be viewed. Determining v″ levels redundantly would allow differences in detection efficiency for each v′ to be factored out of the v″ population ratios. Under the experimental conditions used most of the $N_2(a,v')$ will have relaxed to $N_2(a,v'=0)$ (Ref. 95) and differences in detection efficiency will not be a significant source of error.

Electronic quenching is a major concern in applying LIF to the measurement of ground state population distributions. Under the conditions of these experiments the total $[N_2]$ is typically $\sim 6 \times 10^{16}$ molecules per cubic centimeter. The rate coefficient for electronic quenching of $N_2(a)$ by N_2 is (Refs. 14 and 18) 2.1×10^{-11} cm^3 molecule^{-1} s^{-1}. The first order decay rate, therefore, will be about 1×10^6 s^{-1}. For transfer experiments quenchers with number densities $< 10^{15}$ molecules per cubic centimeter will affect the total $N_2(a)$ decay rate minimally even if these species quench $N_2(a)$ with a gas kinetic rate. Consequently the decay of $N_2(a)$ will, in general, be dominated by $N_2(X)$ quenching and diminutions in the observed LIF signal strength will be due to quenching of the probed v″ levels. One-photon

LIF on the a←X system, therefore, appears to be a pontential method for proving the existence of energy transfer from $N_2(X,v'')$ to various other partners.

The first goal of the one-photon LIF study was to obtain spectra of numerous $N_2(a,v'\leftarrow X,v'')$ transitions. Figure 33 shows a spectrum of the (2-9) transition. The spectrum shows the blue-degraded P, Q and R branches typical of one-photon LIF spectra of $N_2(a\leftarrow X)$. Note the good signal-to-noise ratio of the (2-9) band spectrum which was recorded with relatively low laser energies (3 to 5 μJ) at 191 nm. Nitrogen-purged light pipes were needed to prevent atmospheric O absorption of the laser radiation. Previous data from the Penning-ionization study under similar conditions indicated that the $N_2(X,v)$ distribution fit to a 1700 K Treanor distribution. In this case the $N_2(X,v''=9)$ populations would be 1.6×10^{11} molecules per cubic centimeter. Figure 33 has an ~100:1 signal to noise ratio, giving a detection sensitivity of 1.6×10^{9} molecules per cubic centimeter for one-photon LIF. Thus, one-photon LIF is a very sensitive technique for $N_2(X,v''\geq 9)$ detection.

In one-photon LIF the signal intensity should have a linear dependence on laser energy. The intensity dependence of the $N_2(a^1\Pi_g,v'=2 \leftarrow X^1\Sigma_g^+,\ v''=9)$ LIF signal was measured at 2.5 torr N_2 and 100 W of forward microwave power. The probe laser energy was varied by placing 7-54 Corning glass filters in the laser beam before its entry into the flow tube. The data, presented in Figure 34, show that the expected linear dependence on laser energy is obtained.

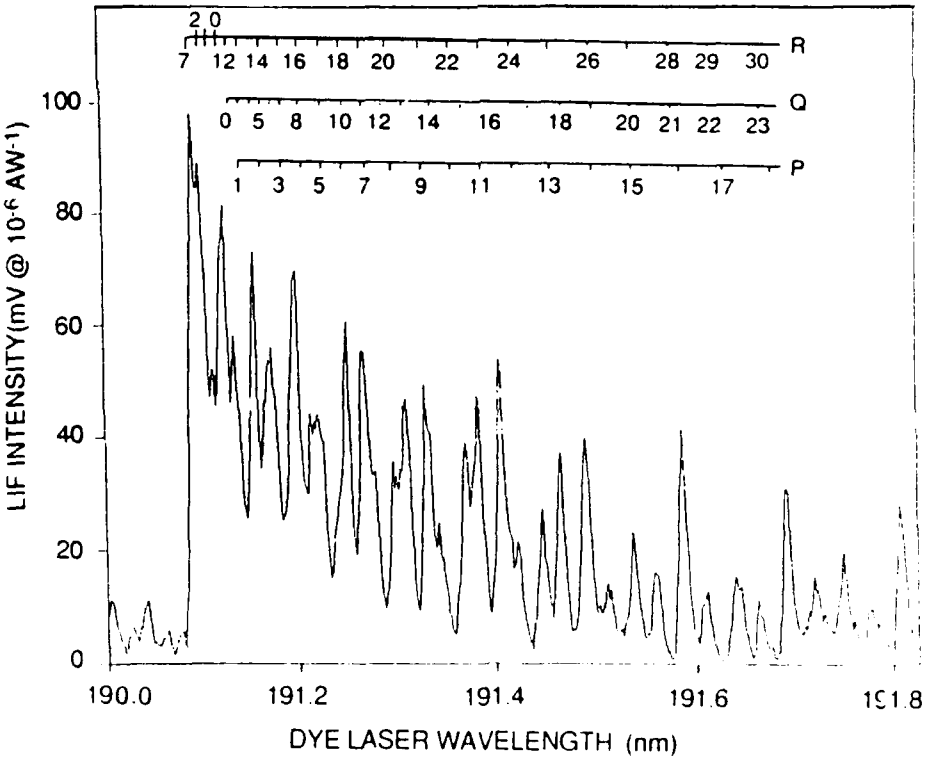

Figure 33. One-photon LIF excitation spectrum of $N_2(a^1\Pi_g,v'=2 \leftarrow X^1\Sigma_g^+,v''=9)$ band.

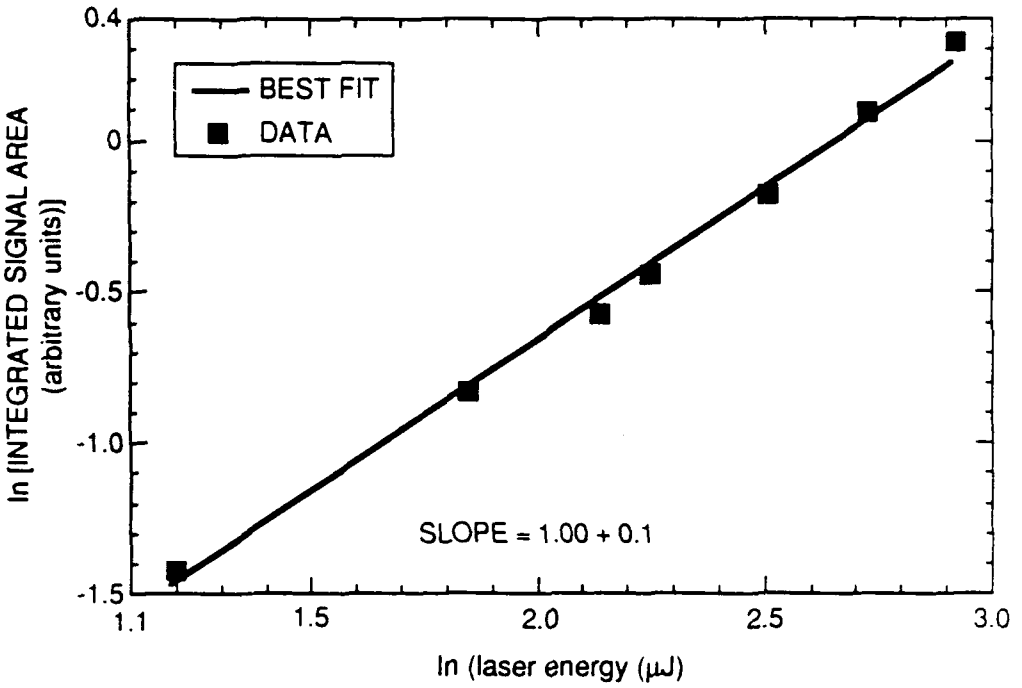

Figure 34. One-photon LIF signal dependence on laser energy.

It was not possible to study the one-photon LIF signal dependence on $N_2(X,v''=9)$ number density. As mentioned earlier there should be a linear signal dependence on $[N_2(X,v'')]$. Because one-photon LIF detection can only be applied to $N_2(X,v''\geq 9)$, exact or relative $N_2(X,v'')$ number densities needed for this study are not available, nor can the $N_2(X,v''\geq 9)$ number densities changing with increasing N_2 flow through a fixed power microwave discharge be predicted. The two-photon LIF work showed a linear dependence of signal on number density and there is no reason to believe the one-photon LIF signal dependence would be any different. Thus a linear one-photon LIF signal dependence on $N_2(X,v'')$ number density is assumed.

One method for studying energy transfer from $N_2(X,v'')$ to another molecule such as IF would be to record $N_2(a)$ fluorescence decays as a function of time. Since under these conditions direct quenching of $N_2(a)$ by IF will not be important (as shown above), quenching of $N_2(X,v'')$ should be observable. A series of plots of LIF intensity versus time with varying amounts of added IF would produce a series of parallel lines with different y-axis intercepts. The y-intercept would give the relative $N_2(X,v'')$ number densities after quenching by IF. This concept is shown in Figure 35. Information from these plots would allow calculation of a rate coefficient for the quenching of $N_2(X,v'')$ by IF.

Figure 36 shows an LIF decay versus time for the (4-13) band. This decay was taken at 2.5 torr N_2 with no added IF. The plot revealed an unexpected problem, a decay that is too fast to analyze with the detection system. Note the rising signal level during the 10 ns laser

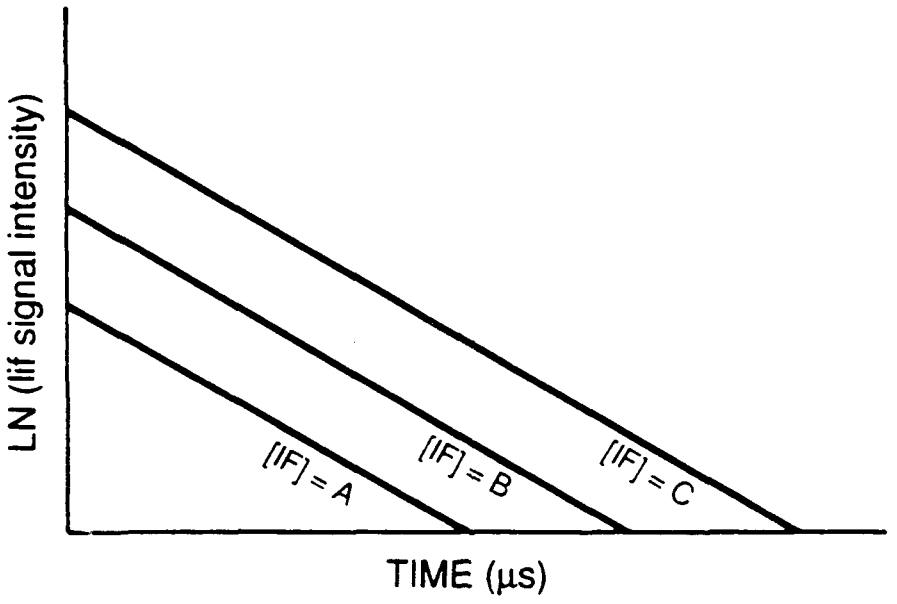

Figure 35. [$N_2(X,v'')$] determination via LIF signal intensity versus time.

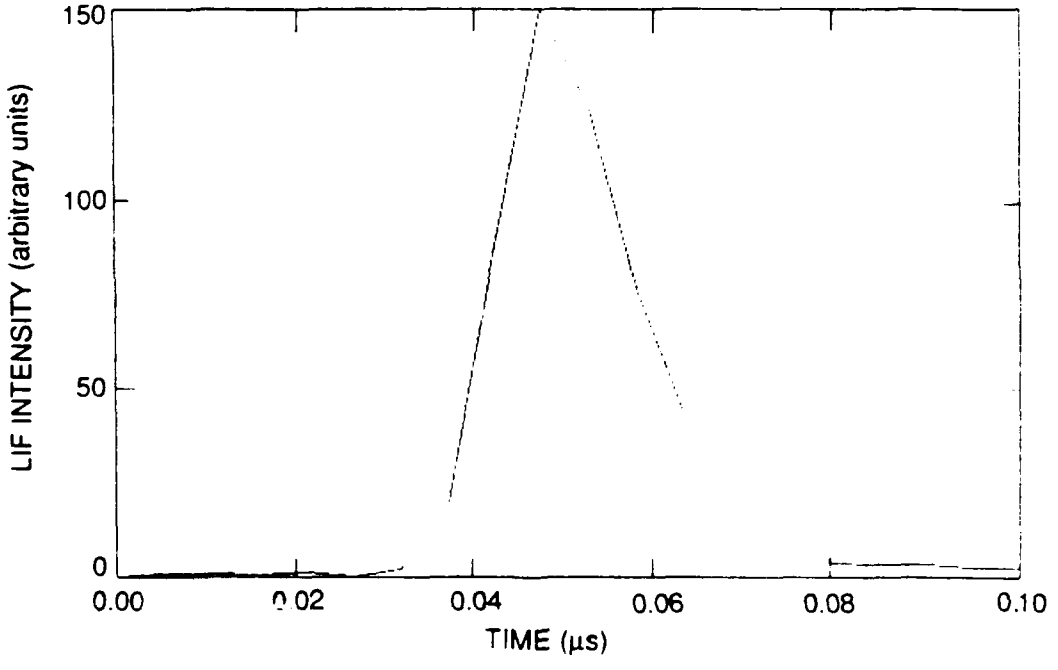

Figure 36. LIF temporal decay of $N_2(a^1\Pi_g, v'=4 \leftarrow X^1\Sigma_g^+, v''=13)$ band.

pulse, and fast decay, ~15 ns. At an N_2 density of 6.4 x 10^{16} molecules per cubic centimeter a decay time of ≈750 ns is expected based on an $N_2(a)$ quenching rate coefficient of 2.1 x 10^{-11} cm^3 $molecule^{-1}$ s^{-1} by N_2 (Refs. 14 and 18). This quenching rate coefficient was measured for $N_2(a,v'=0)$. Figure 36 indicates a decay time of ~15 ns for $N_2(a,v'=4)$. This decay time implies k_Q ~ 8 x 10^{-10} cm^3 $molecules^{-1}$ s^{-1} for quenching of $N_2(a,v'=4)$ by N_2, about 40 times larger than that for $N_2(a,v'=0)$. Field of view effects should not be contributing to the fast decay time. There was also no difference in detection efficiency for the $v' = 0$ and 4 levels. The large difference in the quenching rate constants may be due to collisional pumping of the $a'^1\Sigma_u$ and $w^1\Delta_u$ states. The a, a' and w states form a manifold of nested vibronic levels as they move to $N_2(a^1\Pi_g)$ states higher in energy than $v' = 1$. Previous studies probing $N_2(a)$ quenching concentrated on $v' = 0$ and 1 levels (Refs. 14 and 18). Clearly this measurement is not a comprehensive study of $N_2(a,v'=4)$ quenching by N_2. A different method for determining relative $N_2(X,v'')$ populations needs to be developed. Explaining the large difference in quenching rate coefficients for $N_2(a)$ $v' = 0$ and 4 will require additional work.

The data in Figure 36 can still give relative $N_2(X,v)$ number densities if $N_2(a,v')$ quenching by N_2 is not vibrational level dependent. The integrated area under the curve is a relative measure of the $N_2(X,v'')$ number density. Repeating such measurements for varying amounts of quencher, Q, allows $N_2(X,v)$ quenching kinetics to be studied. The $N_2(X,v'')$ will be quenched by Q and by wall collisions as it flows down the reactor. The rate equation governing the decay of $N_2(X,v'')$ is given by

$$\frac{d[N_2(X,v'')]}{dt} = - k_Q[Q][N_2(X,v'')] - k_{wall}[N_2(X,v'')] \qquad (38)$$

This equation assumes no $N_2(X,v'')$ production following addition of the quencher, Q.

The solution to Equation (38) is

$$\ln \left\{ \frac{[N_2(X,v)]_t}{[N_2(X,v)]_{t=0}} \right\} = - \{k_W + k_Q[Q]\}t \qquad (39)$$

Fixing the reaction time and varying only the quencher number density leads

$$- \frac{d\ln[N_2(X,v)]}{d[Q]} = k_Q l/v \qquad (40)$$

Here the decay time has been replaced by the decay length divided by the flow velocity, l/v. A plot of $\ln[N_2(X,v'')]$ versus Q, as shown in Figure 37, for Q equal to CF_4 and $v''=14$.

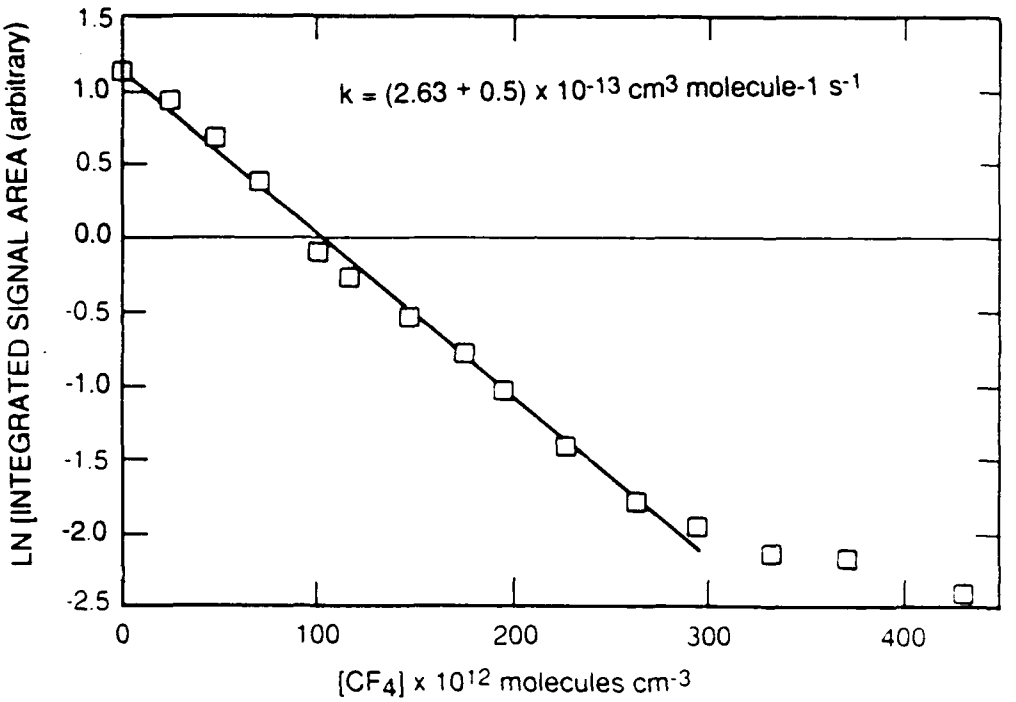

Figure 37. $N_2(X^1\Sigma_g^+, v''=14)$ quenching by CF_4.

The quenching rate coefficient extracted from the data is 2.6×10^{-13} cm^3 molecule^{-1} s^{-1}. Note the flattening of the curve at high CF_4 number densities. This may be due to $N_2(X,v'')$ production in the flow tube after the CF_4 is added, perhaps from N-atom recombination. Subtracting this background from the data gives $k_Q = 3.6 \times 10^{-13}$ cm^3 molecule^{-1} s^{-1}. This may be a lower boundary for k_Q because of feed into $v'' = 14$ from quenching higher levels. This determines only an effective loss rate.

This work does demonstrate that one-photon LIF can be used in kinetic studies involving energy transfer from $N_2(X,v'')$. The reasons one-photon LIF was successful in the previous kinetic study are:

- Technique is nonintrusive
- Higher sensitivity than multiphoton processes
- Signal linear with laser power
- Signal not dependent upon a gain medium.

The last bullet explains why one-photon LIF is quantitative and 1+1 MPI is not. In order to obtain 1+1 MPI signals, the run had to be in a regime where signal gain within the gas was present. This meant the addition of another species into the flow reactor could change the gain. These unpredictable increases or decreases in signal gain forced abandonment of 1+1 MPI as a quantitative tool for $N_2(X,v'')$ kinetic studies.

2.3.3.5 Future Laser-Based Efforts. Future one-photon LIF studies should concentrate on two areas. First the studies on $N_2(X,v'')$ quenching by CF_4 should be repeated under a variety of flow conditions. This would ensure that no experimental artifacts skewed the results. Such a study would allow characterization of this new kinetic tool and predict potential problems which might arise when studying $N_2(X,v'')$ quenching by other species, such as IF.

A second area of study leads back to developing LIF into a quantitative tool for determining absolute $N_2(X,v'')$ number densities. As previously mentioned it may be possible to relate the one-photon and two-photon LIF techniques using a common $N_2(X,v'')$ level. This would allow quantifying the one-photon LIF technique, and determining absolute $N_2(X,v'' \geq 9)$ number densities. If these two techniques cannot be tied together, population ratios of $N_2(X,v'' \geq 9)$ levels would allow fitting Boltzmann or Treanor distributions to the data. If the same experimental conditions are used in a Penning-ionization study, and the same vibrational temperature describes the upper and lower v'' distributions, then extrapolation of the Penning-ionization distribution to describe the $N_2(X,v'' \geq 9)$ levels of the interest in energy-transfer studies will have been proven.

2.3.4 Summary and Conclusions

In the laser-based experiments the usefulness of four $N_2(X,v)$ detection techniques have been rated. These techniques are

1. 2+2 MPI
2. 1+1 MPI
3. Two-photon LIF
4. One-photon LIF.

A direct comparison of 2+2 MPI detection of $N_2(X,v)$ with previous Penning-ionization studies showed that MPI gave quantitative results which were similar to those obtained from Penning-ionization studies, but MPI has a large potential for systematic errors. Problems with the effects of laser beam position and low sensitivity ($\sim 2.5 \times 10^{14}$ molecules cm^{-3}) have discounted 2+2 MPI as a useful quantitative tool for $N_2(X,v'')$ energy transfer studies.

Examination of 1+1 MPI spectroscopy showed it to be much more sensitive than 2+2 MPI. There is an estimated detection limit on the order of 10^8 molecules per cubic centimeter. The 1+1 MPI technique could be used only to detect $N_2(X,v'' \geq 9)$, while 2+2 MPI could only be used to detect $N_2(X,v'' \leq 4)$. This prevents 1+1 MPI from being a quantitative technique for the detection of $N_2(X,v'')$. The problem of signal level dependence on laser beam position and signal gain within the gas forced abandonment of 1+1 MPI as a relative quantitative tool for $N_2(X,v'')$ detection even on a relative basis. It is a sensitive technique, however, for identifying highly vibrationally excited $N_2(X,v'')$ within a gas stream.

Two-photon LIF via the $N_2(a)$ state was investigated in the Phase I study of $N_2(X,v'')$ detection. At that time it was discounted as a quantitative tool due to quenching of the $N_2(a)$

state and thus low fluorescence efficiency, ϕ_f. Also problems with PMT saturation caused by VUV emission from the microwave discharge led to rejection of two-photon LIF. Since that study the detection system has been redesigned and the VUV background emission has been eliminated from the microwave discharge. In the Phase I study the detection limit was 10^{13} molecules per cubic centimeter. Now it may be possible to extend this limit to the 10^{11} or 10^{12} range and anchor one-photon LIF to two-photon LIF.

One-photon LIF has been used to detect $N_2(X,v'' \geq 9)$. The detection limit is estimated to be on the order of 10^9 molecules per cubic centimeter. One-photon LIF can be used to determine relative $N_2(X,v'')$ number densities quantitatively. These experiments used it to determine a rate coefficient for $N_2(X,v''=14)$ quenching by CF_4 of 3.6×10^{-13} cm^3 $molecule^{-1}$ s^{-1}.

3.0 QUANTITATIVE CORRELATIONS

The work on quantitative correlations required first the development of quantitative diagnostic techniques. Penning ionization appeared to be the most straightforward diagnostic to implement quantitatively, so this was done. It is described in detail in Subsection 2.1.

After developing the quantitative Penning-ionization diagnostic, similar techniques were used to quantify $N_2(X,v)$ measurements using 2+2 MPI. While the 2+2 MPI is the least sensitive of the laser-based diagnostics, it is the one which quantifies most easily. The effluents of a 70 W microwave discharge in pure N at 2.5 torr pressure were observed.

THe initial experimental efforts using 2+2 MPI as a quantitative tool for determining $N_2(X,v'')$ number densities, employed the 2.5 cm diameter flow reactor where PSI had previous experience in obtaining 2+2 MPI spectra. These scans had two important functions, the first was to calibrate the dye laser wavelength. The second was to set the dye laser wavelength at a frequency corresponding to an intense transition of the band system of interest $N_2(a,v'=0) \leftarrow N_2(X,v''=0)$. Conditions in the 5 cm diameter flow reactor could then be optimized for the largest ionization signal.

The proof-of-principle experiment was run in the 5-cm diamter flow reactor. With the laser wavelength corresponding to the (0-0) transition frequency the N_2 gas flow and reactor pressure was adjusted until an ionization signal was detected. These parameters were similar to those used in a preceeding Penning-ionization experiment. The results of the two studies, therefore, could be compared. With no microwave discharge, 2.5 torr of N_2, +90 V electrode bias, and 11.5 mJ laser energy, a spectrum of the $N_2(a,v'=0) \leftarrow N_2(X,v''=0)$ band was recorded. Then a second scan was recorded under the same conditions except with a 70 W microwave discharge ignited. Figure 38 displays these two spectra. Note that the two spectra are slightly power-broadened. The dark trace shows the spectrum with no microwave discharge, the light trace shows the spectrum recorded with 70 W forward microwave power. The small drop in signal with the microwave discharge ignited indicates that a fraction of the ground state N molecules have been excited out of the zeroth vibrational state to $N_2(X,v''>0)$. The difference in the areas under the S and R branch bandheads of each of these spectra revealed that 16 percent of the N had been excited from $N_2(X,v''=0)$. Some of the $N_2(X,v''=0)$ may have been dissociated into N-atoms in the microwave discharge, but the fractional dissociation of molecular N is almost certainly below a percent. Following this test, a spectrum of the $N_2(a,v'=1 \leftarrow X,v''=1)$ band was recorded under the same conditions with a 70 W microwave discharge. Figure 39 shows this spectrum. Note that the intensity units of the ordinate are a factor of ten smaller than those in Figure 38. Again the area under the S and R bandheads was integrated so that it could be compared to that of the (0-0) transition.

Using the (0-0) band data with no microwave discharge, the exact $[N_2(X,v''=0)]$ is known from the flow rates and chamber pressure. From the integrated signal area, the laser energy and the Franck-Condon Factor for the 0-0 transition a calibration factor, ζ, can be defined. This calibration factor relates ionization signal levels to number densities for a specific

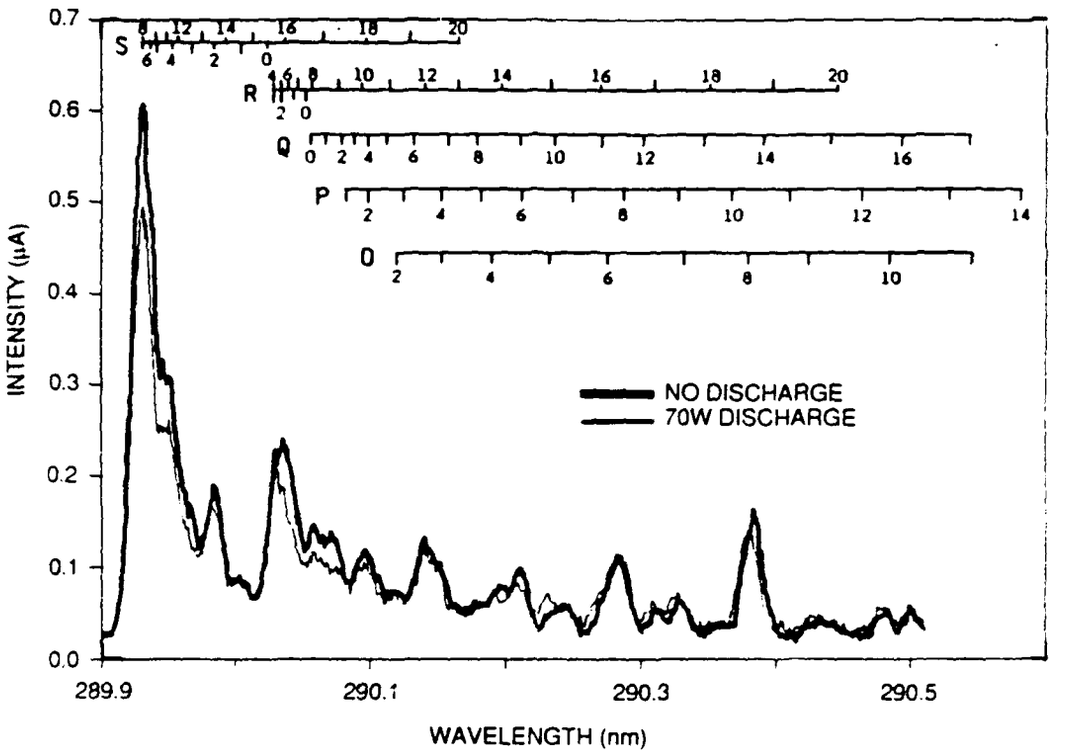

Figure 38. The 2+2 MPI spectrum of the $N_2(a^1\Pi_g, v'=0 \leftarrow X^1\Sigma_g^+, v''=0)$ band, overlay with 70 W microwave discharge and without microwave discharge.

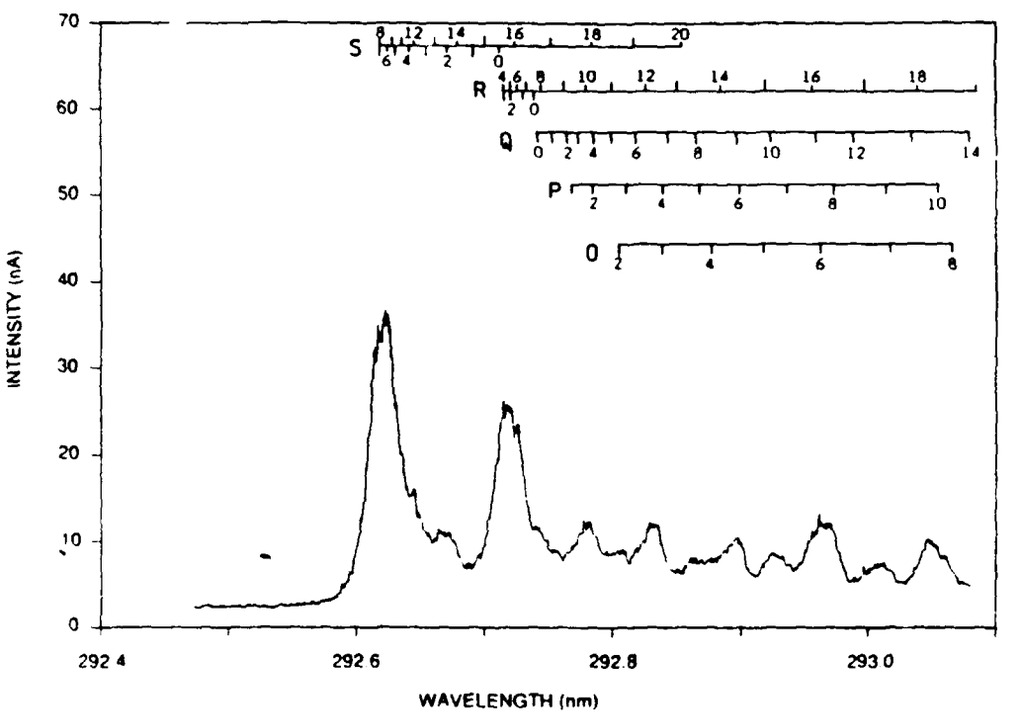

Figure 39. The 2+2 MPI spectrum of $N_2(a^1\Pi_g, v'=1 \leftarrow X^1\Sigma_g^+, v''=1)$ band, 70 W microwave discharge production of $N_2(X^1\Sigma_g^+, v''=1)$.

transition, by correcting for difficult to quantify effects such as electrode collection efficiency and laser beam geometry. This calibration factor can be used with other transitions to obtain information on $N_2(X,v'')$ number densities if the Franck-Condon factors, $q_{v'v''}$, and the experimental laser energies are known. The Franck-Condon factors, $q_{v'v''}$, and laser energies, I_{laser}, account for the fact that not all transitions have the same probability of occurring, and that different transitions are recorded at different laser energies. Equation (41) defines the calibration factor:

$$\zeta = [N_2(X,v''=0)]q_{00}\frac{I_{laser}^2}{I_{signal}} \tag{41}$$

(squared energies are used because the rate-limiting step requires two-photons (Refs. 20, 91-94). A given number of molecules will give a specific signal area at a fixed laser energy and transition probability. When the discharge is turned on and a new signal area is determined for the (0-0) band, this area only needs to be multiplied by the calibration factor to determine the new $[N_2(X,v''=0)]$:

$$[N_2(X,v''=0)]_{discharge\ on} = \frac{\zeta\, I_{signal}^{v=0}}{q_{00}\, I_{laser}^2} \tag{42}$$

The number density of $N_2(X,v''=1)$ is calculated similarly:

$$[N_2(X,v''=1)] = \frac{\zeta\, I_{signal}^{v=1}}{q_{11}\, I_{laser}^2} \tag{43}$$

Table 4 summarizes these data with calculated $N_2(X,v'')$ number densities.

The $N_2(X^1\Sigma_g^+,v'')$ population ratios shown below are used to calculate a Boltzmann vibrational temperature of 1300 K.

$$\frac{[N_2(X,v''=0)]_{discharge\ on}}{[N_2(X,v''=0)]_{discharge\ off}} = 0.84$$

$$\frac{[N_2(X,v''=1)]_{discharge\ on}}{[N_2(X,v''=0)]_{discharge\ off}} = 0.08$$

Table 4. The $N_2X^1\Sigma_g^+$ vibrational populations

Computed from MPI Signal Areas, Anchored to $N_2X^1\Sigma_g^+$,v″ = 0 MPI Signal Levels				
Flow Tube Conditions:		N_2 Flow = 5.84 x 10^{16} molecules cm^{-3} Pressure = 2.5 torr Bulk Flow Velocity = 80 cm s^{-1}		
v″	Discharge Condition	MPI Signal Area	Actual [N_2]	Calculated [N_2,v]
0	Off	5.70 nm-mV	5.84 x 10^{16} cm^{-3}	5.84 x 10^{16} cm^{-3}
0	On	4.81 nm-mV	Unknown	4.93 x 10^{16} cm^{-3}
1	On	0.472 mm-mV	Unknown	3.92 x 10^{15} cm^{-3}

There are a number of potential sources of error in the data presented above. The first and most obvious statistical error has already been mentioned. The uncertainty in the data is ≈25 percent. This study was only a two point determination to show proof of principle, and as such serves its purpose.

Other systematic sources of error stem from the physical process which is being measured. The MPI signals should show a linear dependence on [N_2], a squared dependence on laser energy for a 2+2 MPI process, and no dependence on electrode bias to prevent signal gain in the flowing gas mixture.

Probing the discharge effluents using Penning ionization gave similar results. The Penning-ionization measurements indicated that 79 percent of the N in the effluent remained in the zeroth vibrational level, and that the ratio of the number density of $N_2(X,v=1)$ to that of $N_2(X,v=0)$ was 0.14. Given the experimental errors involved, these values agree reasonably well with the laser-based measurements. Table 5 summarizes the results of the quantitative correlation measurements.

Table 5. Comparison of $N_2(X,v)$ detection by MPI versus Penning ionization

	MPI	Penning
$\frac{[N_2X,v''=0 \text{ Discharge On}]}{[N_2X,v''=0 \text{ Discharge Off}]}$	0.84	0.79
$\frac{[N_2X,v''=1]}{[N_2X,v''=0]}$	0.08	0.14
Vibrational Temperature	1300 K	1700 K

4.0 SOURCE CHARACTERIZATION

Both discharge and chemical sources of $N_2(X,v)$ were characterized using the Penning-ionization diagnostic. The discharge sources examined included microwave (2.54 GHz), rf (13.56 MHz), hollow-cathode, direct current, and dielectric-barrier. The dielectric-barrier discharge is essentially a low-power, ac discharge. Only the microwave and rf discharges generated measurable $N_2(X,v)$, with the microwave discharge being somewhat more efficient. Fairly low power microwave sources can produce copious quantities of $N_2(X,v)$ under appropriate conditions. For example, in the effluents of a 3 percent N in He discharge at 50 W, well over half of the $N_2(X,v)$ is vibrationally excited.

Several chemical sources of $N_2(X,v)$ were also investigated including the reaction of N with NO, the recombination of N_3 radicals, and the N formed in the sequence of reactions that begin by adding H-atoms to NF_2. Because of a number of interferences, the Penning-ionization diagnostic could not be used to examine the last reaction even though the H + NF_2 reaction most likely produces $N_2(X,v)$. It was quite successful for the first two reactions, however, and showed that the reaction of N with NO generates an inverted vibrational distribution, while the recombination of N_3 radicals generates a vibrational distribution similar to a Treanor distribution which has an effective vibrational temperature of 3300 K.

4.1 CHARACTERIZATION OF DISCHARGE SOURCES OF $N_2(X,v)$

4.1.1 Characterization of a Microwave Discharge Source

The vibrational distribution of ground-state N molecules exiting a microwave discharge through a flowing mixture of N diluted in He was characterized. Effects investigated included variations with discharge power, mole fraction of N in the discharge, and flow time between the discharge exit and the observation region.

Figure 40 shows how the effective vibrational temperature, as determined from the modified Treanor distribution, varies as a function of discharge power. Below 20 W, the modified Treanor did not describe the $N_2(v)$ distribution accurately. As discussed, the higher vibrational levels were somewhat more populated than expected based upon the populations in $v' = 0$ and 1. The presence of the Ni screen in the flow does appear to reduce the vibrational temperatures somewhat at the higher discharge powers, but some of this effect might result from the screen's having removed ions and other metastables from the flow. Figure 41 illustrates the growth in the fraction of the total N that is vibrationally excited as a function of discharge power. Above about 50 Watts, nearly two-thirds of the nitrogen is vibrationally excited. The microwave discharge, therefore, is a very efficient source of $N_2(X,v'')$.

Figure 42 demonstrates that the highest effective vibrational temperatures result from mole fractions in the discharge on the order of 0.01. As the N becomes progressively more concentrated, the effective vibrational temperature cools. Figure 43 shows how the absolute

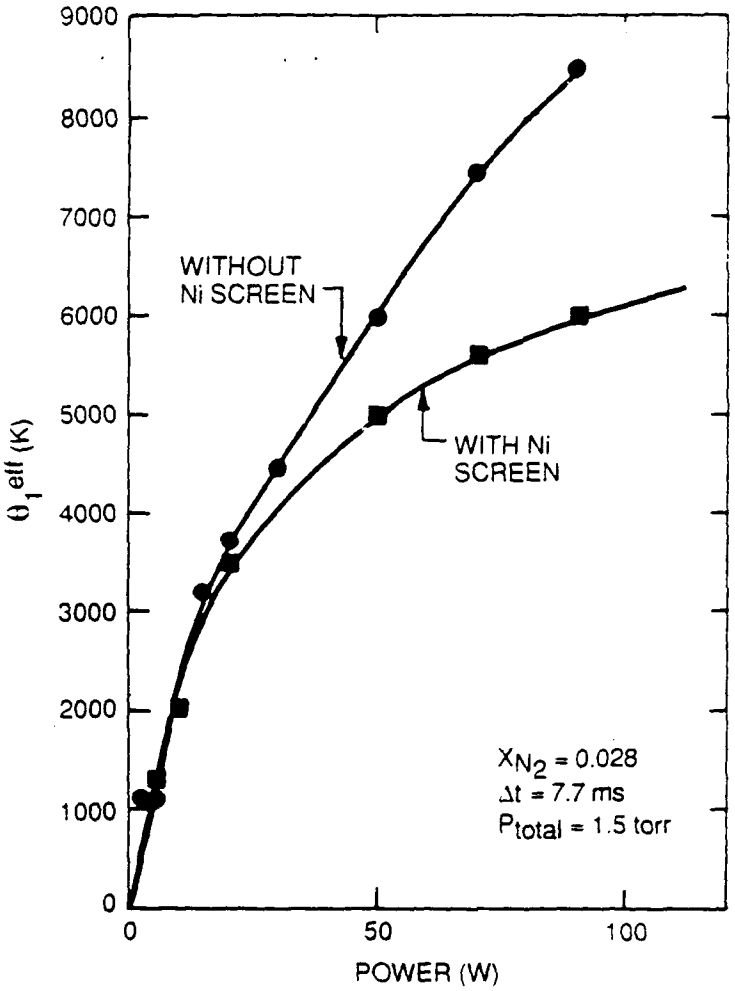

Figure 40. Variation in effective N vibrational temperature as a function of discharge power.

number densities in the various vibrational levels vary with N mole fraction in the discharge. The cooling effect at the largest mole fraction is enough to give comparable or perhaps even somewhat lower number densities in vibrational levels 4 and above than is the case for only half as much total N through the discharge.

Figure 44 shows that very little cooling of the N occurs as it flows down the tube for times up to 30 ms. In other words, quenching of $N_2(v)$ appears to be only a minor channel. The open points were taken under the same conditions, but at different positions along the flow reactor.

The filled points resulted from throttling the pump to reduce the flow velocity by almost a factor of 4. The other effect of throttling the pump was to raise the total pressure, and thus N partial pressure a like amount. The major factor determining the effective vibrational temperature of N in the discharge, therefore, appears to be N mole fraction rather than N partial pressure. Data at higher mole fractions than shown in Figure 44 show a similar

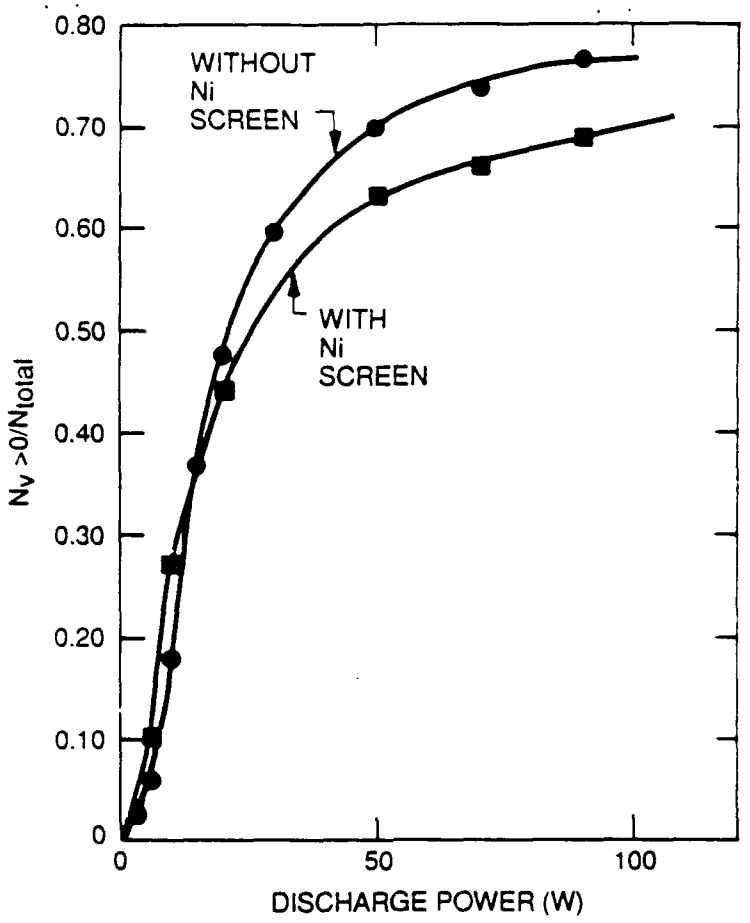

Figure 41. Fraction of total N that is vibrationally excited as a function of discharge power.

trend: only a very moderate vibrational cooling with flow time. Also, $N_2(X,v'')$ number densities in excess of 10 mtorr were produced using this simple discharge technique.

4.1.2 Characterization of Radio Frequency Discharge Effluents

The rf discharge has characteristics similar to the microwave discharge, except that somewhat higher power levels are required to achieve comparable excitation rates. Figure 45 illustrates this point. It compares how the effective $N_2(X,v)$ vibrational temperature of the effluents of radio frequency and microwave discharges vary with discharge power. A 50-W rf discharge generates only as much as $N_2(X,v)$ as does a 20-W microwave discharge, while $\approx$120 W of rf power are necessary to excite $N_2(X,v)$ to levels comparable to that found in a 50-W microwave discharge. Figure 46 shows the variation in effective $N_2(X,v)$ vibrational temperature as a function of N mole fraction in the discharge. The rf discharge behavior is quite similar to that of the microwave discharge. Here again, however, comparable excitation rates can only be achieved if the rf discharge runs at a somewhat higher power than the microwave discharge.

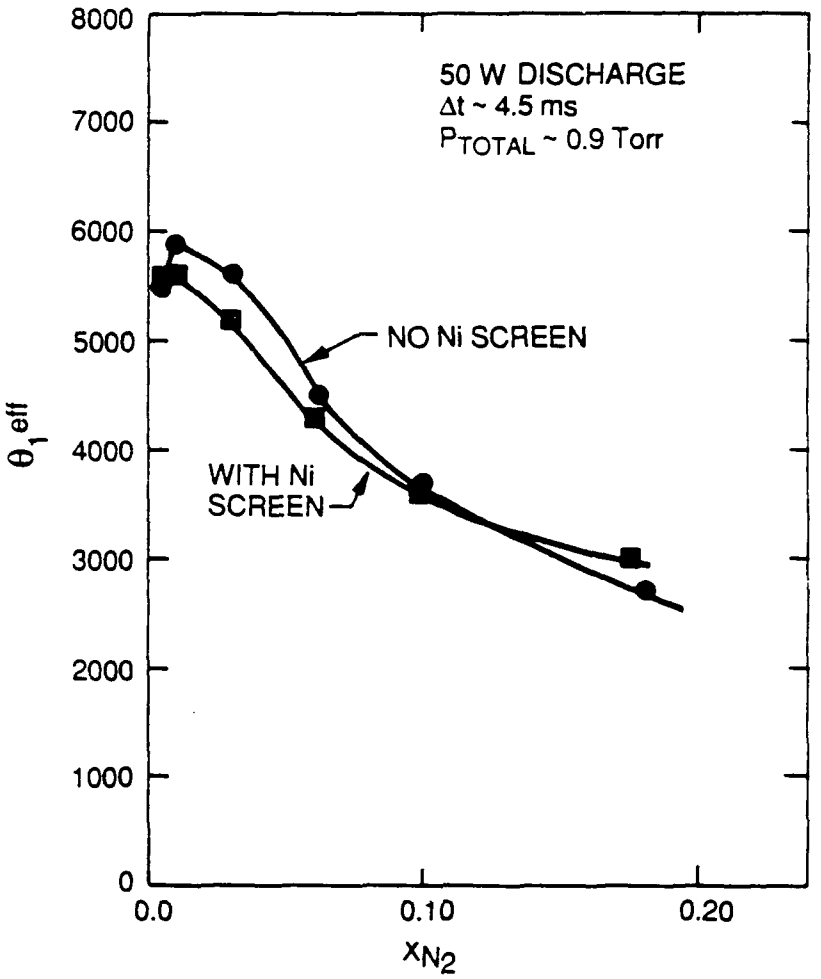

Figure 42. Variation in effective vibrational temperature with nitrogen mole fraction.

4.1.3 Dielectric Barrier and dc Discharges

Penning-ionization spectra taken in the afterglow of dielectric-barrier or dc discharges were identical to those with the discharges off. This result indicates that ≥ 98 percent of the N in the afterglow is in v″ = 0. This null result may not be all that surprising since both discharges operate powers of a few watts or less. Both sources, when operated properly, however, are reasonably efficient sources of electrically excited metastable N in the $A^3\Sigma_u^+$ state.

4.1.4 Discussion

Microwave discharges through N_2/He mixtures are efficient sources of $N_2(X,v)$. The vibrational distribution of the discharge effluent is best characterized by a modified Treanor distribution, with effective vibrational tempertures about 6000 K for 50 W of power and a N mole fraction of 0.01 to 0.02.

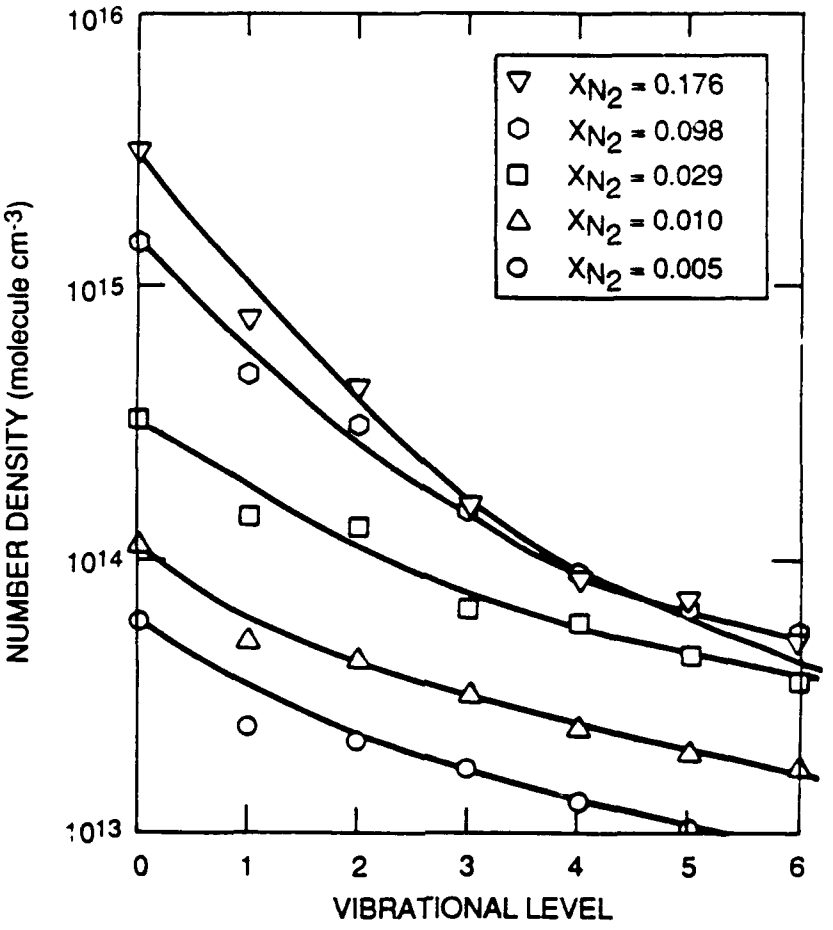

Figure 43. Variation in vibrational level number densities with N mole fraction through the discharge. P_{tot} ~ 0.9 torr, Δt ~ 4.7 ms, 50 W discharge.

The effective vibrational temperature correlates strongly with discharge power and shows a weak inverse dependence on N mole fraction for mole fractions in excess of 0.02. For discharge powers in excess of 50 W, roughly two thirds of the molecular N is vibrationally excited. The measurements show only a weak cooling of the $N_2(v)$ with transit time from the discharge, for times <30 ms.

Placing a Ni screen across the flow downstream from the discharge, deactivates electronically excited N metastables, such as $N_2(A^3\Sigma_u^+)$, $N_2(a'^1\Sigma_u^-)$, $N(^2D,^2P)$, and recombines the N atoms. The Ni screen reduces the effective vibrational temperature of the N only slightly. This configuration, therefore, provides a fairly clean source of $N_2(v)$ for kinetic studies.

The amount of reduction of the metastable and atomic number densities depends, as might be expected, upon the mesh size of the Ni screen and the contact time of the screen with the gas. For one configuration in which two 7-cm long coaxial, cylindrical, 60-mesh Ni screens

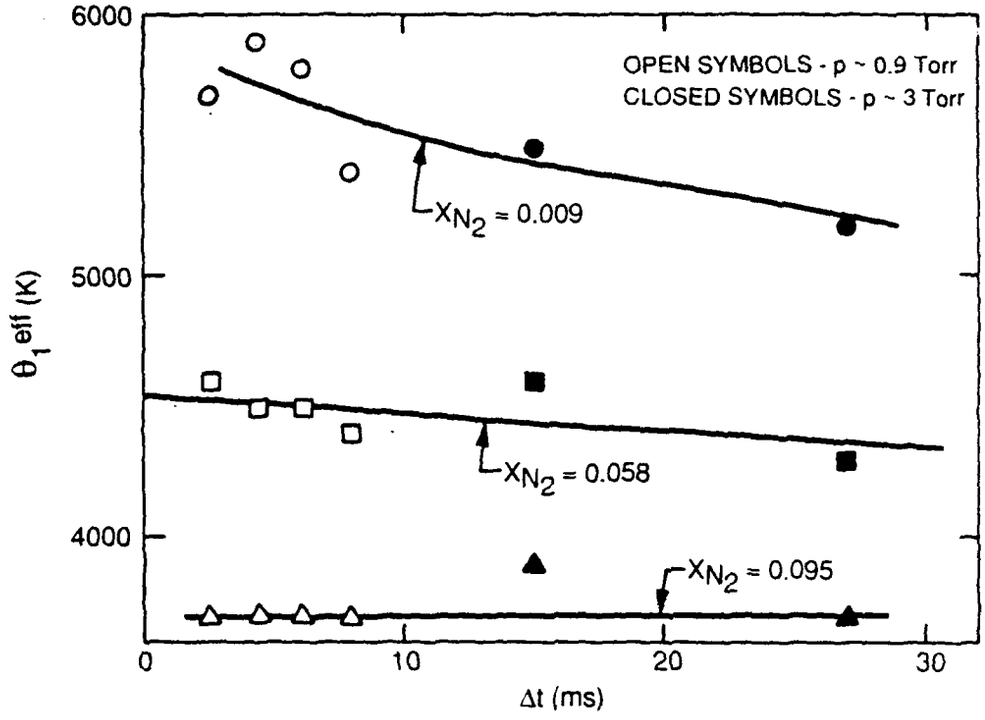

Figure 44. Variation in effective N vibrational temperature with flow time from the discharge. Open symbols, p ~ 0.9 torr; closed symbols, p ~ 3 torr.

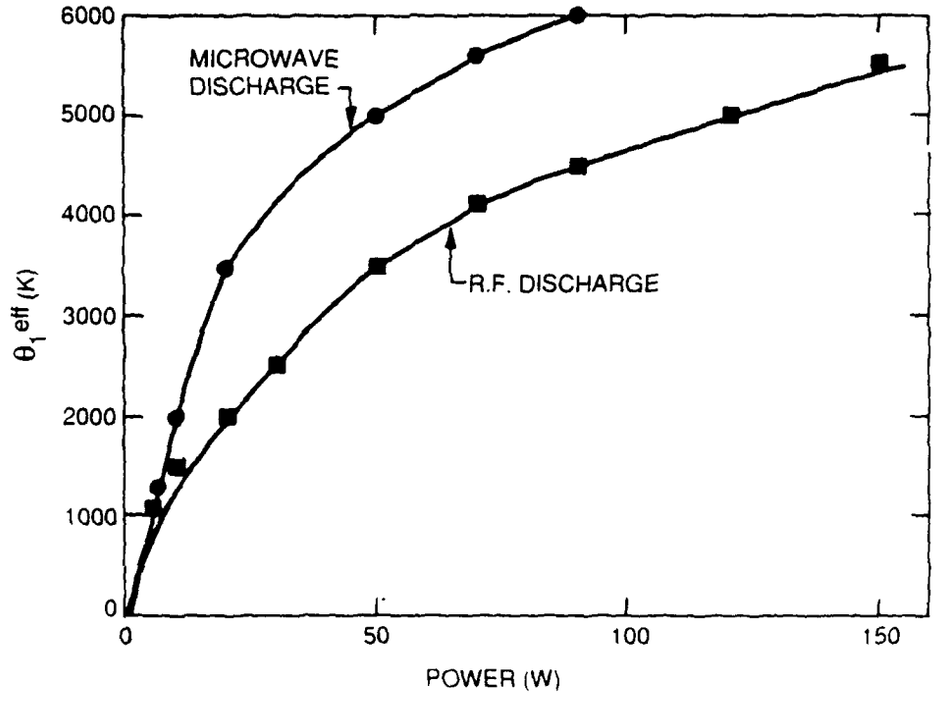

Figure 45. Variation in effective vibrational temperature of $N_2(X,v)$ as a function of discharge power for microwave and rf discharge.

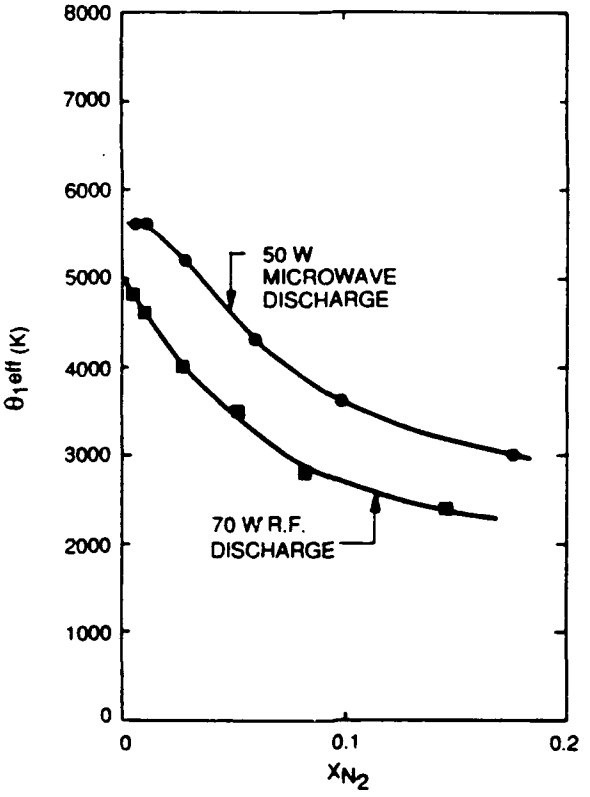

Figure 46. Variation in effective vibrational temperature of $N_2(X,v)$ as a function of N mole fraction for a 50-W microwave discharge and a 70-W rf discharge.

were placed downstream from a microwave discharge through N_2/He mixtures, there was a 60-fold reduction in the N-atom number density and a reduction in $N_2(A)$ number density of over two orders of magnitude with the screen in place as compared to conditions with it removed. In another series of tests, a circular double screen of 16 mesh Ni which could be rotated either to fully cover the cross-sectional area of the flow tube or to be parallel to the axis of the flow tube was used. When a flow of $N_2(A)$ was generated in the absence of N-atoms, there was a factor of 30 reduction in the $N_2(A)$ number density when the screen was perpendicular to the flow-tube axis compared to placing the screen parallel to the flow. When the $N_2(A)$ was accompanied by nitrogen atoms, however, the reduction in the $N_2(A)$ number density was diminished only a factor of 6 when the Ni screen was rotated from the parallel position to be perpendicular to the flow. This last observation may be evidence that $N_2(A)$ is produced in the recombination of N-atoms on Ni.

4.2 CHARACTERIZATION OF CHEMICAL SOURCES OF $N_2(X,v)$

4.2.1 Introduction

A Penning-ionization diagnostic (Ref. 2) has been used to investigate the production of $N_2(X,v'')$ in the following chemical systems:

$$N + NO \rightarrow N_2(v \leq 12) + O \qquad (44)$$

$$H + NF_2 \rightarrow HF + NF(a^1\Delta) \quad (45a)$$

$$NF(a^1\Delta) + H \rightarrow HF + N(^2D) \quad (45b)$$

$$N(^2D) + NF(a^1\Delta) \rightarrow N_2(v \leq 45) + F \quad (45c)$$

$$N_3 + N_3 \rightarrow 3N_2(v \leq 40) \quad (46)$$

$$N + N_3 \rightarrow N_2(X, v \leq 45) \ . \quad (47)$$

Only reaction (44) has been shown previously to produce $N_2(X,v)$ (Refs. 98-100), although its vibrational distribution has never been established. Morgan, Phillips and Schiff (Ref. 98) detected $N_2(X,v)$ from reaction (44) in the form of excess heat given off to a catalytic probe in their flow reactor. They estimated an average energy of 21 kcal mole^{-1} in vibration. Black et al. (Ref. 99) detected $N_2(X,v=1)$ produced from reaction (44) using laser Raman spectroscopy. Van Lonkhuyzen and de Lange (Ref. 100) detected $N_2(X,v)$ from reaction (44) using HeI photoelectron spectroscopy. Their observations led them to infer substantial excitation of $N_2(X,v'' \geq 4)$.

No one is known to have observed directly the production of $N_2(X,v)$ from the other three reactions. Reactions (45) and (47) produce $N_2(B^3\Pi_g)$ efficiently (Refs. 6 and 101). One might expect that efficient quenching of the $N_2(B)$ would result in $N_2(X,v)$ production.

Reaction (46) appears to produce $N_2(B)$ rather inefficiently, if at all (Ref. 102). In addition, $N_2(A)$ appears not to be a major product. Given that the reaction releases 8.8 eV of energy (Ref. 103), one would anticipate that much of this energy would appear as vibration.

The procedure and theory behind Penning-ionization experiments has been discussed in detail previously (Ref. 2). In brief, the interaction between He metastables and N_2 results in Penning ionization of the N_2 into the B-state of the molecular ion. The resulting fluorescence spectrum is analyzed to determine the vibrational distribution of the ground state, neutral N molecules. Because Penning ionization is a vertical process, the vibrational distribution of the product ions is determined solely by the vibrational distribution of the reactant molecules and the Franck-Condon factors which couple the two states. Often, a modified Treanor distribution represents the ground-state distribution (Refs. 2, 34, and 35). Using this model, one can vary the ground-state vibrational temperature until calculated excited-state distributions agree with observations. The best-fit vibrational temperature determines the relative populations in the different levels of ground state N_2. In order to place this relative distribution on an absolute basis, the total amount of N_2 produced in a specific reaction is determined either by a titration reaction or by calibration with a known amount of N_2.

4.2.2 Experimental

The apparatus configurations for these experiments are shown in Figure 47. The basic apparatus is a 5-cm diameter flow tube coated with halocarbon wax and pumped by a Roots blower. Flow rates of all species are determined by calibrated electronic mass flow meters and the pressure is determined by a 0- to 10-torr capacitance manometer. Flow velocities range from 500 to 5300 cm s^{-1}.

Gas purification was accomplished with a glass prepline outfitted for trap-to-trap distillation and purified gases were stored in glass bulbs. In these experiments only the He and NO required purification. The NO was passed through an ascarite trap, then a methanol/liquid N_2 slush bath before storage in a bulb and He was passed through a liquid-N-cooled, molecular-sieve trap before flowing through the flow meters.

4.2.3 $N_2(v)$ Production from the N + NO Reaction

Reaction (44),

$$N + NO \rightarrow N_2(v \leq 12) + O \qquad (44)$$

is exothermic by 3.23 eV and is therefore capable of exciting the N_2 product up to $v = 12$. The N-atoms were produced in a 70 W discharge of 25 percent N_2/He mixtures, and a 10 percent NO/Ar mixture was injected downstream from the discharge (Figure 47(a)). Pressures in the flow tube ranged from 0.8 to 3.8 torr. A glass wool plug, placed between the discharge and the rest of the flow tube, was fairly effective in relaxing vibrationally excited N_2 produced in the discharge. The maximum N-atom density produced from this discharge was 3×10^{13} molecules per cubic centimeter.

For maximum sensitivity, the ratio of N-atoms to N_2 in the discharge needs to be as high as possible to be able to make a clear distinction between N_2 produced in the reaction and N_2 already present in the flow. To increase this ratio, trace amounts of SF_6 were used. This additive increases the rate of N_2 dissociation in microwave discharges (Ref. 104). Adding the SF_6 increased the N/N_2 ratio from 0.1 to 0.3.

Since O-atoms are produced as well as N_2 in this reaction, they can react with excess NO reactant giving the NO/O afterglow, a continuum emission from 375 to 3000 nm (Ref. 49-55). In order to avoid this, N-atoms are titrated with the reactant NO to determine the point at which the added [NO] just equaled the initial [N]. This titration procedure is well known (Ref. 6). In brief, N-atom recombination produces chemiluminescence from the N_2 first-positive bands. The intensity of emission, observed at 580 nm, is proportional to the square of the N-atom number density. Upon adding NO, the first-positive emission decreases until the quantity of NO added balances the amount of N initially in the flow. At this point, the end point of the titration, all N initially in the reactor is converted to O, and no emission is observed. As further NO is added to the reactor, the afterglow emission begins to be observed, and the intensity of the emission varies linearly with the amount of

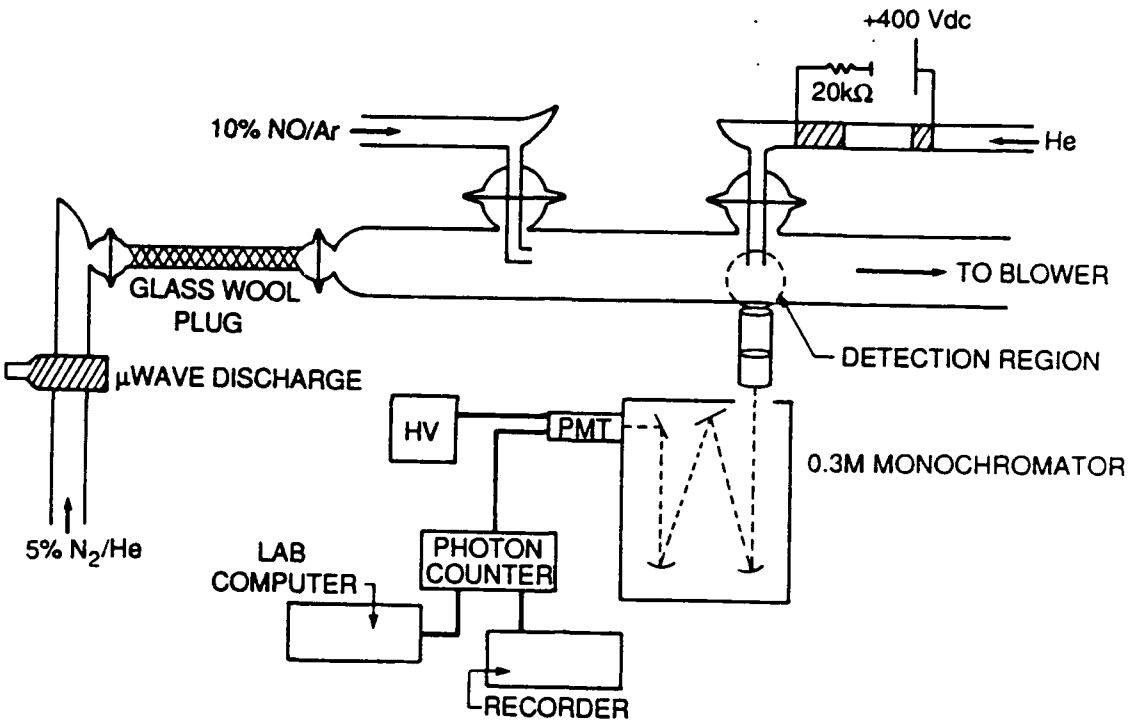

(a) N + NO Reaction

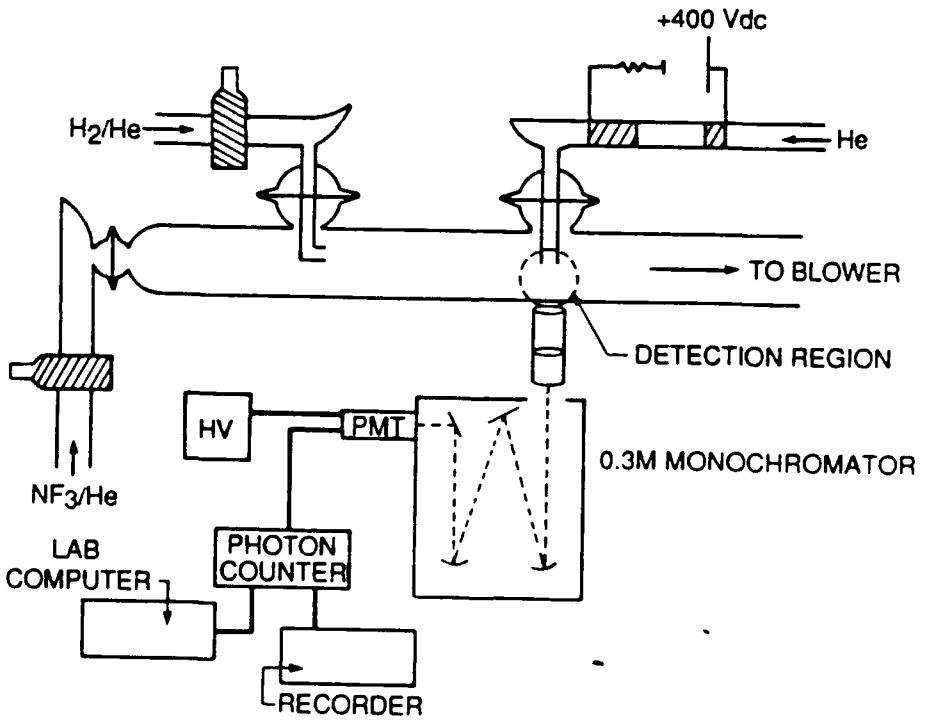

(b) H + NF_2 Reaction

Figure 47. Flow reactor configurations.

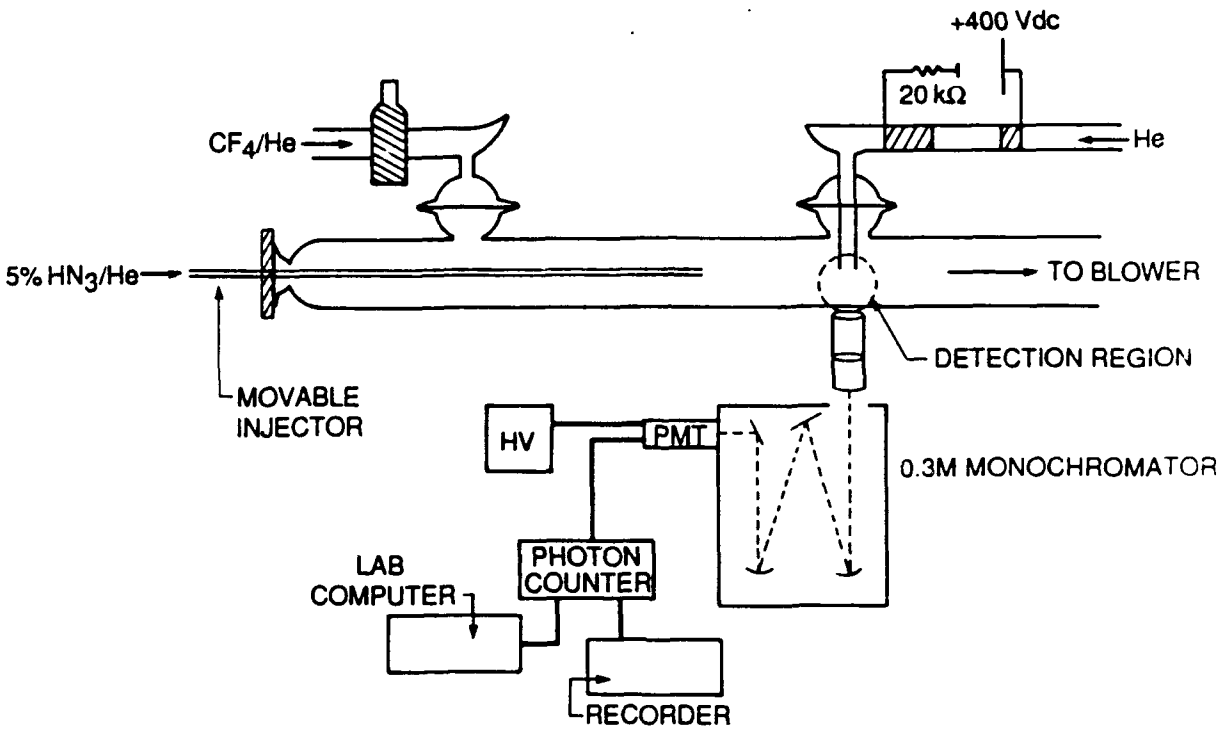

(c) N_3 Recombination

Figure 47. Concluded.

NO added. A typical titration plot is shown in Figure 48. The end point of the titration, then, gives the amount of NO necessary to consume the N-atoms completely.

In the preliminary investigations of this reaction, operations were not at the end point of this titration in some cases. In taking care not to overshoot the end point, too little NO was added. This resulted in unreacted N-atoms interacting with product O-atoms to produce NO(B-X) chemiluminescence which fluoresces in the same spectral region as the N_2^+(B-X) Penning-ionization signal. This extraneous emission interferes with analysis of the Penning-ionization spectra. Care was taken, therefore, to ensure that the NO concentration that was added was precisely the same as the initial N-atom concentration, thus eliminating the extraneous NO(B-X) emission.

Following a titration experiment, the appropriate amount of NO is reacted with the N-atoms. The product N_2 is detected by Penning ionization, where He metastables excite ground state N_2 to the B-state of the molecular ion. The resultant first-negative emission, $N_2^+(B^2\Sigma_u^+ - X^2\Sigma_g^+)$ is then observed from 440 to 470 nm. Since undissociated N_2 will also be detected, spectra are taken in the presence and absence of NO, as shown in Figures 49 and 50. Clearly, a significant amount of $N_2(X,v)$ is being produced as indicated by the increased intensity of the higher vibrational levels. The vibrational distribution of the $N_2(X,v)$ as determined by analytical procedures (Ref. 2) is shown in Figures 51 and 52. This distribution cannot be characterized by either a Treanor or a Boltzmann distribution, so the

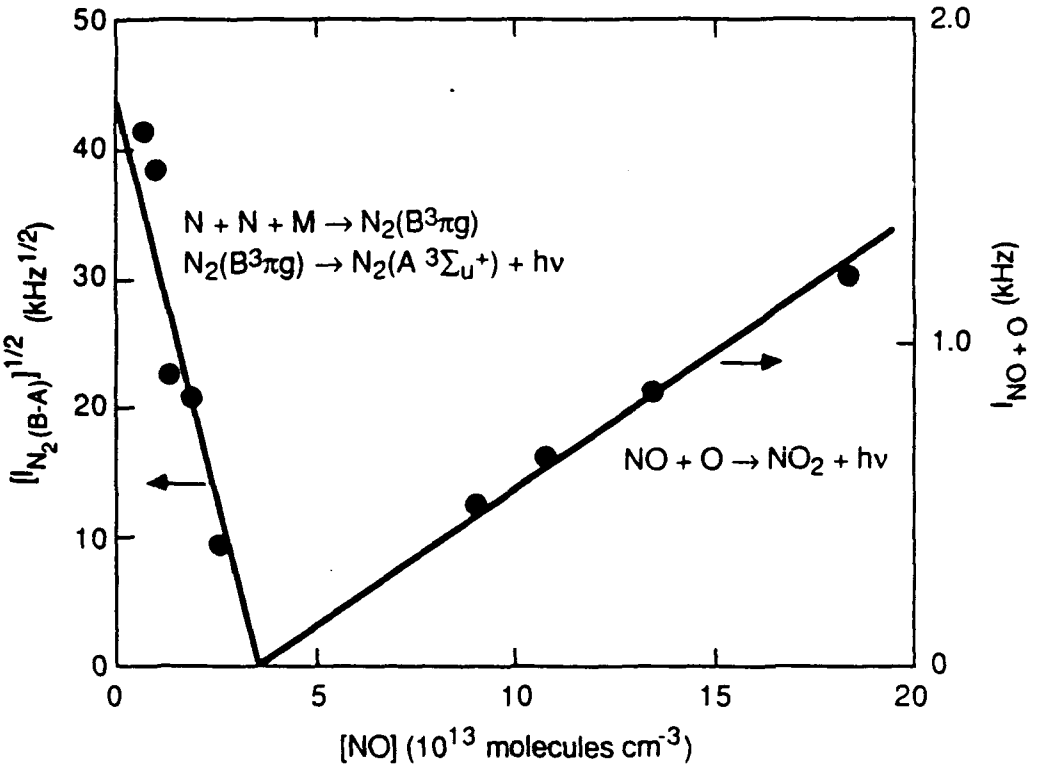

Figure 48. The N + NO titration plot.

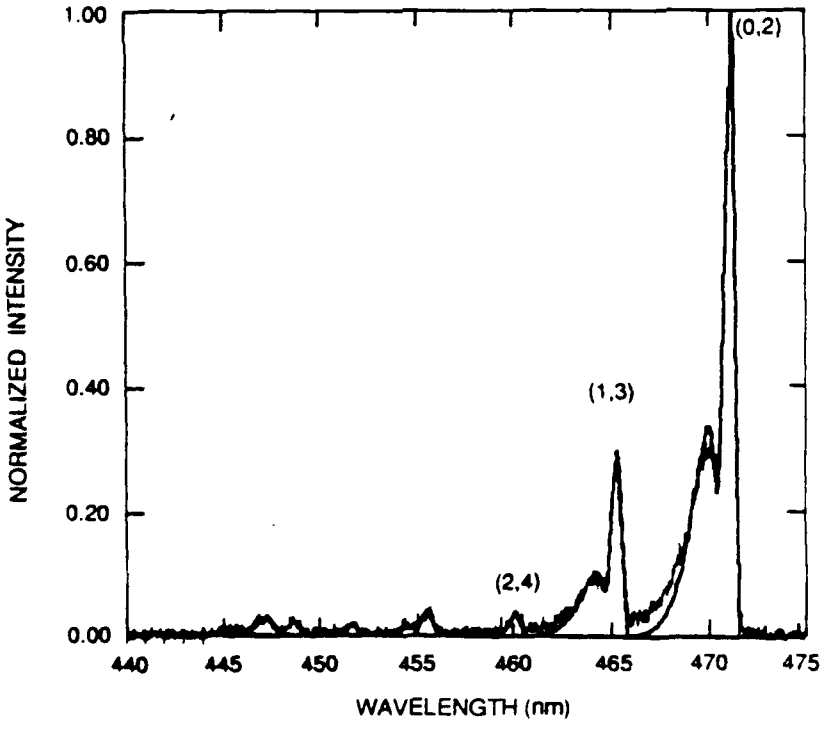

Figure 49. Penning-ionization in absence of added NO.

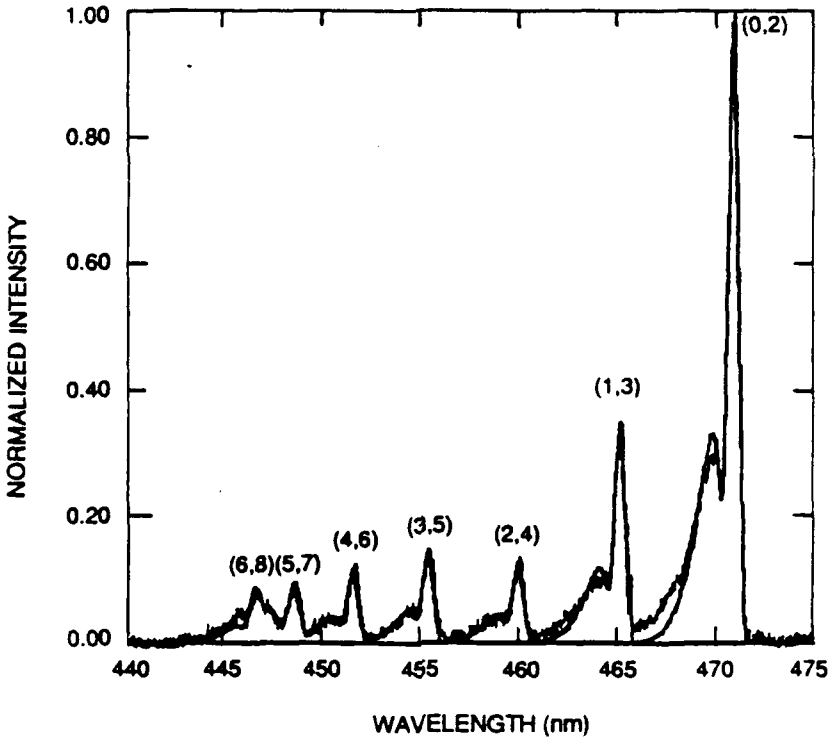

Figure 50. Penning-ionization spectrum of $N_2(v)$ generated from N + NO.

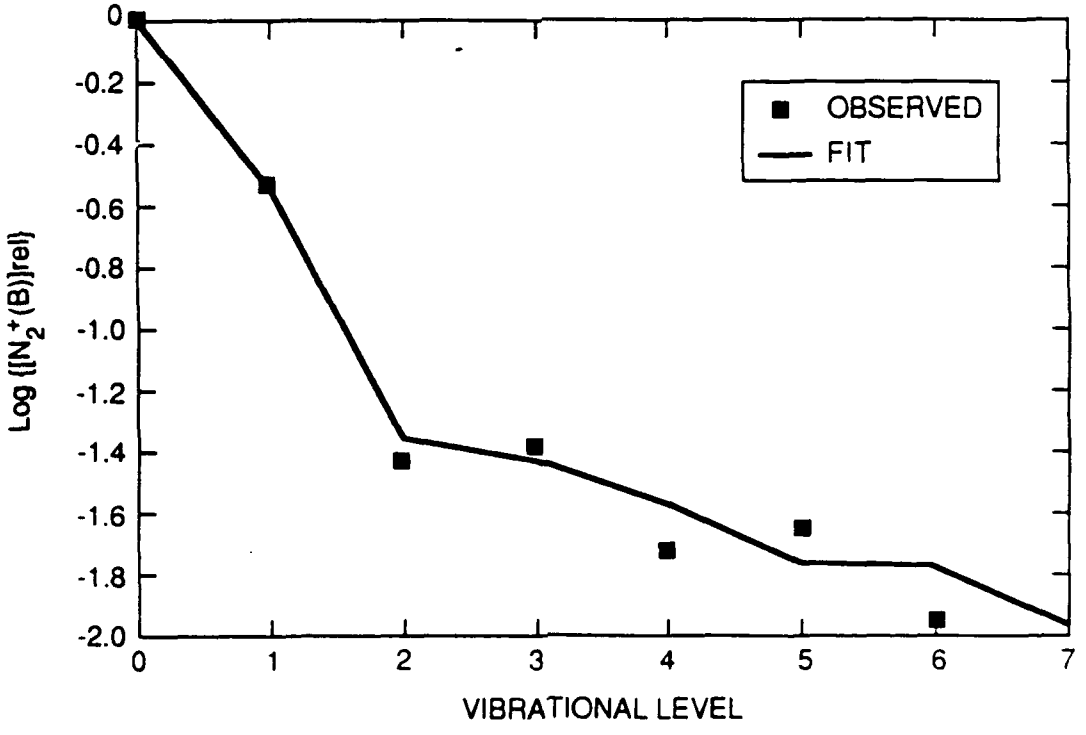

Figure 51. First negative distributions without NO. Iterative producedure is used to fit Penning-ionization data.

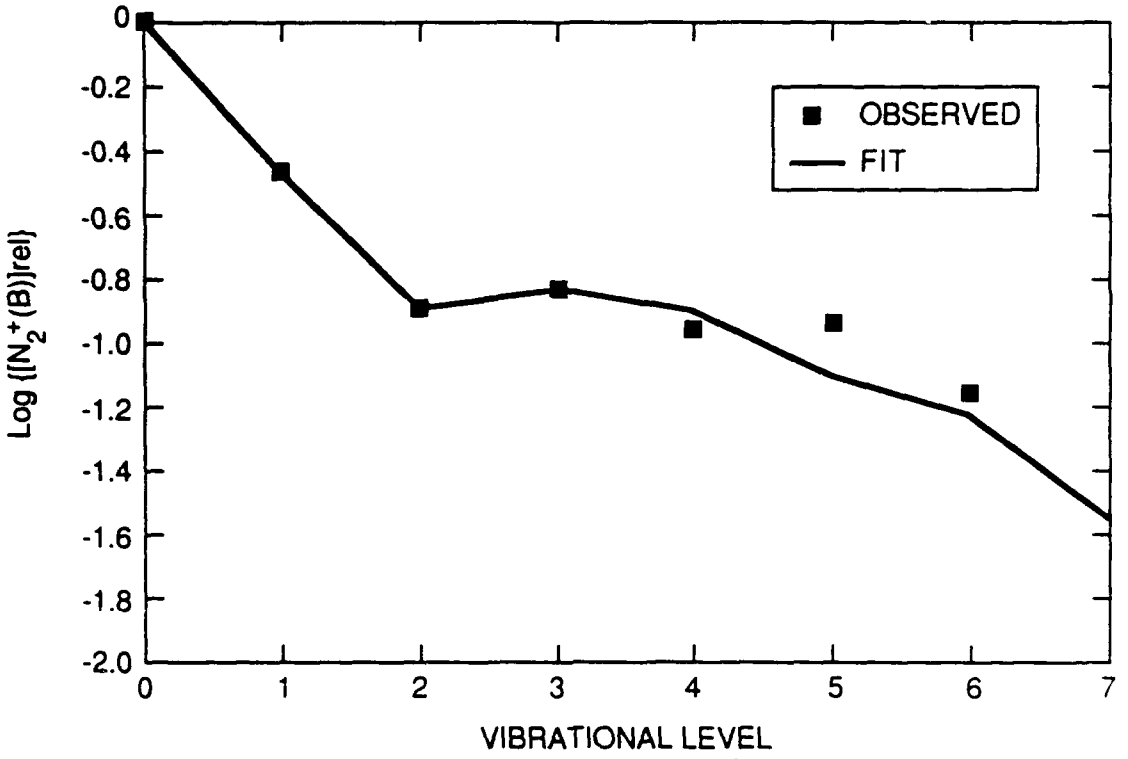

Figure 52. First negative distributions with NO. Iterative procedure is used to fit Penning-ionization data.

iterative technique is used (see Subsection 2.1.3) to determine the ground state vibrational population. This is done for both spectra (NO "on", NO "off"); the arithmetic difference being the vibrational distribution of the $N_2(v)$ produced by the N + NO reaction. This is shown in Figure 53.

Interestingly, the negative v = 0 population indicates a loss of $N_2(X,v''=0)$ when $N_2(X,v''>0)$ is present. This can be understood on the basis of V-V exchange between the undetectable higher vibrational levels and $N_2(X,v=0)$. Thermodynamically, N + NO can produce $N_2(X,v)$ up to v = 12. These high-lying vibrational levels may be vibrationally relaxed by the large reservoir of $N_2(v=0)$ present in the reactor. Treanor et al. (Ref. 34) and Caledonia and Center (Ref. 35) have modeled vibrational distributions in diatomic gases dominated by vibrational relaxation where anharmonic effects and V-V exchange are significant. The V-V exchange rates are several orders of magnitude larger at room temperature than V-T rates so energy exchange through vibrational modes is the only process considered here. Furthermore, although multiquanta events may occur, the gain or loss of a single quantum of vibrational energy is the most likely, so the analysis of these data can be greatly simplified by only considering single quantum exchanges.

During relaxation, rapid V-V exchange can result in reactions of the type:

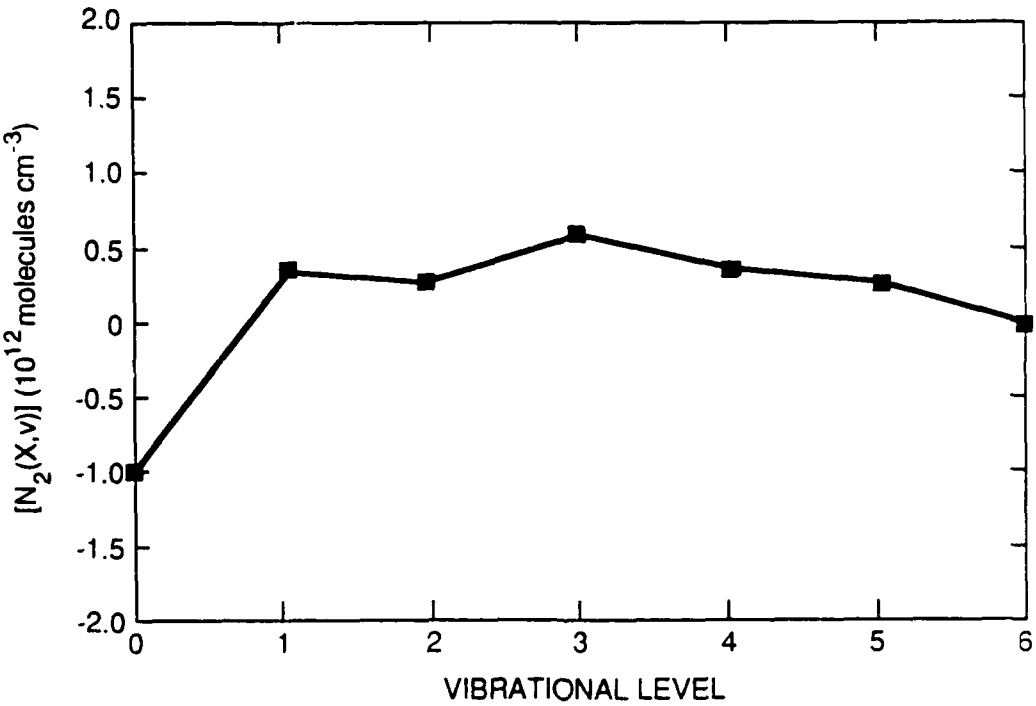

Figure 53. The $N_2(X,v)$ distribution produced from N + NO reaction.

$$N_{v+1} + N_0 \underset{P_{1,0}^{v,v+1}}{\overset{P_{0,1}^{v+1,v}}{\rightleftharpoons}} N_1 + N_v \tag{48}$$

where the subscripts v+1, 0, 1, and v denote the vibrational energy level. The rate of exchange between a high-lying vibrational level v + 1 and v = 0 is given by (Ref. 36):

$$P_{0,1}^{v+1,v} = P_{1,0}^{v,v+1} \exp\left[-(E_1 - E_0 + E_v - E_{v+i})/kT\right] \tag{49}$$

which reduces to

$$\frac{P_{0,1}^{v+1,v}}{P_{1,0}^{v,v+1}} = \exp\left[-2v\omega_e x_e/kT\right] \tag{50}$$

For v = 12, the ratio

$$\frac{P_{0,1}^{v+1,v}}{P_{1,0}^{v,v+1}} = 0.193$$

Given this ratio, the lower limit of N_2 concentrations can be estimated in the pertinent vibrational levels which would facilitate exchange. The exchange reaction

$$N_{v+1} + N_0 \rightleftarrows N_1 + N_v \tag{51}$$

is actually two half-reactions existing synergistically,

$$N_{v+1} \rightleftarrows N_v \tag{52}$$

$$N_0 \underset{k_{1,0}}{\overset{k_{0,1}}{\rightleftarrows}} N_1 \tag{53}$$

The ratio of backward and forward rates $k_{0,1}/k_{1,0}$ is therefore the same in both cases and equal to the ratio for the whole reaction

$$\frac{P_{0,1}^{v+1,v}}{P_{1,0}^{v,v+1}}$$

which is calculated to be 0.193 in this case. In other words,

$$\frac{k_{0,1}}{k_{1,0}} = \frac{P_{0,1}^{v,v+1}}{P_{1,0}^{v,v+1}} = 0.193$$

Taking this a step further, relate this ratio to the concentrations of N (v=0) and (v=1), since at equilibrium

$$\frac{k_{0,1}}{k_{1,0}} = \frac{N_2(v=1)}{N_2(v=0)} = 0.193$$

It is clear that the inequality $[N_2(v=0)] > 5.19[N_2(v=1)]$ must be satisfied for this exchange to be feasible. The Penning-ionization data shows the $N_2(v=0)/N_2(v=1)$ ratios, in the absence of NO, ranging from 6.5 to 8.2, always in excess of the 5.19 stipulation. It seems, then, that these V-V exchange reactions will occur under these conditions and may explain the apparent $N_2(v)$ distribution from the N + NO reaction.

As pressure is increased by throttling the pump, an increasing loss of $N_2(v=0)$ is observed (Figure 54). This also can be explained on the basis of V-V exchange. Throttling the pump results in both an increased collision rate and an increased reaction time. These effects will cause the V-V exchange processes to proceed further toward equilibrium.

The total number of collisions suffered by the N_2 before detection can be calculated using simple kinetic theory (Ref. 76). The number of collisions experienced per unit time is given by

$$\Gamma = \xi p \sigma^2 \sqrt{\pi / mkT} \qquad (54)$$

where $\xi = 1/3 + 2/3\sqrt{2}$, p = partial pressure of the N_2 in atmospheres, m = the reduced mass, σ = collision diameter = 3.75Å, T = temperature in K, and k = the gas constant. The collision frequency, Γ, times the reaction time, 2 ms, gives the total number of N_2 collisions, which is increasing with pressure. A plot of the depletion of N_2 (v=0) versus total number of N_2-N_2 collisions experienced before detection is shown in Figure 55. As expected, the loss of $N_2(v=0)$ is increasing with the number of collisions experienced by the N_2 before detection.

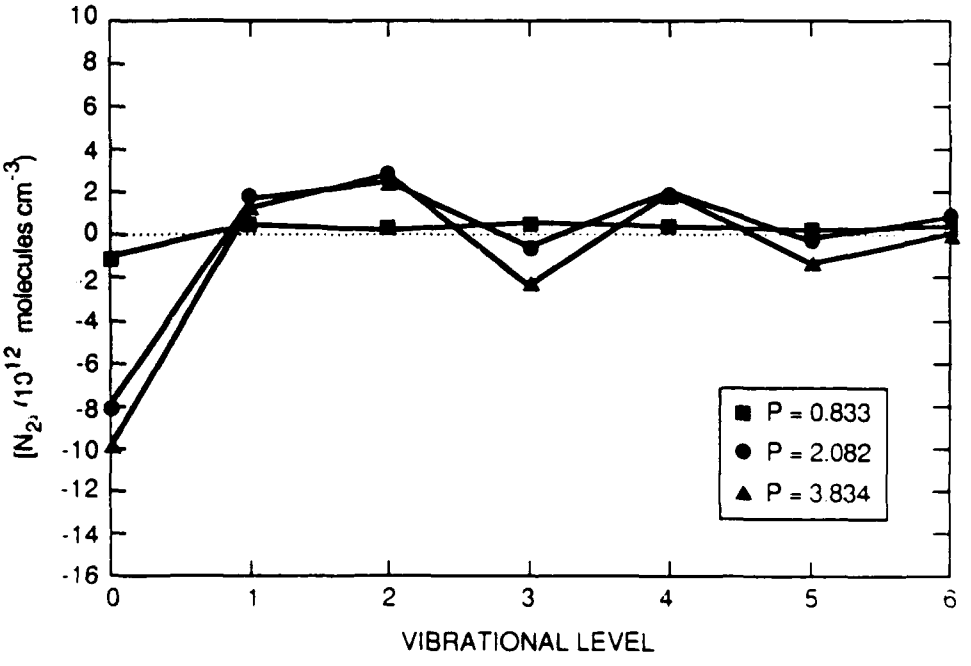

Figure 54. The $N_2(X,v)$ distributions from N + NO at various pressures.

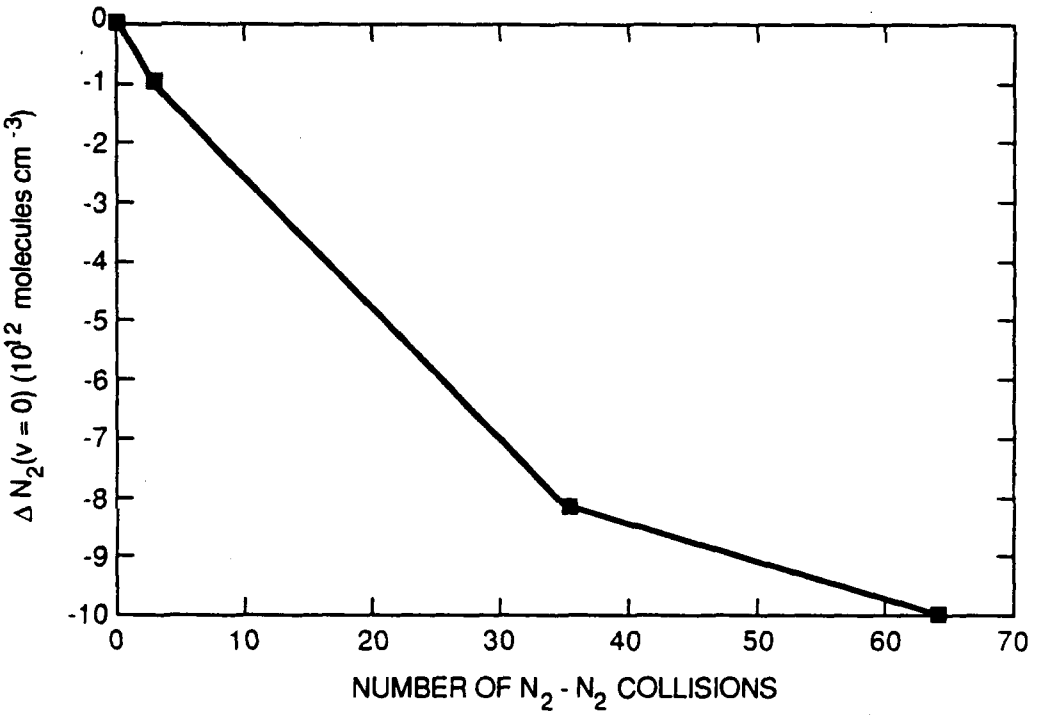

Figure 55. Loss of $N_2(X,v=0)$ with increasing N_2-N_2 collisions.

Vibrational levels above v = 0 display a seemingly complex distribution, which may be due to errors in estimating population densities in these levels. In any case, unlike the systematic loss of $N_2(v=0)$ with increasing pressure, no chemical significance can be attached to the slightly undulating nature of the distribution of $N_2(v)$ above v = 0.

Of course, the effect of $N_2(v=0)$ depletion at all pressures presupposes that the nascent vibrational distribution of the N_2 (v) formed by the N + NO reaction is inverted. This is not unlikely. Inversions are predicted in N_2 when the vibrational temperature greatly exceeds the N_2 characteristic vibrational temperature (3353.3 K) or at very low translational temperatures. At this time, the initial $N_2(v)$ distribution produced by reaction of N + NO cannot be probed, but the effect it has on the overall N_2 distribution can be observed. These observations suggest that the $N_2(v)$ produced in reaction is indeed inverted and undergoes rapid V-V exchange with N_2 (v=0) before detection.

4.2.4 N_2 Production for the H + NF_2 Sequence

The second reaction studied for production of $N_2(v)$ was the H + NF_2 reaction sequence:

$$H + NF_2 \rightarrow HF + NF\ (a^1\Delta) \qquad (45a)$$

$$H + NF(a^1\Delta) \rightarrow HF + N(^2D) \qquad (45b)$$

$$N(^2D) + NF(a^1\Delta) \rightarrow N_2(\leq 45) + F \qquad (\Delta E = -10.05\ eV)\ . \qquad (45c)$$

Previous investigations at PSI have demonstrated that the final step of this highly exoergic reaction generates the $N_2(B^3\Pi_g)$ state (Ref. 8), which is readily quenched. This product energy, then, could be channeled into high vibrational levels of the ground state.

In these experiments, NF_3/He mixtures were discharged at low microwave power ($\sim$7 W) and H_2 was injected downstream (Figure 47(b)). In order to find the optimal conditions for $N_2(X,v)$ production, flow tube pressure, reactant concentration, and discharge power were varied over a wide dynamic range. Also, discharging the H_2 before injection into the flow tube was tried. NO $N_2(X,v)$ was observed during this reaction sequence. There were several aspects of this system which complicated these experiments considerably. First of all, the He metastables were quenched by the rich reacting mixture. The worst offending species of this type was NF_3. Even at low concentrations (10^{13} molecules per cubic centimeter), NF_3 quenches the initial He metastables by at least 30 percent. Secondly, the crucial species, $N(^2D)$, is quenched in reaction with H_2: $N(^2D) + H_2 \rightarrow NH(X) + H$. This quenching will cut off the generation of N_2. Lastly, a number of atomic and molecular emissions interfered with and complicated the spectrum. These were isolated as being due to the following species:

H-atoms
He-atoms
N-atoms
$N_2(X,v)$ from the NF_3 discharge
NH(c-b).

This reaction sequence, although still a probable source of $N_2(X,v)$, is not conducive to measurements using the Penning-ionization diagnostic.

4.2.5 N_3 Recombination Studies

4.2.5.1 $N_2(X,v)$ Production from N_3 Recombination. The third chemical source: $N_3 + N_3$ did produce copious $N_2(X,v)$. The N_3 radicals were produced by the reaction of F-atoms with HN_3 (Ref. 105). A microwave discharge passed through a 10 percent CF_4/He mixture, produced the F-atoms. The HN_3 was made prior to the experiment by the reaction of NaN_3 and stearic acid and stored as a 5 percent mixture in He. The HN_3 was injected through a movable, Teflon-coated injector downstream from the discharge (Figure 47(c)). Typical flow rates were: He (dc discharge), 2272 μmoles s^{-1}; HN_3, 3.5 μmoles s^{-1}; CF_4, 3.3 μmoles s^{-1}; He (microwave discharge), 609 μmoles s^{-1}; and He (injector), 453 μmoles s^{-1}. Pressures in the flow tube ranged from 0.7 to 7 torr.

The N_3 radicals are produced by the reaction of F with HN_3, but they are also consumed in reaction with excess F-atoms to produce $NF(a^1\Delta)$:

$$F + HN_3 \rightarrow HF + N_3 \quad (55)$$

$$F + N_3 \rightarrow NF(a) + N_2 \quad (56)$$

The total rate coefficients for these reactions have been measured by Habdas et al. (Ref. 102) to be 1.1 x 10^{-10} cm^3 $molecule^{-1}$ s^{-1} and 5 x 10^{-11} cm^3 $molecule^{-1}$ s^{-1}, respectively. The NF(a) produced in reaction (56) then reacts with vibrationally excited HF to give NF(b) (Ref. 106):

$$NF(a^1\Delta) + HF^+(v \geq 2) \rightarrow NF(b^1\Sigma^+) + HF(v-2) \qquad (57)$$

To determine the amount of N_3 produced from the F + HN_3 reaction, chemiluminescence from the NF(b) product of reaction (57), readily observable at 528.8 nm, was monitored. A typical titration curve is shown in Figure 56. The NF(b) intensity increases with added HN_3 until the [HN_3] = [F]. At this point, the end point of the titration, all of the atoms are consumed via reaction (57) and excess F-atoms are no longer available to react with the N_3 radicals. Titrations of this type were performed at various injector positions. Figures 56 and 57 are titration curves taken under the same conditions except for reaction distance. The change in apparent shape of the curve and position of the end point is due to insufficient mixing of reactants at short reaction distances. With reaction distances longer than 10 cm, the end point of this titration was essentially constant and gives an initial N_3 number density of 1 x 10^{13} molecules per cubic centimeter.

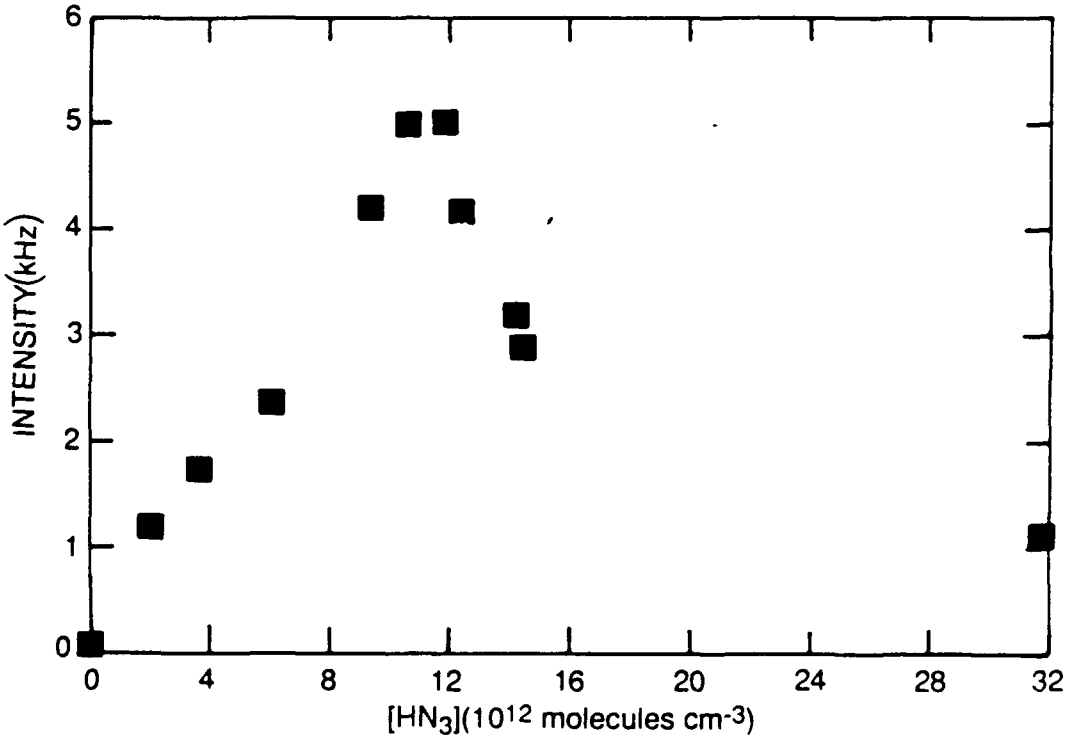

Figure 56. The NF(b) chemiluminescence versus [HN_3] at 528.8 nm: reaction length = 21 cm.

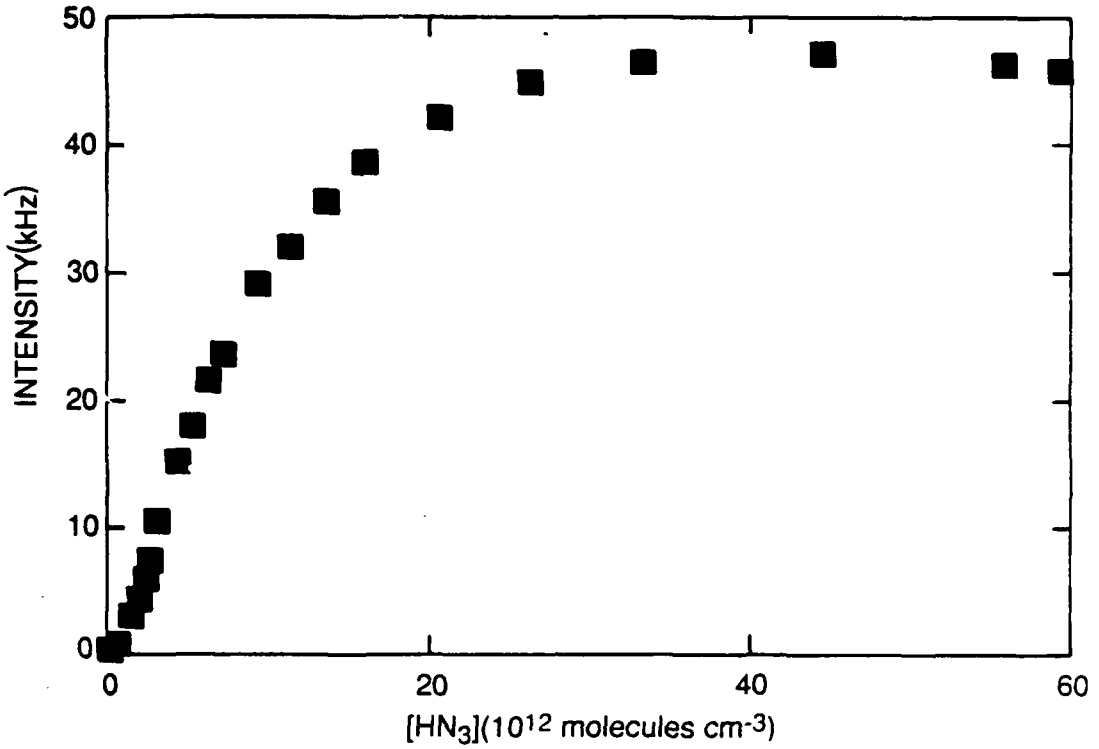

Figure 57. The NF(b) chemiluminescence versus [HN_3] at 528.8 nm: reaction length = 1 cm.

Once created, N_3 radicals will recombine to produce $N_2(X,v)$. Penning-ionization of the N_2 product results in the first-negative spectrum depicted in Figure 58. This spectrum was obtained with a reaction time of 2 ms and at a pressure of 0.783 torr. No emission was observed in the absence of N_3 radicals. To validate that the observed signal was indeed due to N_2 produced by N_3 recombination, the signal was monitored while the injector distance was varied. Figure 59 shows a plot of the reciprocal of the signal intensity versus injector position. The fact that this signal increases with injector distance is evidence of N_2 being produced by a time-dependent chemical reaction.

The excited-state distribution of $N_2^+(B)$ obtained from the best synthetic fit to the first-negative spectrum (Figure 58) is shown in Figure 60. A Treanor distribution with ground-state vibrational temperature of 3200 K would explain the observed $N_2^*(B)$ distribution. An expected ground-state distribution based on this vibrational temperature is shown in Figure 61.

Absolute number densities were determined by monitoring the signal when known amounts of ground-state N_2 were added. Since the analytical procedure determined the relative ground-state vibrational distribution and also that 60 percent of the N_2 produced is in v = 0, absolute number densities for each vibrational level could be determined. These are shown in Table 6.

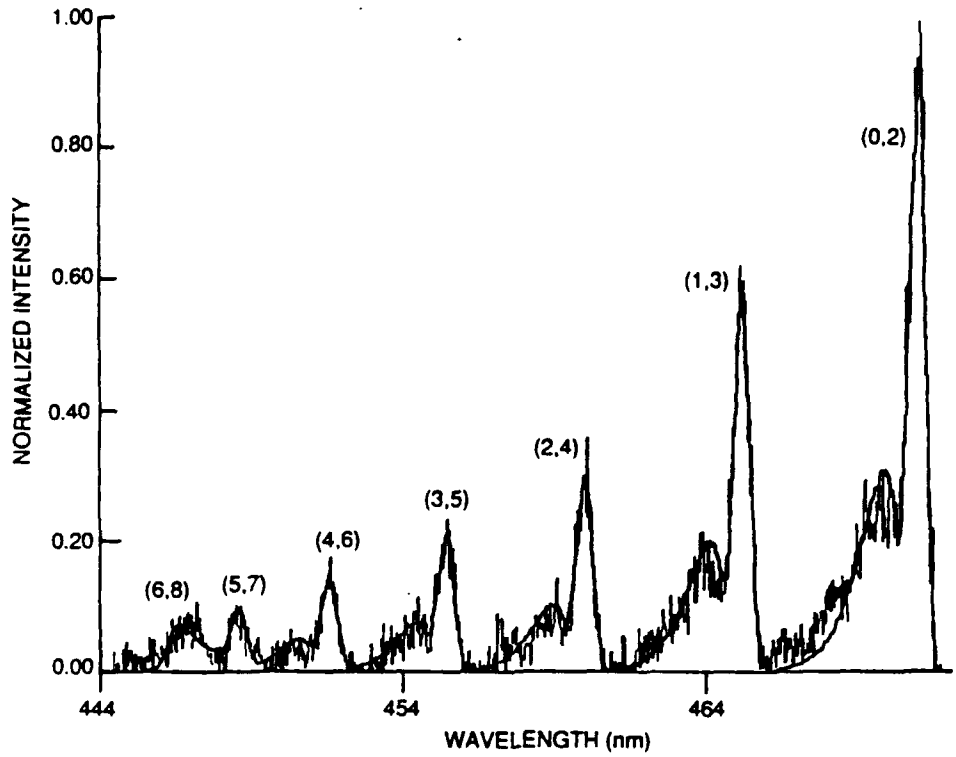

Figure 58. $N_2^+(B^2\Sigma_u^+ - X^2\Sigma_g^+)$ emission from Penning ionization of the product of N_3 recombination

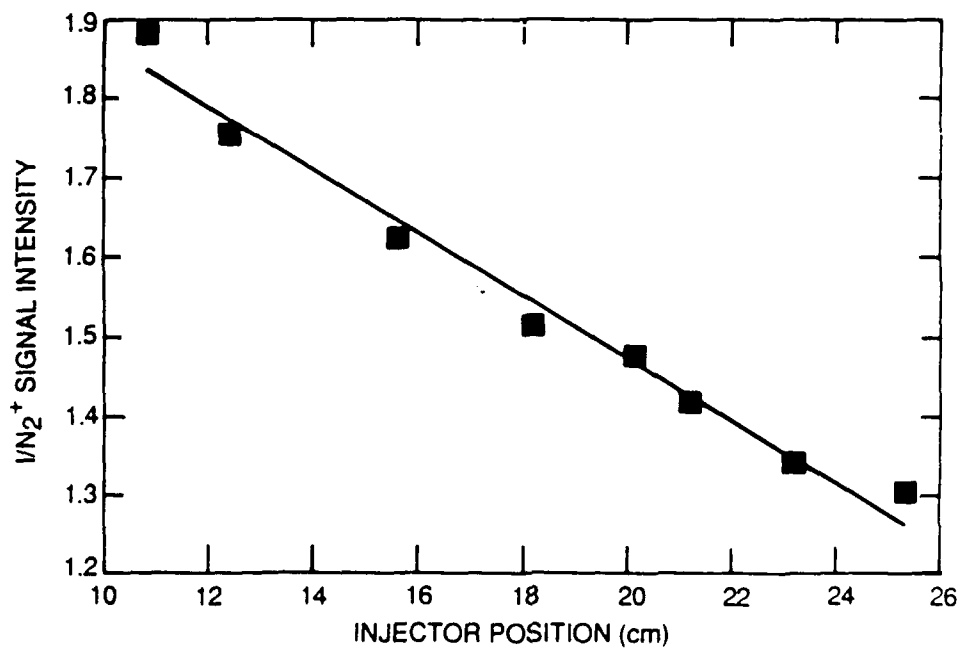

Figure 59. Reciprocal of the signal intensity versus reaction length: $[HN_3] = 2.8 \times 10^{13}$ molecules per cubic centimeter.

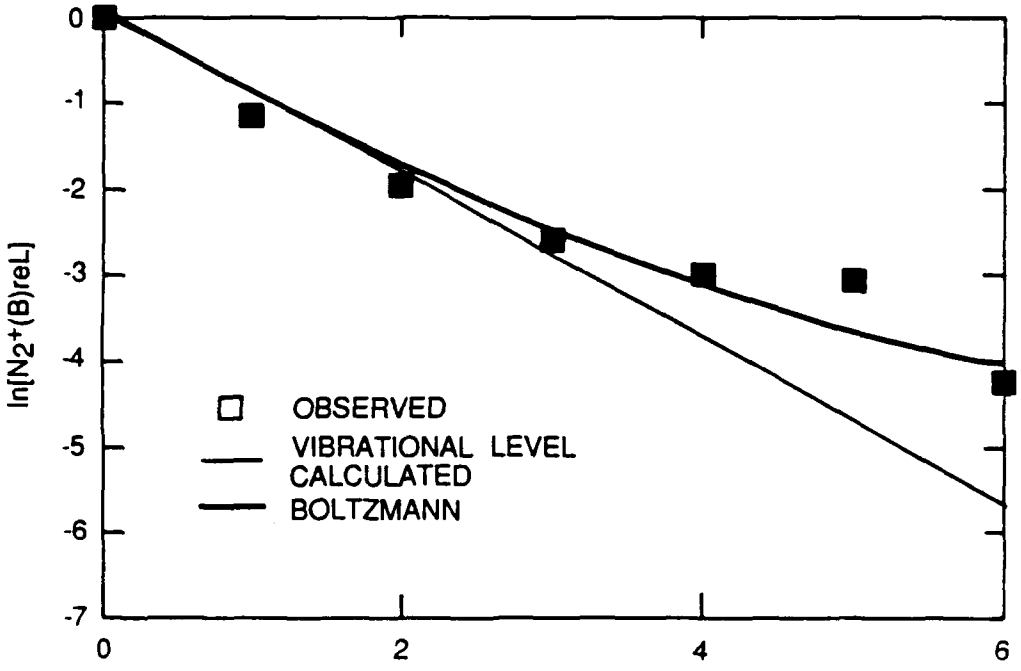

Figure 60. Excited state distributions of $N_2(v)$ from N_3 recombination. Vibrational temperature = 3200 K

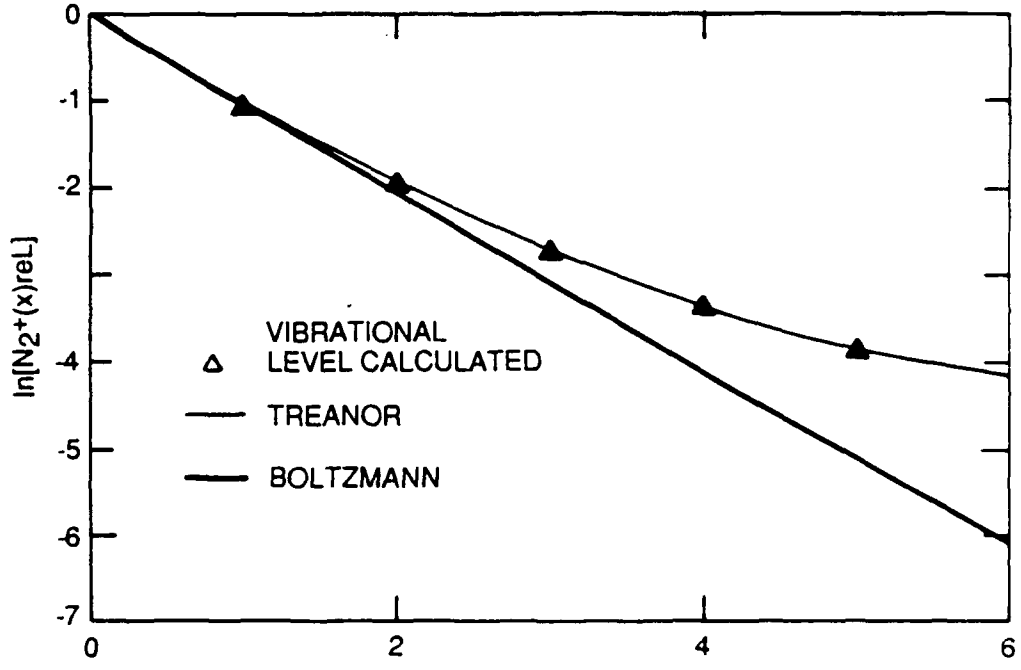

Figure 61. Expected ground state distributions of $N_2(v)$ from N_3 recombination.

Table 6. The N_3 recombination results: absolute number densities for $N_2(X,v)$.

V	$[N_2(v)][N_2(v=0)]$	$[N_2]$ (10^{12} molecules cm^{-3})
0	0.600	2.04
1	0.210	0.714
2	0.085	0.289
3	0.039	0.132
4	0.021	0.072
5	0.013	0.044
6	0.009	0.031

Changing the flow time by varying the reaction distance from 10 to 20 cm had no effect on the vibrational temperature of the N_2 at a pressure of 0.783 torr. This result is, perhaps, not surprising since earlier reports showed that $N_2(v)$ produced in a microwave discharge does not relax appreciably for flow times up to 30 ms (see Subsection 4.1.1). The findings in regard to N_3 recombination, however, are inconclusive, since by moving the injector in these experiments, the flow time is only varied by 2 ms. There was, however, a significant change in the vibrational temperature with flow tube pressure. Figure 62 shows the vibrational distribution at pressures ranging from 0.7 to 7 torr. Increasing the pressure in the flow tube by throttling the pump has the effect of decreasing the flow velocity as well as increasing the partial pressure of individual species. One of these parameters is probably governing the degree of vibrational excitation in the N_2. Further analysis and characterization of this source will be necessary before any conclusions can be drawn concerning this apparent relaxation at high pressures.

4.2.5.2 Kinetics of N_3 Disproportionation. The kinetics of N_3 recombination were investigated since the correct value for this rate coefficient is necessary to consider this reaction as a potential precursor for a chemical laser. Numerous estimates for the N_3-recombination rate coefficient have been published previously (Refs. 102, 107-112). The discrepancies between these previously reported values span more than two orders of magnitude. Table 7 lists the reported rate coefficients.

By keeping the HN_3 in excess, the secondary reaction of F-atoms with N_3 radicals to produce NF does not occur to any significant extent. Once N_3 radicals are produced, they may decay via the disproportionation reaction (58) or wall loss (59) as they travel down the reactor:

$$N_3 + N_3 \rightarrow \text{products} \qquad (58)$$

$$N_3 + \text{wall} \rightarrow \text{products} \qquad (59)$$

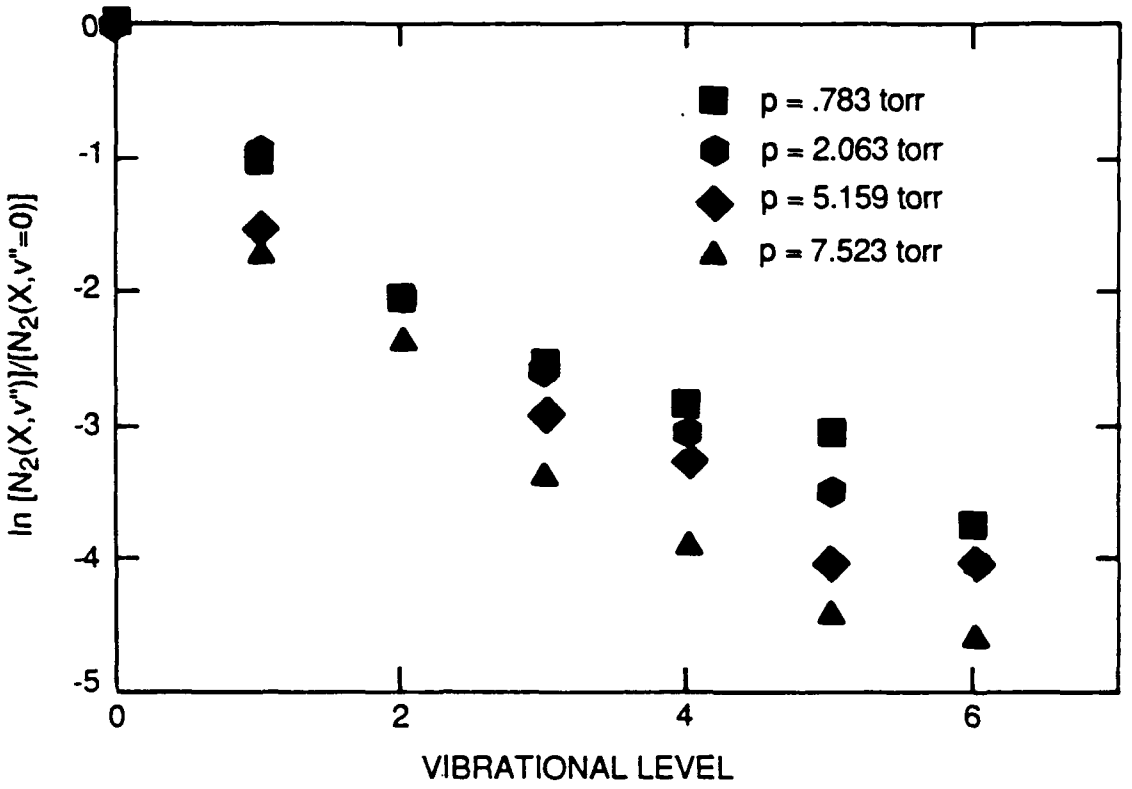

Figure 62. Excited state distribution as a function of flow tube pressure.

By varying the position of the HN_3 injector, the N_3 decay time is varied. The equation governing the loss of N_3 radicals is

$$-\frac{d[N_3]}{dt} = 2k_{58}[N_3]^2 + k_{59}[N_3] \tag{60}$$

Under conditions where wall loss is insignificant, Eq. 60 solves to give

$$\frac{1}{[N_3]_t} = \frac{1}{[N_3]_0} = 2k_{58}t \tag{61}$$

where t = decay length, L, divided by flow velocity, v. Since $[N_3]$ at any time, t, equals the initial $[N_3]_0$ minus the amount of N_3 consumed in the reaction, and the amount of N_3 consumed in a reaction is equal to $2/3[N_2]$ produced, this equation can be rearranged to give

$$\frac{1}{[N_3]_0 - 2/3[N_2]_{produced}} = 2k_{58}\left[\frac{L}{V}\right] + \frac{1}{[N_3]_0} \tag{62}$$

This allows the rate coefficient for N_3 recombination to be determined on the basis of the appearance of the product N_2. This analysis assumes that the $[N_3]_0$ is not dependent on the

Table 7. Previously reported values for the N_3 recombination rate coefficient.

Authors	Technique	k_{58} (cm^3 $molecule^{-1}$ s^{-1})
Clark and Clyne[107]	Discharge flow - absorption	5.0×10^{-12}
Paur[108]	Flash photolysis - absorption	3.3×10^{-10}
Combourieau et al.[109]	Discharge flow mass spectrometry/modeling	$(5\text{-}8) \times 10^{-11}$
Yamasaki et al.[110]	Discharge flow - emission	1.4×10^{-12}-
MacRobert[111]	Discharge flow - mass spectrometer	$(8.8 \pm 2.0) \times 10^{-12}$
Coombe et al.*	Flow reactor	3×10^{-12}
Habdas, Wategaonkar and Setser[102]	Discharge flow	$2_{-1}^{+2} \times 10^{-11}$
Marinelli et al.[112]	Discharge flow - LIF	$2.4_{-0.8}^{+1.1} \times 10^{-12}$

reaction length, which is a valid assumption. Previously, at reaction times greater than 1 ms, the $[N_3]_0$ produced by $F + HN_3$ did not vary significantly. The amount of N_2 produced by N_3 recombination was determined by calibrating the signal at $v = 0$ with a known amount of ground-state N_2.

A plot of the left-hand-side of Equation (62) versus injector position results in a slope equal to $2k_{58}/v$ where v is equal to flow velocity. Such a plot is shown in Figure 63. The rate coefficient calculated from the slope of this line is 2.4×10^{-12} cm^3 $molecules^{-1}$ s^{-1}. Since the y-intercept equals $1/[N_3]_0$, its reciprocal should equal 1×10^{13} molecules per cubic centimeter, the initial $[N_3]$ as determined by titration. Actually, the y-intercept gives an initial N_3 number density of 8.4×10^{12} molecules per cubic centimeter. Therefore a 16 percent error is assumed in the determination of $[N_3]_0$. Incorporating this error, the rate constant is $2.4_{-0.7}^{+1.4} \times 10^{-12}$ cm^3 $molecule^{-1}$ s^{-1}.

4.2.5.3 Application of $N_2(A) + N_2(v)$ Diagnostic to N_3 Recombination Products. Efficient energy transfer has been demonstrated between $N_2(X,v)$ and $N_2(A)$ to create $N_2(B)$ (Ref. 30). Exciting the observed $N_2(B)$ levels from the $N_2(A)$ requires $N_2(X)$ in vibrational

* R. Coombe, "Chemiluminescent Reactions in Azide Radicals," in Presentation to AFOSR Molecular Dynamics Contractors Conference, Hanscom AFB, MA, 15-17 October 1986.

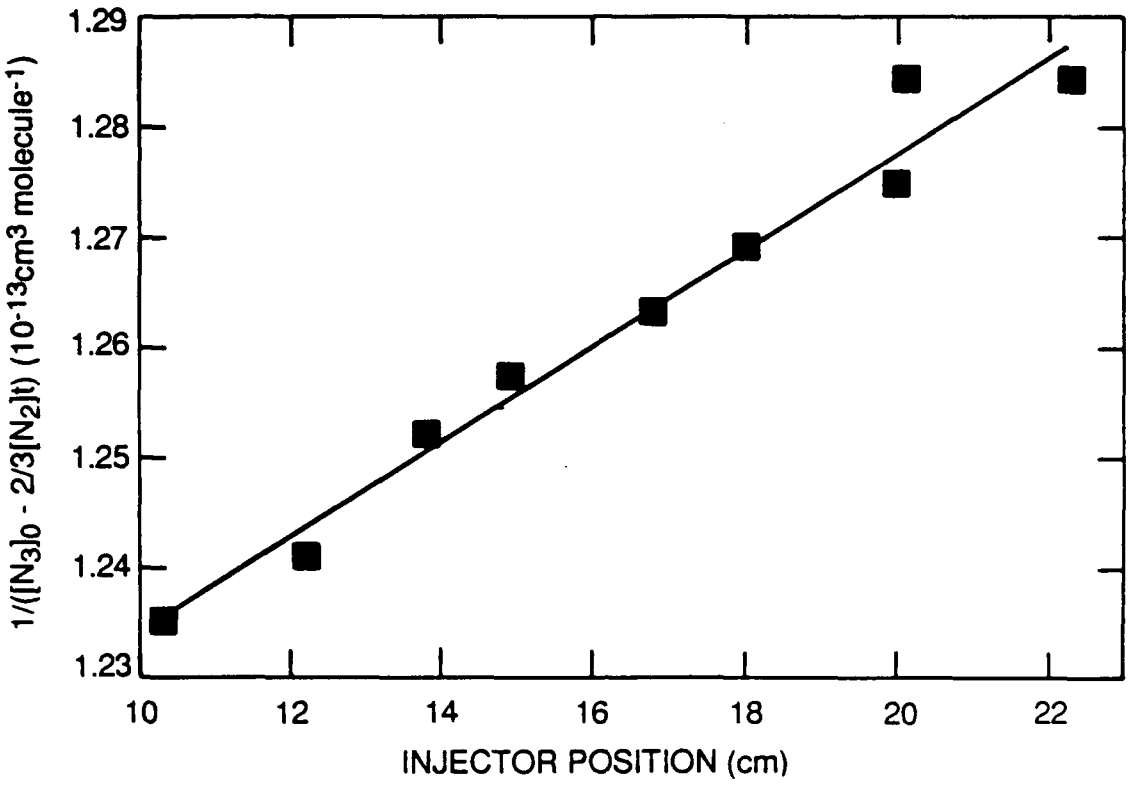

Figure 63. N_3 kinetics plot.

levels 5-14. This makes the $N_2(A) + N_2(X,v)$ reaction a useful diagnostic for $N_2(X,v)$ in these vibrational levels.

Attempted efforts to apply this diagnostic to detect $N_2(X,v)$ generated in the N_3 recombination reaction are reported. This reaction is an attractive test of this diagnostic because it does not produce $N_2(B)$ by itself.

The configuration of the flow reactor is shown in Figure 64. The N_3 is produced from reaction of F-atoms with HN_3. A hollow cathode dc discharge through a flow of 3 to 10 percent Ar in He generates metastable argon atoms. The Ar metastables mix immediately downstream from the discharge with a flow of nitrogen. The argon metastables excite $N_2(C)$ which radiates to the $N_2(B)$ state. Radiative decay and collisional quenching of $N_2(B)$ results in $N_2(A)$ state production. This $N_2(A)$ is injected downstream from the N_3 recombination reaction zone and $N_2(B)$ emission is detected further downstream. Typical flow rates are: He (dc discharge), 2485; Ar, 7.39; He (microwave discharge), 510; He (N_2 carrier), 184; HN_3, 0.934; F_2, 6.128; N_2 (dc discharge), 2.9, with a typical pressure of 2.5 torr.

With N_3 and $N_2(A)$ in the flow tube, one observes a small amount of $N_2(B)$ emission. This emission vanishes when either reactant is removed. This may be evidence of $N_2(v>5)$, though small amounts of N-atoms, produced from metastable Ar dissociation of N_2, may be reacting with unreacted N_3 to give this same effect.

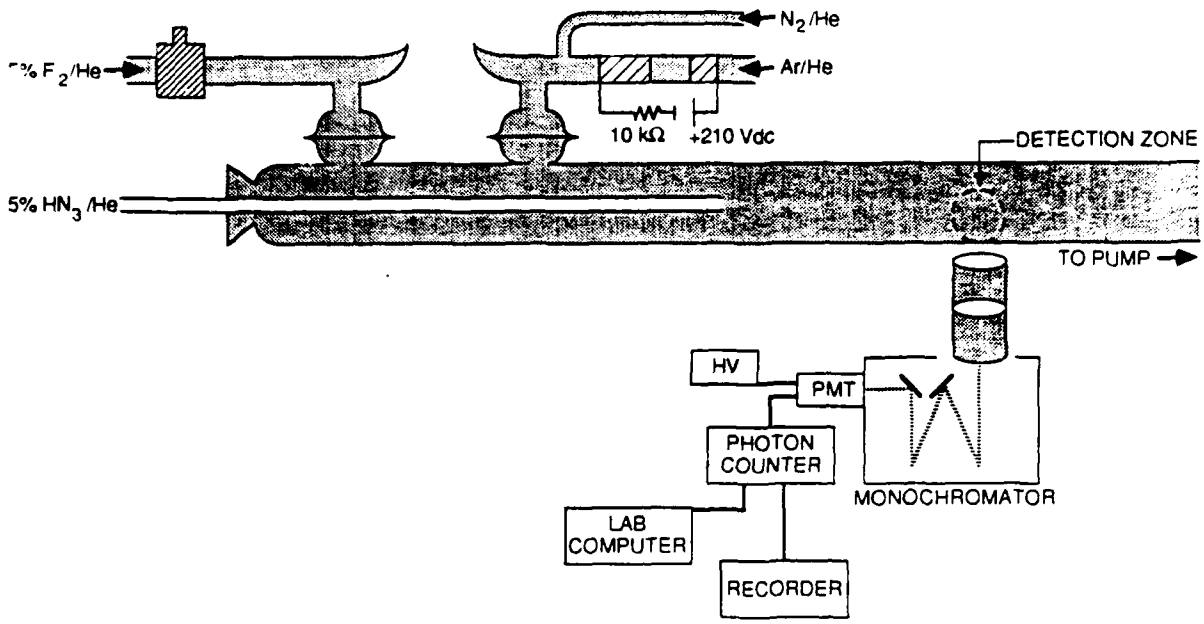

Figure 64. Flow reactor configuration for $N_2(A) + N_2(v)$ studies.

Although quite promising, the initial attempt to react a chemical source of $N_2(v)$ with $N_2(A)$ is inconclusive. An unequivocal test of these results would be to use Xe rather than Ar metastables to generate the $N_2(A)$. Since Xe metastables do not dissociate N_2, this procedure would eliminate the possibility of $N + N_3$ producing the observed $N_2(B)$ emission.

4.2.6 Investigations of the $N + N_3$ Reaction

4.2.6.1 $N_2(X,v)$ From $N + N_3$. Interest in the $N + N_3$ reaction stems from the fact that N-atom/N_3 mixtures will excite IF (Refs. 112 and 113), a lasing species. The source of the excitation, however, has not been definitively identified. The reaction produces intense $N_2(B-A)$ emission although the product yield for $N_2(B)$ remains highly speculative. Reported yields range from 10 to 70 percent (Refs. 112, and 114). Although $N_2(B)$ is not metastable, and therefore not a likely transfer candidate, it can be a precursor to $N_2(A)$ through radiative and collisional quenching. Hence, $N_2(B)$ has been the primary focus of studies of this reaction (Refs. 101, 112 and 114). Very little, however, has been done to examine the ground-state $N_2(X)$ product and the possibility that vibrationally excited N_2 is the energy carrier in this reaction. Using the Penning-ionization diagnostic, an attempt was made to probe the lower vibrational levels of the ground state N_2 produced in this reaction.

The flow tube configuration for these experiments is shown in Figure 65. The N-atoms are produced by a 5 percent mixture of N_2/He passed through a microwave discharge. The azide radicals are produced from the reaction of atoms and HN_3. The F-atoms are produced in a 5 percent F_2/He microwave discharge. The HN_3 was made prior to the experiment using the reaction of NaN_3 and stearic acid and stored as a 5 percent mixture in He. Typical flow rates (μmoles/s) were: He (dc discharge), 2208; He (microwave discharge), 576; HN_3, 0.736; F_2, 5.6; N_2, 5.86.

The N-atom densities are determined in separate experiments by titration with NO as described above. Trace amounts of SF_6 in the discharge increased the N_2 dissociation rate to give N-atom densities of 2.3 x 10^{13} molecules per cubic centimeter. Vibrationally excited N_2 from the discharge was relaxed with a glass wool plug. The concentration of N_3 is determined by titrating F-atoms with HN_3.

In the study of the N_3 + N reaction, the depletion of N_3 via reaction (56) is undesirable since there is need to know the N_3 concentration that will be reacting with the N-atoms. This is easily remedied if the [HN_3] is in excess of the F-atoms. In this case, then, the secondary reaction (56) becomes negligible and all of the N_3 produced in reaction (55) is available for reaction with N-atoms. In these experiments, the initial N_3 number density was 1 x 10^{13} molecules per cubic centimeter.

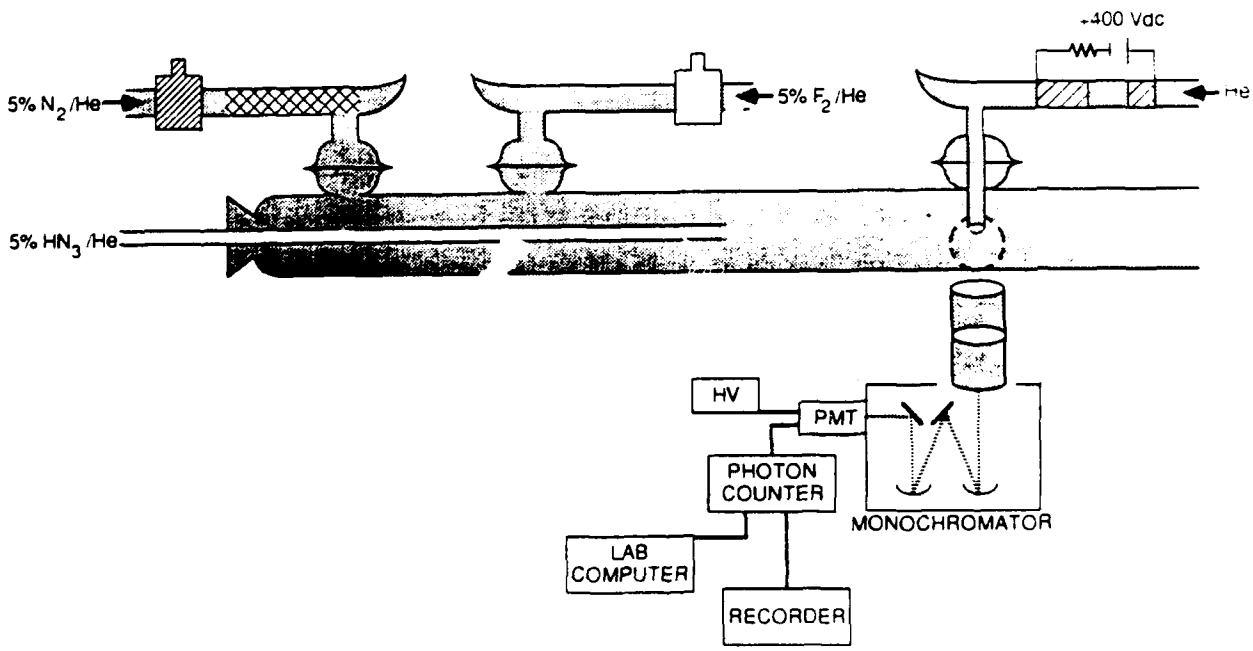

Figure 65. Flow reactor configuration for N + N_3 reaction.

The Penning-ionization diagnostic was used to monitor ground state $N_2(X,v)$ produced in the $N + N_3$ reaction. No evidence for ground-state N_2 in vibrational levels greater than one was observed. Since populations in $v = 0$ and 1 are largely dominated by undissociated N_2 in the discharge, very small changes in these levels with N-atoms present could go undetected, since detection of $< 1 \times 10^{11}$ molecules per cubic centimeter under these conditions is unlikely. The $N_2(X)$ produced by the $N + N_3$ reaction, must have a very small branching ratio, or be otherwise quite vibrationally cold. Perhaps it was formed in levels $v'' >> 6$, and they did not relax enough to be observed.

4.2.6.2 $N_2(B)$ Branching Ratio. It is perhaps not too surprising that $N + N_3$ does not result in high concentrations of $N_2(X,v)$. As mentioned, the branching ratio to produce the product $N_2(B)$ may be as great as 0.7. An additional $N_2(B)$ branching ratio determination wa made by monitoring $N_2(B\text{-}A)$ emission in vibrational levels 2 through 12. The GaAs PMT based detection system was calibrated absolutely using the well known O/NO air afterglow procedure (Refs. 49-51). Therefore is was possible to determine absolute number densities of $N_2(B)$ produced in reaction (47) by monitoring $N_2(B\text{-}A)$ emission intensities. Since only $v = 2\text{-}12$ can be detected, The data were corrected to incorporate $v = 0$ and 1 by assuming that 29 percent is in $v = 2\text{-}10$, as determined experimentally by Marinelli et al. (Ref. 112).

A typical $N_2(B\text{-}A)$ emission spectrum from the $N + N_3$ reaction is shown in Figure 66. The branching ratio of the $N + N_3$ reaction can be estimated to form $N_2(B)$ from:

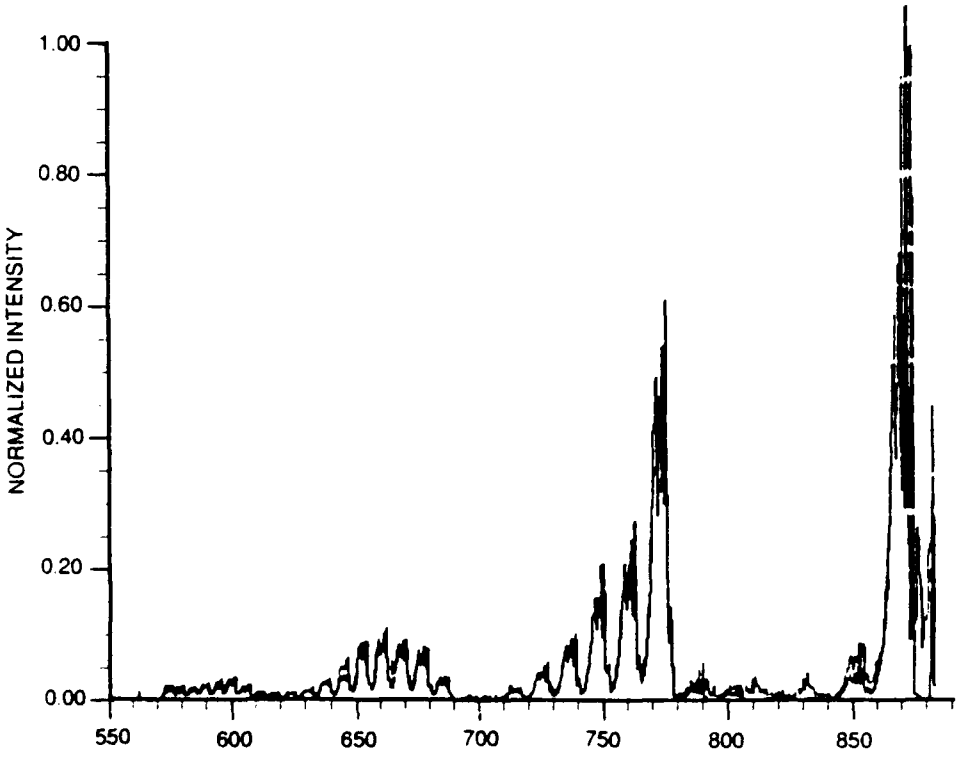

Figure 66. $N_2(B\text{-}A)$ emission from $N + N_3$ reaction.

$$\phi = \frac{N_2(B)]_{observed}}{[N_2(B)]_{maximum}} \tag{63}$$

which is the ratio of $N_2(B)$ detected to the maximum amount of $N_2(B)$ that could be formed. Based on the emission intensities, the concentration of $N_2(B) = 5.45 \times 10^6$ molecules per cubic centimeter. When this is corrected for the unobserved levels of 0 and 1, the number density is estimated to be 1.8×10^7 molecules per cubic centimeter. The maximum produced in this reaction is the steady state $N_2(B)$ number density given by

$$[N_2(B)] = \frac{k_{47}[N]_t[N_3]_t}{k_{rad}} \tag{64}$$

where k_{47} is the $N + N_3$ rate coefficient, and k_{rad} is the radiative rate. The [N] and $[N_3]$ concentrations correspond to the respective concentrations in the c rvation region. The integrated equation for second order reaction kinetics is given by

$$2k_{47}t = \left[\frac{1}{[N]_0[N_3]_0}\right] \ln \left\{\frac{[N_3]_0([N]_0 - x)}{[N]_0([N_3]_0 - x}\right\} \tag{65}$$

where [N], $[N_3]$ refer to the respective initial concentrations and x refers to the amount to N or N_3 which is consumed in reaction at some time, t. The concentration of N and N_3 after time t is simply found by solving for x and subtracting that amount from the initial concentrations. This calculation gives $[N_3]_t = 6.9 \times 10^9$ molecules per cubic centimeter and $[N]_t = 1.3 \times 10^{13}$ atoms per cubic centimeter. Plugging these values into Equation (65) indicates a maximum $[N_2(B)]$ of 7.84×10^7 molecules per cubic centimeter. The branching ratio equals 0.23, which, being within the range of previous measurements, is a good check on experimental technique.

4.2.7 Summary of Experiments on Chemical Production of $N_2(v)$

These chemical reactions have been investigated as sources of $N_2(X,v)$:

$$N + NO \rightarrow N_2\ (X, v \leq 12) + O \tag{44}$$

$$H + NF_2 \rightarrow HF + NF\ (a^1\Delta) \tag{45a}$$

$$NF(a^1\Delta) + H \rightarrow HF + N(^2D) \tag{45b}$$

$$N(^2D) + NF(a^1\Delta) \rightarrow N_2(X, v \leq 45) + F \tag{45c}$$

$$N_3 + N_3 \rightarrow 3N_2(X,v \leq 40) \quad (46)$$

$$N + N_3 \rightarrow N_2(X,v) + N_2 \ . \quad (47)$$

The N_3 recombination is the most efficient source of $N_2(X,v)$ with a vibrational temperature of 3200 K and number densities of $N_2(v=0\text{-}6)$ as high as 3×10^{12} molecules per cubic centimeter easily realized. The $H + NF_2$ reaction, although highly exoergic, gave no evidence for production of $N_2(X,v)$. Interfering atomic and molecular emissions complicated the Penning-ionization spectrum. These were isolated as being due to the following: H-atoms, He-atoms, N-atoms, $N_2(X,v)$ from a NF_3 discharge, and NH(c-b). The conclusion was that this reaction was incompatible with the Penning-ionization diagnostic.

The N + NO reaction also is an efficient source of $N_2(X,v)$. The evidence suggests population densities in high vibrational levels that affect the populations in lower levels by a V-V exchange process. Although these high-lying levels are undetected by the Penning-ionization diagnostic, initial $N_2(X,v)$ distribution is inferred from the N + NO reaction which is inverted and undergoes rapid V-V exchange with the $N_2(v=0)$ reservoir in the flow reactor.

The $N + N_3$ reaction did not appear to produce $N_2(X,v>0)$. Determining population densities in 0 and 1 were somewhat inconclusive becuase of the large amount of ground-state N_2 present in the flow tube.

5.0 ENERGY TRANSFER MEASUREMENTS

Several sets of energy transfer measurements were made on $N_2(X,v)$ during the course of this program and the viability of laser-induced fluorescence of the $N_2(a^1\Pi_g - X^1\Sigma_g^+)$ transition for monitoring the quenching kinetics of $N_2(X,v)$ was demonstrated. Subsection 2.3.3.4 describes this work.

The excitation of $IF(B^3\Pi_{O+})$ by the products of N_3 recombination was investigated briefly. Although the species involved in the excitation was not identified positively, $N_2(A^3\Sigma_u^+)$ rather than $N_2(X,v)$ appeared to be most likely.

The excitation of IF(B) in active N was also studied. Two regimes were used. Most of the effort was spent studying the excitation of $IF(B^3\Pi_{O+})$ by the products of N-atom recombination. The N-atoms were generated in a microwave discharge, and electronic metastables in the effluent were reduced significantly by operating at moderately high pressures and long flow times from the discharge to the observation region. Penning-ionization studies of these effluents indicated the presence of modest amounts of $N_2(X,v)$, but when the $N_2(X,v)$ was removed by flowing the discharge effluents over a glass-wool plug prior to mixing with the IF, the results were unchanged. These studies indicated that rather large number densities of IF(B) could be excited by the products of N-atom recombination, and that furthermore, the IF(B) excitation was significantly enhanced when the ground-state IF was vibrationally excited.

The second series of measurements involved active N produced at low pressures with short transit times from the discharge. In some of these studies, N-atoms and electronically excited metastables were removed from the flow by placing a Ni screen between the discharge and the observation region. The presence of significant quantities of $N_2(X,v)$ in vibrational levels above six was confirmed by observing the N first-positive bands when $N_2(A)$ was added to the flow downstream from the Ni screen. Under these conditions, no IF(B) was observed. When the Ni screen was removed, IF(B) was excited readily. Further diagnostics of the discharge effluents indicated that some $N_2(A)$ was present in the flow, but at number densities only sufficiently large to account for about 40 percent of the observed excitation. These studies show clearly that some effluent from the discharge, in addition to $N_2(A)$, excites IF(B) efficiently, but that this metastable species apparently is not $N_2(X,v)$.

Finally a technique was developed for measuring global quenching rate coefficients for $N_2(B^3\Pi_g, v' = 1\text{-}12)$ and $N_2(X, v'' = 5\text{-}15)$. Several quenching molecules were surveyed and nearly all of them, including CH_4, H_2, CO_2, N_2, CF_4 and N_2O quenched the electronic energy in $N_2(B)$ at near gas kinetic rates. The CH_4 and SF_6 appeared to be inefficient quenchers of $N_2(X,v'')$, whereas H_2, CF_4, N_2 and CO_2 relaxed vibrational energy in $N_2(X,v'')$ with rate coefficients between 1×10^{-15} and 4×10^{-14} cm^3 $molecule^{-1}$ s^{-1}.

5.1 INTRODUCTION

The energy-transfer measurements comprised two primary components. Two techniques were developed to study the total quenching of $N_2(X,v'')$, and the excitation of IF(B) was investigated in energy-transfer reactions between N metastables and IF(X). One of the $N_2(X,v'')$ quenching techniques is based on one-photon LIF measurements, and is detailed in Subsection 2.3.3.4. The other technique is based upon the $N_2(A)$ energy transfer diagnostic (see Subsection 2.2) and is detailed below.

Three sources of metastables were used for the studies on the excitation of IF(B) by excited N. Two of them are two forms of active N, the effluents of an N_2/He microwave discharge operated under two different sets of conditions. The third metastable source is the metastable N generated in azide-radical recombination. Two different regimes were used to generate active N. In one regime the flow times between the discharge and the observation region are long enough so that electronic metastables produced in the discharge will be deactivated by wall collisions and primarily N-atoms and some $N_2(X,v)$ survive to the observation region. Any IF excitation under these conditions is likely to result from transfer from N metastables generated by N-atom recombination or $N_2(X,v)$.

In the second operating regime, the pressures and transit times from the discharge are small enough so that significant number densities of electronically excited metastables, generated in the discharge, will be present in the observation region. These metastables as well as $N_2(X,v)$ might be capable of exciting IF(B). This second regime has been studied extensively under previous contracts (Refs. 3, 5, and 6). The additional studies in this report elucidate the IF(B) excitation mechanism.

5.2 ACTIVE N PRODUCED UNDER "SLOW FLOW" CONDITIONS (REGIME I)

The primary goals in the Regime I experiments were as follows:

1. To address scaling issues pertinent to IF(B) production using the F + CF_3I reaction to produce IF(X).

2. To determine the source of excitation in an N_2^* + IF reaction.

3. To survey the effect other sources of IF(X) have on the production rate of IF(B).

To this end IF(B) production in a flow tube as high as 3.2×10^8 molecules per cubic centimeter has been successfully achieved. In optimizing this signal the N-atom concentration produced in the N_2/He discharge was found to be chemically linked to the amount of excited IF observed. Diagnostic experiments on the effluents of the N_2 microwave discharge showed that

1. Without N-atoms, no IF(B) was produced.
2. N-atoms are depleted by IF.

3. $N_2(X,v)$ has a small, if any, role in the excitation process.
4. $N_2(A)$ is not the excitation source in our system.

Finally, IF was generated using the I_2 + F reaction and enhanced production of IF(B) was found in active N. This suggests that vibrationally excited IF(X) is excited more efficiently in active N than is vibrationally cold IF.

5.2.1 Scaling Experiment

Crucial to the viability of $N_2(X,v)$ as a source of energy in a chemical laser is its transfer efficiency to a lasant. In this section attempts to scale up the amount of IF(B) produced using a copious source of N_2^*, a microwave discharge through N_2/He mixtures are reported.

5.2.1.1 Experimental. The flow tube configuration for these experiments is shown in Figure 67. The IF(X) is produced in chemical reaction between CF_3I and F-atoms. When excess F-atoms are employed, this method quantitatively converts F-atoms to IF molecules. Typical flow rates, in units of μmol s^{-1}, were He (N_2 carrier), 700; He (IF generator), 250; N_2, 30; F_2, 10; CF_3I, 0.5; and pressures were $\approx$4 torr. An N_2/He discharge upstream from the IF injector produces the N_2^*.

Upon adding IF, the Lewis Rayleigh afterglow caused by N-atom recombination, is essentially extinguished downstream from the IF injector. It is replaced with

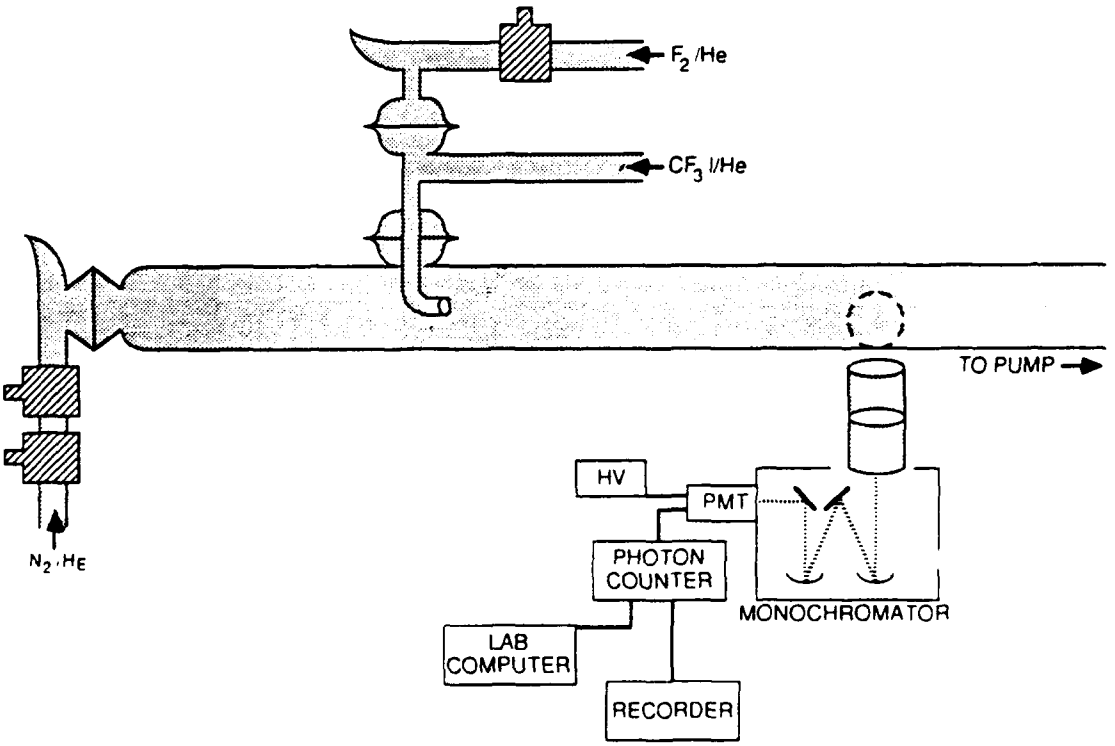

Figure 67. Flow reactor configuration for scaling experiments.

$IF(B^3\Pi_0^+ - X^1\Sigma_g^+)$ emission which appears greenish yellow to the eye. The IF(B-X) emission is monitored tens of milliseconds downstream from the injector. Spectra of the emissions are taken by and stored in a lab computer for later analysis using Labtech Notebook®. A spectral fitting routine described previously (Refs. 4 and 6), allows simulation of an IF(B-X) emission spectra and determination of the relative populations of the individual vibrational levels. Since the system is calibrated these relative populations can be related to an absolute [IF(B,v')]. The sum of [IF(B,v'=0-8)] is taken to be the absolute number density of IF in the B-state.

5.2.1.2 Results. Figure 68 shows a typical IF(B-X) emission spectrum. Some N_2(B-A) which is generated by N-atom recombination, is also apparent. Figure 69 indicates the vibrational distribution of the IF(B) derived from the spectral fitting procedure. In order to increase the number density of IF(B), its intensity was monitored while several parameters were varied. Figures 70, 71, and 72 show the effects of varying CF_3I concentration (Figure 70), N_2 mole fraction (Figure 71), and microwave discharge power (Figure 72) on the IF(0,2) band intensity. This particular band was chosen since it is well isolated from interfering CN(A-X) and N_2(B-A) emissions.

In Figure 70, there appears to be a threshold value of $[CF_3I]$ below which IF(B) is not observed. This is a reproducible effect and has been noticed by other workers in this lab (Ref. 3). The reason is that the F-atom discharge also produces trace quantities of OH. The

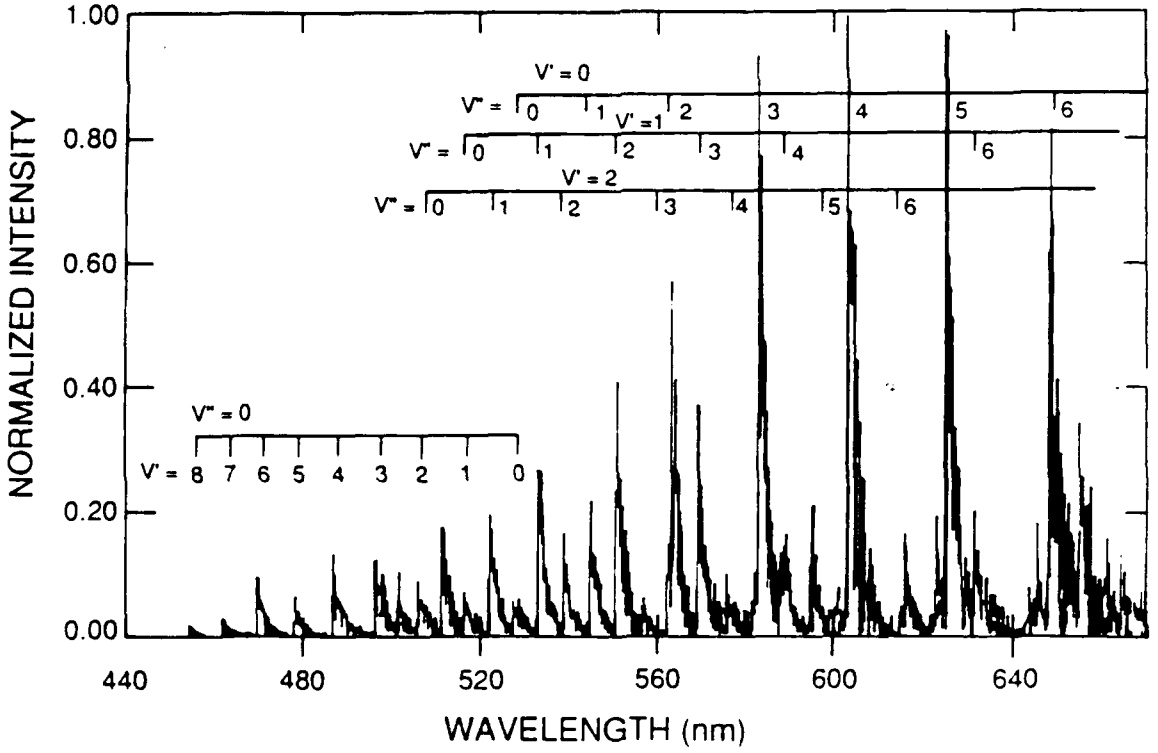

Figure 68. The $IF(B^3\Pi_0^+ - X^1\Sigma_g^+)$ emission from active N_2 excitation of IF(X) produced in the F + CF_3I reaction.

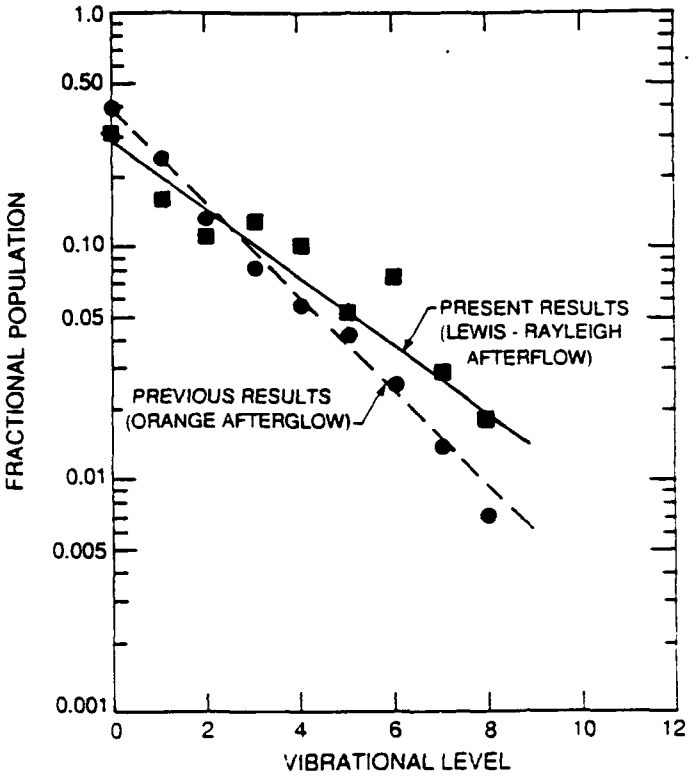

Figure 69. The IF(B) vibrational distributions in active N_2.

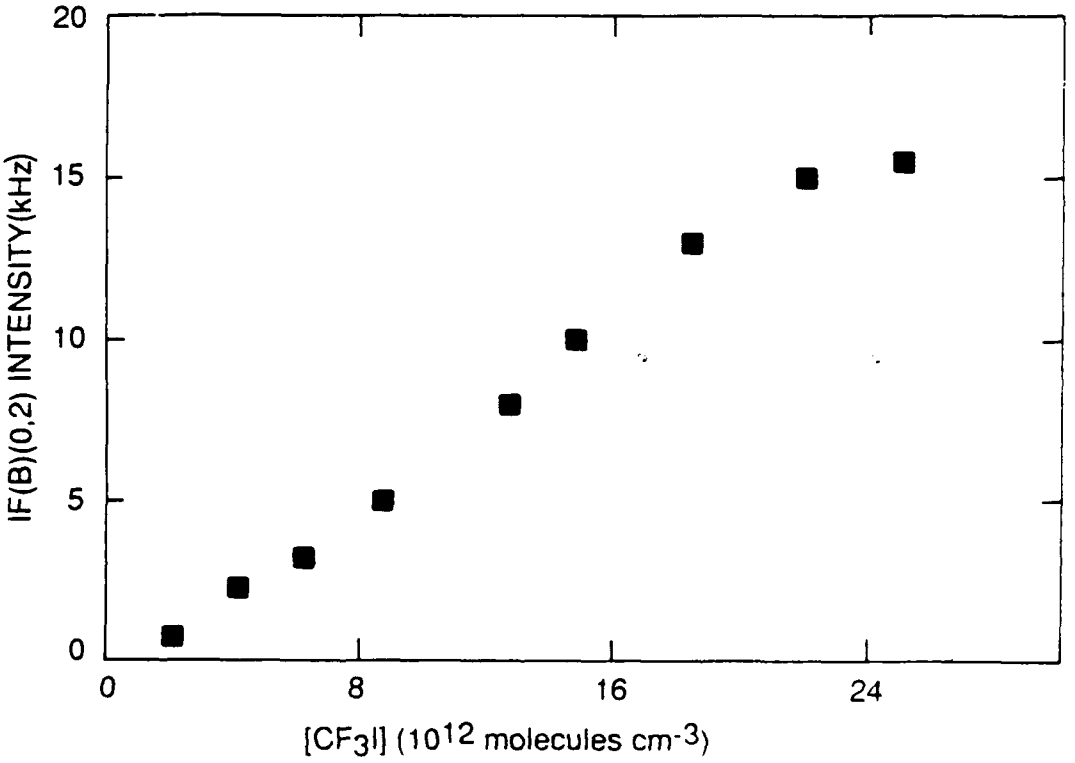

Figure 70. The IF(B) intensity versus $[CF_3I]$.

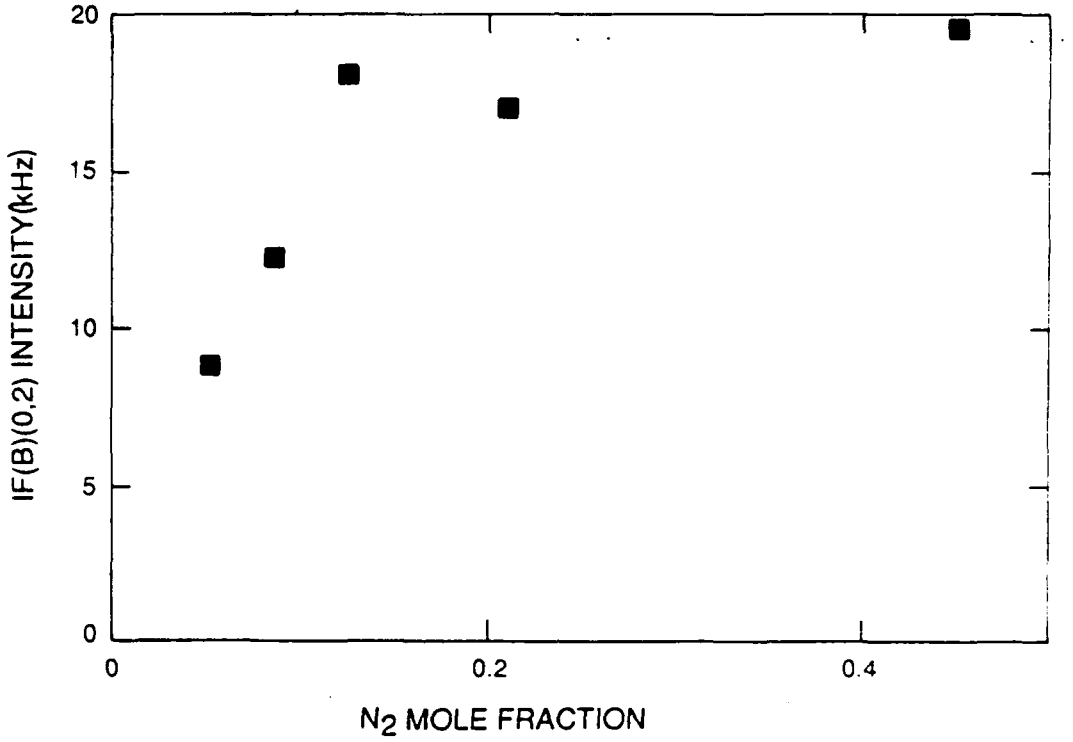

Figure 71. The IF(B) intensity versus N_2 mole fraction in discharge.

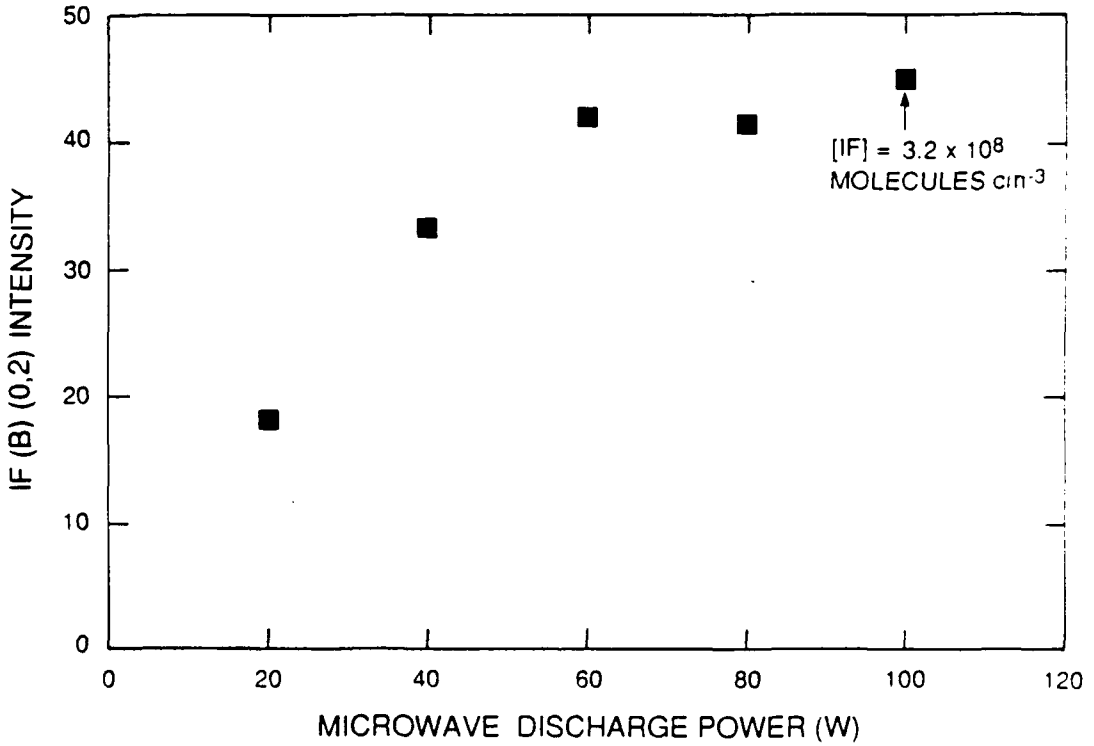

Figure 72. IF(B) intensity versus microwave power.

OH reacts with IF, and, consequently, IF fails to exit the injector until all the OH has been consumed. After reaching this value, the IF(B) then scales linearly with added CF_3I as expected. The F + CF_3I reaction is essentially gas kinetic with a rate constant (Ref. 115) of 8.8×10^{-11} $mole^{-1}$ s^{-1}, so it is a good assumption that CF_3I is converted to IF by excess F-atoms during the 10 ms residence time in the IF injector. The conditions for IF(X) production are somewhat limited due to the desire to maintain flow conditions which are pseudo-first order in excess F-atoms and had flow times in the injector which allowed the reaction to go the completion. However, within these constraints [IF(X)] in excess of 10^{13} molecules per cubic centimeter was reached. The greatest barrier to producing high [IF(B)] lies not in limitations imposed by the production of ground state IF, but by the concentration of transfer agent (N_2^*) to excite it to IF(B). To optimize the [N_2^*] the N_2 mole fraction in the discharge and the discharge power, were varied while monitoring the IF(B-X) emission (Figures 71 and 72).

The significance of the shapes of these curves will be discussed further in the next section. Clearly, however, as illustrated in Figures 71 and 72 the IF(B) signal is strongest at somewhat low N_2 mole fractions and high microwave power. Also using a second microwave discharge in series with the first one enhanced IF(B) production.

With these parameters optimized, that is, having 2 tandem microwave discharges, both powered to 100 W, an N_2 mole fraction of 0.2, and CF_3I added equal to 4.59×10^{13} molecules per cubic centimeter a maximum IF(B) number density of 3.2×10^8 molecules per cubic centimeter was obtained in the flow tube.

It is estimated that 10^{11} molecules per cubic centimeter of IF(B) are required to make a gain measurement. The [N] and/or [IF(X)] would have to be increased significantly before this can happen. Additional N_2 discharges placed in series may be adequate to increase the [N] an order of magnitude. The ground state [IF] was constrained somewhat in these experiments. This may be overcome somewhat by longer F + CF_3I reaction distances before entering the flow tube. Also, the F + CF_3I reaction may not be an ideal IF producer. The I_2 + F reaction, which produces IF(X,v) may be more efficient at producing IF(B). Therefore IF(B) number densities can be enhanced several orders of magnitude over that achieved in these experiments with only minor modifications in apparatus and technique.

5.2.2 N_2^* Diagnostic Experiments

This section summarizes efforts in identifying the energy carrier responsible for IF excitation from an N_2^* source. Although the primary goal of the experiments presented in the previous section was to maximize IF(B) production, in doing so valuable information concerning the identity of the transfer agent was extracted. This comprises the first part of this section. In addition, separate experiments designed to rule out one or more of the more likely energy carriers present in active N were performed. Those experiments form the remainder of this section.

5.2.2.1 Role of N-Atoms. Adding IF to the Lewis-Rayleigh afterglow diminishes its intensity. This is visually apparent and can be examined more quantitatively by monitoring the N_2(B-A) emission. Furthermore, the dominant factor in increasing [IF(B)] production is increased N-atom number densities. As presented in the last section, flow constituents, and power characteristics of the N_2 microwave discharge were varied to maximize [IF(B)] (Figures 71 and 72).

Concomitant NO titrations allowed tracking of the subsequent variation in N-atom concentrations as well. The NO titration procedure has been detailed previously (Refs. 3 and 6). Figures 73 and 74 illustrate the N-atom variations under conditions of Figure 71 and 72 where N_2 mole fractions in the discharge as well as discharge power were varied to increase [IF(B)]. Figure 75 shows even more succinctly the IF(B) (0,2) intensity as a function of [N]. Clearly the IF(B) intensity varies with the N-atom number density, the dependence appearing to be linear above N-atom partial pressures on the order of a millitorr.

5.2.2.2 Discharge Modifications. To verify the significant role N-atoms have in this excitation process the specie were modified in the effluents of the discharge. In some experiments a Ni screen was added to recombine N-atoms catalytically and to collect metastables while passing N_2(X,v") (Ref. 30). Using a glass wool plug, on the other hand allowed most N-atoms to pass but relaxed N_2(X,v) and electronically excited metastables formed in the discharge (Ref. 116).

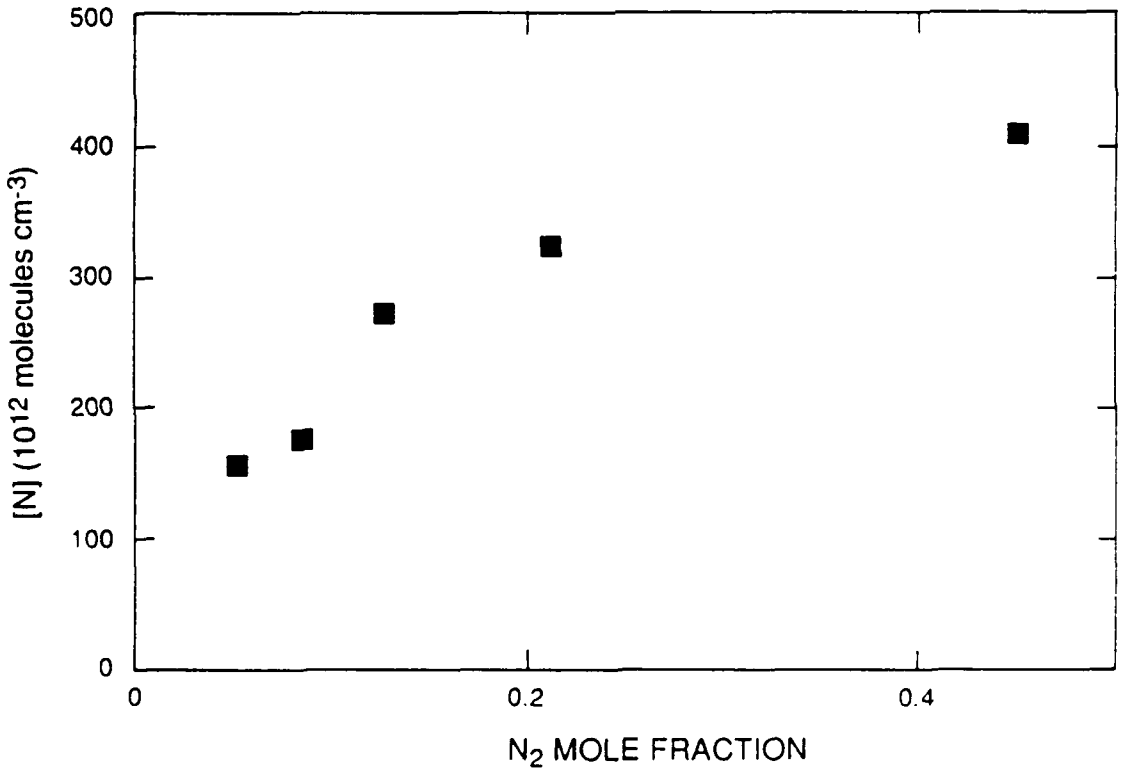

Figure 73. The N_2 mole fraction in discharge dependence of N-atoms produced in an N_2/He microwave discharge.

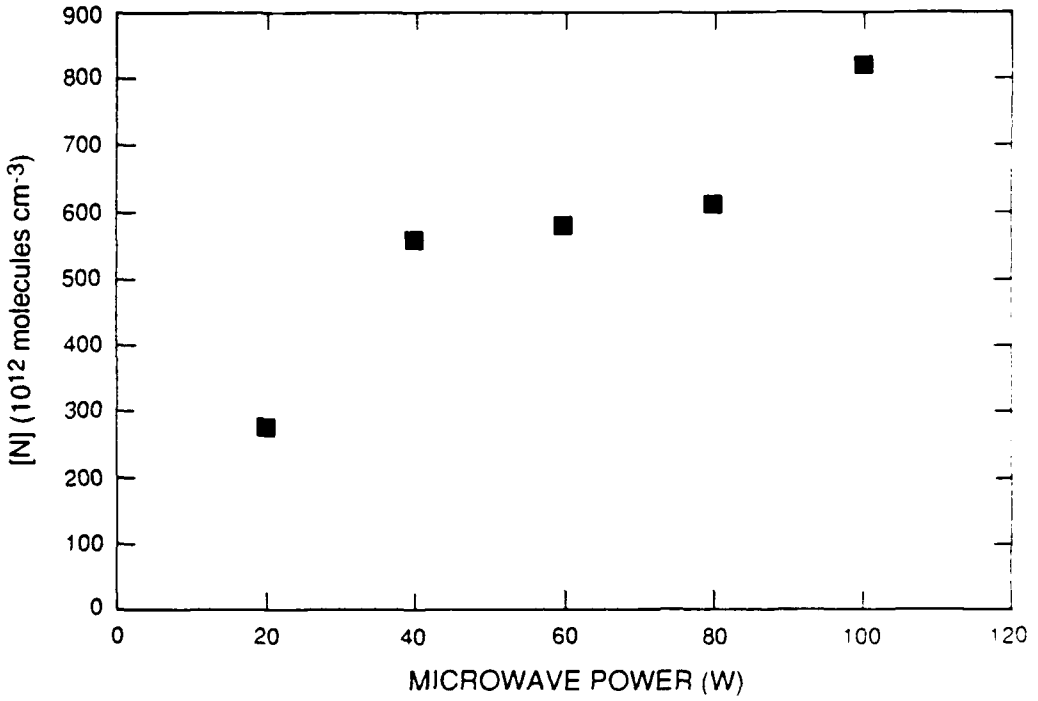

Figure 74. Discharge power dependence of N-atoms produced in an N_2/He microwave discharge.

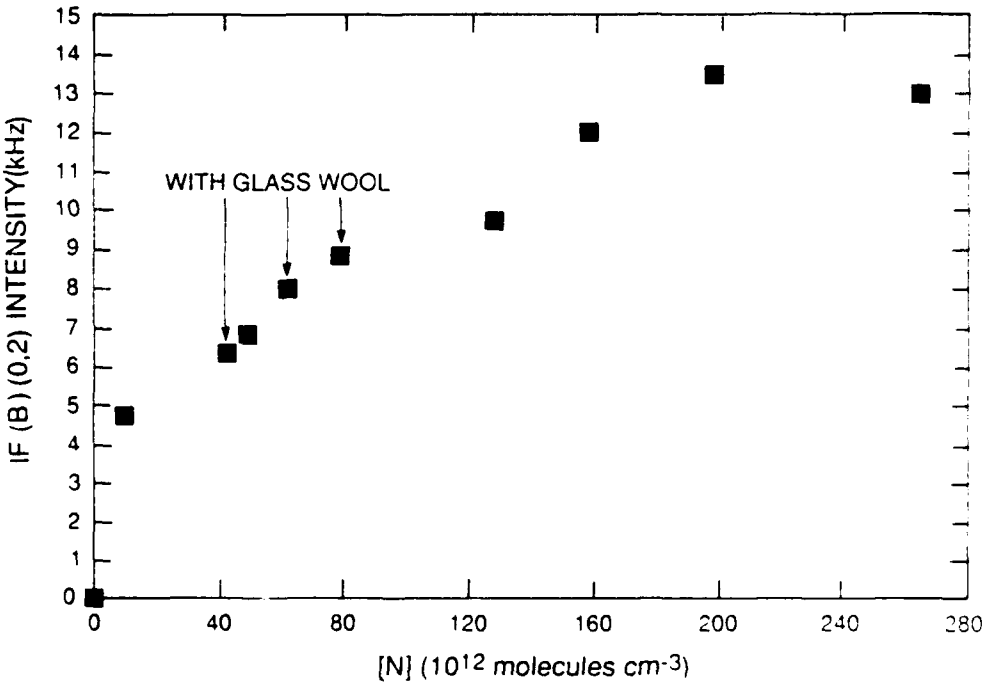

Figure 75. IF(B-X) (0,2) intensity versus [N].

These experiments were done under flow and pressure conditions similar to those in the scaling experiments.

With a Ni screen in place, and all N-atoms removed from the effluents of a N_2/He discharge, no IF(B-X) emission is observed. This means that $N_2(X,v \lesssim 6)$, which does pass through the screen, does not play a major role in exciting IF. The potential role of $N_2(X,v>>6)$ remains an unanswered question.

Replacing the Ni screen with a glass wool plug, which eliminates $N_2(X,v)$, further confirms this result since IF(B) excitation persists. The intensities observed in this case were significantly lower than without the glass wool plug. The NO titrations taken with the glass wool plug determined that the [N] had decreased. Figure 75 shows that the relative IF(B-X) intensities observed with a glass wool plug can be explained by a loss of N-atoms.

5.2.2.3 Penning-ionization Experiments. Lastly, the Penning-ionization diagnostic was used to confirm that discharge produced $N_2(X,v)$ was being relaxed in the glass wool plug and was unaffected by a Ni screen. The theory behind Penning ionization has been described in detail (Ref. 2). In brief, the interaction between He metastables and N_2 results in Penning ionization of the N_2 into the B-state of the molecular ion. The resulting first negative emission, N_2^+ ($B\,^2\Sigma^+_u$ - $X\,^2\Sigma^+_g$) is analyzed, to determine the vibrational distribution of the ground-state, neutral nitrogen molecules. Due to the fact that Penning ionization is a vertical process in the Franck-Condon sense, the vibrational distribution of the product ions are determined solely by the vibrational distribution of the reactant molecules and the Franck-Condon factors which couple the two states. In many cases, a modified Treanor distribution represents the ground state distribution. Using this model, one can vary the ground state vibrational temperature until calculated excited state distributions agree with observations. The best fit vibrational temperature determines the relative populations in the different levels of ground state N_2.

The experimental apparatus is shown in Figure 76. Typical flow rates (in μmol s^{-1}) were He (dc discharge), 1800; He (N_2 carrier), 900; N_2, 70; and pressures were typically 3.8 torr.

The Penning-ionization diagnostic has the limitation of being sensitive primarily to N_2 (v=0-6). Although $N_2(v=9)$ is required to excite IF(B) qualitative information can still be obtained on the extent of N_2 vibrational excitation. First negative emission with a glass wool plug and a Ni screen is shown in Figures 77 and 78. As expected, much of the $N_2(X,v)$ present in the discharge is relaxed by the glass wool plug (Figure 77). It is a fair assumption that populations in $N_2(X,v>6)$ will be increasingly diminished leading to the inference that $N_2(X,v)$ has a small, if any, role in exciting IF(B). This conclusion is further supported by the Ni screen experiments. Figure 78 is the Penning-ionization spectrum of N_2^* through a Ni screen. No evidence has been observed for IF(B) excitation under these conditions although the N_2 is obviously quite vibrationally excited.

In conclusion, the diagnostic experiments have essentially eliminated $N_2(X,v)$ as an energy carrier and have reinforced the role of N-atoms as a precursor to the responsible N_2

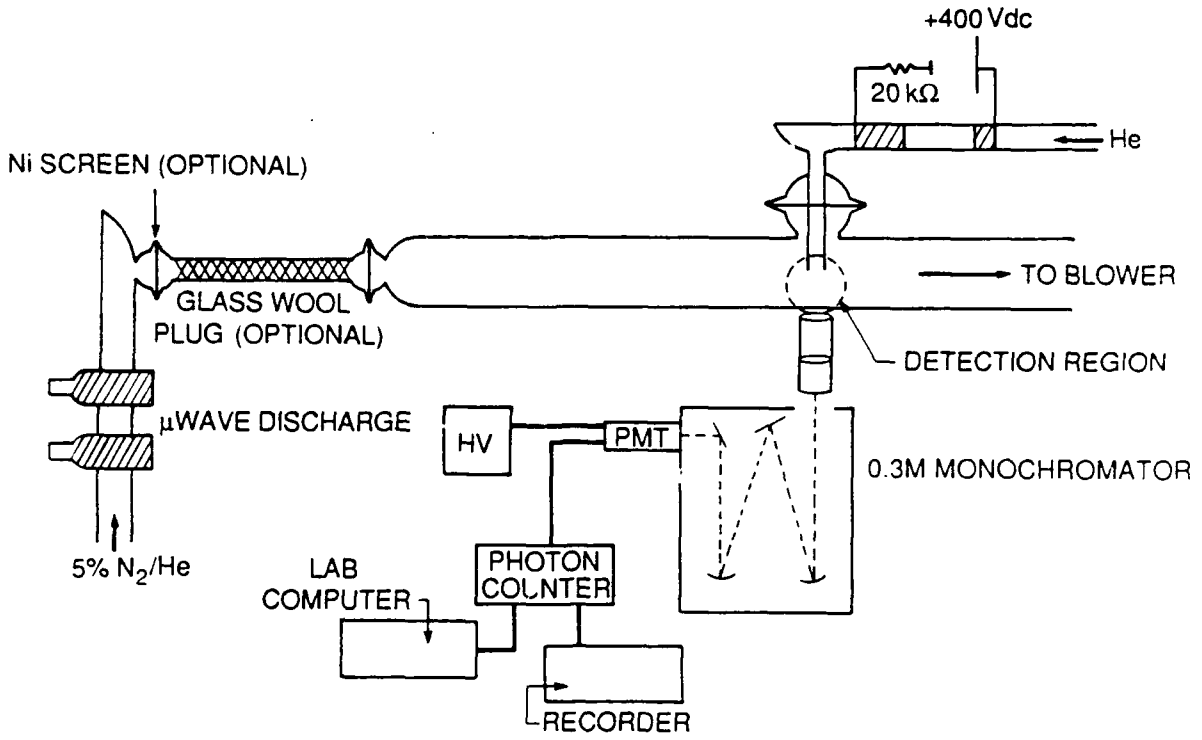

Figure 76. Flow reactor configuration for Penning-ionization studies.

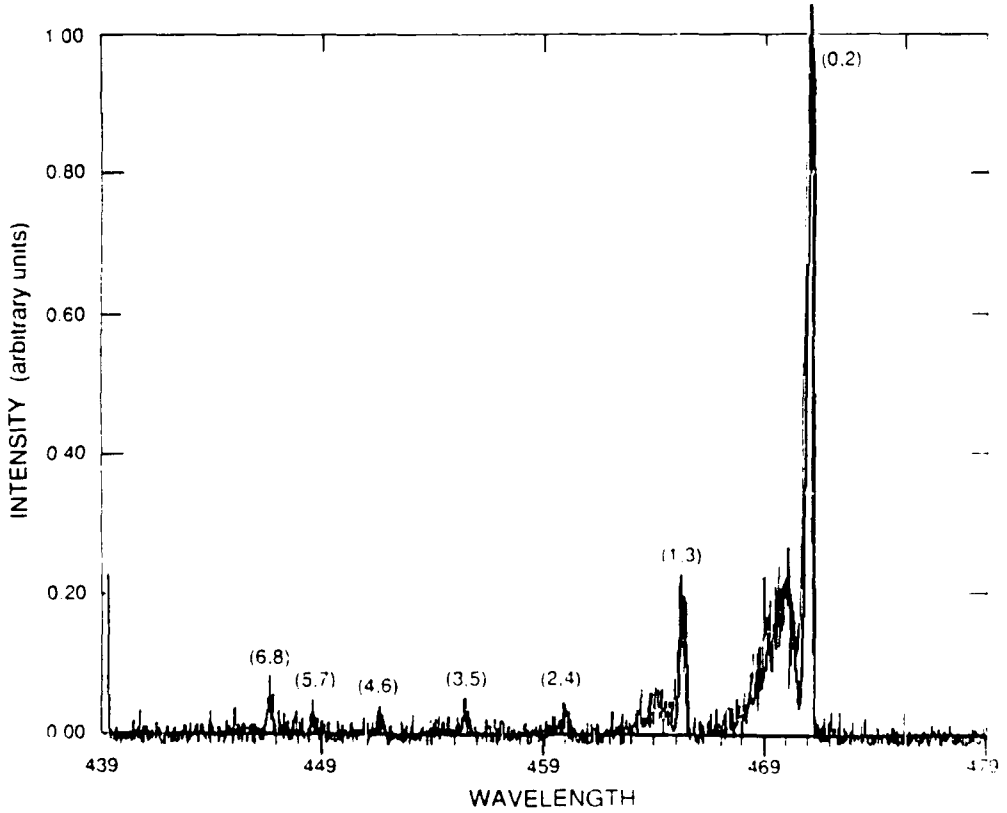

Figure 77. Penning ionization of $N_2(v)$ generated in active N_2 with a glass wool plug.

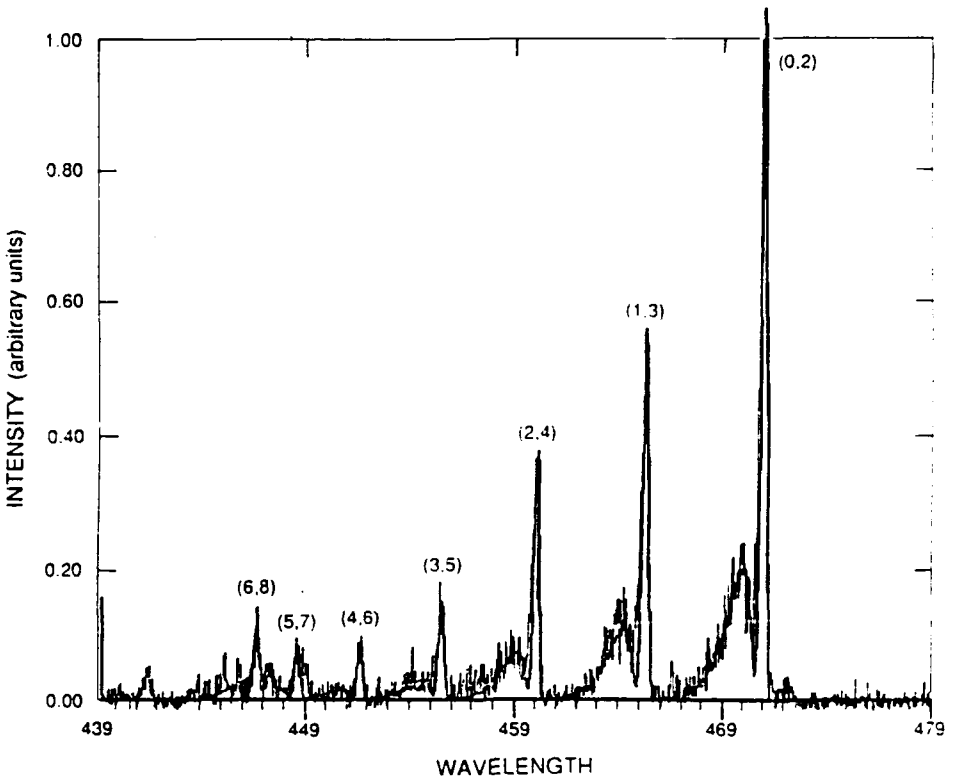

Figure 78. Penning-ionization spectra of $N_2(v)$ generated from active N_2 with Ni screen.

metastable. It should be noted here that $N_2(A)$, a known transfer agent to IF (Refs. 3 and 4), can also be eliminated from consideration in this case after estimating the number density of N_2^* required to excite the observed IF(B). The differential equation describing the rate of change in the IF(B) number density with time is

$$\frac{d[IF^*]}{dt} = k_{ex}[IF][N_2^*] - k_{rad}[IF^*] \qquad (66)$$

Because the IF(B) radiative decay is quite large, the IF(B) is in steady state. Assuming a gas kinetic excitation rate, it is estimated that in order to observe 10^8 molecule per cubic centimeter of IF^* from 10^{13} molecules per cubic centimeter of IF(X), the $[N_2^*]$ must be on the order of 10^{10} molecules per cubic centimeter. The $N_2(A\text{-}X)$ emission is not observed in the flow tube from the effluents of the N_2 discharge which suggests that the $N_2(A)$ concentration must be $< 10^7$ molecules per cubic centimeter, too low to account for the observed IF(B) concentration.

5.2.3 CF_3I versus I_2

The final part of this section presents observations of enhanced IF(B) production efficiency using the F + I_2 reaction to produce IF(X).

5.2.3.1 Experimental. The I_2 + F experimental setup is shown in Figure 79. Typical flow conditions and pressures were comparable to the I + CF_3I experiments. The flow rates were He (N_2 carrier), 870; He (F_2 carrier), 370; Ar (iodine donor carrier), 340; F_2, 4; N_2, 47. Pressures were typically 3.8 torr.

5.2.3.2 Results. With comparable concentrations of I_2 and CF_3I, there is a more efficient production of IF(B) using the I_2 + F reaction. Figure 80 shows the IF(B) (0,2) intensity as a function of concentration of each of these reactants. Under the experimental conditions employed, I_2 + F seems to be about two times more efficient at IF(B) production than the CF_3I + F reaction. This is most likely due to the fact that I_2 + F produces IF(X) which is vibrationally excited (Ref. 117). Since the mean time between generating the IF(X,v) in the I_2 + F reaction was about 4 ms, some vibrational relaxation of the IF(X,v) probably occurred. Shortening the mixing time of the IF(X,v) with the N-atom flow undoubtedly would considerably enhance the IF(B) excitation rate further.

These room temperature measurements using I_2 limited the [I_2] that could be introduced into the flow tube so the highest flows of CF_3I could be compared to I_2. This result, however, implies an increased IF(B) production which could lead to greater [IF(B)] at higher ambient temperatures. The choice of reaction to produce IF(X) can have a large impact on scaling concerns.

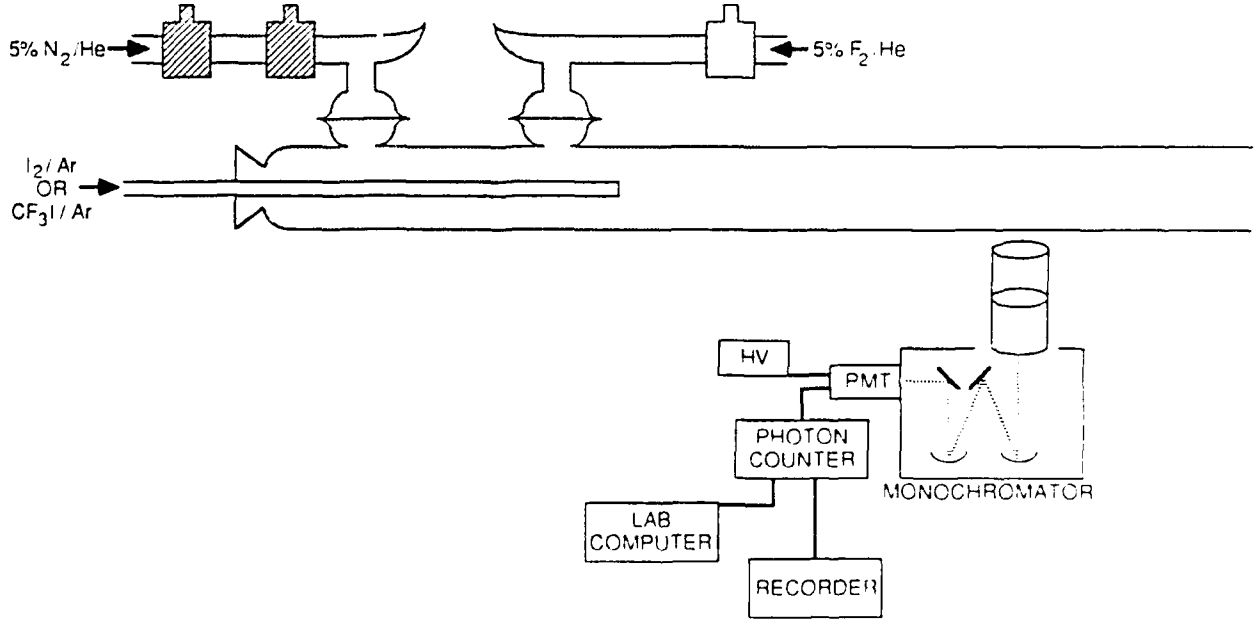

Figure 79. Flow reactor configuration for IF(B) excitation studies comparing I donor.

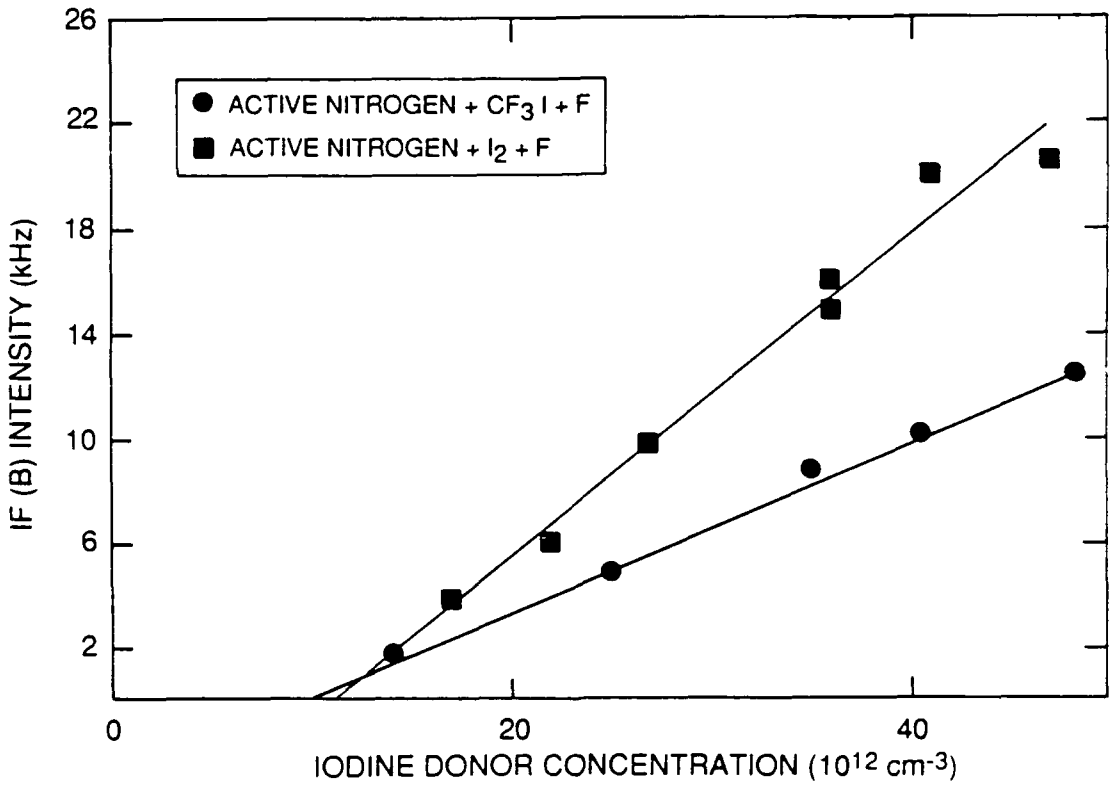

Figure 80. The IF(B) intensity versus I donor concentration.

5.3 ACTIVE NITROGEN PRODUCED UNDER "FAST FLOW" CONDITIONS (REGIME II)

5.3.1 Introduction

Previous studies on the excitation of IF($B^3\Pi_0^+$) in active nitrogen indicated that $N_2(X,v'' > 9)$ could be the metastable in the active N that was responsible for the excitation (Refs. 3, 5, and 6). At the time those studies were done there was no clear diagnostic of the higher vibrational levels of $N_2(X,v'')$, nor was there a clean source of $N_2(X,v'')$ that was free from other metastable species. During the course of Phase II, a clean source and a diagnostic for the higher vibrational levels of $N_2(X,v'')$ were developed (Ref. 30). In brief, flowing active N through a Ni screen recombines most of the atoms exiting the discharge and deactivates the electronic metastables, but allows copious amounts of $N_2(X,v'')$ to pass through. The diagnostic is to add metastable N molecules, $N_2(A^3\Sigma_u^+)$, to the flow and to observe the resultant N first-positive emission, $N_2(B^3\Pi_g - A^3\Sigma_u^+)$. This diagnostic is sensitive to vibrational levels of $N_2(X,v'')$ between 5 and 15.

The IF($B^3\Pi_0^+$) excitation in the presence of $N_2(X,v'')$ generated by this clean source, has been looked for/sought using downstream addition of $N_2(A)$ to confirm the presence of the $N_2(X,v'')$ as well as to allow an estimation of its number density. The small amounts of IF(B) excitation observed appear to be from residual $N_2(A)$ that was not deactivated on the Ni screen, rather than from the $N_2(X,v'')$. Additional studies with the Ni screen removed

showed substantial IF(B) excitation. In those studies, roughly 40 percent of the IF(B) excitation could be attributed to $N_2(A)$ in the active-N stream. The balance of the excitation is caused by an unidentified metastable. The identity of this metastable, however, is not $N_2(X,v'' \leq 15)$.

5.3.2 Experimental

These experiments were done in a 4.6-cm ID, quartz flow reactor (see Figure 81) that has been described previously (Refs. 2 and 30). The $N_2(X,v'')$ is generated at the upstream end of the flow reactor in a microwave discharge through a flow of N dilute in He. The discharge effluents flow through a Ni screen prior to turning a right angle and entering the flow reactor. At the downstream end of the flow reactor, two injectors, spaced 10 cm apart, introduce first IF and then $N_2(A)$.

The IF is generated in the injector from the reaction between CF_3I and F-atoms. The F-atoms are produced in a microwave discharge through a mixture of CF_4 in He at the upstream end of the injector. Downstream from this discharge, CF_3I is added to the injector, and the F-atoms and CF_3I flow together for several milliseconds before exiting the injector into the main flow reactor. The residence time in the injector is adjusted to ensure complete reaction of the F with the CF_3I. The walls of the injector are teflon coated to retard surface recombination of the IF that is generated in the injector.

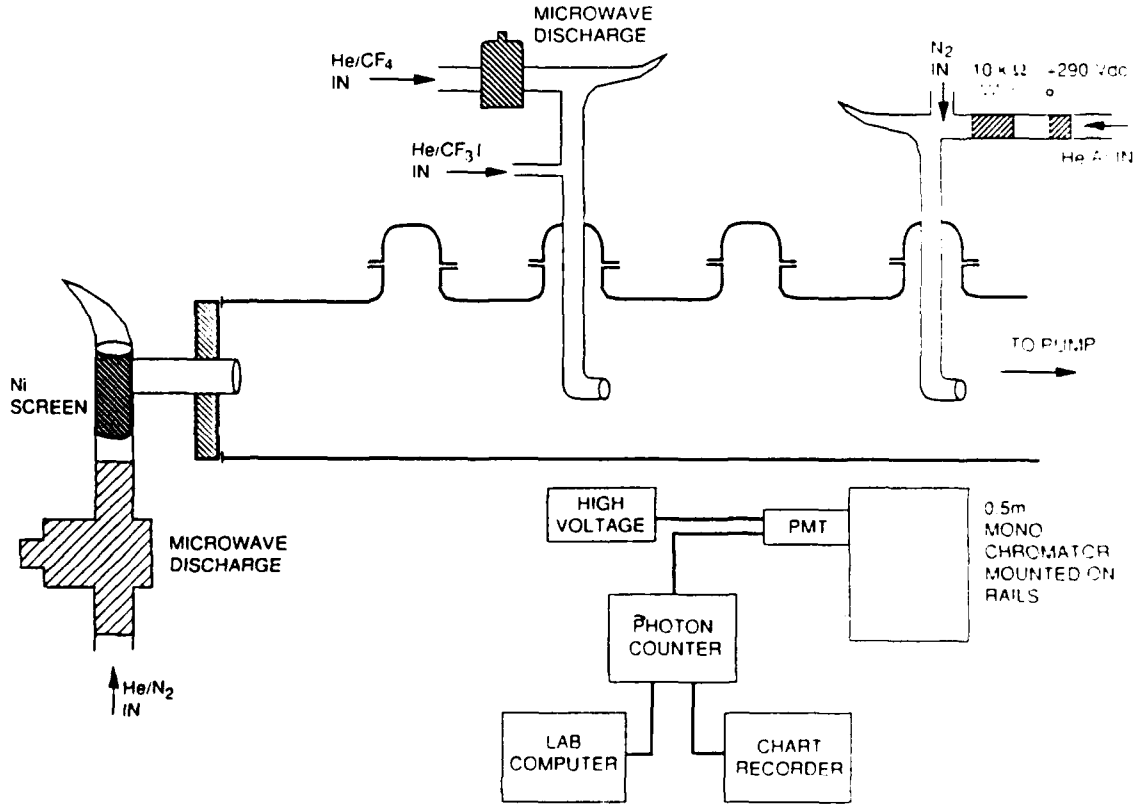

Figure 81. Flow reactor for studying the excitation of IF(B) by $N_2(X,v'')$.

The $N_2(A)$ is generated in the second injector from the reaction between metastable Ar atoms and N molecules. The Ar metastables are produced in a hollow-cathode, dc discharge through a mixture of about 5 percent Ar in He. The N-metastable number densities at the exit of the injector are fairly modest, roughly 10^8 molecules per cubic centimeter but these number densities were adequate for the experimental measurements.

Spectral observations of emissions inside the flow reactor used a 0.5 m monochromator which was sensitive between 200 and 900 nm. All spectra were taken several centimeters downstream from the $N_2(A)$ injector. The relevant spectra consisted of scans of the N Vegard-Kaplan bands, $N_2(A^3\Sigma_u^+ - X^1\Sigma_g^+)$, between 250 and 370 nm which revealed the number densities of $N_2(A)$, the nitrogen first-positive bands between 550 and 900 nm, the intensities of which were used to estimate $N_2(X,v'')$ number densities, and the $IF(B^3\Pi_O^+ - X^1\Sigma^+)$ bands between 440 and 650 nm. All spectra were analyzed using a spectral fitting procedure documented previously (Ref. 22). This procedure gives the number densities of all emitting states in the spectrum, including correcting for spectral overlap from interfering systems. Einstein coefficients used in the spectral analysis included those of Shemansky (Ref. 118) for $N_2(A\text{-}X)$, Piper et al. (Ref. 22) for $N_2(B\text{-}A)$, and Marinelli and Piper (Ref. 119) for IF(B-X).

5.3.3 Results

As a check on the system, the excitation of IF(B) by $N_2(A)$ was examined first. This system had been studied in some detail previously (Ref. 4), and the results were confirmed by Cha and Setser (Ref. 120). Mixing IF and $N_2(A)$ together resulted in the $IF(B^3\Pi_O^+ - X^1\Sigma^+)$ system. The relative vibrational distribution is slightly more relaxed than observed previously, but the earlier results were done in a primarily Ar buffer, while the current experiments used a He buffer. Helium is roughly five times more efficient than Ar at relaxing vibrational energy in IF(B) (Ref. 121). Measurements of the rate coefficient for exciting IF(B) by $N_2(A)$ gave a rate coefficient of 7×10^{-11} cm^3 molecule^{-1} s^{-1} which agrees with the previously reported value (Ref. 4) of 8×10^{-11} cm^3 molecule^{-1} s^{-1}.

Next the excitation of IF(B) by $N_2(X,v'')$ was investigated. For these experiments the product of the IF(B) excitation rate coefficient times the exciting metastable number density for excitation by $N_2(X,v'')$ was compared to that by $N_2(A)$. Since IF(B) is in steady state within the monochromator's field of view, its formation and decay rates will be equal:

$$k_{ex}[IF][N_2^*] = k_{rad}[IF^*] = I_{IF^*} \tag{67}$$

The product of the excitation rate coefficient times the number density of the metastable responsible for the excitation is

$$\frac{dI_{IF^*}}{d[IF]} = k_{ex}[N_2^*] \tag{68}$$

Figure 82 is a plot of the IF(B) intensity as a function of added IF number density for excitation by $N_2(A)$ and $N_2(X,v'')$. The ratio of the slope of the line for $N_2(A)$ excitation to that for $N_2(X,v'')$ excitation is 22. This discrepancy means either that $N_2(X,v'')$ is much less efficient at exciting IF(B) than is $N_2(A)$, or else that some small number density of $N_2(A)$ persists downstream from the Ni screen, and that this residual $N_2(A)$ number density is 22 times less than the number density of the $N_2(A)$ which was added through the $N_2(A)$ injector. Such a small $N_2(A)$ number density would have been below the detection limit.

In the first instance, i.e., excitation by $N_2(X,v'')$, the number density of $N_2(X,v''=5\text{-}15)$ was 2.7×10^{14} molecules per cubic centimeter. This number density and the slope of the line in Figure 82 indicates that the rate coefficient for exciting IF(B) by $N_2(X,v'')$ can be only 1×10^{-18} cm^3 $molecule^{-1}$ s^{-1}. In reality, this number must be considered to be an

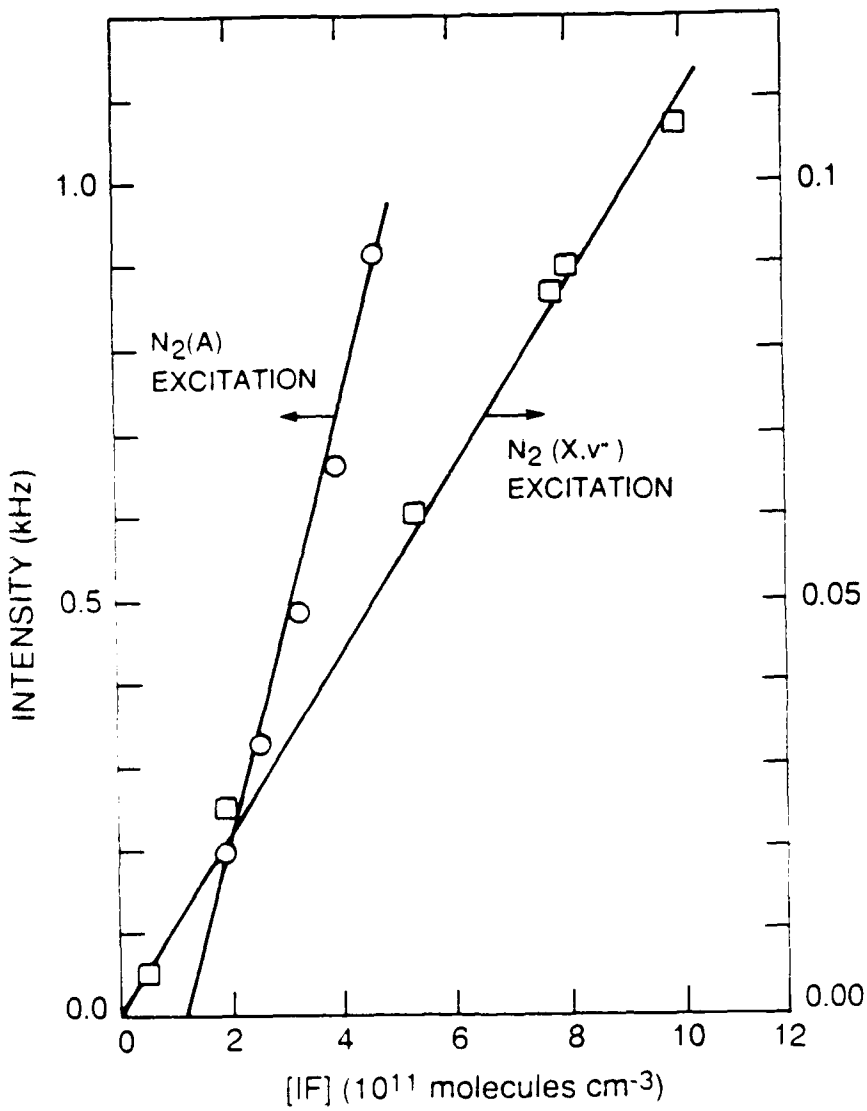

Figure 82. Excitation of the IF(B) 0,4 band by $N_2(A)$ and $N_2(X,v'')$.

upper limit because there is good reason to believe that the actual excitation is by residual $N_2(A)$ in the afterglow.

Two pieces of evidence point to the likelihood that $N_2(A)$ persists downstream from the discharge. The microwave discharge makes not only $N_2(X,v'')$, but also a small amount of NO due to impurities in the gasses used. The $N_2(A)$ excites the NO resulting in fluorescence of the NO γ bands (Ref. 83), $NO(A^2\Sigma^+ - X^2\Pi)$. The intensity of the NO γ bands can be used as a tracer for $N_2(A)$. The ratio of intensities of the NO γ bands in the presence of $N_2(A)$ to that with the $N_2(A)$ off, i.e., in the presence only of $N_2(X,v'')$, is 20, essentially the same ratio as found for the two cases of IF(B) excitation. A weak residual fluorescence from $N_2(B)$ was observed when the $N_2(A)$ was turned off. The most likely source of this $N_2(B)$ is excitation of $N_2(X,v'')$ by $N_2(A)$. Here again the ratio of the $N_2(B)$ with the $N_2(A)$ on to that with it off was 22. All three observations point to the persistence of residual $N_2(A)$ downstream from the Ni screen, and indicate that any excitation of IF(B) by $N_2(X,v'')$ is entirely negligible.

A possible alternative for the first-positive emission observed in the absence of added $N_2(A)$ would be that generated from N-atom recombination. The N-atom number densities downstream from the Ni stream were checked by titrating with NO. The NO quantitatively converts any N-atoms in the flow to O-atoms (Ref. 122). In the presence of excess NO, any atomic O in the flow will recombine with the NO to give the well known air afterglow emission (Refs. 49-55). A weak air afterglow was observed, and its variation in intensity with the number density of added NO indicated an initial N-atom number density downstream from the Ni screen of 1.1×10^{11} atoms per cubic centimeter. Previous experience (Ref. 77) had been such that small number densities of N-atoms at the low pressures employed, 1.06 torr, would result in unobservable first-positive emission by the detection system. The Ni screen was quite efficient at removing N-atoms from the flow. The NO titrations of the discharge afterglow under identical conditions, but with the Ni screen removed, indicated an N-atom number density of 6.4×10^{12} atoms per cubic centimeter.

Finally, the Ni screen was removed and the excitation of IF(B) in the microwave-discharge afterglow was examined. In this case the ratio of the rate coefficient for IF(B) excitation times the metastable N number density from active N excitation to that from $N_2(A)$ excitation was 14.2. Scans over the $N_2(A\text{-}X)$, Vegard-Kaplan, bands, however, showed that the ratio of the $N_2(A)$ number densitiy from the active N to that from the $N_2(A)$ source alone was 5.5. Thus only 40 percent of the excitation in the active N comes from $N_2(A)$ in the flow. The rest comes from some other N metastable. In previous work, it was thought that $N_2(X,v'')$ might be that additional metastable. The results of this work show conclusively that $N_2(X,v'' \leq 15)$ is incapable of exciting IF(B) to any appreciable extent. Conceivably somewhat higher vibrational levels could be involved. Thus the identity of this metastable is unknown.

5.4 IF(B) EXCITATION BY THE PRODUCTS OF N_3 RECOMBINATION

This section relates observations of IF excitation by the products of N_3 recombination. The N_3 recombination reaction was used as a source of $N_2(X,v)$ because it produces high yields.

5.4.1 Experimental

The flow tube configuration for these experiments is shown in Figure 83. The IF is produced by chemical reaction between CF_3I and F-atoms and the N_3 radicals by the reaction of F with HN_3. When excess F-atoms are employed, these methods quantitatively convert CF_3I or HN_3 to IF or N_3 molecules, respectively. Typical flow rates (in micromole s^{-1}) are: He (F_2 diluent), 457; He (F_2 diluent), 497; F_2 (IF generator), 25; F_2 (N_3 generator), 4.41; HN_3, 8.6; and CF_3I, 8. Typical pressures are 1 to 2 torr.

5.4.2 Results

The IF(B-X) emission is observed when the products of N_3 recombination and IF interact. The IF(B-X) spectrum displayed in Figure 84 exhibits vibrational excitation up to v = 8. The vibrational distribution is shown in Figure 85. To excite IF at all, 2.3 eV are required which corresponds to $N_2(v=9)$. At this time, there is no information on the number density of N_2 at this vibrational level, so $N_2(v)$ cannot definitively be identified as the source.

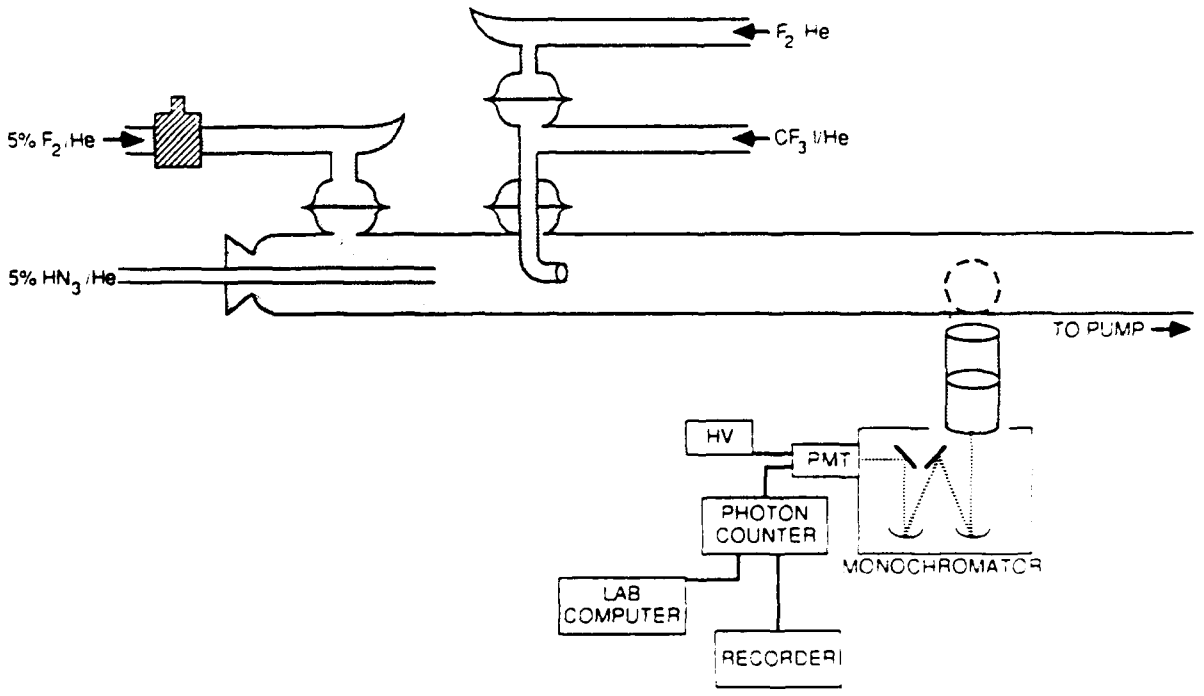

Figure 83. Flow reactor configuration for $N_2(v)$ + IF studies.

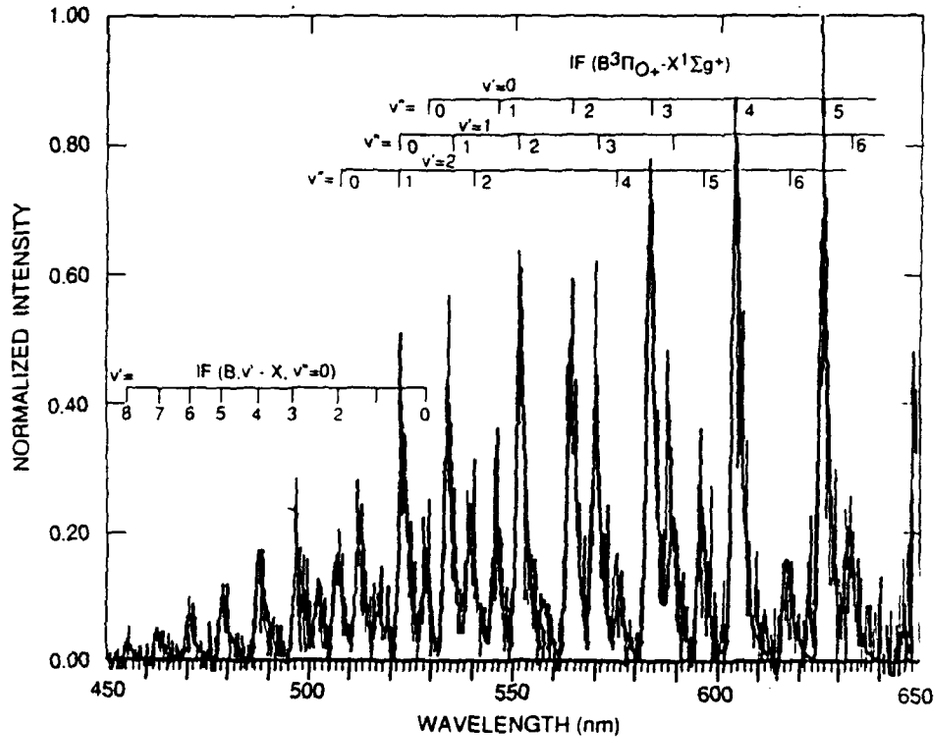

Figure 84. IF(B) excited by N_3 + N_3 recombination products.

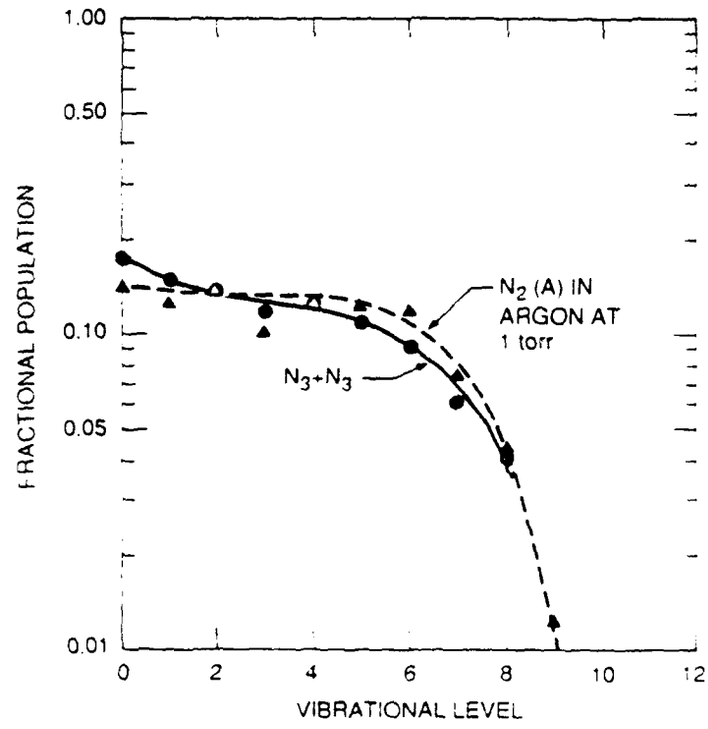

Figure 85. The IF(B) vibrational distributions from N_2^* excitation.

Another likely source for IF excitation is $N_2(A)$ (Refs. 3 and 4). A typical IF vibrational distribution from this source is also shown in Figure 85. This IF(B) distribution looks quite similar to that excited from the products of N_3 recombination, suggesting that $N_2(A)$ could be the responsible metastable in the $N_3 + N_3$ source. The $N_2(A\text{-}X)$ emission was not observed in the products of the N_3 recombination reaction. This places an upper limit on the $N_2(A)$ number density of about 10^7 molecules per cubic centimeter, and an upper limit on the branching ratio for the $N_2(A)$ formation in $N_3 + N_3$ of about 10^{-5}. The upper limit $N_2(A)$ number density is sufficient to excite the weak IF(B-X) fluorescence that was observed, however, so that failure to observe $N_2(A\text{-}X)$ emission doesn't discount $N_2(A)$ as an excitation source for IF(B).

5.5 QUENCHING OF $N_2(X,v'')$ AND $N_2(B)$

5.5.1 Introduction

One component necessary for understanding energy-transfer reactions of $N_2(X,v'')$ is to know the rates at which various molecules quench $N_2(X,v'')$. To this end a technique was developed for determining global quenching rate coefficients for $N_2(X,v''=5\text{-}15)$. This technique relies upon the diagnostic wherein the intensity of nitrogen first-positive emission, excited in the reaction between $N_2(A)$ and $N_2(X,v'')$, is proportional to the number density of $N_2(X,v'')$ (Ref. 30). Because adding a quencher to the reactor can quench not only the $N_2(X,v'')$ but also the first-positive emission itself, one must also determine $N_2(B)$ quenching rate coefficients. Thus, using this technique will result in quenching rate coefficients for both species.

5.5.2 Experimental

These experiments used the 4.6 cm ID quartz flow reactor which is described elsewhere (Ref. 30). Briefly, the $N_2(X,v'')$ is prepared first by discharging a mixture of Ni dilute in He and then passing the effluents of the discharged mixture through a Ni screen prior to their entry into the flow reactor. At the downstream end of the flow reactor, $N_2(A)$ is injected into the flow and the resulting N_2 first-positive emission is detected using a monochromator that is sensitive to radiation between 200 and 900 nm. The quenching reagent is added to the flow through a loop injector that can be moved along the length of the flow tube. The details of the experimental apparatus and procedures can be found elsewhere (Ref. 30).

5.5.3 Experimental Technique

When the loop injector is placed immediately behind the $N_2(A)$ inlet and quencher is added, the number density of $N_2(X,v'')$ remains essentially unchanged because it is mixed with the quencher for too short a time to effect significant quenching. Any diminution in the first-positive emission, therefore, results from quenching of $N_2(B)$. When the loop injects its reagent at the upstream end of the flow reactor, the $N_2(X,v'')$ and quencher flow together for many milliseconds. This allows adequate time for the $N_2(X,v'')$ to be quenched unless the quenching rate coefficients are exceedingly small. Any difference in diminution of the

first-positive emission with the injector in the upstream position as compared to the downstream position can be attributed to quenching of the $N_2(X,v'')$ by the added reagent. These concepts are detailed mathematically below.

In the absence of added quencher, the intensity of the N_2 first-positive emission is given by

$$I_0 = k_r[N_2(B)] = k_{ex}[N_2(X,v'')][N_2(A)] \tag{69}$$

where, k_{ex} is the rate coefficient for $N_2(B)$ excitation in the reaction between $N_2(A)$ and $N_2(X,v'')$, and k_r is the radiative decay rate of the $N_2(B)$ (Ref. 22). These experiments were run at low pressures, primarily of He so as to minimize quenching by the bath gas in the flow tube. Bath-gas quenching is neglected, therefore, in Equation (69). When the quencher is introduced to the flow reactor, the first-positive emission intensity is given by

$$I = k_r[N_2(B)] = \frac{k_{ex}[N_2(A)][N_2(X,v'')]}{1 + \frac{k_Q[Q]}{k_r}} \tag{70}$$

where k_Q is the rate coefficient for $N_2(B)$ quenching by the quencher Q. Taking the ratio of the intensity in the absence of quencher to that in the presence of quencher gives the classical Stern-Volmer formula for electronic quenching, viz.

$$\frac{I_0}{I} = 1 + \frac{k_Q[Q]}{k_r} \tag{71}$$

The rate coefficient for $N_2(B)$ quenching is given, therefore, by the product of the $N_2(B)$ radiative decay rate times the slope of a plot of I_0/I versus [Q] for data taken with the injector in the downstream position.

With the injector in the upstream position, quenching of the $N_2(X,v'')$ also becomes possible, and the first-positive emission intensity becomes

$$I = k_r[N_2(B)] = \frac{k_{ex}[N_2(A)][N_2(X,v'')]_0 \, e^{-k_v[Q]\Delta t}}{1 + \frac{k_Q[Q]}{k_r}} \tag{72}$$

where k_v is the rate coefficient for $N_2(X,v'')$ quenching, Δt is the time the quencher and the $N_2(X,v'')$ are mixed, and the subscript o refers to conditions in the absence of added quencher. The $N_2(X,v'')$ quenching rate coefficients can be determined, therefore, from the ratio of Stern-Volmer factors at short to long delay times:

$$k_v = \frac{\ln(I_d/I_u)}{[Q]\Delta t} \qquad (73)$$

where the subscripts u and d refer to intensity measurements with the injector in the upstream and downstream position, respectively.

These formalisms presume that the $N_2(A)$ that is added to the reactor is not diminished by addition of the quencher. This is not necessarily always the case. In cases where the A-state also is quenched, the actual A-state number density must be determined for each set of experimental conditions, and divided into the first-positive intensities. This procedure will correct for A-state quenching, and makes this technique applicable, therefore, for studies of quenchers which react rather efficiently with $N_2(A)$. Because of the short time that $N_2(A)$ is actually in the flow reactor before the fluorescence is observed, A-state quenching generally will not be large even for reagent molecules which normally quench the A-state efficiently.

5.5.4 Results

The initial studies of reaction between $N_2(A)$ and $N_2(X,v'')$ included the variation in B-state excitation as a function of A-state vibrational level (Ref. 30). CH_4 was added to the reactor to relax the vibrational energy in the A-state. In the analysis, some vibrational relaxation of the $N_2(X,v'')$ by the CH_4 was presumed, but no electronic quenching. Subsequently, it was found that this supposition is in error and that, in fact, CH_4 is very efficient at quenching first-positive emission, but is quite poor at relaxing the vibrational energy of $N_2(X,v'')$. The quenching of $N_2(B)$ by CH_4 has been studied, therefore, in a little more detail than the other molecules investigated. Observations on all the other molecules are essentially survey measurements in which a two-point determination was made of the $N_2(B)$ and $N_2(X,v'')$ quenching rate coefficients.

When the first-positive emission spectrum was scanned in the presence of 10 mtorr of CH_4, a significant diminution in intensity was noted. This diminution was the same at 9 ms interaction as it was when the interaction time was < 1 ms. This indicated that CH_4 is indeed a significant quencher of $N_2(B)$, but that it didn't quench $N_2(X,v'')$ under the conditions employed.

The quenching of several bands of the first-positive system as a function of added CH_4 was studied. Figure 86 shows the Stern-Volmer quenching plot for two of these levels. The data indicate rate coefficients for quenching $N_2(B)$ by CH_4 which range from about 5×10^{-10} cm^3 molecule^{-1} s^{-1}, for $v' = 2$ and 3, to 7 and 9×10^{-10} cm^3 molecule^{-1} s^{-1} for $v' = 6$ and 8, respectively.

Table 8 summarizes the survey data obtained from these experiments. The upper limit values are calculated from the assumption that there would be a 10 percent decrease in first-positive intensity. Since the experiments were essentially proof-of-concept measurements, the experimental values can have uncertainties of up to a factor of 2. In

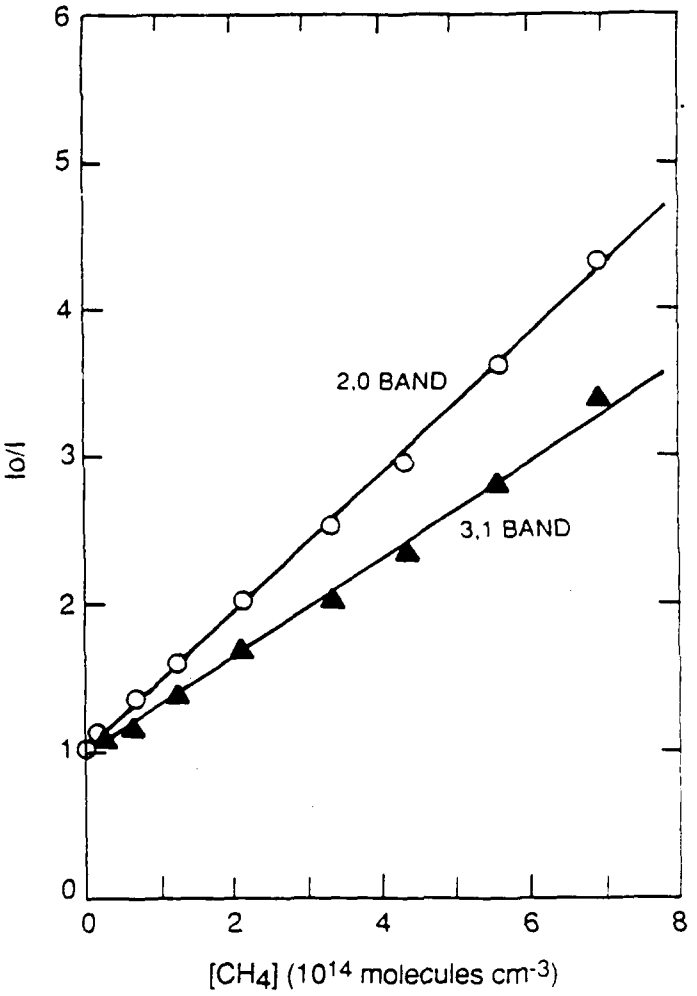

Figure 86. Stern-Volmer plot for $N_2(B)$ quenching by CH_4.

Table 8. Rate coefficients[a] for global quenching of $N_2(B)$ and $N_2(X,v'')$

Quencher	$N_2(B)$	$N_2(X,v'')$
CH_4	6×10^{-10}	$< 3 \times 10^{-14}$
H_2	1.3×10^{-10}	9×10^{-16}
CO_2	5×10^{-10}	4.4×10^{-14}
N_2	4×10^{-11}	2×10^{-15}
CF_4	$> 10^{-11}$	$> 10^{-15}$
SF_6	$< 1 \times 10^{-11}$	$< 2 \times 10^{-15}$
N_2O	6×10^{-10}	---

a. Units of cm^3 $molecule^{-1}$ s^{-1} at 300 K.

addition, only global quenching-rate coefficients are presented. Rate coefficients for quenching individual levels may well vary considerably from one another, as for CH_4, and also for $N_2(B)$ quenching by N_2 (Ref. 10).

Most gases studied quenched $N_2(B)$ quite strongly, including CF_4, which was observed only qualitatively. N_2, CO_2, CF_4, and H_2, weakly, also quenched $N_2(X,v'')$, but CH_4 and SF_6 had essentially no effect upon the number density of $N_2(X,v'')$. There were no observations of N_2O with the injector in the upstream position, so there is no information as to its efficiency at relaxing $N_2(X,v'')$. Previous observers, however, have indicated that N_2O is moderately efficient at quenching the vibrational energy in Ni (Ref. 116).

SF_6 exhibited rather strange behavior. In the global sense, it quenched neither the $N_2(B)$, nor the $N_2(X,v'')$. The first-positive vibrational distributions in the absence and presence of SF_6 were quite different, however, with some levels increasing in intensity as SF_6 was added, while others diminished in intensity. This observation appears to indicate that SF_6 can relax vibrational energy within the B-state manifold.

In summary, a novel technique has been presented for measuring the quenching of $N_2(X,v'')$ and $N_2(B)$ by a variety of quenchers.* Observations indicate that most species quench $N_2(B)$ at rates in excess of gas kinetic, whereas even efficient vibrational quenching of $N_2(X,v'')$ proceeds at rates four to five orders of magnitude less than gas kinetic.

---

* Subsequent to the completion of this work, additional analysis resulted in small corrections to some of the rate coefficients. The basic effect was to reduce the rate coefficients for $N_2(B)$ quenching by about 30 percent. In addition the rate coefficient for $N_2(X,v)$ quenching by H_2 was found to be twice as great a given in Table 8. See L.G. Piper, "Energy Transfer Studies on $N_2(X^1\Sigma_g^+,v)$ and $N_2(B^3\pi_g)$," PSI-1045/SR-467, Physical Sciences Inc., Andover, MA, 1990.

6.0 PROGRAM SUMMARY

A number of diagnostics for $N_2(X,v'')$ have been developed and these diagnostics have been used to characterize sources of $N_2(X,v'')$, both discharge and chemical, as well as to study energy-transfer reactions involving $N_2(X,v'')$. The program involved four major areas of study: 1) development of $N_2(X,v'')$ diagnostics; 2) quantitative correlations between diagnostic techniques; 3) characterization of $N_2(X,v'')$ sources, both discharge and chemical; and 4) the study of energy transfer reactions involving $N_2(X,v'')$.

The diagnostic development work involved developing a number of laser-based diagnostics and two others that are based upon metastable energy-transfer reactions. The laser-based diagnostics included both multiphoton ionization and laser-induced fluorescence. Both techniques involve initial excitation to $N_2(a^1\Pi_g)$ via either one- or two-photon transitions. Two-photon excitation to the intermediate state could be effected from ground-state vibrational levels below $v'' = 4$, whereas the single-photon excitation could be done only from levels above $v'' = 9$. Levels as high as 26 in a microwave discharge afterglow were observed. Both two-photon techniques are fairly insensitive, requiring $N_2(X,v'')$ number densities in excess of 10^{14} molecules per cubic centimeter, but could be made quantitative under carefully controlled conditions. The one-photon excitation techniques had sensitivity limits on the order of 10^8 molecules per cubic centimeter, but could be used quantitatively only in a relative sense.

The energy-transfer based diagnostics involved Penning ionization of the $N_2(X,v'')$ by metastable atoms, which resulted in fluorescence from $N_2^+(B^2\Sigma_u^+)$, and excitation of N first-positive fluorescence, $N_2(B^3\Pi_g - A^3\Sigma_u^+)$, in an energy-transfer reaction between $N_2(X,v'')$ and $N_2(A^3\Sigma_u^+)$. The Penning-ionization technique has sensitivity at least as good as 10^{11} molecules per cubic centimeter and gives absolute number densities of $N_2(X,v'')$. It is sensitive to vibrational levels below 6. The $N_2(A)$ energy-transfer diagnostic is only semiquantitative; bulk $N_2(X,v'')$ number densities can be estimated only to factors of 2 or 3; but it is sensitive to vibrational levels 5 through 15.

Quantitative detection of $N_2(X,v'')$ using 2+2 MPI was compated to that using Penning ionization. There was reasonable agreement, but the large experimental errors inherent in the MPI technique along with its poor overall sensitivity do not make it a particularly attractive diagnostic for most applications.

A number of discharge and chemical sources using the Penning-ionization diagnostic were characterized. Both microwave and rf discharges through mixtures of N in He generated significant amounts of vibrationally excited N, with the microwave source being substantially more efficient. Under some conditions, more than two thirds of the N exiting the microwave discharge was vibrationally excited. No $N_2(X,v'')$ was detected in the effluents of hollow-cathode, dc or dielectric-barrier discharges in N_2/He mixtures.

Chemical sources found to generate significant quantities of $N_2(X,v'')$ were the reaction between N-atoms and NO and the recombination of N_3 radicals. The $N_2(X,v'')$ generated in the

sequence of reactions beginning with the reaction between H and NF_2 and the reaction between N-atoms and N_3 could not be determined. The reaction between N and NO produces an inverted population of $N_2(X,v'')$ while the recombination of N_3 radicals produces $N_2(X,v'')$ in a Treanor distribution with a vibrational temperature of about 3200 K.

The capability of measuring $N_2(X,v'')$ quenching using one-photon laser induced fluorescence was developed. Measurements on the quenching of $N_2(X,v''=14)$ by CF_4 gave a quenching rate coefficient of 3.6×10^{-13} cm^3 $molecule^{-1}$ s^{-1}. This technique is suitable for kinetic measurements involving $N_2(X,v'')$.

A second technique was developed for studying the vibrational quenching of $N_2(X,v''=5\text{-}15)$ which is based on the $N_2(A)$ energy-transfer diagnostic. This technique also results in measurements of $N_2(B)$ quenching rate coefficients. The diagnostic was used to survey the quenching of $N_2(X,v''=5\text{-}15)$ and $N_2(B)$ by CH_4, H_2, CO_2, N_2, CF_4, SF_6, and N_2O.

The excitation kinetics of IF(B) were studied using several different sources of N metastables. Under conditions of relatively high pressure and long transit times from the discharge to the observation region, IF(B) appeared to be excited by the N metastables produced in N-atom recombination. We also found that if the ground-state IF were vibrationally excited, the IF(B) excitation rate was significantly enhanced. Studies on the excitation of vibrationally cold IF(X) in these afterglows resulted in easily achievable number densities of IF(B) in excess of 3×10^8 molecules per cubic centimeter.

Under conditions of low pressure and short transit times from the discharge to the observation region, $N_2(X,v'' \leq 15)$ did not excite IF(B). Only 40 percent of the IF(B) excitation in the active N produced under these conditions, however, could be attributed to the presence of $N_2(A)$ in the afterglow. The bulk of the excitation is by some as yet unidentified metastable species.

REFERENCES

1. Marinelli, W.J. and Kessler, W.J., Laser-Based Diagnostics for $N_2(X,v)$, PSI-2015/TR-669, Physical Sciences Inc., Andover, MA, 1987.

2. Piper, L.G. and Marinelli, W.J., "Determination of Non-Boltzmann Vibrational Distributions of $N_2(X,v'')$ in He/N_2 Microwave-Discharge Afterglows," J. CHEM. PHYS. 89, 2918, 1988.

3. Piper, L.G., Marinelli, W.J., Green, B.D., Rawlins, W.T., Murphy, H.C., Donahue, M.E., and Lewis, P.F., Kinetics of Iodine Monofluoride Excitation by Energetic Nitrogen, PSI TR-460, Physical Sciences Inc., Andover, MA, August 1985.

4. Piper, L.G., Marinelli, W.J., Rawlins, W.T., and Green, B.D., "The Excitation of $IF(B^3\Pi_O{}^+)$ by $N_2(A^3\Sigma_u{}^+)$," J. CHEM. PHYS. 83, 5602, 1985.

5. Piper, L.G. and Marinelli, W.J., "The Excitation of IF by Active Nitrogen," J. PHYS. CHEM. 93, 4033, 1989.

6. Piper, L.G., Davis, S.J., Murphy, H.C., Cummings, W.C., Walkauskas, L.P., DeFaccio, M.A., Cowles, L.M., Rawlins, W.T., Marinelli, W.J., and Green, B.D., CONAN: Chemistry of Nitrogen-A Nascence, Final Technical Report PSI-076/TR-593, Physical Sciences Inc., Andover, MA, January 1987.

7. Piper, L.G., Krech, R.H., and Taylor, R.L., "The Generation of N_3 in the Thermal Decomposition of NaN_3," J. CHEM. PHYS. 71, 2099, 1979.

8. Davis, S.J. and Piper, L.G., "The Production of $N_2(B^3\Pi_g, v=1\text{-}12)$ in the Reaction Between $NF(a^1\Delta)$ and $N(^2D)$," J. CHEM. PHYS. 94, 4515, 1990.

9. Piper, L.G., "State-to-State $N_2(A^3\Sigma_u{}^+)$ Energy Pooling Reactions I. Formation of $N_2(C^3\Pi_u)$ and the Herman Infrared System," J. CHEM. PHYS. 88, 231, 1988.

10. Piper, L.G., "State-to-State $N_2(A^3\Sigma_u{}^+)$ Energy-Pooling Reactions II. The Formation and Quenching of $N_2(B^3\Pi_g, v=1\text{-}12)$," J. CHEM. PHYS. 88, 6911, 1988.

11. Piper, L.G. and Caledonia, G.E., "Long-Lived States in Nitrogen Afterglows," Paper JA-5, 38th Gaseous Electronics Conference, Monterey, CA, October 1985. Bull. A.P.S 31, 157, 1986.

12. Shaub, W.M., Nibler, J.W., and Harvey, A.B., "Direct Determination of Non-Boltzmann Vibrational Level Populations in Electric Discharges by CARS," J. CHEM. PHYS. 67, 1883, 1977.

13. Mutel, B., Bridoux, M., Crunelle-Cras, M., Dessaux, O., Grase, F., Goudmand, P., and Moreau, G., "Study of the Formation and Relaxation of $N_2(X^1\Sigma_g^+)v$ in Active Nitrogen by Pulsed Multichannel Raman Spectroscopy," CHEM. PHYS. LETT. 104, 290, 1984.

14. van Veen, N., Brewer, P., and Bersohn, R., "Detection of the $a^1\Pi_g$ $(v'=0) \leftarrow X^1\Sigma_g^+$ $(v''=0)$ Transition in N_2 by Laser-Induced Fluorescence," J. CHEM. PHYS. 77, 4326, 1982.

15. Young, S.J. and Horn, K.P., "Measurement of Temperatures of Vibrationally Excited N_2," J. CHEM. PHYS. 57, 4835, 1972.

16. Schmeltekopf, A.L., Ferguson, E.E., and Fehsenfeld, F.C., "Afterglow Studies of the Reaction of He^+, $He(2^3S)$, and O^+ with Vibrationally-Excited N_2," J. CHEM. PHYS. 48, 2966, 1968.

17. Bass, A.M., Absorption Spectrum of the 'Pink' Afterglow of Nitrogen in the Vacuum Ultraviolet," J. CHEM. PHYS. 40, 695, 1964.

18. Marinelli, W.J., Kessler, W.J., Green, B.D., and Blumberg, W.A.M., "Quenching of $N_2(a^1\Pi_g, v'=0)$ by N_2, O_2, CO, CO_2, CH_4, H_2 and Ar," J. CHEM. PHYS. 90, 2167, 1989.

19. Marinelli, W.J. Kessler, W.J., Green, B.D., and Blumberg, W.A.M., "The Radiative Lifetime of $N_2(a^1\Pi_g, v=0\text{-}2)$," J. CHEM. PHYS. 91, 701, 1989.

20. Johnson, P.M. and Otis, C.E., "Molecular Multiphoton Spectroscopy with Ionization Detection," ANN. REV. PHYS. CHEM. 32, 139, 1981.

21. Young, R.A., Black, G., and Slanger, T.G., "Vacuum-Ultraviolet Photolysis of N_2O. II. Deactivation of $N_2(A^3\Sigma_u^+)$ and $N_2(B^3\Pi_g)$," J. CHEM. PHYS. 50, 303, 1969.

22. Piper, L.G., Holtzclaw, K.W., Green, B.D., and Blumberg, W.A.M., "Experimental Determination of the Einstein Coefficients for the N_2(B-A) Transition," J. CHEM. PHYS. 90, 5337, 1989.

23. Nadler, I. and Rosenwaks, S., "Studies of Energy Transfer Processes in Triplet States of N_2. I. Energy Pooling by Vibrationally Selected $N_2(A^3\Sigma_u^+, v)$ Molecules," J. CHEM. PHYS. 83, 3932, 1985.

24. Sadeghi, N. and Setser, D.W., "Collisional Coupling of $N_2(B^3\Pi_g)$ and $N_2(W^3\Delta_u)$ States Studied by Laser-Induced Fluorescence," CHEM. PHYS. LETT. 77, 304, 1981.

25. Sadeghi, N. and Setser, D.W., "Collisional Coupling and Relaxation of $N_2B(^3\Pi_g)$ and $N_2(W^3\Delta_u)$ Vibrational Levels in Ar and Ne," J. CHEM. PHYS. 79, 2710, 1983.

26. Rotem, A. and Rosenwaks, S., "Laser-Induced Fluorescence Studies of Molecular Nitrogen," OPT. ENGIN. 22, 564, 1983.

27. Piper, L.G. and Donohue, K., "The Production of $N_2(X,v'')$ and $N_2(A^3\Sigma_u^+)$ in the Recombination of N_3 Radicals," PSI-1045/SR-489, Physical Sciences Inc., Andover, MA, 1990.

28. Young, S.J., "Measurement of Vibrational Temperature of CO and N_2 Using the $He(2^3S)$ Penning Ionization Technique," J. CHEM. PHYS. 38, 1603, 1973.

29. Piper, L.G., Gundel, L., Velazco, J.E., and Setser, D.W., "Excitation of Nitrogen and Carbon Monoxide Ionic Emissions by $He(2^3S)$, He^+, and He_2^+," J. CHEM. PHYS. 62, 3883, 1975.

30. Piper, L.G., "The Excitation of $N_2(B^3\pi_g, v=1\text{-}12)$ in the Reaction Between $N_2(A^3\Sigma_u^+)$ and $N_2(X, v\geq 5)$," J. CHEM. PHYS. 91, 864, 1989.

31. McCarroll, B., "An Improved Microwave Discharge Cavity for 2450 MHz," REV. SCI. INSTRUM. 41, 279, 1970.

32. Cummings, W.P. and Piper, L.G., "Production of $N_2(A^3\Sigma_u^+)$ in the Low Pressure Dielectric Barrier (Ozonizer) Discharge," APPL. SPECTROSC., 44, 656, 1990.

33. Fraser, M.E., Rawlins, W.T., and Miller, S.M., "Infrared (2 to 8 μm) Fluorescence of the $W^3\Delta_u \rightarrow B^3\Pi_g$ and $w^1\Delta_u \rightarrow a^1\Pi_g$ Systems of Nitrogen," J. CHEM. PHYS. 88, 538, 1988.

34. Treanor, C.E., Rich, J.W., and Rehm, R.G., "Vibrational Relaxation of Unharmonic Oscillators with Exchange Dominated Collisions," J. CHEM. PHYS. 43, 1798, 1968.

35. Caledonia, G.E. and Center, R.E., "Vibrational Distribution Functions in Unharmonic Oscillators," J. CHEM. PHYS. 55, 552, 1971.

36. Dilonardo, M. and Capitelli, M. "Non-Equilibrium Dissociation of Nitrogen," REV. PHYS. APPL. 13, 115, 1978.

37. Loftus, A., and Krupenie, P.H., "The Spectrum of Molecular Nitrogen," J. PHYS. CHEM. REF. DATA 6, 113, 1977.

38. Hayes, G.N. and Oskam, H.J., "Population of $N_2(B^3\Pi_g)$ by $N_2(A^3\Sigma_u^+)$ During the Nitrogen Afterglow," J. CHEM. PHYS. 59, 1507, 1973.

39. Kulagin, Yu.A. and Shelepin, L.A., "Metastable-State Population Kinetics," ZH. PRIKL. SPEKTROSK. 39, 827, 1983.

40. Piper, L.G. and Caledonia, G.E., "Long-Lived States in Nitrogen Afterglows," Bull. A.P.S. 31, 157, 1986.

41. Kenty, C., "Collisions Involving Metastable N_2 Molecules in Dischargs and Afterglows in a Rare Gas Plus N_2," Proceedings of the Third International Conference on Physics of Electronic and Atomic Collisions, M.R.C. McDowell, ed., p. 1133, Amsterdam: North Holland, 1964.

42. Dessaux, O., Goudmand, P., and Mutel, B., "Selective Effects of Homogeneous and Heterogeneous Reactions in the System N_2^*-CO," J. QUANT. SPECTROSC. RADIAT. TRANS. 30, 311, 1983.

43. Piper, L.G., "Characterization of $N_2(X,v)$ in the Effluents of Common Laboratory Discharges Using $He^*(2^3S)$ Penning Ionization," PSI-1045/SR-445, Physical Sciences Inc., Andover, MA, 1989.

44. Setser, D.W., Stedman, D.H., and Coxon, J.A., "Chemical Applications of Metastable Argon Atoms. IV. Excitation and Relaxation of Triplet States of N_2," J. CHEM. PHYS. 53, 1004, 1970.

45. Stedman, D.H. and Setser, D.W., "Chemical Applications of Metastable Argon Atoms II. A Clean System for the Formation of $N_2(A\ ^3\Sigma_u^+)$," CHEM. PHYS. LETT. 2, 542, 1968.

46. Roy, C.R., Dreyer, J.W., and Perner, D., "Rate Constants for the Quenching of $N_2(A^3\Sigma_u^+; v_A = 1\text{-}6,8)$ by Rare Gases," J. CHEM. PHYS. 63, 2131, 1975.

47. Michejda, J.A., Dubé, L.J., and Burrow, P.D., "Detection of Vibrationally Excited Nitrogen by Trapped Electron and Electron Transmission Methods," J. APPL. PHYS. 52, 3121, 1981.

48. Grum, F. and Wightman, T.E., "Absolute Reflectance of Eastman White Reflectance Standard," APPL. OPT. 16, 2775, 1977.

49. Fontijn, A., Meyer, C.B., and Schiff, H.I., "Absolute Quantum Yield Measurements of the NO-O Reaction and Its Use a Standard for Chemiluminescent Reactions," J. CHEM. PHYS. 40, 64, 1964.

50. Vanpee, M., Hill, K.D., and Kineyko, W.R., "Absolute Rate Constant Measurements for the Radiative Combination of Atomic Oxygen with Nitric Oxide," AIAA J. 9, 135, 1971.

51. Golomb, D. and Brown, J.H., "The Temperature Dependence of the NO-O Chemiluminous Recombination. The RMC Mechanism," J. CHEM. PHYS. 63, 5246, 1975.

52. Woolsey, G.A., Lee, P.H., and Slafer, W.D., "Measurement of the Rate Constant for NO-O Chemiluminescence Using a Calibrated Piston Source of Light," J. CHEM. PHYS. 67, 1220, 1977.

53. Sutoh, M., Morioka, Y., and Nakamura, M., "Absolute Rate Constant for the Chemiluminescent Reaction of Atomic Oxygen with Nitric Oxide," J. CHEM. PHYS. 72, 20, 1980.

54. Pravilov, A.M., and Smirnova, L.G., "Spectral Distribution of the Chemiluminescence Rate Constant in the O+CO(+M) and O+NO(+He) Reactions," KINET. AND CATAL. 19, 202, 1978.

55. Bradburn, G. and Lilenfeld, H., "Absolute Emission Rate of the Reaction Between Nitric Oxide and Atomic Oxygen," J. PHYS. CHEM. 92, 5266, 1988.

56. Piper, L.G., Caledonia, G.E., and Kennealy, J.P., "Rate Constants for Deactivation of $N_2(A\ ^3\Sigma_u^+\ v'=0,1)$ by O," J. CHEM. PHYS. 75, 2847, 1981.

57. Piper, L.G., "State-to-State $N_2(A^3\Sigma_u^+)$ Energy-Pooling Reactions I. The Formation of $N_2(C^3\Pi_u)$ and the Herman Infrared System," J. CHEM. PHYS. 88, 231, 1988.

58. Shemansky, D.E., "N_2 Vegard-Kaplan System in Absorption," J. CHEM. PHYS. 51, 689, 1969.

59. Thomas, J.M., Jeffries, J.B., and Kaufman, F., "Vibrational Relaxation of $N_2(A\ ^3\Sigma_u^+, v'1,2,3)$ by CH_4 and CF_4," CHEM. PHYS. LETT. 102, 50, 1983.

60. Eyler, E.E. and Pipkin, F.M., "Lifetime Measurements of the $B^3\Pi_g$ State of N_2 Using Laser Excitation," J. CHEM. PHYS. 79, 3654, 1983.

61. Shemansky, D.E., "$A^3\Sigma_u^+$ Molecules in the N_2 Afterglow," J. CHEM. PHYS. 64, 565, 1976.

62. Mitchell, K.B., "Fluorescence Efficiencies and Collisional Deactivation Rates for N_2 and N_2^+ Bands Excited by Soft X-Rays," J. CHEM. PHYS. 53, 1795, 1970.

63. Brennen, W. and Shane, E.C., "The Nitrogen Afterglow and the Rate of Recombination of Nitrogen Atoms in the Presence of Nitrogen, Argon and Helium," J. PHYS. CHEM. 75, 1652, 1971.

64. Jonathan, N. and Petty, R., "Studies of the Nitrogen Yellow Afterglow at Low Pressures," J. CHEM. PHYS. 50, 3804, 1969.

65. Bayes, K.D. and Kistiakowsky, G.B., "On the Mechanism of the Lewis-Rayleigh Nitrogen Afterglow, J. CHEM. PHYS. 32, 992, 1960.

66. Ferguson, E.E., Fehsenfeld, F.C., and Schmeltekopf, A.L., "Flowing Afterglow Measurements of Ion-Neutral Reactions," Advances in Atomic and Molecular Physics edited by D.R. Bates, Academic Press, New York, NY, 1970.

67. Bolden, R.C., Hemsworth, R.S., Shaw, M.J., and Twiddy, N.D., "Measurements of Thermal-Energy Ion-Neutral Reaction Rate Coefficients for Rare-Gas Ions," J. PHYS. B 3, 45, 1970.

68. Farragher, A.L., "Ion-Molecule Reaction Rate Studies in a Flowing Afterglow System," TRANS. FARADAY SOC. 66, 1411, 1970.

69. Huggins, R.W. and Cahn, J.H., "Metastable Measurements in Flowing Helium Afterglow," J. APPL. PHYS. 38, 180, 1967.

70. Walker, R.E., "Chemical Reaction and Diffusion in a Catalytic Tubular Reactor," PHYS. FLUIDS 4, 1211, 1961.

71. Poirier, R.V. and Carr, R.W., "The Use of Tubular Flow Reactors for Kinetic Studies Over Extended Pressure Ranges," J. PHYS. CHEM. 75, 1593, 1971.

72. Cher, M. and Hollingsworth, C.S., "Chemiluminescent Reactions of Excited Helium with Nitrogen and Oxygen," ADV. CHEM. SER. 80, 118, 1969.

73. Kolts, J.H. and Setser, D.W., "Decay Rates of Ar(4s, $^3P_2$), Ar(4s, $^3P_0$), Kr(5s $^3P_2$), and Xe(6s, $^3P_2$) Atoms in Argon," J. CHEM. PHYS. 68, 4848, 1978.

74. Shaw, M.J. and Stock, H.M.P., "Product Ion Diffusion in Flowing Afterglows," J. PHYS. B. 8, 2752, 1975.

75. DeSouza, A.R., Gousset, G., Touzeau, M., and Khiet, Tu., "Note on the Determination of the Efficiency of the Reaction $N_2(A^3\Sigma) + O(^3P) \rightarrow N_2 + O(^1S)$," J. PHYS. B. 18, L661, 1985.

76. Hirschfelder, J.O., Curtiss, C.F., and Bird, R.B., Molecular Theory of Gases and Liquids, John Wiley and Sons, Inc., New York, NY, 1964.

77. Piper, L.G., "The Excitation of $N(^2P)$ by $N_2(A^3\Sigma_u^+, v'=0,1)$," J. CHEM. PHYS. 90, 7087, 1989.

78. Deperasinska, I., Beswick, J.A., and Tramer, A., "A Distorted Wave Calculation for Electronic Energy Transfer in Molecular Collisions. Application to $N_2(A\ ^3\Sigma_u^+)$ + $CO(X\ ^1\Sigma^+) \rightarrow N_2(X\ ^1\Sigma_g^+)$ + $CO(a\ ^3\Pi)$ System," J. CHEM. PHYS. 71, 2477, 1979.

79. Coombe, R.D. and Lam, C.H-T., "Photodissociation of Bromine Azide II. Production of $Br_2(D'^3\Pi_{2g})$," J. CHEM. PHYS. 80, 3106, 1984.

80. Katayama, D.H., Miller, T.A., and Bondybey, V.E., "Collisional Deactivation of Selectively Excited N_2^+," J. CHEM. PHYS. 72, 5469, 1980.

81. Herbelin, J., "Electronic Energy Transfer Between NF(b) and IF(X)," CHEM. PHYS. LETT. 133, 331, 1987.

82. Pravilov, A.M., Smirnova, L.G., and Vilesov, A.F., "The Mechanism of $N_2(B^3\Pi_g)$ Deactivation of N_2," CHEM. PHYS. LETT. 144, 469, 1988.

83. Piper, L.G., Cowles, L.M., and Rawlins, W.T., "State-to-State Excitation of $NO(A^2\Sigma^+, v'=0,1,2)$ by $N_2(A^3\Sigma_u^+, v'=0,1,2)$," J. CHEM. PHYS. 85, 3369, 1986.

84. Katayama, D.H., Dentamaro, A.V., and Welsh, J.A., "State Specific Electronic Quenching Rates for $^{14}N_2^+$ and $^{15}N_2^+$," J. CHEM. PHYS. 87, 6983, 1987.

85. Jihua, G., Ali, A., and Dagdigian, P.J., "State-to-State Collisional Interelectronic and Intraelectronic Energy Transfer Involving CN $A^2\Pi v=3$ and $X^2\Sigma^+ v=7$ Rotational Levels," J. CHEM. PHYS. 85, 7098, 1986.

86. Kenty, C., "Some Afterglow Spectra Observable in Incandescent Lamps," PHYS. REV. 89, 336, 1953.

87. Kenty, C., "Active Nitrogen in the Rare Gases and Its Excitation of Metal Vapors," J. CHEM. PHYS. 23, 1555, 1955.

88. Kenty, C., "New Evidence for the importance of $N_2(^3\Delta_u)$ in Discharge and Afterglows in N_2 Plus a Rare Gas," J. CHEM. PHYS. 41, 3996, 1964.

89. Kenty, C., "Diffuse Continua-Emitting Discharges in the Rare Gases With and Without Nitrogen," J. CHEM. PHYS. 47, 2545, 1967.

90. Rotem, A., Nadler, I., and Rosenwaks, S., "Laser-Induced Fluorescence Studies of Collisional Coupling of $N_2(B^3\Pi_g)$ with $N_2(W^3\Delta_u)$ and $N_2(A^3\Sigma_u^+)$," CHEM. PHYS. LETT. 83, 281, 1981.

91. Peticolas, W.L., "Multiphoton Spectroscopy," ANN. REV. PHYS. CHEM. 18, 233, 1967.

92. Zare, R.N., "Laser Chemical Analysis," SCIENCE 226, 298, 1984.

93. Leone, S.R., "Laser Probing of Chemical Reaction Dynamics," SCIENCE 227, 889, 1985.

94. Dixit, S.N. and McKoy, V., "Theory of Resonantly Enhanced Multiphoton Processes in Molecules," J. CHEM. PHYS. 82, 3546, 1985.

95. Marinelli, W.J., Green, B.D., DeFaccio, M., and Blumberg, W.A.M., "Vibrational Relaxation and Intersystem Crossing in $N_2(a^1\Pi_g)$," J. PHYS. CHEM. 92, 3429, 1988.

96. Butler, J.E., "Efficient Baffles for Laser Light Scattering Experiments," APPL. OPT. 21, 3617, 1982.

97. Cool, T.A., "Quantitative Measurement of NO Density by Resonance Three-Photon Ionization," APPL. OPT. 23, 1559, 1984.

98. Morgan, J.E., Phillips, L.F., and Schiff, H.I., "Studies of Vibrationally Excited Nitrogen Using Mass Spectrometric and Calorimeter-Probe Techniques," DISCUSS. FARADAY SOC. 33, 118, 1962.

99. Black, G., Sharpless, R.L., and Slanger, T.G., "Measurements of Vibrationally Excited Molecules by Raman Scattering, I. The Yield of Vibrationally Excited Nitrogen in the Reaction $N + NO \rightarrow N_2 + O$," J. CHEM. PHSY. 58, 4792, 1973.

100. van Lonkhuyzen, H. and de Lange, C.A., "Non-Boltzmann Vibrational Excitation of Nitrogen Detected by UV Photoelectron Spectroscopy," CHEM. PHYS. LETT. 107, 420, 1984.

101. David, S.J. and Coombe, R.D., "The Chemiluminescent Reaction of $N(^4S_u)$ Atoms with Azide Radicals," J. PHYS. CHEM. 89, 5206-5212, 1985.

102. Habdas, J., Wategaonkar, S., and Setser, D.W., "The $F + HN_3$ System: A Chemical Source for $NF(a^1\Delta)$," J. CHEM. PHYS. 91, 451-458, 1987.

103. Clark, T.C. and Clyne, M.A.A., "Kinetic of Chemiluminescent Reactions of the Gaseous Azide Radical," TRANS. FARADAY SOC. 66, 877, 1970.

104. Young, R.A., Sharpless, R.L., and Stringham, R., "Catalyzed Dissociation of N_2 in Microwave Discharges," J. CHEM. PHYS. 40, 117, 1964.

105. Pritt, A.T., Patel, D., and Coombe, R.D., "Yields of Singlet Nitrenes from Halogen Atom-Azide Molecule Reactions," INT. J. CHEM. KINET. 16, 977, 1984.

106. Habdas, J. and Setser, D.W., "Vibrationally to Electronic Energy Transfer from HF(v=2,3) to NF($a^1\Delta$)," J. PHYS. CHEM. 93, 229-235, 1989.

107. Clark, T.C., Ph.D. Dissertation, Queen Mary College, London, U.K., 1969 (unpublished).

108. Paur, R.J., Ph.D. Dissertation, Indiana University, Bloomington, IN, 1973 (unpublished).

109. Combourieu, J., Lebras, G., Poulet, G., and Jourdain, J.L., XVIth Int. Combustion Symp., Boston, MA, 1976.

110. Yamasaki, K., Fueno, T., and Kajimoto, D., "Studies of the Reaction N + N_3 → $N_2(B^3\Pi_g)$ + $N_2(X^1\Sigma_g^+)$," CHEM. PHYS. LETT. 94, 425, 1983.

111. MacRobert, S., Ph.D. Dissertation, Queen Mary College, London, U.K., 1983 (unpublished).

112. Marinelli, W.J., Kessler, W.J., and Woodward, A.M., Vibronic Exchange Visible Laser. Azide Radical Reactions, PSI-9451/TR-746, Physical Sciences Inc., Andover, MA, December 1987.

113. David, S.J., Ongstad, A.P., MacDonald, M.A., and Coombe, R.D., "Chemical Generation of Excited IF($B^3\Pi_{O+}$)," CHEM. PHYS. LETT. 136(3,4), 352, 1987.

114. David, S.J. and Coombe, R.D, "Rate of Reactions of the Azide Radical," J. PHYS. CHEM. 90, 3260-3263, 1986.

115. Morris, R.A., Donohue, K., and McFadden, D.L., "Atomic Hydrogen and Fluorine Reactions with Trifluoroiodomethane," J. CHEM. PHYS. 93, 1358, 1989.

116. Morgan, J.E. and Schiff, H.I., "The Study of Vibrationally-Excited N_2 Molecules with the Aid of an Isothermal Calorimeter," CAN. J. CHEM. 41, 903, 1963.

117. Davis, S.J., Woodward, A.M., Piper, L.G., and Marinelli, W.J., Chemical Pump Sources for IF(B), AFWL-TR-87-92, Kirtland AFB, NM, July 1988.

118. Shemansky, D.E., "N_2 Vegard-Kaplan System in Absorption," J. CHEM. PHYS. 51, 689, 1979.

119. Marinelli, W.J. and Piper, L.G., "Franck-Condon Factors and Absolute Transition Probabilities for the IF($B^3\Pi_0^+$ - $X^1\Sigma^+$) Transition," J. QUANT. SPECTROSC. RADIAT. TRANS. 34, 321, 1985.

120. Cha, H. and Setser, D.W., "NF($b^1\Sigma^+$) Quenching Rate Constants by Halogens and Interhalogens and the Excitation Rate Constant for IF(B) Formation," J. PHYS. CHEM. 91, 3758, 1987.

121. Wolf, P.J. and Davis, S.J., "Collisional Dynamics of the IF $B^3\Pi(O^+)$ State. III. Vibrational and Rotational Energy Transfer," J. CHEM. PHYS. 87, 3492, 1987.

122. Brocklehurst, B. and Jennings, K.R., "Reactions of Nitrogen Atoms in the Gas Phase," PROG. REACT. KINET. 4, 1, 1967.